The application of esca to structure, bonding and reactivity of some polymer systems, with particular reference to surface modifications

Alan Dilks

UNIVERSITY OF DURHAM

A thesis entitled

THE APPLICATION OF ESCA TO STRUCTURE, BONDING AND REACTIVITY OF SOME POLYMER SYSTEMS, WITH PARTICULAR REFERENCE TO SURFACE MODIFICATIONS

Submitted by

Alan Dilks, B.Sc.

(Van Mildert College)

A candidate for the Degree of Doctor of Philosophy

1977

To Sheila and my parents

ACKNOWLEDGEMENTS

I am indebted to my supervisor, Dr. D. T. Clark for his help, encouragement and enthusiasm towards the work of this thesis, and my sincere gratitude is due to him. I would also like to thank my colleague, H.R. Thomas for his friendship and many helpful discussions as well as practical assistance, particularly in the work on sample charging phenomena. Thanks are also due to Dr. G. H. C. Freeman at the National Physical Laboratory, Teddington for supplying instrumentation and expertise for the measurement of vacuum ultraviolet spectra.

Gratitude is also expressed to the Science Research Council for provision of ESCA instrumentation and a research studentship, and to the Institute of Petroleum for financial support without which this work would not have been possible.

Finally I would like to thank Messrs. Coulson, Hodgson and Venmore for their able fabrication of the plasma reactor used for kinetic studies, and to Mrs. M. Wilson for her great patience and secretarial skill in typing this manuscript.

A. Dilks

Durham, 1977

MEMORANDUM

The work described in this thesis was carried out at the University of Durham between October 1974 and June 1977. It has not been submitted for any other degree and is the original work of the author except where acknowledged by reference.

Work in this thesis has formed the whole, or part, of the following publications:

1. Application of ESCA to Studies of Structure and Bonding in Polymers, D.T. Clark, A. Dilks, J. Peeling and H.R. Thomas, Faraday Disc.Chem.Soc., 60 183 (1975)

2. Some Aspects of Shake Up Phenomena in Some Simple Polymer Systems, D.T. Clark, D.B. Adams, A. Dilks, J. Peeling and H.R. Thomas, J.Elect.Spec., 8 51 (1976)

3. ESCA Studies of Polymers. VII. Shake Up Phenomena in Some Alkane-Styrene Copolymers, D.T. Clark and A. Dilks, J.Polym.Sci., Polym.Chem.Edn., 14 533 (1976)

4. ESCA Studies of Polymers. XIII. Shake Up Phenomena in Substituted Polystyrenes, D.T. Clark and A. Dilks, J.Polym.Sci., Polym.Chem.Edn., 15 15 (1977)

5. Plasma Modification of Polymers Studied by Means of ESCA, D.T. Clark and A. Dilks, A.C.S. Centennial Meeting, New York, April 1976, 'International Symposium on Advances in Characterization of Metal and Polymer Surfaces', Ed. L.H. Lee, 101, Academic Press, New York (1977)

6. Difference ESCA Spectra as a Convenient Probe for Surface Modification of Polymers, D.T. Clark and A. Dilks, J.Elect. Spec. 11 225 (1977)

7. ESCA Applied to Polymers. Part XV. R.F. Glow Discharge Modification of Polymers, Studied by Means of ESCA, in Terms of a Direct and Radiative Energy Transfer Model, D.T. Clark and A. Dilks, J.Polym.Sci., Polym.Chem.Edn., in press (1977).

8. ESCA Applied to Polymers. Part XVIII. R.F. Glow Discharge Modification of Polymers in Helium, Neon, Argon and Krypton, D.T. Clark, and A. Dilks, J.Polym.Sci., Polym.Chem.Edn., in press (1977)

9. ESCA Applied to Polymers, Part XXI. An Investigation of Sample Charging Phenomena, D.T. Clark, A. Dilks and H.R. Thomas, J.Polym.Sci., Polym.Chem.Edn., in press (1977)

10. The Application of ESCA to Polymer Degradation, D.T. Clark, A. Dilks and H.R. Thomas in, 'Developments in Polymer Degradation', Ed. N. Grassie, in press (1977)

11. The Application of Plasmas to the Synthesis and Surface Modification of Polymers, D.T. Clark, A. Dilks and D. Shuttleworth, in the proceedings of the 'Durham Polymer Surfaces Symposium' Ed. D.T. Clark and W.J. Feast, J.Wiley and Sons, London, in press (1977)

ABSTRACT

X-ray photoelectron spectroscopy (ESCA) is used to study structure bonding and reactivity of polymeric materials. Particular emphasis is placed on the investigation of surface modification of polymers, on the monomolecular depth scale, effect by inductively coupled radiofrequency glow discharges excited in a variety of inert gases and oxygen.

Low energy satellite structures, deriving from $\pi^* \leftarrow \pi$ shake up transitions accompanying direct core ionization are identified in the spectra of unsaturated systems and demonstrated to be characteristic of the polymer structure and sensitive to substituent effects. The shake up transitions are essentially localized within a given pendant group or backbone feature and are exploited on a semi-quantitative basis, as a monitor of the extent of unsaturation in the surface of the polymer, providing a valuable extra level of information.

The equilibrium static charge consequent upon the various electron fluxes arriving at and leaving the sample during the ESCA experiment has been correlated to polymer structure within a depth scale of the same order as electron mean free paths and is shown to be worthwhile studying in its own right. The effect of sample charging with respect to energy referencing employing extraneous hydrocarbon contamination in the spectrometer is shown to be small.

Shake up and charging phenomena along with several other facets of the ESCA experiment including angular dependence of relative and absolute signal intensities, analytical depth profiling, difference spectroscopy and Madelung charge potential

calculations, as well as the primary sources of data (absolute and relative binding energies, and relative peak intensities) have been employed in an extensive investigation into the surface modification of polymers by means of inert gas and oxygen plasmas. For the inert gas plasmas the rates for direct and radiative energy transfer processes are determined within the framework of a kinetic model, and are shown to have a strong dependence on the sustaining gas, the power, the pressure and the plasma configuration. The depth to which direct energy transfer processes are important is determined to range from about one monolayer for krypton to three monolayers for helium. Radiative energy transfer to the bulk polymer is best effected by neon and some aspects of the vacuum ultraviolet radiation emitted from the plasmas are also presented.

Modification by the oxygen containing plasmas is demonstrated to be extensive but confined within approximately one monolayer, in the initial stages. The rate and extent of oxidation is a strong function of polymer structure for pure oxygen plasmas (r.f. low power, low pressure) and is thought to be initiated by a crosslinking mechanism. This is affirmed by comparison with plasmas excited in helium/oxygen mixtures.

CONTENTS

		Page
CHAPTER ONE:	Electron Spectroscopy for Chemical Applications (ESCA)	
1.	Introduction	1
2.	Processes Involved in ESCA	8
2.1	The ESCA Experiment	8
2.2	Auger Emission and X-ray Fluorescence	12
2.3	Electronic Relaxation	18
2.4	Shake-up and Shake-off	21
3.	Chemical Shifts	28
3.1	Equivalent Cores Approximation	29
3.2	Charge Potential Model	32
3.3	Inversion of the Charge Potential Model	37
4.	Fine Structure	39
4.1	Multiplet Splitting	39
4.2	Spin-Orbit Splitting	43
4.3	Electrostatic Splitting	45
5.	Valence Bands	47
6.	Energy Referencing	49
7.	Signal Intensities	55
7.1	Fixed Angle Studies	56
7.2	Analytical Depth Profiling	61
7.3	Angular Dependence of Signal Intensities	63
8.	Line Shape Analysis	65
9.	Instrumentation	71
9.1	X-ray Equipment	72
9.2	Sample Chamber	76
9.3	Analyser	78
9.4	Electron Detection	80
CHAPTER TWO:	ESCA as a Tool for the Study of Structure, Bonding and Reactivity of Polymers	
1.	Introduction	82
2.	Sample Preparation	83
2.1	Powders	84
2.2	Solution Cast Films	84
2.3	Pressed or Extruded Films	85
2.4	'In situ' Preparation	86
2.5	Sample Contamination	86

Page

3. Energy Referencing 87

4. Information Available from ESCA 89

5. Linear Polymers 91

5.1 Homopolymers 91
5.2 Copolymers 101

6. Crosslinked Polymers 110

7. Surface Modified Polymers 115

7.1 Chemical Modification 117
7.2 Modification by Plasmas and Discharges 122
7.3 Mechanical Modifications 127

CHAPTER THREE: Shake up Phenomena in Polymers

1. Introduction 131

2. Experimental 134

2.1 Samples 134
2.2 ESCA Spectra 135
2.3 U.V./Visible Spectra 136

3. Theoretical 137

4. Shake up Phenomena in Poly(para-substituted)Styrenes 139

4.1 Core Level Spectra 139
4.2 Shake up Spectra 143
4.3 U.V./Visible Spectra 150
4.4 Theoretical Interpretation of the Shake up Spectra 153
4.5 Derivative Spectra 166

5. Shake up Phenomena in Homopolymers 168

5.1 Core Level and Shake up Spectra 168
5.2 Theoretical Interpretation of the Shake up Spectra 171

6. Shake up Phenomena in Copolymers 179

6.1 U.V./Visible Spectra 181
6.2 Shake up Spectra 183

7. Conclusions 190

CHAPTER FOUR: Sample Charging Phenomena in Polymers

1. Introduction 192

2. Experimental 196

Page

2.1 Samples 196
2.2 Instrumentation 199
2.3 Sample Charge and Time Dependent Studies 201

3. Charging Induced by a Non-monochromatic X-ray Source 202

3.1 Equilibrium Charging of Polymers 202
3.2 Surface Sensitivity of Sample Charging 208
3.3 Sample Charging as a Function of the Operating Parameters of the X-ray Source 215
3.4 Time Dependence of Sample Charging 218

4. Charging Induced by a Monochromatic X-ray Source 221

4.1 Some Instrumental Dependent Factors Governing Sample Charging 221
4.2 Sample Charging as a Function of Film Thickness 225

5. Conclusions 227

CHAPTER FIVE: Surface Modification of Polymers by Inert Gas Plasmas - Part I

1. Introduction 228

2. Experimental 236

2.1 Samples 236
2.2 Instrumentation 238
2.3 Plasma Configurations 238
2.4 Kinetic Studies 241

3. Preliminary Observations on the Argon Glow Discharge Modification of Polymers 243

4. Angular Dependence of Absolute and Relative Peak Intensities 254

5. Kinetic Studies of the Glow Discharge Modification of Polymers 262

5.1 The Kinetic Model 262
5.2 Glow Discharge Modification of an Ethylene/Tetrafluoroethylene Copolymer by Plasmas Excited in Argon 265

6. Mechanistic Aspects of the Plasma Modification of an Ethylene/Tetrafluoroethylene Copolymer Film 279

CHAPTER SIX: Surface Modification of Polymers by Inert Gas Plasmas - Part II

1. Introduction 286

2. Experimental 287

		Page
2.1	Samples and Gases	287
2.2	Kinetic Studies	288
2.3	Direct Electron Sampling	288
2.4	Vacuum Ultraviolet Spectra of the Plasmas	291
3.	Some Physical Aspects of Inert Gas Plasmas	292
3.1	Observations on the Energy Distribution of Electrons Samples from Radiofrequency Plasmas Excited in Inert Gases	293
3.2	Ions and Metastables in Inert Gas Plasmas	298
3.3	Observations on the Vacuum Ultraviolet Radiation Emitted from Radiofrequency Plasmas Excited in Inert Gases	300
4.	Kinetic Studies of the Glow Discharge Modification of the Ethylene/Tetrafluoroethylene Copolymer by Plasmas Excited in the Inert Gases	307
4.1	Plasmas Excited in Helium, Neon, Argon, Krypton and Xenon	307
4.2	Plasmas Excited in Gas Mixtures	321
4.3	Modification of Other Polymers by Inert Gas Plasmas	326
4.4	Angular Dependence Studies	328
4.5	Charging Phenomena	332
5.	Elucidation of Some Mechanistic Aspects of the Initial Stages of Crosslinking	333
5.1	Theoretical Interpretation of the ESCA Spectra of the Crosslinked Copolymer	333
5.2	Difference Spectra	340
5.3	Valence Band Spectra	346
6.	Conclusions	349
CHAPTER SEVEN:	Surface Modification of Polymers by Oxygen Plasmas	
1.	Introduction	350
2.	Experimental	352
3.	Absolute and Relative Binding Energies of Carbon-Oxygen Structural Features	352
4.	Modifications Effected by Oxygen Containing Plasmas	360
4.1	Pure Oxygen Plasmas	360
4.2	Helium/Oxygen Plasmas	375
5.	Mechanistic Aspects of the Plasma Oxidation of Hydrocarbon Polymers	377
6.	Conclusions	382

CHAPTER ONE

Electron Spectroscopy for Chemical Applications (ESCA)

1. Introduction

In common with most other spectroscopic methods X-ray photoelectron spectroscopy is a technique originally developed by physicists and is now extensively utilized by inorganic, organic and physical chemists as a tool for investigating structure and bonding.[1]

At the beginning of the 20th century Robinson[2-4] (in England) and de Broglie[5] (in France) investigated the energy distribution of electrons in various elements by the X-ray irradiation of thin foils, producing photoemission via the photoelectric effect. The distribution of the electron energies for the transmitted photoelectrons was recorded photographically and analysed using a homogeneous magnetic field. The electron distributions obtained were characterised by long tails with distinct edges at the high energy end since the radiation source consisted of a continuous spectrum (bremsstrahlung) with the characteristic line spectrum of the anode material superimposed. Measurement of these edge positions gave a determination of the energies of the photoelectrons ejected from the different atomic levels and therefore with a knowledge of the energy of the exciting X-ray line, binding energies were calculated. Except for a few isolated attempts[6-10] to extend the work of Robinson and de Broglie, X-ray photoelectron spectroscopy went into a recession until the early 1950's when Siegbahn and co-workers at the University of Uppsala, Sweden, developed an iron-free magnetic double-focussing electron spectrometer with high resolution properties.[11] In 1954 attempts were made to record high resolution photoelectron spectra

excited by X-rays and the observation of a sharp line which could be resolved from the edge of each electron veil changed the course of future development of the technique. The photoelectrons to which this line corresponded had the important property that they did not suffer energy losses and, therefore possessed the binding energy of the atomic level from which they came and could be measured to a precision of a few tenths of an electron volt.[12]

Although core electrons are not explicitly involved in bonding (even though most of the total energy of a molecule resides in the core electrons), the core energy levels of a molecule encode a considerable amount of information concerning the chemical environment of the atom.[13,14] However, the chemical effects were difficult to measure accurately and very often difficult to interpret theoretically. Siegbahn and co-workers first studied these chemical effects for copper and its oxides[15] and the value of X-ray photoelectron spectroscopy for measurement of chemical 'shifts' became apparent from this work, but its general utility was appreciated only as recently as 1964.[16-17]

Much of the early work of Siegbahn and co-workers was extensively documented in 1968 in 'ESCA. Atomic, Molecular and Solid State Structure Studied by Means of Electron Spectroscopy'.[18] Later work was summarized in 1969 in the well thumbed pages of 'ESCA Applied to Free Molecules'.[19]

In addition to the name ESCA originally coined by Siegbahn the technique is also known as:

1) X-ray Photoelectron Spectroscopy (XPS).

2) High Energy Photoelectron Spectroscopy (HEPS).

3) Induced Electron Emission Spectroscopy (IEES).

4) Photoelectron Spectroscopy of the Inner Shell (PESIS).

The designation ESCA (Electron Spectroscopy for Chemical Applications) is however, descriptive and aesthetically pleasing and will be used throughout this thesis.

As we shall see ESCA is an extremely powerful tool with wide ranging applicability and the principal advantages of the technique may be summarized as follows:

(1) The sample may be solid, liquid or gas and sample sizes are small being 1 mg. solid, 0.1 µl. liquid and 0.5 cc. (STP) of a gas.

(2) The technique is for all practical purposes non-destructive in that the X-ray flux is quite small ($\sim$ 0.1 millirad/sec.).[20] This is especially advantageous over Auger spectroscopy where the electron beam produces many surface changes, particularly in polymeric systems where cross-linking and degradation can occur.

(3) The technique is independent of the spin properties of the nucleus and can be used to study any element of the periodic table with the exception of H and He.

(4) Materials may be studied 'in situ' in their working environments with a minimum of preparation.

(5) The technique provides a large number of information levels from a single experiment and has a higher sensitivity than most other analytical techniques.

(6) The data is often complementary to that obtained by other

techniques and has unique capabilities centred to the development of a number of important fields.

(7) For solids, ESCA has the unique capability of differentiating the surface from subsurface and bulk phenomena, allowing analytical depth profiling.

(8) The information obtained is directly related to the molecular structure and bonding, and is applicable to both the inner shells and valence levels of the molecule enabling a quite thorough analysis of the electronic structure of the system to be made.

(9) The information levels are such that 'ab initio' investigations are feasible and the theoretical basis is well understood resulting in considerable interest to theoreticians.

Having elaborated on the advantages of ESCA it is important to consider also the disadvantages which are surprisingly few.

(1) The overall costs are quite high.

(2) The ultra high vacuum system associated with ESCA requires provision of vacuum interlocks for routine sample handling.

(3) Whilst the technique has superior depth resolution (in the range of $\sim$ 100 Å) the spatial resolution is poor and typically an area of 0.3 $cm.^2$ is sampled.

(4) If the surface differs from the bulk then it is not possible to say anything about the bulk structure by means of ESCA without sectioning the sample.

(5) To take full advantage the technique often requires a relatively high level of theoretical competence. (However it must be emphasized that the technique has capability for exploitation at many levels).

The hierarchy of information levels available in ESCA is shown in Table 1.1. It is the composite nature of these information levels which endows ESCA with such wide ranging capabilities and has seen the technique emerge into one of the most powerful tools available to chemists and physicists today.

Table 1.1 Hierarchy of Information Levels Available in ESCA

(1) Absolute binding energies relative peak intensities, shifts in binding energies. Element mapping for solids, analytical depth profiling, identification of structural features etc. Short range effects directly longer range indirectly.

(2) Shake up - shake off satellites. Monopole excited states; energy separation with respect to direct photoionization peaks and relative intensities of components of 'singlet and triplet' origin. Short and longer range effects directly (Analogue of U.V.).

(3) Multiplet effects. For paramagnetic systems, spin state, distribution of unpaired electrons (Analogue of E.S.R.).

(4) Valence energy levels, longer range effects directly.

(5) Angular dependent studies. For solids with fixed arrangement of analyzer and X-ray source, varying take off angle between sample and analyzer provides means of differentiating surface from sub-surface and bulk effects.

Variable angle between analyzer and X-ray source, angular dependence of cross sections, asymmetry parameter β, symmetries of levels.

The great advantages of ESCA as a technique, in being able to study in principle the core and valence levels of any element (regardless of nuclear properties such as magnetic or electric quadrupole moments), coupled with the low sample requirements and the ability to study involatile insoluble solids, is nowhere more apposite than in the study of polymers. In applying the technique to the investigation of polymer structures there are several distinct aspects about which one would hope to gain information (Table 1.2).

Table 1.2 ESCA Applied to Polymers

A. Aspects of Structure and Bonding (Static Studies)

(i) Gross chemical compositions
  (a) elemental compositions,
  (b) % incorporation of comonomers in copolymers,
  (c) polymeric films produced at surfaces.

(ii) Gross structural information
  e.g. for copolymers, block, alternating or random nature. Domain structure in block copolymers.

(iii) Finer details of structure
  (a) structural isomerisms,
  (b) experimental charge distributions in polymers.

(iv) Valence bands of polymers.

(v) Identification of polymers, structural elucidation.

(vi) Monopole excited states.

B. Aspects of Structure and Bonding (Dynamic Studies)

(i) Surface treatments e.g. CASING, plasma modification.

(ii) Thermal and photochemical degradation.

(iii) Polymeric films produced at surfaces by chemical reaction e.g. fluorination (including the use of ESCA for depth profiling and quantitative measurement of film thickness).

(iv) Chemical degradation of polymers, e.g. oxidation, nitration etc.

C. Electrical Properties

(i) Mean free paths of electrons as a function of kinetic energy.

(ii) Photoconductivity of polymers.

(iii) Statics and dynamics of sample charging.

(iv) Triboelectric phenomena.

This thesis is particularly concerned with aspects of the surface modification of polymers. Information is gained on the structure, bonding and reactivity of such systems by means of the primary sources of information (i.e. absolute and relative binding energies and relative signal intensities) as well as secondary sources of information (i.e. shake-up phenomena, angular dependence of relative signal intensities and sample charging phenomena). The following chapter provides an introduction to the application of ESCA to the study of structure, bonding and reactivity of polymers including a brief review of the research in the field to date. In chapters 3 and 4 the applicability of two secondary sources of information namely shake-up phenomena (Chapter 3) and sample charging phenomena (Chapter 4) to the study of polymeric materials is

investigated in some detail. The remainder of the thesis is concerned with the surface modification of polymeric materials, on the monomolecular depth scale, by external agents with particular emphasis on inductively coupled radiofrequency glow discharges excited in argon (Chapter 5), other inert gases (Chapter 6) and oxygen (Chapter 7). The rationale behind the choice of these particular systems is presented in the relevant chapters. Since much of the latter part of this thesis involves the use of radiofrequency glow discharge techniques a short introduction to these methods is included at the beginning of Chapter 5.

It should become apparent from this thesis that ESCA is the single most powerful tool presently available for the study of surface modification of polymers on the monomolecular depth scale due to its extreme surface sensitivity and the minimal amount of sample preparation necessary.

2. Processes involved in ESCA

2.1 The ESCA Experiment

The interaction of a monoenergetic beam of soft X-rays with an atom in a molecule or lattice results in the photoejection of electrons with specific kinetic energies.[18]

The most commonly employed X-ray sources utilized are $Al_{K\alpha_{1,2}}$ and $Mg_{K\alpha_{1,2}}$ with corresponding photon energies of 1486.6 eV and 1253.7 eV respectively. With the knowledge of the photon energy and the measurement of the kinetic energy of the photoemitted electrons, ESCA provides a technique for the determination of the binding energies of, in principle, all electrons from the core to the valence levels. The

lifetimes of the core hole states are typically in the range 10^{-13} - 10^{-15} sec.[21] emphasizing the extremely short time scales involved in ESCA compared with most other spectroscopic techniques.

The total kinetic energy of an emitted photoelectron (KE, which may include the contributions from the vibrational, rotational and translational motions as well as electronic) is given by the equation

$$KE = h\nu - BE - E_r \qquad (1.1)$$

where $h\nu$ is the energy of the incident photon, h is Planck's constant and ν is the frequency of the X-ray radiation, B.E. is the binding energy of the photoemitted electron which is defined as the positive energy required to remove an electron to infinity with zero kinetic energy, and E_r is the recoil energy of the atom. Siegbahn, et al,[18] have calculated that the recoil energy of atoms decreases with increasing atomic number e.g. H = 0.9 eV, Li = 0.1 eV, Na = 0.04 eV, K = 0.02 eV and Rb = 0.01 eV. Therefore it is evident that the E_r term only has significance for the lighter elements, when compared with the instrumental linewidths obtained with the present study of elements from carbon upwards in the periodic table. With present resolution of typical ESCA spectra in the study of solid materials the excitations from the translational, rotational and vibrational motions are seldom observed. ESCA is primarily concerned, therefore, with the various electronic states of the atom.

Therefore the equation for a free molecule reduces to equation 1.2

$$KE = h\nu - BE \qquad (1.2)$$

It is important to understand the relationship that exists between the binding energies observed experimentally by ESCA for solids versus free molecules when compared with values calculated theoretically by ab initio and semi-empirical LCAO-MO-SCF treatments.

The most convenient reference level for a conducting sample is the Fermi level. In a metal this level, sometimes referred to as the 'electron chemical potential', is defined as the highest occupied level.

The work function, ϕ_s, for a solid is defined as the energy gap between the free electron (vacuum) level and the Fermi level in the solid. The vacuum levels for the solid sample and the spectrometer may however be different and the electron will experience either a retarding or accelerating potential equal to $\phi_s - \phi_{spec}$ where ϕ_{spec} is the work function of the spectrometer.[18] In ESCA it is the kinetic energy of the electron when it enters the analyzer that is measured and taking zero binding energy to be the Fermi level of the sample the following equation results,

$$BE = h\nu - KE - \phi_{spec} \qquad (1.3)$$

The binding energy referred to the Fermi level does not depend on the work function of the sample but on that of the spectrometer and this represents a constant correction to all binding energies.

It is evident that for conducting samples in electrical contact with the spectrometer the Fermi level serves as a convenient reference level. For insulating samples, such as polymers, the Fermi level is not so well defined analytically but lies somewhere between the filled valence levels and the

empty conduction band.[18]

Equation 1.3 assumes equilibrium conditions during the ejection of an electron, which may or may not occur when the resistance of the sample is high compared with the electrical currents needed to replace the electron vacancies due to photoemission.

Several investigations have shown that the primary photoelectrons are rapidly slowed down by the interaction with matter and can generate intense currents of slow 'secondary' electron clouds at the surface of the sample.[22-24] These secondaries play an important role in establishing the electrical equilibrium at the surface of the sample and have been typically found to be approximately 20% of the photoelectron flux in a conducting sample and 99% of the flux in an insulating sample.

In practice, the problem of extracting absolute binding energies is circumvented by the use of reference standards for calibration of the binding energy scale. This is dealt with in more detail in a subsequent section where energy referencing is discussed.

Several processes may accompany photoionization and they may be divided into two main categories depending on the time scale relative to the photoionization process. Auger electron emission and X-ray fluorescence are slow processes compared to photoionization and hence have negligible effects on the kinetic energy of the photoejected electron. Electronic relaxation processes, shake-up and shake-off, on the other hand occur on a similar time scale to photoionization and result in a modification of the kinetic energy of the

photoejected electron.

2.2 Auger Emission and X-ray Fluorescence

De-excitation of the hole state can occur via both fluorescence and Auger processes, for elements of low atomic number the latter being more probable.[18] These fundamental processes are shown schematically in Fig. 1.1.

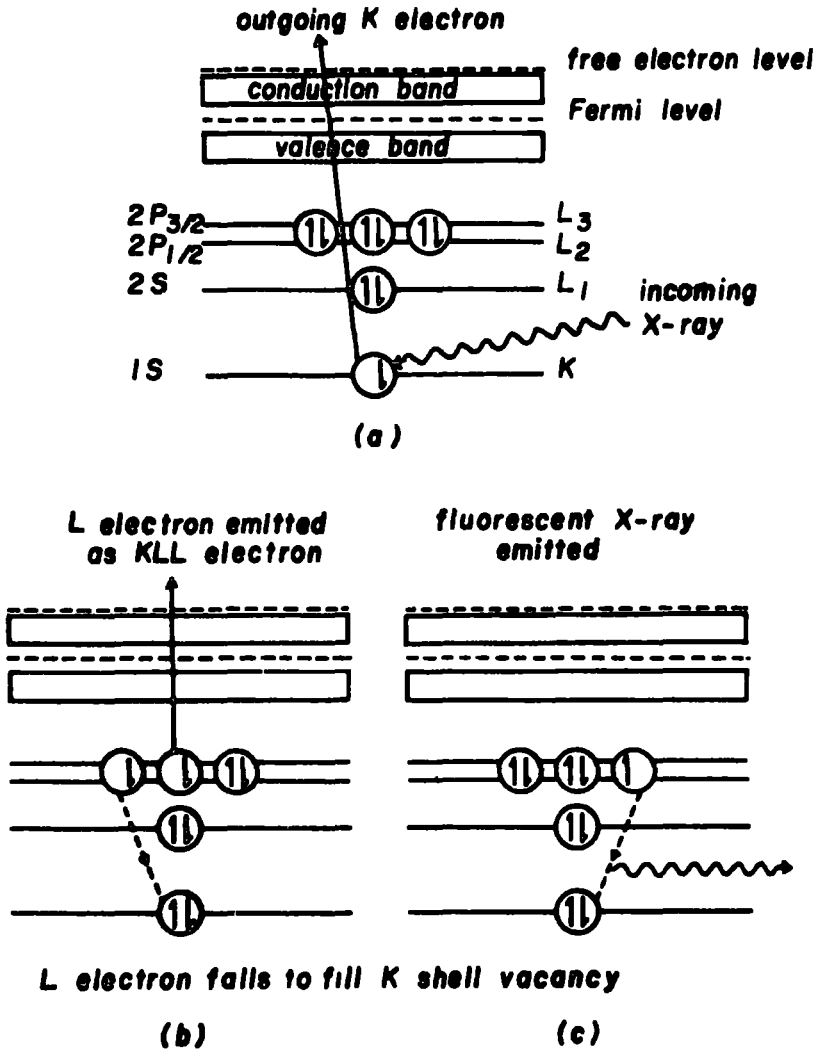

Figure 1.1. Photoionization, Auger and X-ray Fluorescence.

Auger emission may be viewed as a two step process involving the ejection of an electron from an inner shell by a photon followed by an electron dropping down from a higher level to the vacancy in the inner shell with the simultaneous

emission of a second electron (Fig.1.1).[25-30] When the electron drops from a valence shell to fill the inner shell vacancy the chemical shifts involved are related to both outer and inner shells and in a few suitable cases information can be gained on the binding energies of both levels.

Where the electronic vacancy in the inner shell is filled by an electron from another inner shell (Coster-Kronig transitions) the Auger spectrum is useful for analysis of inner shell transitions. These are very efficient and lead to very short lifetimes with well resolved Auger spectra.[29,30] (These processes also cause a broadening in the ESCA spectrum due to their short lifetimes).

The wavefunction overlap is such that the probability for Coster-Kronig processes are more than an order of magnitude greater than for Auger processes involving valence electrons. For a Coster-Kronig process to occur the difference in the binding energies of the two inner shells must be sufficiently large to eject an electron from an orbital in the higher shell. These processes only occur in elements of atomic number < 40.

For a general Auger transition which involves any set of levels KLM, a peak should appear at:

$$E_{(Z)} = E_K - E_L - E_M\,(Z + \Delta) - \phi_A \qquad (1.4)$$

where: Z is the atomic number

$\Delta = 1$ (due to the extra positive charge from the loss of an electron

ϕ_A is the work function of the analyzer

E_K is the energy from a K level transition

E_L is the energy from a L level transition

E_M is the energy from a M level transition

This equation can, however, lead to errors in some cases because the final state of the doubly ionized atom must be defined. The additional definition is needed because the energies involved in the transitions in the Auger process are governed by the coupling scheme amongst electronic wavefunctions in the initial (singly ionized) as well as the final (doubly ionized) electronic configuration. LS coupling dominates for light elements and jj coupling for heavy elements. The rate of emission of Auger electrons is determined, essentially, by the K shell ionization rate. The other mode of de-excitation, X-ray emission (Fig.1.1) is very inefficient for the lighter elements and is negligible for energies less than 500 eV, while Auger efficiency is approximately comparable to X-ray emission at about 2000 eV (Fig. 1.2).

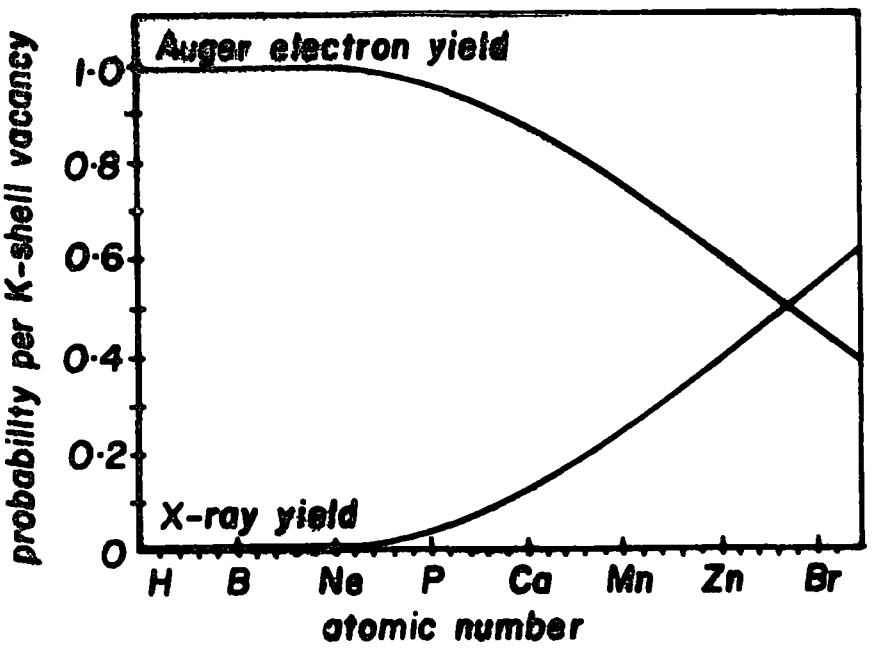

Fig.1.2. Efficiency of Auger and X-ray Fluorescence processes as a function of atomic number.

The relative efficiencies between X-ray fluorescence and Auger current is relatively constant with atomic number when lower energy transitions are involved for the heavy elements.

The decrease in X-ray fluorescence with decreasing energy is due to the fact that it is an electromagnetic (dipole) process and depends mostly on the acceleration of the orbiting electron. The Auger process, however, is dependent upon the electrostatic forces accompanied by a vacancy in the inner shell.

Essentially there are three types of chemical information which may in principle be obtained from Auger spectra. However, it should be pointed out that the extraction of this information is by no means straightforward since differences in energy levels are involved. The first is the chemical shift due to the shifts of the inner shell energy levels arising from changes in valence electron distributions. The second pertains to the valence levels themselves. The valence band spectra are usually quite pronounced due to the redistribution (relaxation) of electrons upon formation of a new electronic configuration. The third type of information that may be obtained is much more vague and is referred to as 'molecular orbital energy spectra' and is of course also involved with part of the valence levels. If the molecular orbitals are known for a specific compound then the valence energy levels can be compared. This technique although it has the limitation that to-date molecular orbitals cannot be assigned to specific energy levels the symmetry of its component wave functions can be used to 'infer' point group symmetry of an atom in a crystal to locate it within a unit cell.

Auger Electron Spectroscopy (AES) as conventionally applied is based on the analysis of the energy of electrons that are ejected from a sample as a consequence of excitation by primary electron beams typically ~2 kV, rather than X-ray photons. This technique is truly a surface analysis technique in that the penetration depth for the exciting electrons is typically only about 5 atomic layers.[31] Under ideal conditions atoms have been detected down to 10^6 atoms/cm.^{3} at the surface.

It should be noted that Auger spectroscopy which is an extremely powerful technique for studying metal and semiconductor surfaces is not a viable alternative to ESCA in studying polymers since the dose rates for the relatively well focussed primary electron beam is typically three orders of magnitude larger than that delivered by the photon beam in ESCA and radiation damage is therefore a severe problem.[32] A further complication also arises in analytical depth profiling by Auger spectra excited by electron beams since the mean free path of the incident electrons must be considered as well as that of the ejected electrons.

The emission of X-rays instead of electrons leads to X-ray fluorescence (secondary-emission analysis) and is an excellent means of qualitative analysis for constituents of atomic number greater than eight. Concentrations down to 0.1% for most elements and 0.01% for elements around Fe, Co, Ni have been detected. X-ray emission tables exist which enable a particular element to be observed at the position of its strongest lines, and thus all of its lines can be identified in the spectrum once its presence is known.[33]

The relative sensitivities of these three techniques, together with other familiar analytical methods, are shown in Table 1.3.

Table 1.3. Sensitivities of Various Analytical Techniques

Bulk Techniques	Minimum Detectable Quantity (g.)
Infrared	10^{-6}
Atomic absorption	10^{-9} - 10^{-12}
Vapour phase chromatography	10^{-3} - 10^{-7}
High pressure liquid chromatography	10^{-6} - 10^{-9}
Mass spectrometry	10^{-10} - 10^{-15}
Surface Techniques	
ESCA	10^{-10}
Neutron activation	10^{-12}
Ion scattering spectrometry	10^{-15}
X-ray fluorescence	10^{-7}
Auger spectroscopy	10^{-14}
Secondary ion mass spectrometry	10^{-13}

Auger chemical shifts can be larger than those corresponding to direct photoemission. The concept of the Auger parameter, defined as the difference in kinetic energy between the photoelectron line and an intense core-type Auger line, has recently been introduced by Wagner.[34]

The concept of a parameter, defined by the difference between two line energies from the same element in the same sample is attractive because static charge and work function corrections are unnecessary, and vacuum level data can be compared to Fermi level data directly. Thus the concept of the Auger parameter seems useful. When the chemical shift in the

Auger line is greatly different from that of the photoelectron line the range in the Auger parameter, in eV can be almost as great as the range in Auger line energy.

It has been amply demonstrated that, for example, for sodium the parameter is a sensitive function of the polarizability of its environment. The data for sodium spreads from 579.3 eV for sodium metal to 569.7 eV for the gaseous atoms a span of 9.6 eV. The sodium salts occupy a 3.4 eV range precisely in the centre between these extremes. At the end nearest sodium gas are the least polarizable anions and at the end nearest sodium metal are the most polarizable ones.

It is not expected that the Auger parameter, for the first series of transition metals or the rare earths will be very useful because of complications arising from multiplet splitting and shake up processes in paramagnetic systems.

For first row elements the Auger spectra are complex due to the involvement of many valence states and the Auger chemical shifts tend to be small. For these reasons the application of the Auger parameter concept to polymer systems has not been exploited.

2.3 Electronic Relaxation

It is well established that photoionization of core electrons is accompanied by substantial electronic reorganization (referred to as electronic relaxation) predominantly associated with the valence electrons.[35-37] Experimental and theoretical studies have indicated that for a given core level the magnitude of relaxation energy (RE) is a sensitive function of the electronic structure of a molecule.[38-42]

Koopmans' method for the calculation of the absolute values of the binding energies relies solely on the ground state properties of a wave function.[43] (Eigenvalues of the Hamiltonian of the neutral molecule). Binding energy, however, depends on the properties of both the final and initial wavefunctions. Koopmans' approximation predicts absolute values of binding energies which are somewhat too large and in some cases the differences in binding energies of the same atomic level in different chemical environments are also incorrectly described with this model. A more sophisticated non-empirical approach (still within the Hartree-Fock formalism[42,44-46]) is to carry out LCAOMO SCF calculations on both the neutral molecule and core ionized states. The problem in the solution of these equations (apart from the very high cost of computer time) is associated with the fact that the Hartree-Fock operator itself depends on the one electron eigenfunctions. Although exact solutions are limited to a few special cases, the concept of self-consistent fields (SCF) provides in principle a formalism for approximate solutions to any desired degree of accuracy. The difference in the energy of the ionized and the ground state, calculated within the Hartree-Fock formalism (ΔSCF), provides an accurate calculation of the binding energy. The relationship between the experimental, Koopmans' and Δ SCF binding energy is schematically shown in Fig.1.3.

$$RE = (BE)_{Koopmans'} - (BE)_{\Delta SCF} \qquad (1.5)$$

An alternative possibility is the direct energy minimization of a functional corresponding to the binding energy in the so called transition formalism which may also be carr-

ied out in an LCAOMO SCF framework.

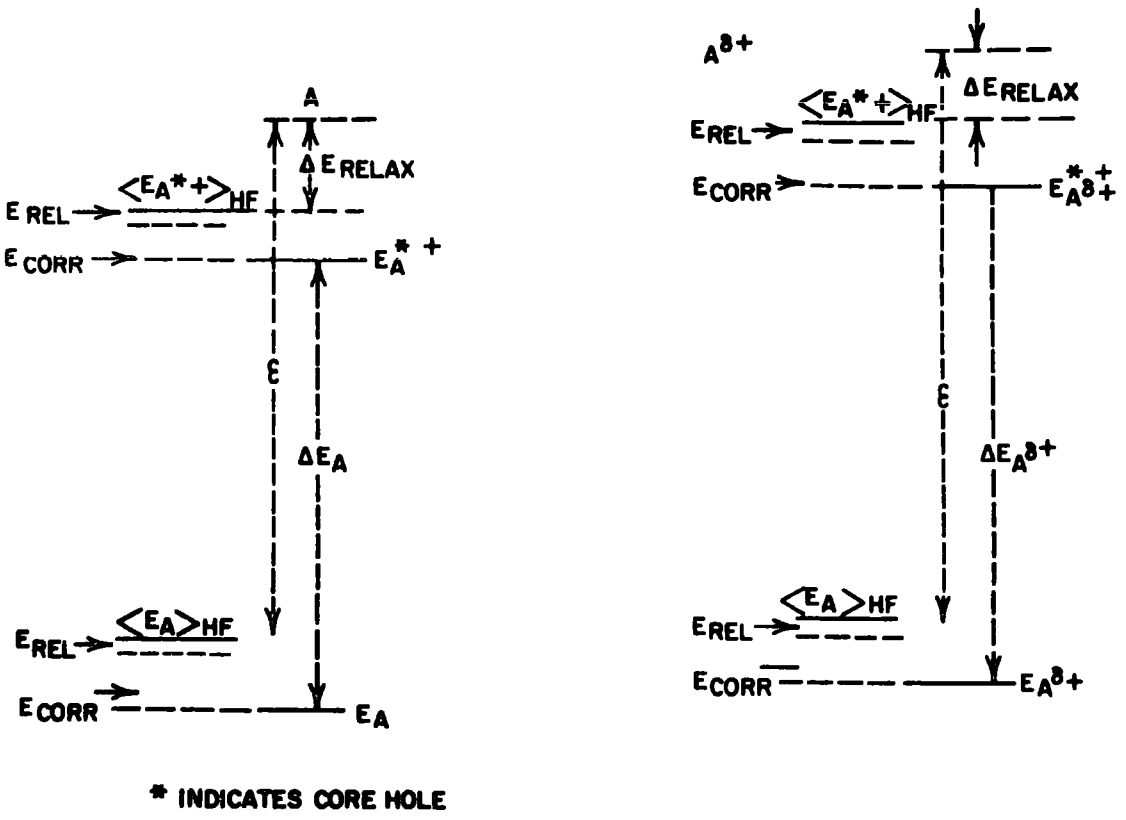

Figure 1.3. Relationship between experimental, Koopmans' and Δ SCF binding energies.

In Fig.1.3,

E_{CORR} = electron correlation energy

R_{REL} = relativistic energy

both of which are ignored by Koopmans' and ΔSCF methods.

The correction terms arising from the correlation[47] energy and relativistic[48-50] energy have been shown to be small for first row atoms and are ignored by both Koopmans'

and ΔSCF methods.

Relaxation energies associated with core ionization of first row atoms, on the other hand are considerable[42,51] (e.g. ~13 eV) and are attributable to reorganization of the valence electrons in response to the apparent increase in nuclear potential. Relaxation of the core levels themselves contributes very little to the total. This relaxation process changes the spatial distribution of the remaining n-1 electrons which is taken into account in the ΔSCF method but not in Koopmans' theorem. A change in potential at the nucleus will be much larger if a core rather than a valence electron is ionized because core electrons have a larger screening coefficient. This is reflected in the value of relaxation energies which are usually smaller by a factor of ten for valence as compared with core electrons. For example values of RE's for the C_{1s} and the 1π orbitals in CO calculated within the ΔSCF formalism are 11.4 eV and 1.8 eV respectively.[42,51]

The differences in relaxation energies for closely related molecules are small and therefore make only minor contributions to shifts in binding energies. This is consistent with the tendency of Koopmans' theorem and ΔSCF calculations to give the same estimates of shift despite the fact that Koopmans' theorem neglects the effect of electronic relaxation.[42]

2.4 Shake-up and Shake-off

The removal of a core electron (which is almost completely shielding as far as the valence electrons are concerned) is accompanied by substantial reorganization (relaxation) of the valence electrons in response to the effective increase in nuclear charge. As well as the relaxation processes described

in the previous section this perturbation also gives rise to a finite probability for photoionization to be accompanied by simultaneous excitation of a valence electron from an occupied to an unoccupied level (shake-up) or ionization of a valence electron (shake-off) as shown in figure 1.4. These relaxation

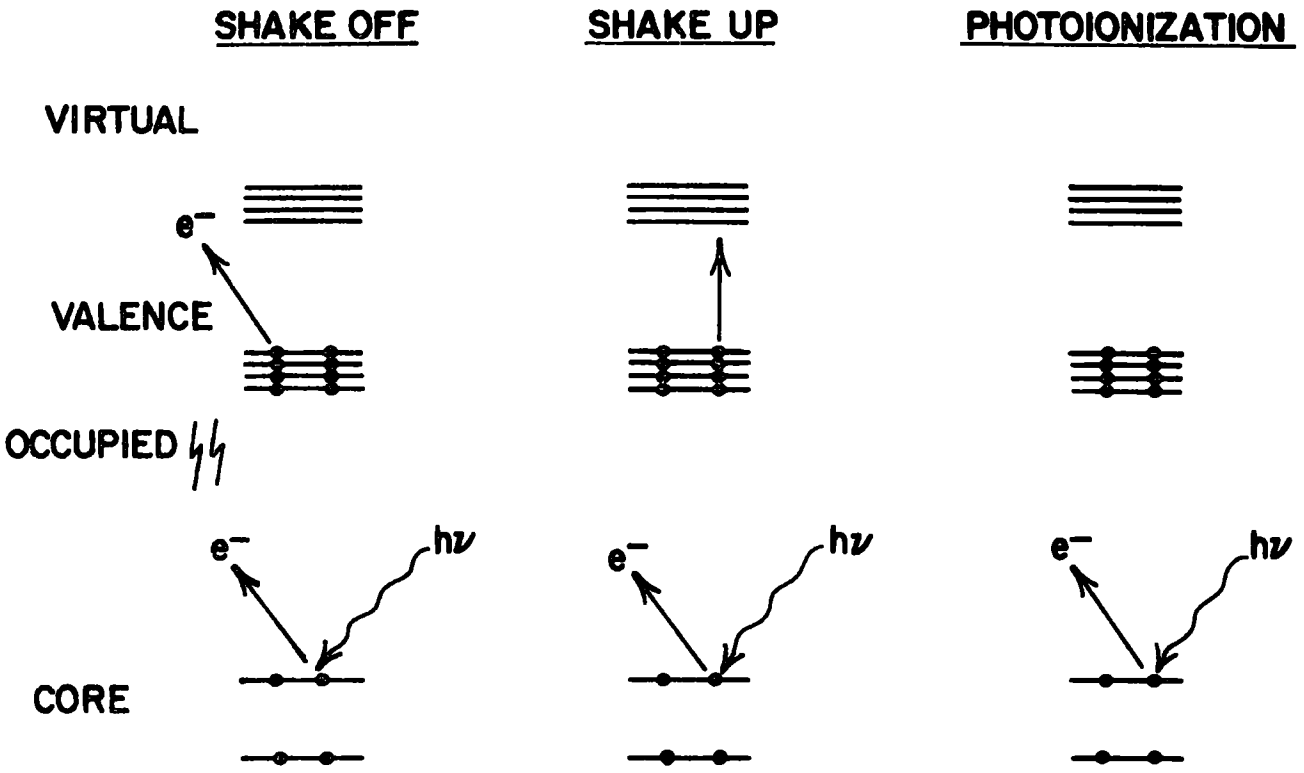

$$\psi_i = \sum_{\mu=1}^{n} C\mu i \; \phi\mu \qquad \psi_f' = \sum_{v=1}^{n} kvf \; \phi'v$$

$$P_{f \leftarrow i} = N \left| \sum_{\mu=1}^{n} k\mu f \; C\mu i \; \langle \phi\mu' | \phi\mu \rangle \right|^2$$

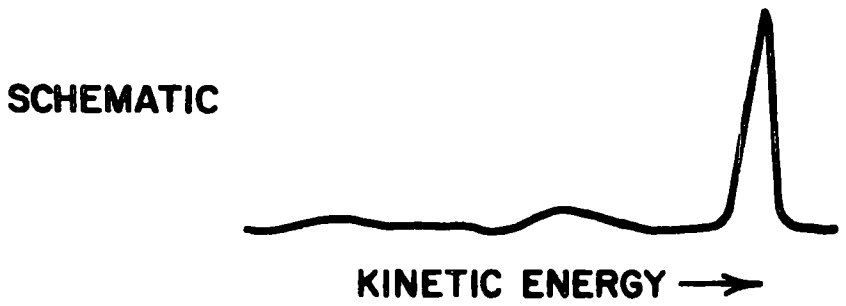

Figure 1.4. Photoionization, Shake-up and Shake-off.

processes result in excited states of the core ionized species.

These processes deriving their energy from the single electron process will lower the K.E. of the primary photoelectron. Therefore, a revision is needed to equation 1.2 to account for these multi-electron processes:

$$KE = h\nu - BE - \bar{E} \qquad (1.6)$$

where $\bar{E}$ is the energy of the multi-electron process.

It may be shown that excitations to these states follow monopole selection rules, ($\Delta J = \Delta L = \Delta S = \Delta M_J = \Delta M_L = \Delta M_S = 0$), as indicated in equations 1.7 to 1.9.

$$\Psi_i = \sum_{u=1}^{n} Cui \; \phi \; u \qquad (1.7)$$

$$\Psi'_f = \sum_{v=1}^{n} Kvf \; \phi' v \qquad (1.8)$$

$$P_{f \leftarrow i} = N \left| \sum_{u=1}^{n} Kuf \; Cui \; \langle \phi' u | \phi u \rangle \right|^2 \qquad (1.9)$$

where, Ψ_i is the initial state wave function

Ψ'_f is the final state wave function.

In the sudden approximation, transition intensities are directly related to the sums of one centre overlap terms involving the occupied orbitals of the initial system and virtual orbitals of the hole state species.[52] These monopole excited states are analogues of the more familiar dipole allowed excited states of the neutral molecule studied in conventional electronic spectroscopy. There are subtle differences however and this can be readily appreciated by the schematic in figure 1.5.

If we consider electronic transitions for a closed shell system as depicted on the left hand side of figure 1.5 in a

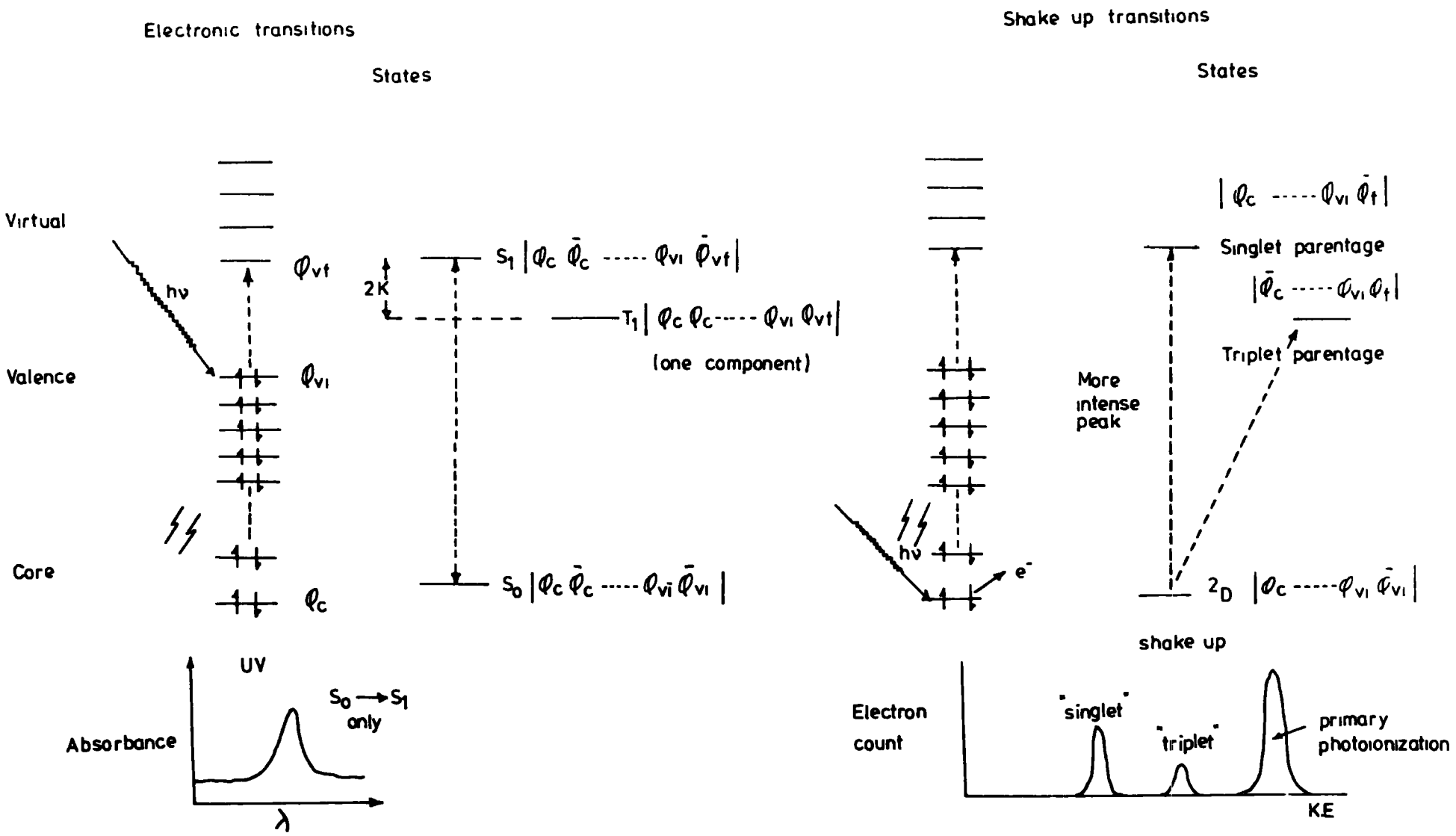

Figure 1.5. Schematic illustrating dipole excited states of a neutral system and monopole excited states of a core hole state.

simple orbital model we may generate a singlet and triplet state from the same excitation configuration, the latter being lower in energy than the former, the energy gap being given by twice the exchange integral. Except under special conditions the only transitions observed with substantial intensities are the dipole allowed singlet to singlet transitions. Consider now excitation involving a core hole state in the doublet manifold as depicted on the right hand side of figure 1.5. We may consider two possibilities for a given excitation configuration. Firstly if we consider the shake up transition to be such that the unpaired electron in the valence level and that excited to the virtual orbital have opposite spins we may consider this doublet state to be of 'singlet origin' by analogy with the excited singlet state of a given excitation configuration, previously discussed. However we may also generate a doublet state by having the electrons in the valence level and that promoted to the virtual orbital with the same spin whilst the remaining core electron has opposite spin. This by analogy corresponds to the shake up state of 'triplet origin'. Again the 'triplet' state is lower in energy than that of singlet origin, however since both represent doublet states, transitions from the ground state of the core hole state may be viewed as both being allowed. In principle therefore we should have as experimental observables the energy separations and intensities for the components of the shake up states of given excitation configuration. We might anticipate naively that the shake up state of singlet origin would be the more intense and in the following discussion this will largely be implicit. The detailed theoretical treatment of shake up states in general is by no means as simple as has been

portrayed, however the simplistic model presented here is conceptually very useful and forms a good starting point for more sophisticated treatments.[53] Fortunately as will become apparent if we restrict ourselves to the interpretation of trends and differences particularly of shake up intensities a rather good description may be obtained at relatively modest computational expense.[53-56] As we have previously discussed relaxation energies are also characteristic of a given core level and also vary within narrow limits as a function of the bonding environment of the atom on which the core level is located.[51] For C_{1s} levels for neutral systems for example, binding energies measured with respect to the fermi level as energy reference, fall in the range 285-295 eV whilst relaxation energies might typically fall in the range 12 $\pm$ 2 eV.[42] The direct relationship between shake up and shake off processes and relaxation energies may be readily understood from theoretical relationships first established by Manne and Åberg.[57] They showed that the weighted average over the direct photoionization and shake up and shake off peaks corresponds to the binding energy appropriate to the unrelaxed systems and this is shown schematically in figure 1.6. Since relaxation energies fall within such a narrow range for a given core level it is clear that shake up and shake off are perfectly general phenomena which are present in every system, the feature which changes from one system to another being the weighting coefficients (probabilities) for each transition. It is clear that transition probabilities for high energy shake off processes should be relatively small and that transitions of highest probability should fall reasonably close to the centroid. In principle relaxation energies should be available from exper-

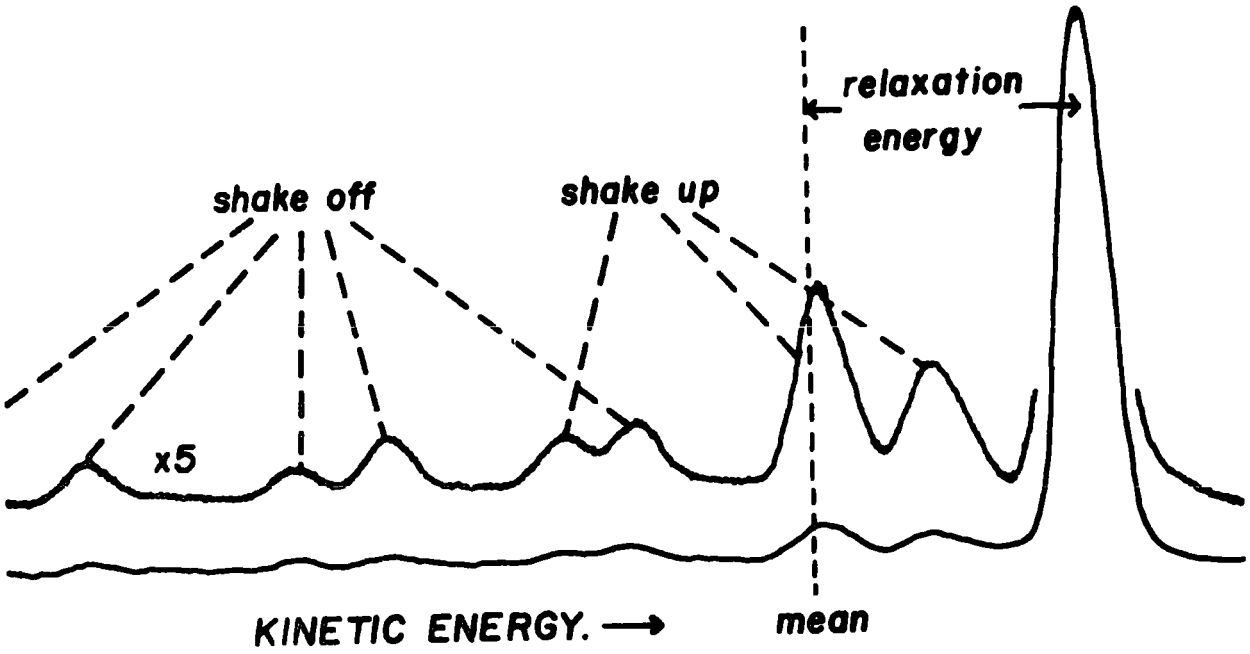

Figure 1.6 Relationship between relaxation energy, Koopmans' Theorem (mean) and the relative intensities of direct photoionization shake-up and shake-off.

iment provided all of the relevant shake up and shake off processes can be estimated in terms of energies and intensities. In practice this is not a feasible proposition particularly for solids since the overall situation is considerably complicated by the presence of the general inelastic tail (arising from photoemission from a given core level followed by energy loss by a variety of scattering processes) which provides a broad energy distribution usually peaking for organic systems $\sim$20 eV below the direct photoionization peaks. This generally obscures any underlying high energy shake off processes such that it is only for systems exhibiting relatively high intensity low energy shake up peaks that information derived from this source can conveniently be exploited.

3. Chemical Shifts

Core levels are essentially localized on atoms, their energies are characteristic for a given element and are sensitive to the electronic environment of an atom.[1] Thus for a given core level of a given element while the absolute binding energy for that level is characteristic for the element, Table 1.4, differences in electronic environment of a given atom in a molecule give rise to a small range of binding energies (i.e. 'chemical shifts') often representative of a particular structural feature.

Table 1.4. Approximate core binding energies (eV)

	Li	Be	B	C	N	O	F	Ne
1s	55	111	188	284	399	532	686	867
	Na	**Mg**	**Al**	**Si**	**P**	**S**	**CL**	**Ar**
1s	1072	1305	1560	1839	2149	2472	2823	3203
2s	63	89	118	149	189	229	270	320
$2p_{\frac{1}{2}}$	31	52	74	100	136	165	202	247
$2p_{3/2}$	31	52	73	99	135	164	200	245

The quantitative interpretation of chemical shift data has been investigated theoretically by five distinct approaches.

1. Koopmans' theorem.
2. Core hole state calculations. (ΔSCF)
3. Equivalent cores approach.
4. Madelung charge potential model.
5. Quantum mechanical potential model (at the nucleus).

The application of Koopmans' theorem and the core hole state approach (Δ SCF) to the calculation of the absolute binding energy has been discussed in section 2.3. The bulk of this

section will therefore concentrate on an evaluation of the equivalent cores method and the Madelung charge potential model. The quantum mechanical potential model is of lesser importance and discussions of this can be found elsewhere.[58-60]

3.1 Equivalent Cores Approximation

The equivalent cores approximation was developed by Jolly and Hendrickson[61] to calculate shifts in core electron binding energies from ground state thermodynamic data, and states, 'When a core electron is removed from an atom in a molecule or ion, the valence electrons relax as if the nuclear charge on the atom had increased by one unit'. Thus atomic cores that have the same charge are considered to be chemically equivalent. The following example illustrates how this principle may be used to estimate the gas phase shift in C_{1s} binding energy between the carbon atoms in methane and fluoromethane.

(i) The carbon 1s electron binding energy in methane B_{CH_4} is given by the energy of the process

$$CH_4 \longrightarrow {}^{*}CH_4^{+} + e^{-} \qquad \Delta E = B_{CH_4}$$

where * indicates a vacancy in a core level (C_{1s} in this case)

(ii) $${}^{*}CH_4^{+} + N^{5+} \longrightarrow NH_4^{+} + {}^{*}C^{5+} \qquad \Delta E = \delta_o$$

This reaction is the exchange of the $^{*}C^{5+}$ core and the equivalent N^{5+} core. According to the principle of equivalent cores the energy of this reaction, δ_o, is zero.

Summing reactions (i) and (ii) gives

(iii) $$CH_4 + N^{5+} \longrightarrow NH_4^{+} + {}^{*}C^{5+} + e^{-} \qquad \Delta E = B_{CH_4} + \delta_o$$

A similar reaction may be written for CH_3F, or any other compound containing a carbon atom.

(iv) $CH_3F + N^{5+} \longrightarrow NH_3F^+ + {}^*C^{5+} + e^-$ $\quad \Delta E = B_{CH_3F^+} \delta_1$

The difference of reactions (iii) and (iv) gives

(v) $CH_3F + NH_4^+ \longrightarrow NH_3F^+ + CH_4$ $\quad \Delta E \triangleq B_{CH_3F} - B_{CH_4} + (\delta_1 - \delta_o)$

The strong form of the equivalent cores approximation given above states that $\delta_1 = \delta_o = 0$ and hence the difference in C_{1s} binding energies between methane and fluoromethane is given by the energy of reaction (v). However, reaction (v) still gives the shifts in binding energy if $\delta_1 = \delta_o$ i.e. if the energy of core exchange is independent of the molecular environment (this is known as the weak form of the equivalent cores approximation). Some typical gas phase data are shown in Table 1.5, and in general indicate good agreement between experimental and thermodynamic shifts.[62] The main restriction to the use of the equivalent cores method is the lack of

Table 1.5. Experimental and Thermodynamic Binding Energy Shifts

Atomic level	Compound	Experimental Shift	Chemical Reaction Energy
N_{1s}	NH_3	0	0
N_{1s}	$(CH_3)_2NH$	- 0.7	- 0.7
N_{1s}	$(CH_3)NH_2$	- 0.3	- 0.4
N_{1s}	N_2	4.35	3.5
N_{1s}	NO	5.5	4.4
C_{1s}	CH_4	0	0
C_{1s}	CO	5.4	4.1
C_{1s}	CO_2	6.8	6.9
C_{1s}	CF_4	11.0	12.3

and/or inaccuracy of thermodynamic data especially with regard to the positive ions involved in the reactions. The

theoretical validity of the equivalent cores concept, however, has been amply demonstrated by Clark and Adams[63,64] in their work on small molecules.

The heats of reaction may be obtained from SCF calculations on the molecules and ions in their ground states. Pople and co-workers[65,66] have shown that for reactions involving closed shell species even minimal basis set (STO 3.G) calculations, which are computationally relatively inexpensive, can reliably reproduce heats of reaction. Particularly accurate results are obtained in the case of reactions in which the number and type (i.e. single, double, etc.) of bonds are the same in both reactants and products since correlation energy changes are very small. Such processes have been designated 'isodesmic reactions' and it is exactly this type of reaction which is involved in the equivalent cores method of calculating shifts. Since heats of reaction are involved there is also the possibility that semi-empirical calculations, which are computationally inexpensive, may be used to predict, at least qualitatively, the required shifts. Thermodynamic data refer to the isoelectronic cations with their nuclei in the equilibrium positions but since photoionization is a rapid process compared with nuclear motion it is more realistic to consider the cations to have the same geometry as the parent molecule. This condition may be imposed in molecular orbital calculations. Also by using the same geometry for the molecules and isoelectronic cations in ab initio calculations many of the two electron integrals may be retained and this greatly reduces the amount of computing time required. By

the very nature of the equivalent cores approximation if the element being studied has more than one core level then identical shifts in binding energy are predicted for all core levels.

3.2 Charge Potential Model

The charge potential model relates core electron binding energies with the charge on the atom from which the core ionization takes place and the potential from the charges in the remainder of the molecule.

Chemical shifts in ESCA were first interpreted in terms of an ionic model by Siegbahn and co-workers.[18] If a charge is removed from, or added to the valence level of a molecule, as in the formation of a covalent bond or ion, the electrostatic potential within the valence shell is changed. If an amount of charge is removed from the valence electron distribution of an atom to infinity, the potential energy is lower by the amount:

$$\Delta E = \frac{q}{r} \qquad (1.10)$$

where r is the radius of the valence shell. When the electron is not removed to infinity but to a finite distance, R, from the molecule, the lowering of the potential energy (shift) is given by

$$\Delta E = \left(\frac{1}{r} - \frac{1}{R}\right)_q \qquad (1.11)$$

although in the ionic crystal model the lattice effects have to be calculated. As far as core level electrons are concerned, neighbouring ions can, to a first approximation, be regarded as point charges since the orbital overlap is negligibly small. Therefore, for the crystal model, a summation of the potentials from the point charges in the crystal will

determine the binding energy of the core electron. In this model, the crystal potential V_i at the centre of atom i is:

$$V_i = \sum_{J \neq i} \frac{q_j}{r_{ij}} \qquad (1.12)$$

where r_{ij} are the centre-to-centre inter-ionic distances and q_j is the charge anion j.

This model was extended to covalent compounds[19] and the change in potential as a consequence of the redistribution of the valence electrons on the formation of a bond can be divided into two components: (a) the component associated with the change of the valence electron population on the atom and (b) the component associated with a two centre interaction, originating from the electron distribution in the remainder of the molecule, which is considered as point charges distributed throughout the molecule. Therefore the binding energies, E_i, are:

$$E_i = E^o + kq_i + \sum_{j \neq i} \frac{q_j}{r_{ij}} \qquad (1.13)$$

where q_i is the charge on atom i

k is the average interaction between a core and valence electron on the atom

r_{ij} are the interatomic distances

E^o is a reference level binding energy.

The assumption of a point charge model is equivalent to assuming that there is no overlap between the core electron density on atom i and the valence electron densities on the other atoms in the molecule. This assumption is the basis for the utilization of the CNDO/2 molecular orbital calculations in relating ESCA chemical shifts.[1] In fact the relationship

1.13 may be derived theoretically from an expansion of Koopmans' theorem[43] in the zero differential overlap approximation. Such an analysis[1] shows that the one centre parameter k is approximately equal to the coulomb repulsion between a core and valence electron on atom i.

Using all valence electron CNDO/2 SCF MO[67] calculations the quantitative discussion of data on quite complex molecules becomes feasible. For example the date in Table 1.6 pertaining to the C_{1s} and O_{1s} levels for a series of compounds gives the charge potential correlations shown in Fig.1.7.

Table 1.6. Absolute Binding Energies for the C_{1s} and O_{1s} Levels of the Model Compounds from the Charge Potential Model

Molecule	Theoretical Binding Energies in eV			
	-C-O-	C=O	C=O	C-O-
CH_3OH	533.7	-	-	286.5
CH_3CH_2OH	533.6	-	-	286.8
CH_3COCH_3	-	533.2	287.8	-
$CH_3CH_2OCH_2CH_3$	533.2	-	-	286.6
$HCOOCH_2CH_3$	534.4	533.2	289.1	287.4
$CH_3COOCH_2CH_3$	534.2	532.9	289.1	287.2
$CH_3COOCH(CH_3)_2$	534.1	532.9	289.0	287.4
$CH_3COOCH_2CH(CH_3)_2$	534.2	532.9	289.1	287.2
$CH_3COCH_2COOCH_2CH_3$	534.2	532.8 533.1	289.1 288.0	287.2

The correlations are very good and from the slopes and intercepts values of k and E_o may be established. Since the charge potential model may be related to Koopmans' Theorem

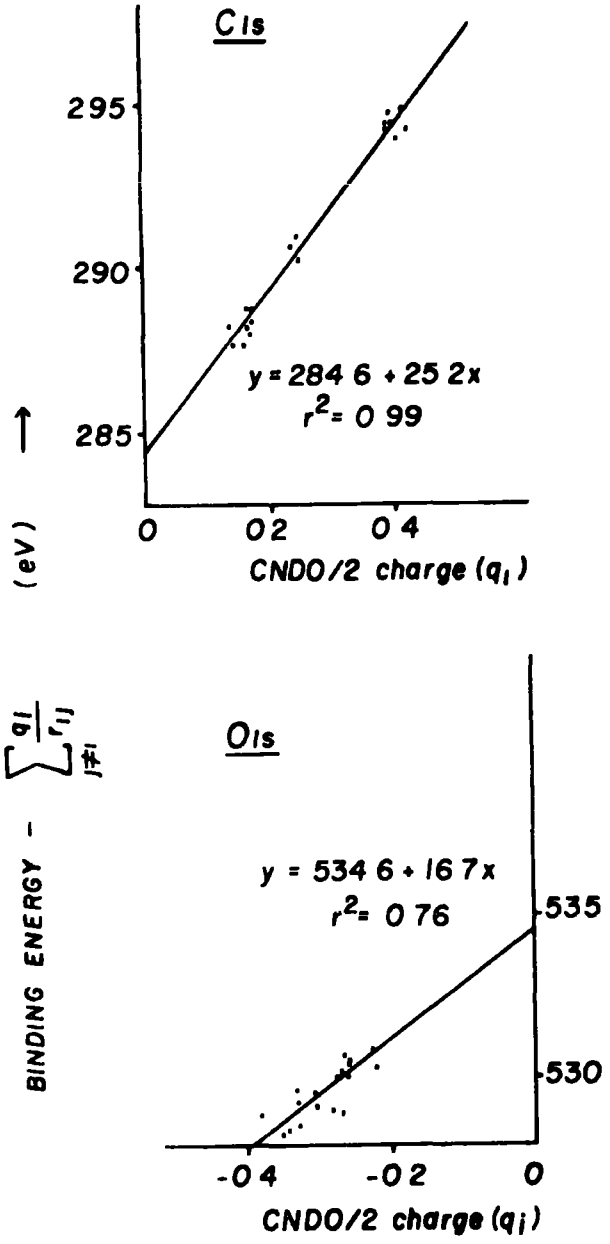

Figure 1.7. C_{1s} and O_{1s} charge potential correlations.

which neglects electronic relaxation of the valence electrons (on ejection of a core electron), it must suffer from some of the same deficiencies. Since electronic relaxation will depend on the electronic structure of a molecule it is only for closely related series of molecules that one might expect

Koopmans' Theorem to provide a quantitative interpretation of shifts in core binding energies. Similarly for the charge potential model we might expect different values of k and E_o for different series of closely related compounds. This is indeed the case. Some values appropriate to series of organic molecules are given in figure 1.8 where it is evident that with charges computed from CNDO/2 calculations the value of k clusters around 25.0 eV for C_{1s} levels. The charge potential model works well for series in which the relaxation energy is either constant or follows a simple trend. This is the case for C_{1s} levels, but not the case however for O_{1s} levels and is clearly reflected in the correlation coefficients (r^2) in figure 1.7. Similar correlations can be made for other levels, e.g. F_{1s}, Cl_{2p}, N_{1s}, etc.

SERIES	k(Cls)
monosubstituted benzenes	24·6
$\underline{C}Cl_3\text{-}X$, $\underline{C}HCl_2\text{-}X$	28·7
$\underline{C}H\text{-}\underline{C}OX$	25·0
perhydro/perfluoro aromatics	25·0
per-H, per-Cl, per-F six membered ring heterocycles	22·4
fluorobenzenes	23·5
five membered ring heterocycles	25·4

Figure 1.8. k values for the C_{1s} levels of related systems.

It is worth considering briefly the relationship between shifts in core binding energies and organic chemists intuitive ideas concerning 'charge distribution'. Since valence electron distributions in molecules are continuous functions the assignment of 'charges' to atoms within a molecule is somewhat arbitrary and depends on how the overlap density is partitioned between atoms. As such, theoretically calculated charge densities are only crude guides to the electron density about an atom. Nevertheless the idea of charge distributions in molecules within its limitations is a useful concept.

3.3 Inversion of the Charge Potential Model

The uses of the charge potential model in studies of structure and bonding in organic molecules is illustrated in Fig.1.9. Starting on the left hand side if we have geometries and appropriate charge distributions (e.g. CNDO/2) we may use the experimental shifts to obtain values of k and E^{o} for a given level of a given element.

We are now in a position to invert the charge potential model by feeding in the geometry, appropriate values of k and E^{o} (as determined from studies on related systems) and the measured binding energies to obtain 'experimental' charge distributions. An example is shown in Fig.1.10 on the application of the inverted model to a simple halocarbon.

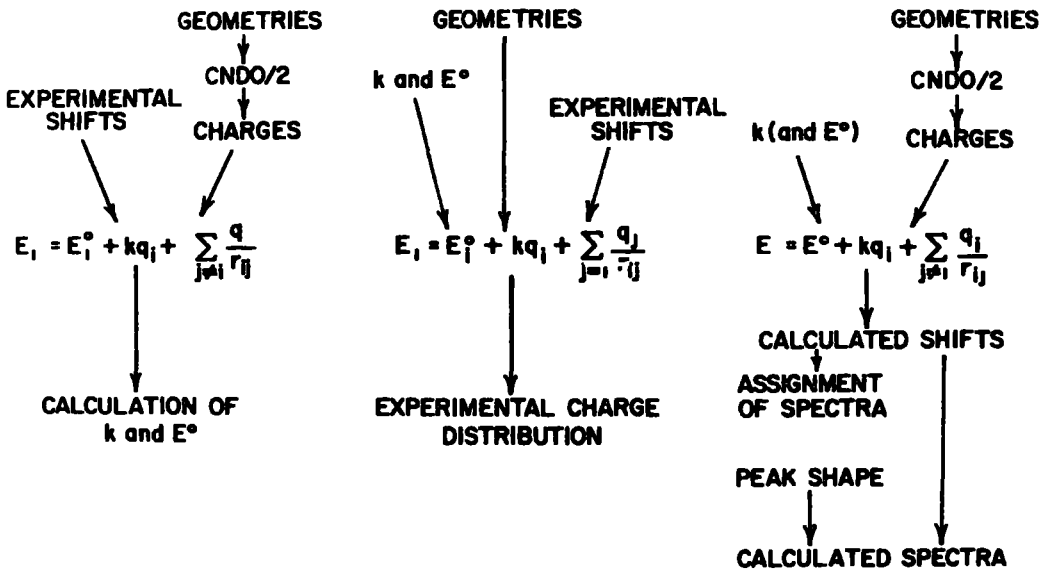

Figure 1.9. Applications of the charge potential model.

Binding energy 690 294 288 187 (eV)

Experimentally Determined	Known		From Charge Potential Model
E^F	E_o^F	K^F	q^F
E^{CF_3}	E_o^C	K^C	q^{CF_3}
E^{CCl_3}	E_o^C	K^C	q^{CCl_3}
E^{Cl}	E_o^{Cl}	K^{Cl}	q^{Cl}

Geometry

Figure 1.10. Inverse charge potential model.

4. Fine Structure

4.1. Multiplet Splitting

The chemical shifts in binding energies can be attributed to differences in the electronic environments of the relevant atoms. Multiplet splittings on the other hand arises for paramagnetic systems and indeed the phenomenon of multiplet splittings accompanying core ionization was predicted for transition metal ions by Watson and Freeman[68] (in advance of the experimental observations by Fadley and coworkers)[69] for the 3s level in some fluorides and oxides of manganese and iron which contain unpaired 3d electrons. The interpretation is relatively straightforward only for s-hole states. The following discussion considers s-hole states and is based on van Vleck's vector coupling model which was originally conceived for atoms.[70] This gives the following

results for s-hole states where S is the total spin of the ℓ^n configurations in the ground state. The two possible final states have a total spin of $S \pm \frac{1}{2}$. The splitting ΔE (i.e. the energy difference between the states $S + \frac{1}{2}$ and $S - \frac{1}{2}$) is proportional to the multiplicity of the ground state

$$\Delta E = (2S + 1)K \qquad (1.14)$$

where K is the exchange integral between the core (c) and valence (v) electrons under consideration and is defined by

$$K = \langle \Phi_v(1)\ \Phi_c(2) \left| \frac{1}{r_{12}} \right| \Phi_v(2)\ \Phi_c(1) \rangle \qquad (1.15)$$

The intensities of the peaks are proportional to the degeneracies of the final spin states

$$\text{i.e. } (2(S + \tfrac{1}{2}) + 1) : (2(S - \tfrac{1}{2}) + 1) = (2S + 2) : 2S \qquad (1.16)$$

The magnitudes of multiplet splittings are independent of sample charging effects and reference level.

Multiplet splittings in photoelectron spectra have recently been discussed in some detail by Fadley.[71] The magnitude of the splitting for a given ion (or atom) can give valuable information concerning the localization or delocalization of the unpaired valence electrons in compounds[18,72,73] since the greater the spin density on an atom the greater the splitting. If the total population of unpaired electrons can be assigned among the atoms with a fraction f_i assigned to the i^{th} atom, then the multiplet splitting on the i^{th} atom ΔE^i is approximated by[72]

$$\Delta E = f_i\ (2S + 1)\ K_i \qquad (1.17)$$

A simple example is provided by Siegbahn et al.[19] In their study on N_2, NO and O_2 molecules in the gas phase they found that the N_2 molecule did not possess core level splitting since the core level (1s) after photoemission was degenerate with

respect to spin, whereas NO and O_2 core levels were split, e.g. upon photoemission from a core level in oxygen or nitrogen in NO the molecular ion NO^+ was left in either a triplet or singlet state respectively. The splitting observed in the 1s spectrum can be attributed to the exchange interaction between the core electrons and the two unpaired 2π electrons having different energies. The O_2 molecule has a similar molecular orbital structure but has two unpaired electrons in its outer π-type orbital. Figure 1.11 describes the orbital levels in N_2, NO and O_2 and Figure 1.12 the ESCA 1s levels of the molecules.

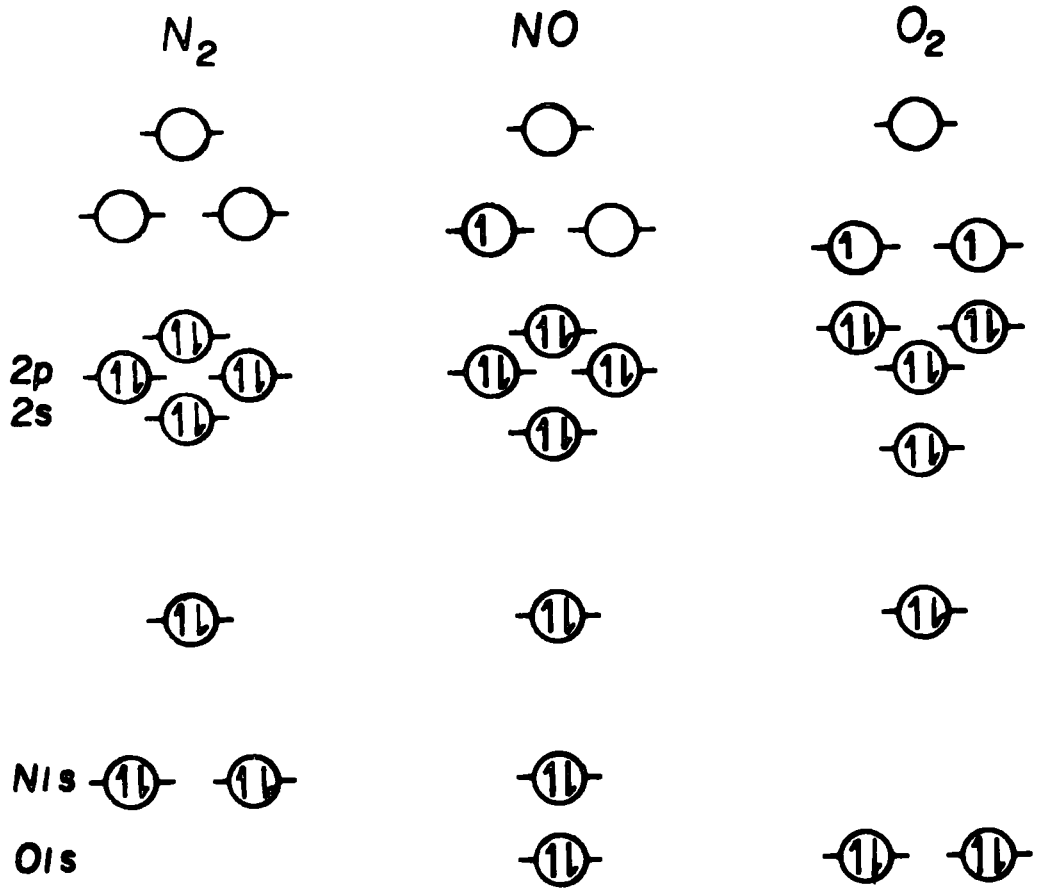

Figure 1.11. Schematic of the electronic configurations of N_2, NO and O_2.

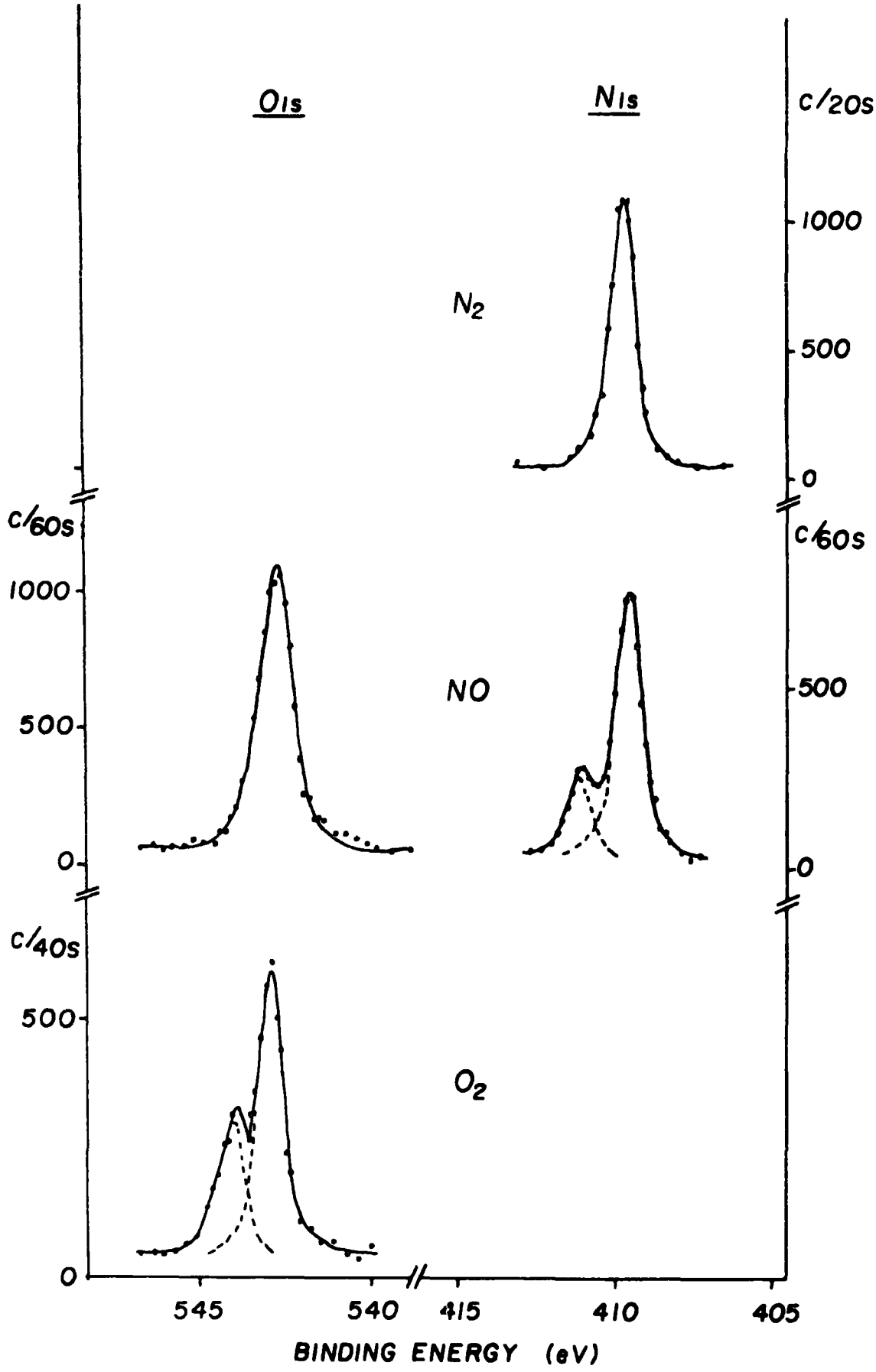

Figure 1.12. O_{1s} and N_{1s} core level spectra of N_2, NO and O_2

4.2 Spin-Orbit Splitting

If photoionization occurs from an orbital which has an orbital quantum number (ℓ) greater than 1 (i.e. p, d and f) then a doublet structure is observed in the ESCA spectrum.[18] This doublet occurs from a coupling of the two magnetic moments of the spin (S) and the orbital angular momenta (L) of the electrons to yield a total momentum(J). When spin-orbit coupling is weak, compared to electrostatic interactions, the orbital angular momenta will couple to give a resultant L instead of coupling to the spin angular momenta. A system of coupling where all the individual spin momenta (S) are coupled, and all the individual orbital momenta (L) are coupled and the resulting momenta coupled is known as a Russell-Saunders coupling scheme ($L + S = J$).[74] The other case where spin-orbit coupling energy is large with respect to the electrostatic energy is the orbital and spin momenta of the individual electrons will couple into a resultant j_1 or j_2. The coupling of the j_1 and j_2 with electrostatic interaction will yield a final J. This situation where orbital and spin momenta are individually coupled and the resultants coupled is known as the jj coupling scheme.[74]

It can be shown that the Russell-Saunders coupling scheme dominates for the lighter elements, up to approximately the lanthanides, and the jj coupling scheme for the heavier elements.[75]

The intensities of the signals in the doublet structure observed are proportional to the ratio of the degeneracies of the states which is quantum mechanically defined by $(2J + 1)$.

The relative signal intensities of the J states for the

s, p, d and f levels are shown in Table 1.7.

Table 1.7. Intensity Ratios for Different Levels

	Orbital quantum number	Total quantum number $J = (\ell \pm s)$		Intensity Ratio $(2J + 1)/(2J + 1)$
s	0	$\frac{1}{2}$		No splitting
p	1	$\frac{1}{2}$	3/2	1:2
d	2	3/2	5/2	2:3
f	3	5/2	7/2	3:4

In Fig. 1.13 examples of the $s(C_{1s})$, $p(Cl_{2p})$, $d(Ag_{3d})$ and $f(Au_{4f})$ levels are shown as observed in the ESCA experiment.

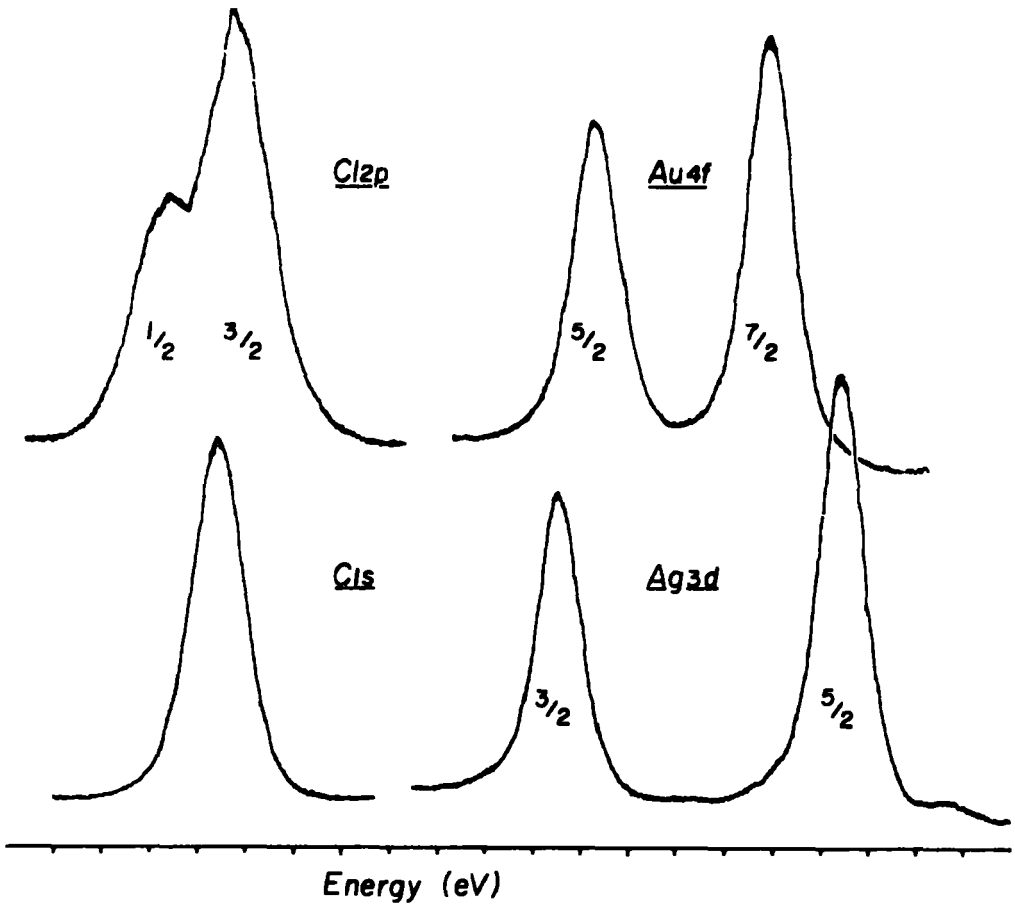

Figure 1.13. Spin-orbit splittings in Cls, Cl2p, Ag3d and Au4f core levels.

4.3. Electrostatic Splitting

Splittings in the $5p_{3/2}$ levels of uranium (Fig.1.14) and thorium metals and their compounds, and in some compounds of gold have been observed.[76,77] These were interpreted as arising from the differential interaction of the internal electrostatic field with the $M = \pm 1/2$ and $M = \pm 3/2$ spin states of the $5p_{3/2}$ electrons, and a definite correlation was found between this type of splitting obtained by photoelectron spectroscopy, and the quadrupole splittings obtained from Mossbauer spectroscopy[78] which arise from the interaction of the nuclear quadrupole moment with an inhomogeneous electric field. Novakov[79] has also observed the known 2 eV crystal field splitting of the valence 3d levels in $CoSO_4$. Bancroft et al have observed a splitting in the spectrum of tin compounds[80] and crystal field splittings should be observable in other systems.[81]

Due to the inherently amorphous structure of organic polymers it is highly unlikely that quadrupole fields will be induced within the bulk structure giving rise to this phenomenon. For this reason no further mention will be made in this text on electrostatic splitting as it has been dealt with adequately by other authors.[76-81]

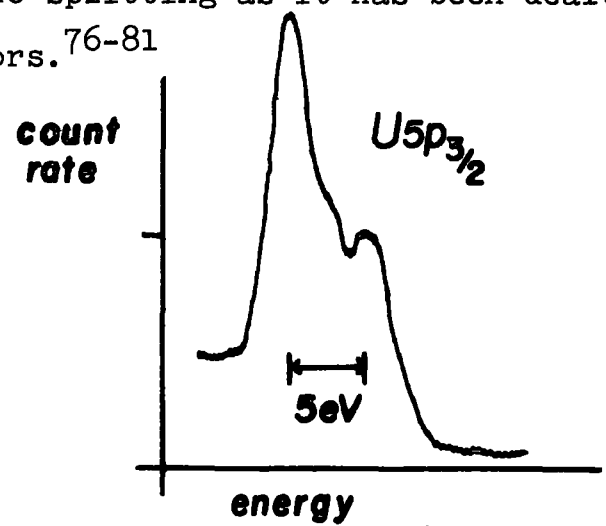

Figure 1.14. Electrostatic splitting in $U5p3/_2$ core level.

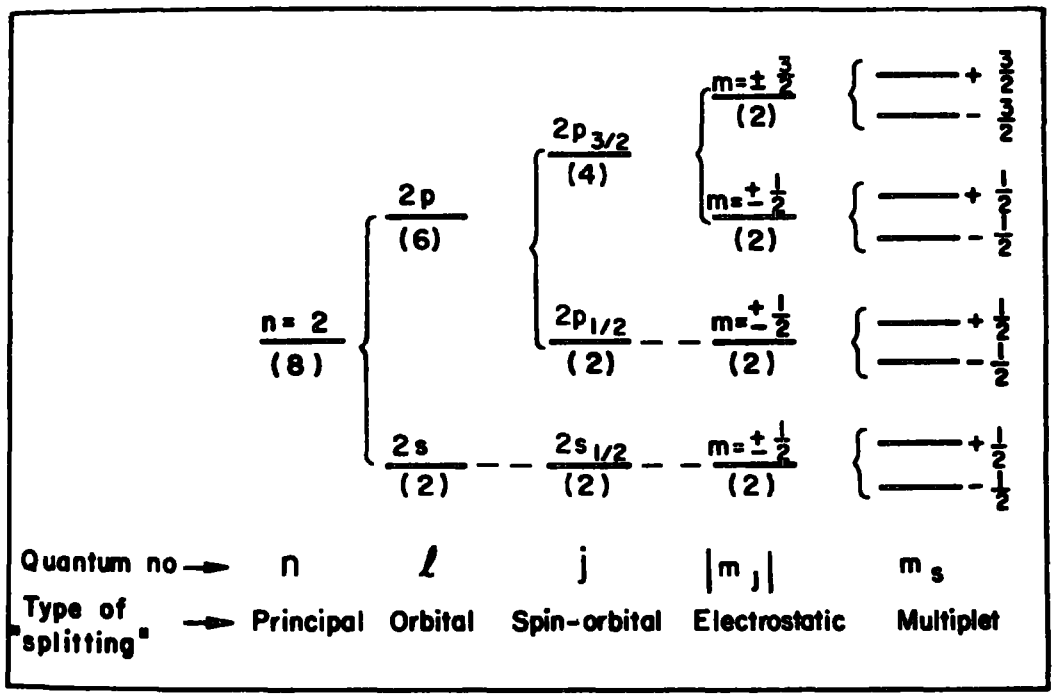

Figure 1.15. Schematic of the types of splitting encountered in ESCA.

Figure 1.15 summarizes the fine structures which may be encountered in ESCA.

5. Valence Bands

Information concerning structure and bonding can be largely inferred from shifts in core binding energies which reflect differences in valence electron distributions. The direct investigation of the valence levels in polymers is also relevant to the detailed interpretation of the electrical properties of the material.

The valence energy levels of simple molecules have been extensively studied in the gas phase by low energy photoelectron spectroscopy.[82] The inherent widths of the exciting radiations which are most commonly used, He(I) and He(II) (photon energies ∿21 eV and ∿40 eV respectively) are such that in favourable cases vibrational progressions may be resolved which considerably aids assignment. Although the development of ultraviolet photoelectron spectroscopy, (UPS) as the technique has come to be known, has primarily been in the hands of chemists, the application to the study of the valence bands of solids has primarily been the province of the physicist (the technique often being referred to as u.v. photoemission) and has dealt mainly with metals studied as evaporated films under UHV conditions.

The study of the valence bands of polymers by UPS is still in its infancy, primarily due to experimental difficulties.

In the case of simple molecules the study of the valence energy levels by ESCA has two distinct disadvantages compared with the corresponding UPS measurements. (It should be

emphasized however, that comparison between the two is very valuable since differential changes in cross sections with photon energy are useful for assigning the symmetries of occupied orbitals). Firstly, cross sections for photoionization are generally lower than for the longer wavelength photon sources used in UPS, and secondly the resolution is much poorer, (viz. photon linewidths He(I) $\sim$ 5 meV,[82] $Mg_{K\alpha_{1,2}}$ $\sim$700 meV).[18]

Figure 1.16 compares the valence band spectrum of carbon monoxide obtained using He(I) and $Al_{K\alpha_{1,2}}$ photon sources.

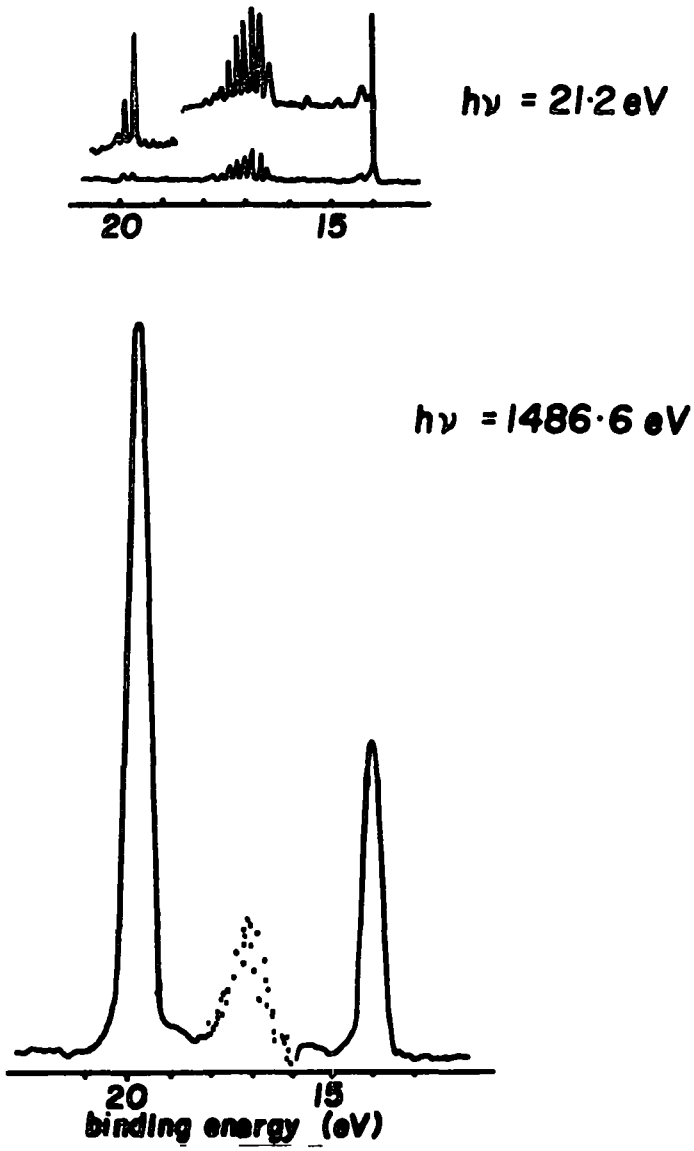

Figure 1.16. Valence band of CO using He(I) and $Al_{K\alpha_{1,2}}$ photon sources.

In studying involatile materials such as polymers however, the disadvantages are considerably offset. Thus since there are so many vibrational modes possible, resolution of ESCA valence signals becomes less of a problem since even with a He(I) source only broad unresolved bands are obtained.

There are three obvious advantages of employing X-ray compared with U.V. photon sources in the study of valence levels in the solid state.

Firstly, with a low energy photon source not all of the valence energy levels may be studied, only the higher occupied levels. Secondly, since the kinetic energy range for electrons will typically be in the range 0-21 eV (HeI), 0-40 eV (HeII) it will become clear in a subsequent section that this is a region of rapidly varying mean free paths for the photoemitted electrons. This causes difficulties in interpreting the UPS data, whereas this difficulty does not arise in ESCA since the electron mean free paths are virtually constant across the valence band. Thirdly, in studying metals the use of a high-energy photon source also minimizes the modulation arising from final state effects and hence gives a close experimental measure of the density of states.

A further discussion of valence bands of polymers obtained by ESCA is given in Chapter Two.

6. Energy Referencing

It has been noted in Section 2.1 that for insulating samples, such as polymers, the Fermi level is not well defined and a means of energy referencing is required due to sample charging effects. For samples studied as solids

three situations may clearly be distinguished. In the first the sample is in electrical contact with the spectrometer. This is usually the case for thin films deposited in situ on a conducting substrate in the spectrometer source. Since the path length for the incident X-ray beam is very large,[18] ~10,000Å, depending on the conditions, it is possible for films of the order of 1000Å to have sufficient charge carriers to remain in electrical contact with the spectrometer. This can most readily be shown to be the case by applying a D.C. bias voltage to the sample probe. If the sample is in electrical contact the apparent shift in energy scale will exactly follow the magnitude of the D.C. bias. The application of a significant negative voltage to the samples will shift the position of the true zero of the kinetic energy scale and the secondary electron energy distribution (SEED) can be then observed, since the electrons near zero kinetic energy without biasing now have enough kinetic energy to overcome the surface potential barrier due to the photoelectron flux. Ascarelli and Missoni[23] have demonstrated that the determination of the sample vacuum level for direct energy referencing can be accomplished by this technique. If the sample has been deposited on a substrate such as gold and is in electrical contact it is possible to measure the core levels of the sample whilst monitoring the $Au_{4f_{7/2}}$ core level (84 eV) and this provides a very convenient means of energy referencing.[1]

The second situation which arises is for thick insulating samples. It is often convenient to study samples mounted on double sided 'Scotch' tape either as powders or as discrete films. In this circumstance there is only a fortuitous possibility that the sample will be in electrical contact with the

spectrometer and in general it will be 'floating' at some potential due to surface charging and indeed this charging process may be time dependent. If care is taken in the measurements, the charge built up on a sample and its time dependence may be used to investigate electrical and chemical characteristics of samples and an example of this is given in Chapter Four. The most reliable method of energy referencing for polymers is to follow the slow build of hydrocarbon contamination at the surface. With a base pressure of $\sim 10^{-8}$ torr the partial pressure of extraneous hydrocarbon material is such that taken in conjunction with the low sticking coefficient for most organic and polymeric systems it normally takes several hours before any signal arising from hydrocarbon (binding energy 285 eV[†]) is apparent.[18] It is of course possible to deliberately leak in straight chain hydrocarbon material to follow the build up at the surface. Such material almost always goes down in uniform coverage and at submonolayer coverage acquires the same surface potential as the sample.[24] This is not necessarily the situation with regard to metals deposited on the surface since there is a marked tendency for gold (the common reference metal) vapour to proceed initially by way of a nucleation process which results in islands of electrically isolated gold on the surface.[83] Although generally speaking the gold islands follow the surface charge and do not react with the polymer, exceptions to both cases have been documented in the literature. Betteridge and co-workers[84] have shown

---

[†] This must of course be independently established for a given spectrometer. It almost certainly arises from long chain hydrocarbon material.

that in some particular systems the width and position of the gold signals can change with time, temperature and substrate material and Ginnard and Riggs[85] have demonstrated that for gold deposited on polyethylene and polytetrafluoroethylene the absolute shift from the gold signal increases as the gold layer increases in thickness, probably due to the higher photoelectron flux from the gold, a phenomena referred to as differential sample charging. In addition since gold is normally evaporated from a filament the possibility of surface damage, reaction or evaporation of substrate during deposition cannot be discounted. The use of the so-called 'gold decoration' technique is therefore not recommended for organic and polymeric materials.[86] Since the factors which determine both absolute and relative binding energies of core levels may be shown to be very short range in nature[1] it is often possible to study smaller molecules which contain the appropriate structural features as thin films in electrical contact with the spectrometer which may be straightforwardly referenced. Comparison may then be drawn between this model and the insulating sample in question thus allowing direct correction for sample charging. A further possibility which has received considerable attention in recent years is the use of electron 'flood guns';[87] the prime motivation being the very large sample charging for thick insulating samples in spectrometers employing monochromatic X-ray sources. The removal of bremsstrahlung as a source of secondary electrons can lead to shifts in the kinetic energy scale in the hundred eV range and can be compensated by flooding the sample with low energy electrons. Samples can become negatively charged however and the

method needs great care to achieve an accuracy comparable with that for the other methods. An alternative source of low energy electrons (developed in this laboratory) is to illuminate the sample region with U.V. radiation from a low pressure, low power mercury lamp via a quartz viewing port in the sample region of the spectrometer.[52] Sufficient secondaries are generated from photoemission from the metal surfaces that sample charging is reduced to a low level. (See Chapter Four).

The third situation which can arise is for films 1-10 micron thick which have been deposited onto a conducting substrate. Such films behave as 'leaky' capacitors in that they exhibit rather striking time dependent charging and discharging characteristics and follow an applied bias potential in a particular manner.[88] Since the dynamic equilibrium which is established under X-ray irradiation invariably produces an overall positive charge on the sample the application of a positive bias voltage causes a smaller shift in the kinetic energy scale than the applied voltage whereas a negative bias voltage produces a larger shift in the kinetic energy scale than the applied voltage. From a study of these effects and from the secondary electron distribution the energy referencing may readily be established. The investigation of such effects as a function of film thickness in the range 1 - 100 micron provides an interesting insight into the electrical characteristics of polymer samples and the typical behaviour which is observed is shown in figure 1.17.

The energy reference in each case for the measurements described above is the fermi level and although the exact location of this level in relation to the valence and conduction

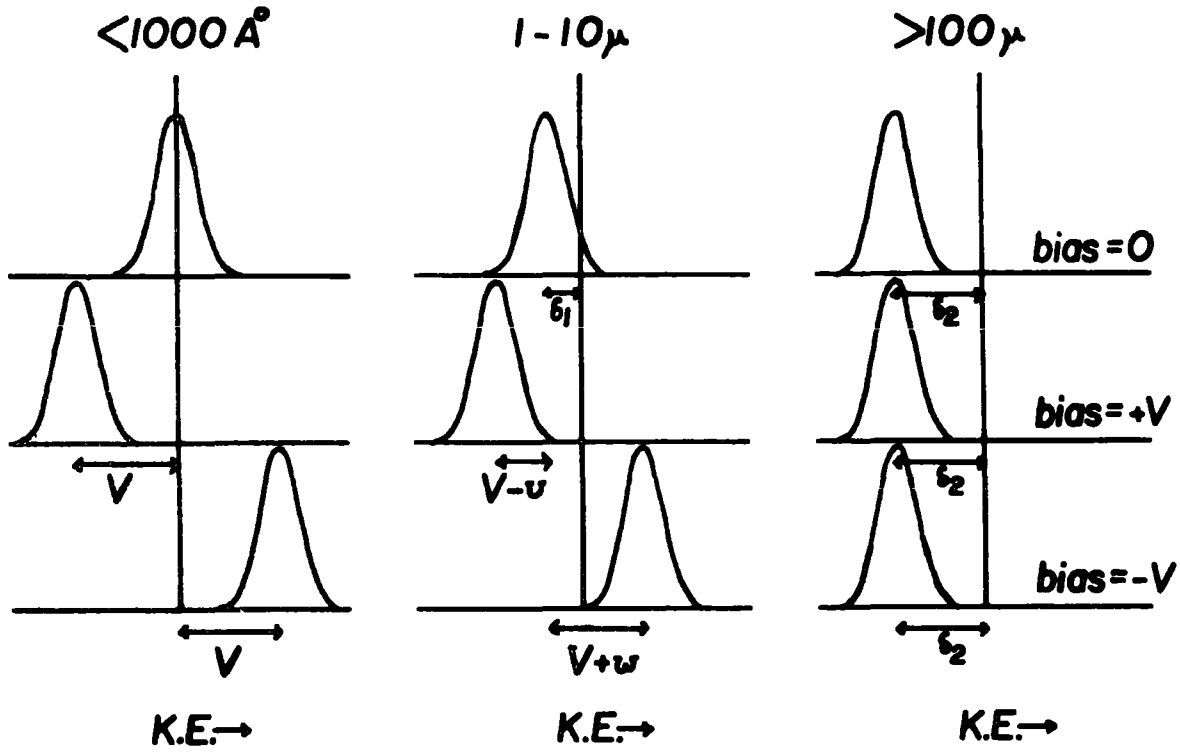

Figure 1.17. Typical behaviour of polymer films with an electrical bias applied to the substrate.

bands is generally unknown for polymers, as we have noted under the conditions of X-ray irradiation it is possible for an 'insulator' to be in electrical contact with the spectrometer, i.e. their fermi levels are the same.[1] Despite the difficulties associated with defining an analytical expression for the fermi level of an insulator, the use of the fermi level as energy reference is operationally convenient. If the work function of the insulator is known we may calculate the binding energy with respect to the vacuum level.

Although sample charging has been widely regarded as somewhat of a nuisance which must be circumvented, our own view has been that the study of sample charging is of interest in its own right. Thus the study of the phenomena provides

an interesting means of studying photoconductivity in polymeric films and will be discussed in detail in Chapter Four on surface charging phenomena.

7. Signal Intensities

Figure 1.18 shows a schematic of the general geometry of the ESCA experiment involving a flat solid sample. hν represents the incident X-rays and e^- the fraction of the photoemitted electrons which enter the analyser. Φ is the angle between the X-ray source and the analyser entrance slit and θ describes the angle of the sample in relation to the analyser. (Low values of θ ($\sim 0^\circ$) correspond to grazing incidence of the X-rays and high values of θ ($\sim 90^\circ$) correspond to grazing exit from the sample of the photoemitted electrons which are analysed). These parameters will be referred to in the ensuing discussion.

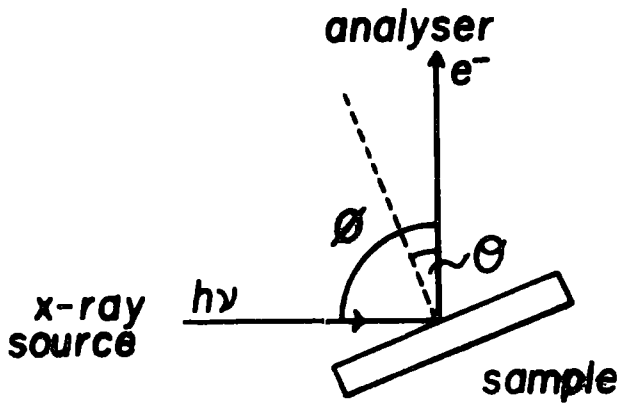

Figure 1.18. Schematic of the sample geometry relative to the X-ray gun and analyser.

7.1 Fixed Angle Studies

For an 'infinitely thick' homogeneous sample the intensity of the elastic (no-energy loss) peak for photoemission from a core level, i, may be expressed as equation 1.18[89,90]

$$dI_i = F\alpha_i N_i k_i e^{-x/\lambda_i} dx \qquad (1.18)$$

where: I_i is the intensity arising from core level, i,

F is the X-ray flux, essentially unattenuated over the sampling depth

α_i is the cross section for photoionization of core level i

N_i is the number of atoms per unit volume on which the core level, i, is localized

k_i is a spectrometer factor

λ_i is the electron mean free path

This equation may be recast into the integrated form

$$I_i = \int_o^\infty F\alpha_i N_i k_i e^{-x/\lambda_i} dx \qquad (1.19)$$

$$I_i = F\alpha_i N_i k_i \lambda_i \qquad (1.20)$$

For a full understanding of the factors governing the intensity of a given signal in ESCA, it is important to discuss them individually and to elaborate on the parameters on which they themselves are dependent.

The X-ray flux in the sample, F, is primarily determined by the power applied to and the efficiency of the X-ray gun. At low values of θ it has been shown, theoretically and experimentally by Henke[91,92] that refraction of collimated X-rays in the outermost surface layers of the sample causes an effective increase in flux in the sampling region as seen by ESCA, resulting in an enhancement of the signal intensity. However,

in practice this phenomenon is rarely experienced since samples are seldom optically flat, X-ray beams are not collimated and the angles, θ, for which this applies are very small, which due to other factors involved in conventional spectrometers results in a very low signal intensity.

The cross section for photoionization of core level, i, α_i is a parameter which describes the probability of the core level being ionized when irradiated by a photon[93] and only includes the fraction of the total number of electrons photoemitted within the angle of acceptance of the analyser focussing lens. α_i is a function of the core level to which it relates and of the energy of the incident photon. α_i may be calculated from the fundamental properties of the atom[94] or determined experimentally from gas phase ESCA experiments.[19] The radial distribution of electrons photoemitted from an atom however is not uniform and it has been shown experimentally and theoretically that α_i is a function of ϕ (Fig.1.19), the angle of detection with respect to the incident photons.[90]

It is well established that the cross section, in the dipole approximation, for randomly oriented polyatomic molecules and unpolarized light is of the form:[95,96]

$$\alpha_i = \alpha_i^{TOT}/_{4\pi}\left[1 - \tfrac{1}{4}\beta_i(3\cos^2\phi - 1)\right] \qquad (1.21)$$

where β_i is the asymmetry parameter[97] of the core level and α^{TOT}_i is the total cross section of the level.

With the use of conventional spectrometers α_i may be considered as a constant for any given set of experiments employing the same X-ray photon energy since the angle between the X-ray source and the analyser entrance slit, ϕ, is usually fixed.

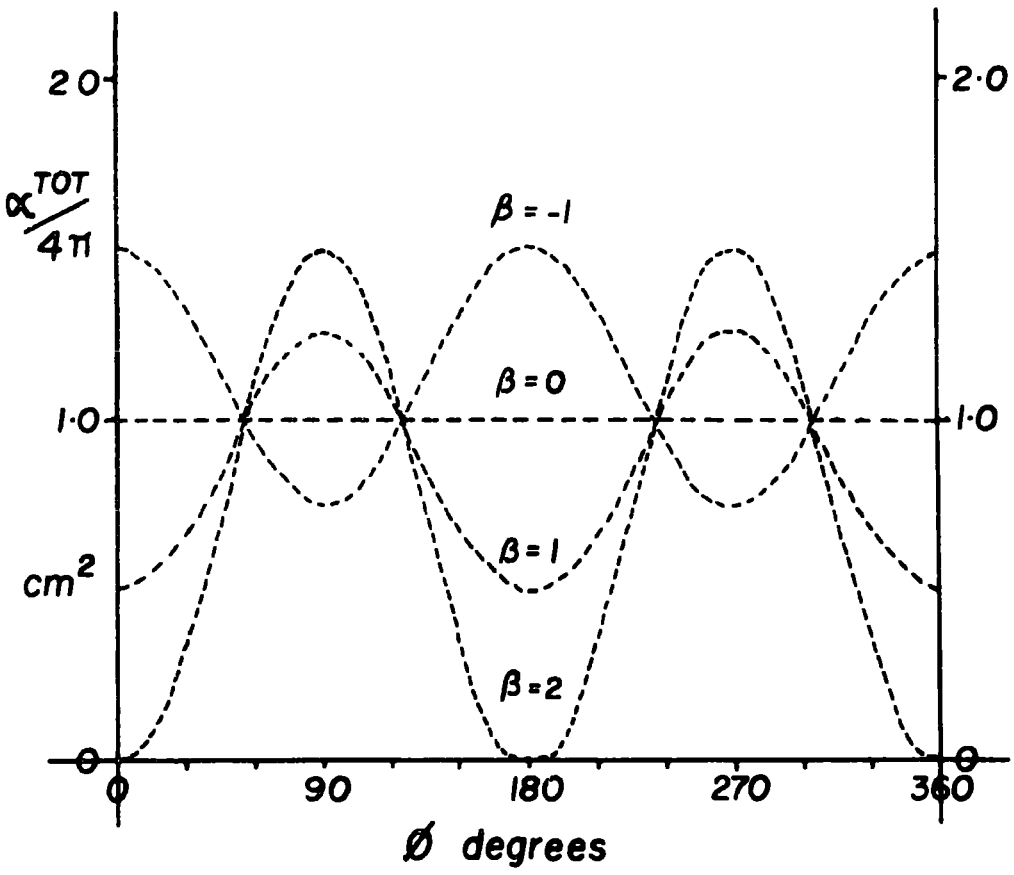

Figure 1.19. Variation of photoionization cross-section with detection angle.

With $Mg_{K\alpha_{1,2}}$ and $Al_{K\alpha_{1,2}}$ the cross section for photoionization for core levels of most elements of the periodic table are within two orders of magnitude of that for the C_{1s} levels, therefore ESCA has a convenient sensitivity range for all elements. The cross sections for core levels are generally considerably higher than for valence levels and this taken in conjunction with the fact that core orbitals are essentially localized on atoms and therefore having binding energies characteristic of a given element, means that in ESCA the predominant emphasis is on the study of core levels.

The spectrometer factor, k_i which varies from one instrument to another, includes effects due to detector efficiency,

transmission characteristics of the analyser (which are both dependent on the kinetic energy of the core electrons being analysed) and geometric factors such as the solid angle of acceptance of the analyser.

The electron mean free path, (sometimes referred to as the escape depth for the photoemitted electrons), λ_i is defined as the distance in the solid through which the photoemitted electrons will travel before $^1/e$ of them have not suffered energy loss through inelastic collision. Theoretical calculations of electron mean free paths have been undertaken by Penn.[98] λ_i is a function of the kinetic energy of the photoemitted electron and typically ranges in magnitude from ~ 4Å for electrons of about 80 eV kinetic energy to ~ 30Å for electrons of about 1500 eV. Further discussion of electron mean free paths, particularly as related to analytical depth profiling will appear in subsequent sections and their importance in the study of surface modifications of polymers will become clearly apparent throughout the experimental chapters of this thesis.

The sampling depth, (not to be confused with electron mean free path), is defined as the depth from which 95% of the signal, arising from a given core level, derives and may be related to λ by:

$$\text{Sampling depth} = -\lambda \ln 0.05 \simeq 3\lambda \qquad (1.22)$$

As an example, for carbon 1s levels studied by a $Mg_{K\alpha_{1,2}}$ X-ray source the kinetic energy of the photoemitted electrons is ~ 960 eV and the mean free path of the electron is ~ 15 Å.[99] 50% of the signal seen by ESCA derives from the outermost, 10 Å of the sample and 95% from the top 45 Å.

Clearly ESCA is indeed a very powerful tool for surface analysis.

The final factor to be discussed is the number of atoms per unit volume in the sample on which the core level is localized, N_i. Although N_i is not <u>directly</u> related to the density of the sample it is a general case that for similar materials of differing density the ESCA signal for a given core level will be more intense for the higher density material (e.g. high density polyethylene vs. low density polyethylene).[52] The most important consequence of N_i is that the relative signal intensities for the core levels of various atoms in a homogeneous (assuming the surface is representative of the bulk) sample are directly related to the overall stoichiometries of the atoms in the sample, due to the fact that the peak intensity from a given core level is directly proportional to the number per unit volume of the atom in the sample.

$$\frac{I_i}{I_j} = \frac{F\alpha_i N_i k_i \lambda_i}{F\alpha_j N_j k_j \lambda_j}$$

where I_i is the signal intensity for core level i and I_j is the signal intensity for core level j. If i and j are the same core level in differing chemical environments (e.g. C_{1s} in <u>CH_3</u>-<u>CF_3</u>) then $k_i\alpha_i\lambda_i = k_j\alpha_j\lambda_j$ and $\frac{N_i}{N_j} = \frac{I_i}{I_j}$.

If i and j are different core levels then $k_i\alpha_i\lambda_i \neq k_j\alpha_j\lambda_j$ and $\frac{N_i}{N_j} = \frac{I_i k_j \alpha_j \lambda_j}{I_j k_i \alpha_i \lambda_i}$. The ratio $\frac{k_j\alpha_j\lambda_j}{k_i\alpha_i\lambda_i}$ may be determined experimentally from standard samples of known stoichiometry containing i and j. Since k_i and k_j vary from one spectrometer to another and also the angle between the X-ray source and the analyser these ratios must be determined for the particular spectrometer and cannot be listed.

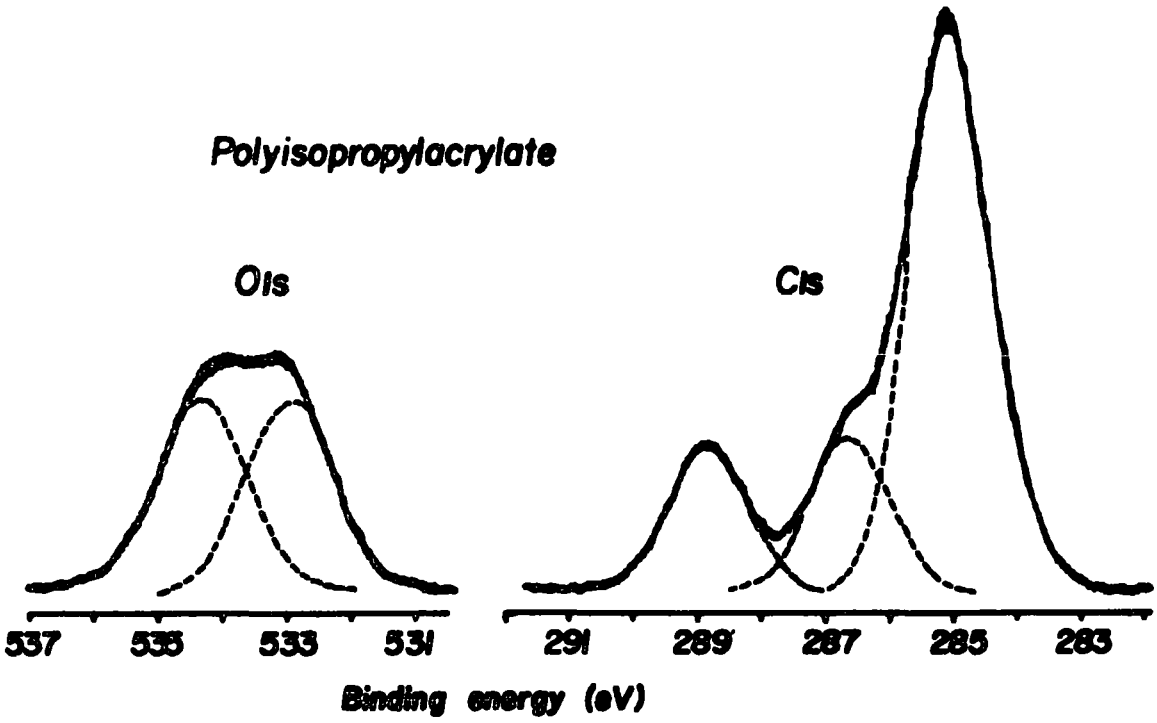

Figure 1.20. O_{1s} and C_{1s} spectra of Polyisopropyacrylate.

As an example, figure 1.20 shows the C_{1s} and O_{1s} spectra of polyisopropylacrylate. The signal intensities relative to the total integrated C_{1s} signal are 16.7%, 16.7% and 66.7% for the $\underline{C}$ = O, $\underline{C}$ - O and $\underline{C}$H C_{1s} levels and 28.3% and 28.3% for the C - $\underline{O}$ and C = $\underline{O}$, O_{1s} levels. This corresponds to a stoichiometry of 1:1:4:1:1 for these levels respectively since

$$\frac{k_{O_{1s}} \alpha_{O_{1s}} \lambda_{O_{1s}}}{k_{C_{1s}} \alpha_{C_{1s}} \lambda_{C_{1s}}} = 1.67$$

for our particular spectrometer geometry. These stoichiometries are precisely as are found in the polyisopropyacrylate repeat unit.

7.2 Analytical Depth Profiling

The situation which is of most common occurrence, when investigating samples for which the surface is not representative of the bulk, is that of a single homogeneous component or of a surface coating of thickness d on a homogeneous base.

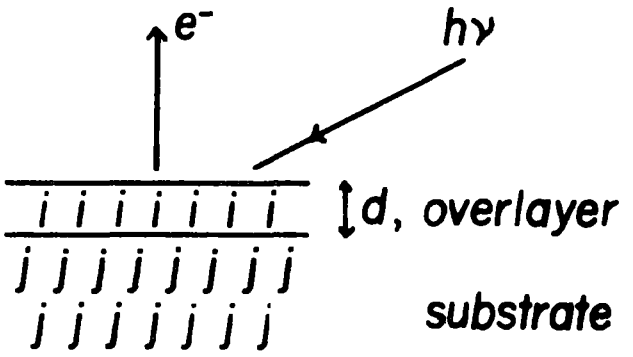

Figure 1.21. Substrate/overlayer model.

This is often termed the substrate/overlayer model and is illustrated in figure 1.21. The intensity of a signal arising solely from the overlayer can be expressed from equation 1.19 integrating between x = 0 and x = d.

$$I_1^{over} = F\alpha_1 N_1 K_i \lambda_i \ (1-e^{-d/\lambda_1}) \qquad (1.23)$$

Similarly, integrating between x = d and x = ∞ gives the intensity of a signal arising solely from the substrate.

$$I_1^{subs.} = F\alpha_j N_J K_J \lambda_j \ e^{-d/\lambda_J} \qquad (1.24)$$

Figure 1.22 gives a general correlation between the electron mean free path and its kinetic energy. It is clear that the data falls into a broad band. The trends however are quite clear. In the energy range of interest to ESCA (>300 eV) the mean free path increases with kinetic energy. As a consequence of this the attenuation of a signal arising from a core level in the substrate by an overlayer coverage will depend strongly on the kinetic energy of the photoemitted electrons. (For example, if a surface coating is put on a sample containing fluorine the F_{1s}/F_{2s} intensity ratio will decrease).

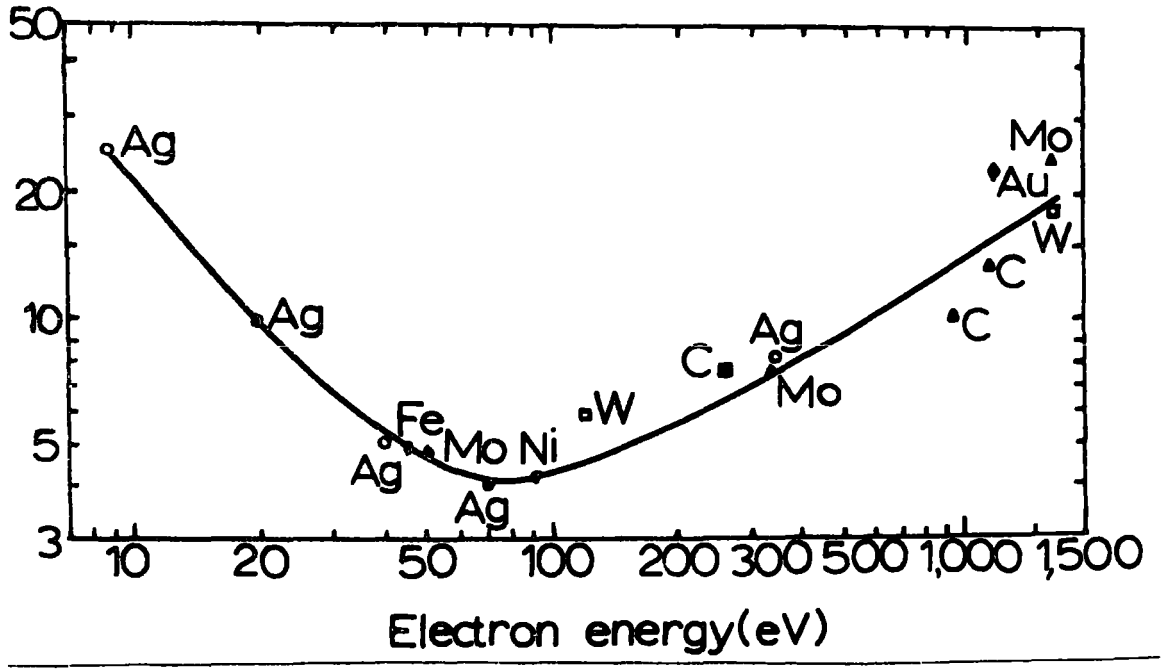

Figure 1.22. Mean free paths of photoemitted electrons, (Å) versus electron energy, (eV).

In order to analytically depth profile a sample it is necessary to determine accurately the electron mean free paths at the kinetic energies of interest, through the material of interest. The electron mean free paths most commonly used in this thesis are those of C_{1s} (~960 eV) and F_{1s} (~560 eV) using $Mg_{K\alpha_{1,2}}$ exciting radiation through polymeric materials. These have been recently directly determined in this laboratory by Clark and coworkers,[99,100] to be ~14 ± 3Å and ~10 ± 3Å respectively. A discussion on these values will appear in Chapter Five.

7.3 Angular Dependence of Signal Intensities

It should be pointed out that equation 1.19 does not accommodate two further effects of varyirg the angle θ. The first is illustrated in figure 1.23. The figure draws a comparison between a narrow X-ray beam and a beam which is broader than the width of the sample, w. For the narrow beam the total flux which hits the same is not affected by varying θ within

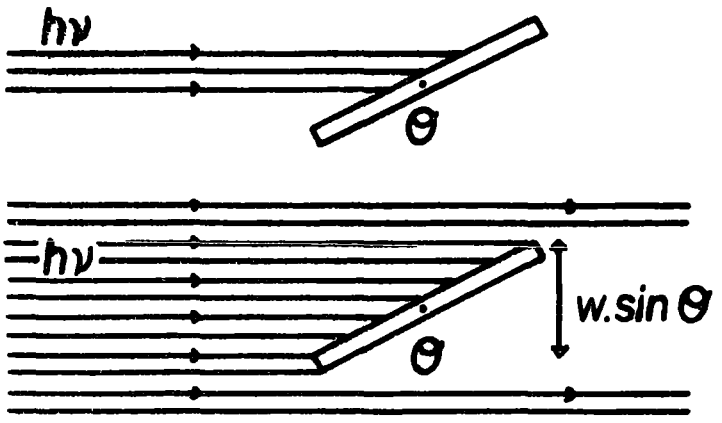

Figure 1.23. Narrow and wide X-ray beams.

limits. However for the broader beam the total flux hitting the sample varies as W sin θ . Therefore as θ is increased this effect tends to increase the signal intensity. (This effect also applies for the narrow beam when θ is very small). The second effect is concerned with the electrons which are photoemitted in the direction of the analyser. For a given value of θ the entrance slit of the analyser 'sees' a sample area proportional to W cos θ . Therefore as θ is increased this effect tends to decrease the signal intensity.

The convolution of these two effects, acting in the opposite sense produces an overall function of θ , $f_i(\theta)$ for a core level i, which exhibits a maximum value.

Equation 1.20 therefore may be replaced by equation 1.25

$$I_i = f_i(\theta) F \alpha_i N_i k_i \lambda_i \qquad (1.25)$$

where $f_i(\theta)$ can be determined empirically.

Inclusion of angular effects into equations 1.23 and 1.24 gives:

$$I_i^{over} = f_i(\theta)\, F\alpha_i N_i k_i \lambda_i\, (1 - e^{-d/\lambda_i \cos\theta}) \qquad (1.26)$$

$$I_j^{subs} = f_j(\theta)\, F\alpha_j N_j k_j \lambda_j\, e^{-d/\lambda_j \cos\theta} \qquad (1.27)$$

Detailed investigations of these angular phenomena are presented in Chapter Five.

8. Line Shape Analysis

The need for line shape analysis arises from the unfavourable ratio of chemical shift to line width ratio which is one of the major weaknesses of ESCA compared to say NMR or NQR.[1] The dominant contribution to the linewidths with most commercial instrumentation is the inherent width of the polychromatic X-ray photon source. With the improvements in instrumentation, e.g. monochromatization of the photon source for simple systems the need for line shape analysis may well largely disappear and unambiguous analysis of more complex systems become feasible.

The measured linewidths for core levels (after taking into account spin orbit splittings, if these are not resolved) may be expressed as

$$(\Delta E_M)^2 = (\Delta E_X)^2 + (\Delta E_S)^2 + (\Delta E_{Cl})^2 \qquad (1.28)$$

Where: ΔE_M is the measured width at half height, the so-called full width at half maximum (FWHM).

ΔE_X is the FWHM of the X-ray photon source.

ΔE_S is the contribution to the FWHM due to the spectrometer (i.e. the analyzer abaritions).

ΔE_{Cl} is the natural width of the core level under investigation. (For solid samples this takes into account the solid state effects not directly associated with the lifetime of the hole state, but rather with slightly differing binding energy

due to differences in lattice environments).

The contributions to ΔE_M from ΔE_X for the commonly used photon sources (i.e. Mg and Al) are essentially Lorentzian line shapes. The characteristics for the energy distribution in $Al_{K\alpha}$ radiation are essentially comprised of four major component [101] lines; α_1, α_2, α_3 and α_4 with positions relative to the α_1 line of -.42, +9.7 and +11.6 eV respectively, with relative intensities of 100, 50, 10.8 and 5.5. While for $Mg_{K\alpha}$ radiation for the α_1, α_2, α_3, and α_4 the relative positions to α_1 are -.33, +8.4 and +10.2 with relative intensities of 100, 50, 12.8 and 6.9.[101] The α_3 and α_4 lines being significantly removed from the α_1 and α_2 lines manifest themselves as satellite peaks to the high kinetic energy side of the intense primary photoionization signal in the ESCA spectrum.

The contributions to ΔE_M from ΔE_S are considered to be Gaussian line shapes and are primarily due to analyser, focusing and detector imperfections. Whereas for the ΔE_{Cl} the contributions are Lorentzian and are dependent upon the Auger and X-ray fluoresence processes upon photoionization of a core level.

The convolution of these line shapes produce a hybrid shape with a Gaussian distribution dominating the overall line shape and with Lorentzian character in the tails. It has been demonstrated however that the use of pure Gaussian shapes introduces only small errors in lineshape analysis.[19]

The methods for resolving complex line shapes in the ESCA spectrum arising from the convolution of several signals falls into two main categories. The first involves mathematical methods of enhancing the resolution of the spectrum whilst the

second involves curve fitting procedures, in either analogue or digital fashion.

Derivative spectroscopy is a technique for obtaining first or higher derivatives of a signal with respect to kinetic energy of the electrons.[102-104] Among the advantages are more characteristic spectra of materials for use in quantitative analysis and increased resolution of overlapping signals. Martin[105] has shown that for some examples the FWHM was reduced by factors of about three and five for second and fourth order derivatives. For the overlap of two equal bands he showed that the use of the second order derivative was sufficient if they were separated by one half width or more. In a treatment by Smith[106] both Gaussian and Lorentzian line shapes were considered and the resolution of a symmetric doublet was found to be the same for the normal and first derivative curves, but the second derivative curve showed an improvement in resolution of 1.78 times and 1.35 times for the Lorentzian and Gaussian line shapes respectively.

The drawbacks are in the fact that the increased resolution must be at the expense of another parameter of the signal, hence the statistical accuracy of the derivative spectra is reduced (i.e. the signal/noise ratio is smaller) and the relative intensities of the component signals are for all practical purpose lost. Further errors occur which are inherent in the mathematical approximations used to calculate the derivatives. The most useful feature which applies to ESCA is that the second or fourth derivatives of a spectrum provide information on the number of components making up the overall line shape and an approximation to their kinetic energies. This information is often essential for the use of

curve fitting procedures. An example is shown in figure 1.24 for a symmetric oxygen doublet and a recent review on the subject has been published by O'Haver and Green.[107]

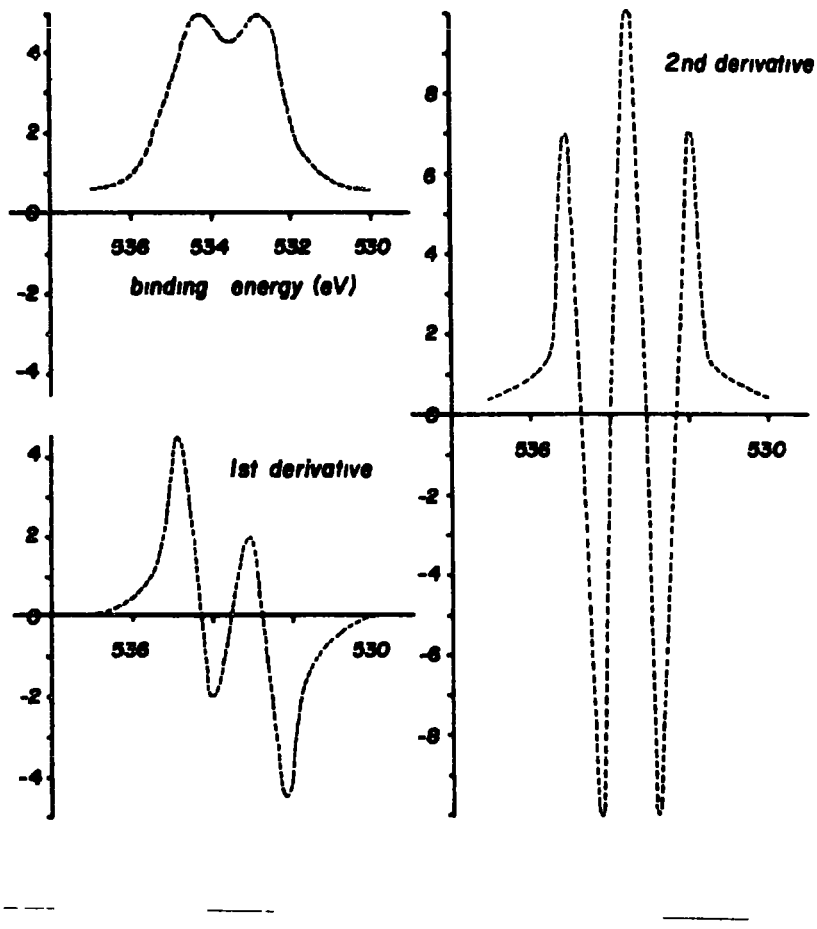

Figure 1.24. Smoothed O_{1s} spectrum (Polyethyleneterephthalate) and its 1st and 2nd order derivatives.

The application of Fourier transform techniques to enhance resolution in ESCA has only appeared recently and is very much still in its infancy. Beatham and Orchard[101] have concluded that the deconvolution of spectra excited by polychromatic radiation can, with data of sufficient quality, yield a virtual resolution approaching that which can be achieved with monochromatized radiation.

Since the full potential of this technique has not yet been fully exploited for application to ESCA no use of it has been made in this thesis, therefore no further discussion will appear, although Fourier transform deconvolution may become important in the near future.

The second category for resolving complex line structures involves curve fitting techniques. In general since one needs to have several variables under close control at any one time an analogue computer analysis is by far more convenient than digital analysis on large computers.[1] The basic philosophy behind such an analysis is set out in figure 1.25.

As an example of a polymer system for which the 'unique fit' situation applies figure 1.26 shows an experimental spectrum of polyvinylchloride in the C_{1s} and Cl_{2p} regions and the analogue curve resolution. The repeat unit, $(CH_2 - CHCl)_n$, contains two types of carbon, one bonded with two hydrogen atoms and one bonded to one hydrogen and one chlorine atom. It is expected based upon theoretical calculations within the Madelung charge potential model to find the C_{1s} levels of these two carbon environments separated by ~1.4 eV. The curve fitting reproduces this precisely. The Cl_{2p} level is a spin-orbit split doublet arising from the $\frac{1}{2}$ and 3/2 degeneracies and, based on the discussion in section 4.2, should have an intensity ratio of 1:2, which is in agreement with the curve resolution, as are the area ratios in the C_{1s} spectrum of 1:1 and the single Cl_{2p} envelope, with respect to the polymer repeat unit.

For more complex lineshapes a detailed background knowledge of prototype systems is essential. The discussion of such information is beyond the scope of this introduction but

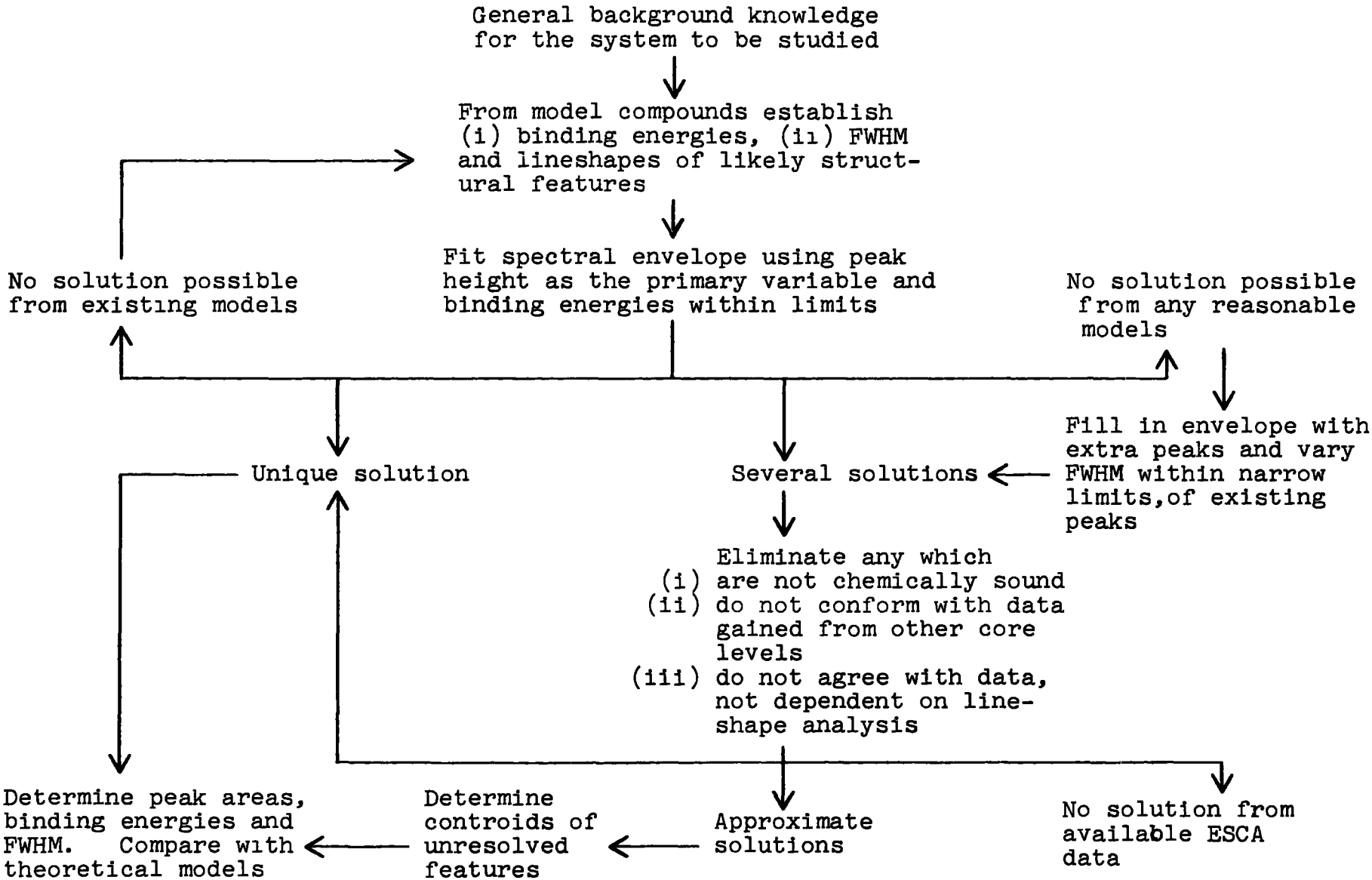

Figure 1.25. Line-shape analysis by curve fitting; schematic of logic procedure.

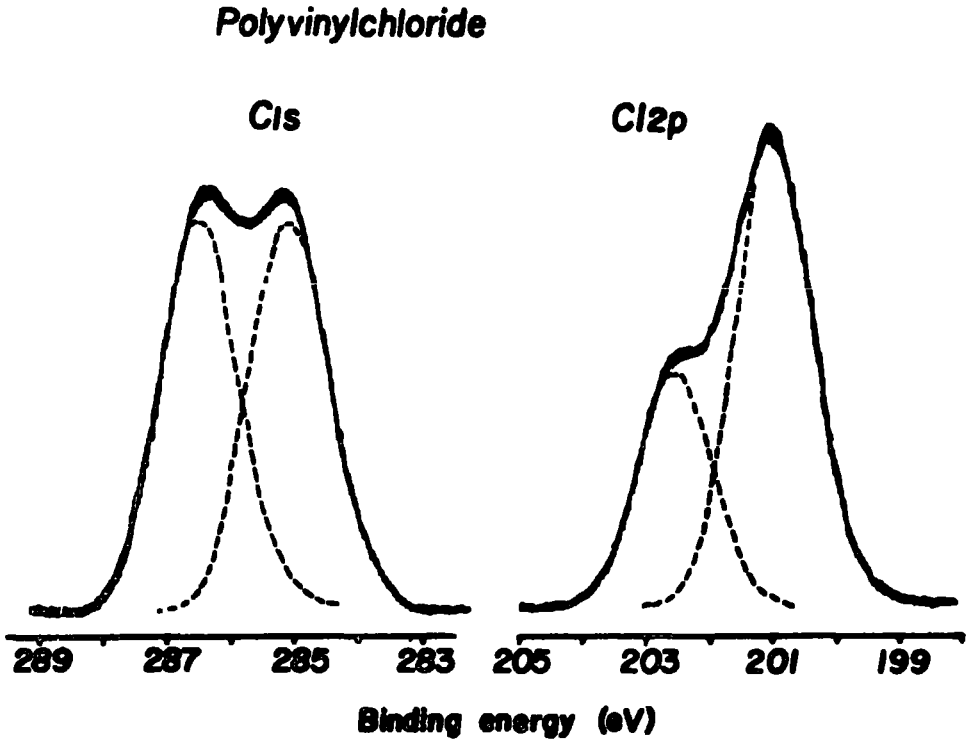

Figure 1.26. C_{1s} and Cl_{2p} spectra of Polyvinylchloride.

the relevant data will accompany the analyses presented in the experimental chapters of this thesis.

9. Instrumentation

The first commercial ESCA instrument appeared in 1970. Since that time several designs have been placed on the market. The work in this thesis was carried out on an A.E.I. ES200 AA/B spectrometer. A schematic of the essential components is given in Figure 1.27.

The description of the spectrometer can be split under four headings:

(a) X-ray equipment

(b) Sample chamber

(c) Analyser

(d) Electron detection

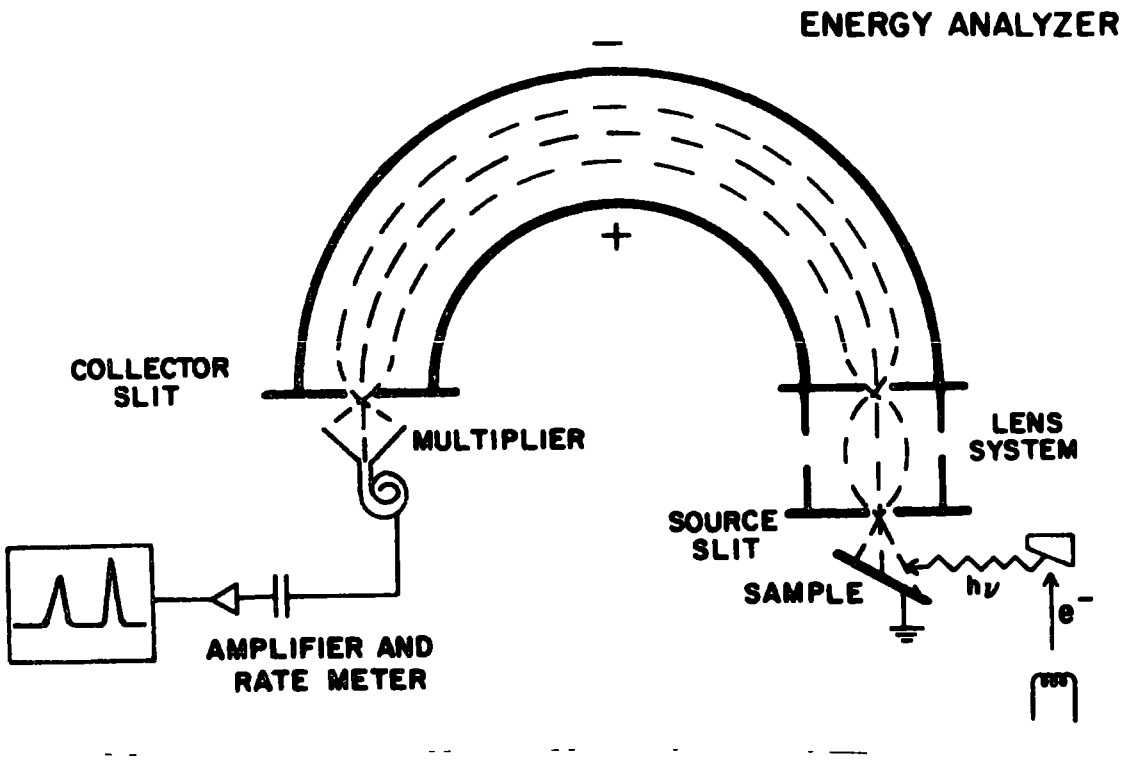

Figure 1.27. Schematic of the ESCA instrumentation.

9.1 X-ray Equipment

The equipment consists of a Marconi-Elliott type GX5 high voltage generator that may be operated in the pressure region $<10^{-5}$ torr. The voltage and current output is integrally variable from 0-60kV and 0-80mA respectively. The ESCA spectrometer is equipped with two X-ray photon sources of Henke design[92]; non-monochromatized $Mg_{K\alpha_{1,2}}$ (typical operating conditions: 12kV, 15mA) and monochromatized $Al_{K\alpha_{1,2}}$ (typical operating conditions: 15kV, 35mA). The X-ray flux is of the order of 10^{-1} rad/sec.[20] which for the majority of polymeric samples causes little or no radiation damage.

The component linewidths for a non-monochromatic X-ray source in the particular cases of Mg and Al targets are ~0.7 eV and 0.9 eV respectively.[18] In the particular instrument used throughout this work the linewidth of the Al source is reduced by monochromatization.[19]

A typical, non-monochromatic X-ray spectrum is shown in Figure 1.28.

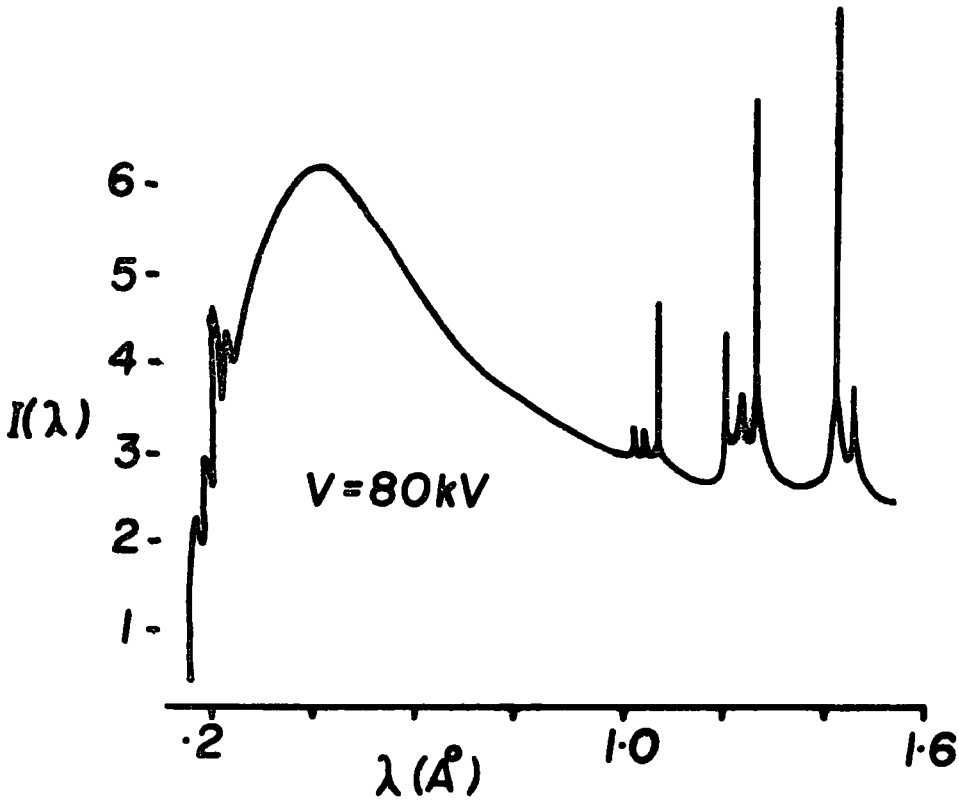

Figure 1.28. X-ray spectrum of a tungsten anode.

The vertical scale is the energy content per unit wavelength emitted by an X-ray tube with a ^{74}W anode.[108]. The spectrum is composed of a characteristic line spectrum superimposed on a continuum.

The continuum's shape depends only on the energy of the incident electrons on the anode, not on the nature of the anode and the λ_o cutoff at short wavelengths is inversely proportional to the electron K.E., and follows the equation:

$$h\nu_o = E \qquad (1.29)$$

where h is Planck's constant. The total X-ray energy per electron, E_T, is proportional to the integral over λ of the continuum and obeys the equation:

$$E_T = kZE^2 \qquad (1.30)$$

where $k \sim 0.7 \times 10^{-4}$ for E_T and E in meV where Z is the atomic number of the anode. The fraction of the electron kinetic energy converted into X-ray energy is:

$$E_T/E = kZE \qquad (1.31)$$

For a typical case of Z = 90 and E = 0.05 MeV, E_T/E is only about 0.3%.

The characteristic line spectra depend only on the atomic number of the anode and not on the incident electrons, however line spectra are obtained only when the electron K.E. satisfies the relation:

$$E > E_T = h\nu = hc/\omega \qquad (1.32)$$

where ν is the frequency and ω the wavelength in question. The total X-ray energy emitted in a particular line increases with incident electron K.E. according to the empirical relation,

$$I \propto (E - E_T)^n \qquad (1.33)$$

when $n \sim 1.5$.

The line spectra of interest from the Al and Mg anodes normally used in ESCA are from the K series transitions and particularly the $K\alpha_{1,2}$ lines. However, the unmonochromatized spectra of the $Mg_{K\alpha}$ radiation contain the continuum and particularly the K(α_7', α_3, α_4, α_5, α_6 and $K\beta$)where the $K\alpha_3$ satellite is 9.5% relative intensity from the primary $K\alpha_{1,2}$ lines (8.4 eV higher K.E.) and the $K\alpha_4$ satellite is 4.5% relative intensity from the primary $K\alpha_{1,2}$ lines (10.1 eV higher K.E.).

Al_{K_α} radiation can be monochromatized by a crystal (quartz) diffraction technique,[19] to eliminate the satellites (and the continuum) and produce pure $K_{\alpha_{1,2}}$ radiation. (Unfortunately monochromatization of the Mg_{K_α} lines is not presently possible with crystal diffraction since no suitable crystal is currently available with the proper lattice spacing).

For Al_{K_α} essentially three techniques are available, (a) 'slit-filtering', (b) 'dispersion-compensation' and (c) 'fine-focussing', all using crystal diffraction of the X-ray radiation and these techniques in principle can attain ultimate linewidths of 0.2 eV. The fine-focussing technique[109] uses a high power electron gun and requires a rotating anode (~5-10,000 r.p.m.). Figure 1.29 illustrates these three techniques. In the spectrometer used in this work method (a) is used.

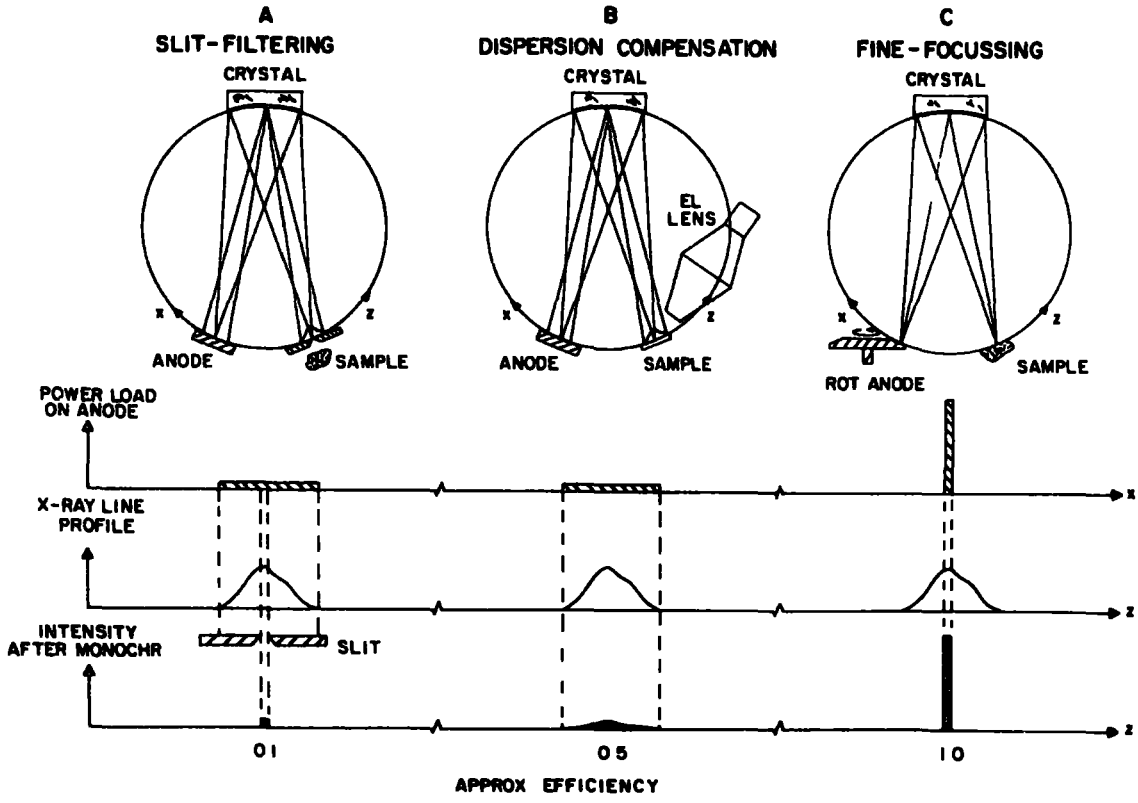

Figure 1.29. Monochromator designs.

9.2 Sample Chamber

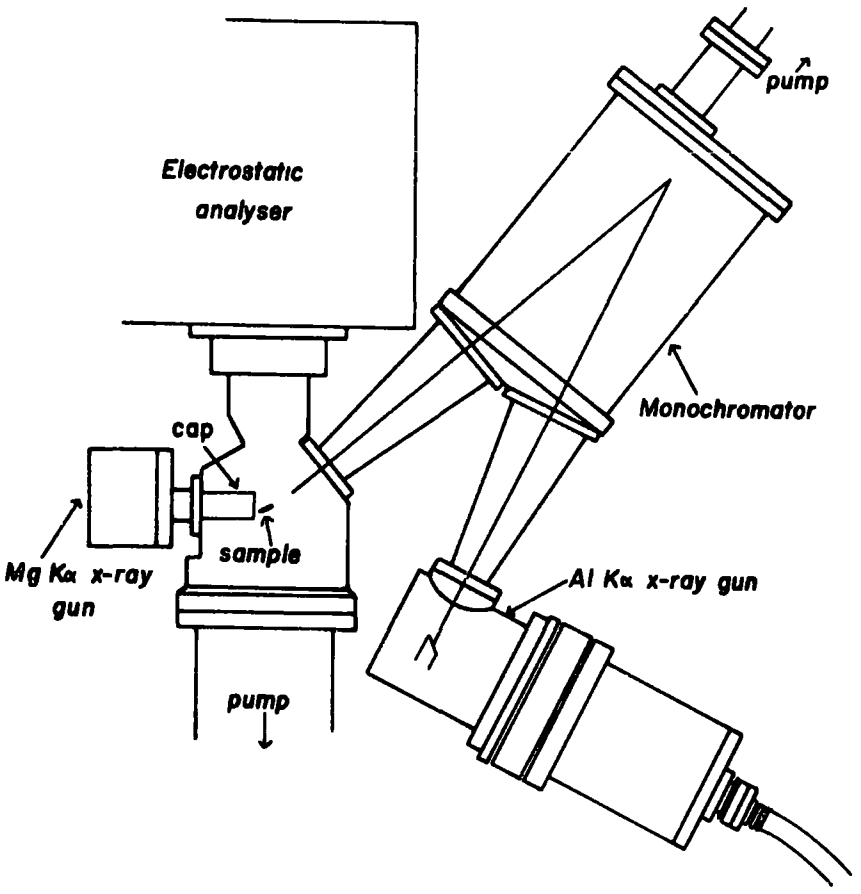

Figure 1.30. General layout of the AEI ES 200B spectrometer.

Figure 1.30 is a drawing of the A.E.I. ES200B[110] spectrometer showing the relative position of the sample, X-ray sources and analyser. The aperture of the Mg X-ray source consists of an end cap and an aluminium foil window (∿0.003" thick) which separates the X-ray source from the sample and ensures that electrons scattered from the target or filament in the X-ray gun do not enter the sample chamber. As an aside here it is worth noting that work in this laboratory has led to the conclusion that the major source of hydrocarbon contamination of samples arises from the heating of the end cap[111]

and window causing hydrocarbon species to 'boil off'. To remedy this our particular spectrometer X-ray end cap has been equipped with a cooling jacket through which either cold water or liquid nitrogen may be passed.

The Al X-ray source on the other hand is remote from the sample and hence no window or cooling device (apart from anode cooling) is required. However a polyester film is incorporated into the design at the entrance to the sample chamber to prevent extraneous hydrocarbon species from contaminating the quartz crystals.

The sample chamber is equipped with several access ports for sample introduction and various pre- and post-treatment options. The preferred method of sample introduction in this work is via an insertion lock system and gate valve. A solid sample is mounted on the tip of a sample probe usually by means of double sided 'Scotch' insulating tape and passed through the insertion lock on Viton 'O' ring seals. This technique is advantageous in two main respects; (i) rapid turn round time for the running of samples, (ii) rotating the probe shaft allows angular dependent studies to be performed, but limits the base pressure of the system to $\sim 10^{-8}$ torr. The temperature of the sample probe tip is variable from liquid nitrogen temperatures to $\sim 400^{\circ}C$.

The facility for cooling the sample probe tip allows liquid and volatile solid samples to be studied in a condensed phase introducing them from a reservoir shaft or direct inlet shaft passed through a second insertion lock. Gases may also be analysed directly using a leak valve.

9.3 Analyser

The analyser on the A.E.I. ES200 AA/B is a hemispherical double focussing electrostatic analyser, which was originally described by Purcell[112] in 1938, enclosed within two mu-metal shields for magnetic shielding. The resolution of the hemispherical analyser is based upon three variables:

(1) mean radius of the hemispheres, R,

(2) width of the entrance slit,

(3) width of the exit slit.

Therefore the resolution, $\Delta E/E$, where E is the energy of the electrons is

$$\Delta E/E = R/W \qquad (1.34)$$

where W = combined widths of entrance and exit slits.

It is quite easily seen that to improve the resolution three terms can be varied:

(1) reduce the slit width, which has the effect of reducing the signal intensity,

(2) increase the hemispherical radius, which increases engineering cost and complexity and pumping requirements,

(3) retard the electrons before entering the analyser so as to reduce their K.E.

With reasonable compromises made on the slit width to obtain sufficient signal intensities and the hemispherical sizes to prevent mechanical distortion and high engineering cost and practical vacuum pump sizes the ES200 AA/B retards the electrons before they enter the analyser by passing them through a lens assembly. This lens system actually serves a double purpose:

(1) The lens system allows the analyser to be located at a convenient distance physically from the source chamber which permits a maximum flexibility in sample handling.

(2) A retarding potential on the electrons allows more flexibility on the resolution requirements of the analyser.[113]

The electrons passing through the analyser can be focussed at the collector by either of two methods:

(1) Electronically scanning the retarding potential applied to the lens while keeping the hemispherical potential constant, or

(2) Simultaneously scanning the retarding potential applied to the lens and the hemispherical potential and keeping a constant ratio between the two, which is the technique used on the ES200 AA/B used here.

The overall resolution $\Delta E_{M/E}$, of the system also depends upon contributions from sources other than the analyser.

(1) The width of the X-ray radiation line, ΔE_X.

(2) The natural width of the electron energy distribution in the level being studied, ΔE_{Cl}.

(3) The line broadening due to spectrometer irregularities, which can vary with electron emission energy, E and slit widths, ΔE_S.

(4) The line broadening due to solid state effects in the sample, ΔE_{SS}.

For a solid sample equation 1.28 becomes:

$$(\Delta E_M)^2 = (\Delta E_X)^2 + (\Delta E_{Cl})^2 + (\Delta E_S)^2 + (\Delta E_{SS})^2 \qquad (1.35)$$

(This relationship is strictly valid only for Gaussian line-shapes).

ΔE_S can be varied on the ES200 AA/B by means of adjustable entrance and collector slits on the analyser.

9.4 Electron Detection

The detector contains a collector aperture (exit slit), described above, which passes the selected K.E. electrons into an electron multiplier. The output pulses from the channel multiplier are amplified and fed into a data handling system. The signals into the data handling system generate the ESCA spectra by one of two methods:

(1) The continuous scan, where the electrostatic field is increased from the present starting K.E. continuously while the signals from the multiplier are monitored by a rate meter. When the signal to background ratio is sufficiently high a graph of the electron counts per second versus the K.E. of the electrons is plotted directly onto an X-Y recorder.

(2) The step scan, where the field is increased by preset increments (typically 0.1 eV) and at each increment (a) the counts may be measured for a fixed length of time or (b) a fixed number of counts may be timed. The data obtained from the step scans is stored in a multichannel analyser. Many scans can be accumulated to average random fluctuations in background. Using this technique the signal to noise ratio increases as the square root of the number of scans.

In both the continuous and step scan modes where the data acquisition time is relatively long care must be taken

to avoid long term sample changes. For example, hydrocarbon contamination and/or time dependent sample charging result in an overall change in the spectrum with time producing erroneous spectra. However, in general the acquisition time is short compared to these effects.

CHAPTER TWO

ESCA as a tool for the study of structure, bonding and reactivity of polymers

1. Introduction

The application of ESCA to studies of structure, bonding and reactivity of polymeric systems is a topic of considerable current interest and the numerous reviews which have appeared over the past few years attest to the increasing awareness of the wide ranging capability of the technique in this area.[1,21,52,114-118] This chapter presents a consise summary of some aspects of the investigations which have been carried out to date, with a bias towards areas of particular interest to this thesis. Since the research discussed in this chapter was pioneered by Clark and coworkers at the University of Durham the examples quoted are taken mainly from their work which has appeared in the literature over the past few years.

Work began in the latter part of 1970;[1,114] the general philosophy behind the initial foundation work being to start by studying simple well characterised systems to build up banks of data (on relative peak intensities, absolute binding energies and chemical shifts) from which trends may be discerned and comparison drawn with simple monomers. This allows the development of a theoretical framework to quantify the results, and hence provides a strong basis for studying more complex systems.

Until early 1974 the emphasis was put on the study of a series of linear fluoropolymers[114,119] with the data obtained being utilized to extend the work to random[120,121] and block copolymers[122] and to more complex systems such as the argon ion bombardment of an ethylene tetrafluoroethylene copolymer[114] in a simulation of the casing procedure and the surface fluorination of polyethylene.[114,123,124] The rationale behind the

choice of fluorine containing systems may be summarized as follows. Since fluorine is the most electronegative element in the periodic table it induces large shifts in the C_{1s} binding energy of the carbon atom to which it is directly attached, and a proportionately smaller shift for the next carbon atom along the chain. This provides the most favourable situation for delineating the likely areas of applicability of ESCA in this field. Secondly, fluoropolymers are academically and technologically important systems, they are often difficult to study by other spectroscopic techniques, due to their insolubility and intactability, but lend themselves very nicely to investigation by ESCA.[114]

From 1974 up until the present time the ESCA investigation of polymeric materials has diversified to encompass non-fluorine containing systems,[125-129] and particular interest has been in the study of plasma polymerization[100,130,131] and surface modification of polymers.[126,132-137]

Before discussing specific examples of the application of ESCA to polymers it is appropriate at this point to present some experimental aspects and comment on the information which is likely to be available from the data.

2. Sample Preparation

The choice of the method of sample preparation is often governed by the physical state of the sample when prepared or as received and for dynamic studies of the nature of the experiment. For the AEI ES 100 and 200 series spectrometers as used in this work the objective is to mount the sample onto the tip of a sample probe which may be passed into the spectrometer via an insertion lock system allowing the vacuum within

the spectrometer to be maintained. The size of the sample is then limited by the dimensions of the insertion lock and is for the majority of examples discussed here ~ 7 x 18 x 1 mm, although the area actually irradiated is of the order of 7 x 10 mm in the centre of the sample.

2.1 Powders

When the polymer sample is available as a powder it is often convenient to study it as such by applying the powder to double sided 'Scotch' adhesive tape mounted on the probe tip. Care must be taken such that no extraneous signals are observed from the sample backing and that no chemical reaction occurs between the sample and substrate. 'Scotch' tape is of silicone composition, conveniently providing intense Si_{2p} and O_{1s} core levels as a monitor of sample coverage. Uneven topography of samples prepared in this way generally leads to lower signal/noise ratios than polymers studied as films.

2.2 Solution Cast Films

If the polymer is sufficiently soluble then thin films may be deposited directly onto a backing, (often clean gold foil ready for mounting on the sample probe tip) by conventional dip or bar coating, or spin casting. Since ESCA is such a surface sensitive technique it is important to use clean apparatus and pure solvents containing no involatile residues (e.g. anti-oxidants, etc.) which would segregate at the surface on evaporation of the solvent. With readily oxidized systems or with systems with sites capable of hydrogen bonding with extraneous water it is imperative to maintain a suitable inert atmosphere during the slow evaporation of solvent.

2.3 Pressed or Extruded Films

Because of problems of contamination in the solvent casting of films, it may be convenient to study polymers in the form of pressed or extruded films mounted on a suitable backing (e.g. gold). For elastomers it is often possible to 'melt' a small amount of the sample and allow it to spread in the form of a thin film on the tip of a sampling probe or to slice a thin film from a larger sample. In preparing samples from powders it is often convenient to press films between sheets of clean aluminium foil at an appropriate temperature and pressure. There are two precautions to be taken in doing this:

(a) the temperature and pressures used should be such that no decomposition or adhesion of surface contamination occurs,

(b) since typically only the top $\sim 50\text{Å}$ of the sample is studied by ESCA it is important to avoid chemical reaction at the surface during preparation. For example pressing polyethylene films in air at the minimum temperature and pressure necessary, results in considerable surface oxidation. This may be obviated by pressing in an inert atmosphere (e.g. N_2 or Ar).[123]

In the chapters of this thesis concerned with surface modification of polymers the majority of the samples are in the form of freestanding extruded films, typically $\sim 30\mu$m thick, which may conveniently be mounted by means of double sided tape.

2.4 'In situ' Preparation

A convenient and often contamination-free method of preparing polymer films is by direct polymerization onto the probe tip, or suitable substrate mounted on the probe tip, usually from the gas phase by ultra violet or electron irradiation, glow discharge polymerization[100] or pyrolysis of appropriate monomers.[99]

Surface treatment of polymers already mounted on the probe tip may also be achieved 'in situ'. For example ultraviolet or electron irradiation and in the context of this thesis glow discharge modifications.[133-137] The experimental set up for 'in situ' preparations often involves pre-treatment chambers bolted directly onto the spectrometer. A long probe is used which may be advanced into the sample chamber of the spectrometer. This technique opens up opportunities for dynamic studies by successively repeating the treatment and analysis cycle.

2.5 Sample Contamination

The most common form of contamination experienced for a polymer sample is hydrocarbon in nature originating either from its preparation and handling or from extraneous hydrocarbon in the sample chamber of the spectrometer[1,111,114] originating from the diffusion pump oil. It is often the case that the contamination is specifically at the surface of the sample and in most cases can be effectively removed by lightly stroking the surface with a soft tissue soaked in spectroscopic grade solvent.

The rate of deposition of hydrocarbon contaminants in the spectrometer, onto a sample, is largely dependent on the stick-

ing probability for the process and the partial pressure of extraneous hydrocarbon in the system. For the study of clean metal surfaces, for example, which have high sticking probabilities hydrocarbon contamination may be a severe problem and clean, ultra high vacuums ($<10^{-10}$torr) are mandatory. The sticking probabilities for polymers however are very much lower and impose less stringent restrictions on the spectrometer pressures. ($\sim10^{-8}$ torr).

Contamination from silicone grease used in vacuum systems may be readily monitored from the Si_{2p} region of the ESCA spectrum, and contamination caused by transfer of aluminium to the surface of a film when prepared by pressing between sheets of aluminium foil may be monitored from the Al_{2p} region, and eliminated by optimizing the pressing conditions.[114]

The final form of contamination most frequently found in polymers is oxidation of the surface regions or the bulk when heating in air is involved in the sample preparation[123,125] (e.g. melt casting, hot pressing). This may be overcome by employing an inert atmosphere, preferably argon.

3. Energy Referencing

Of their very nature, most polymers are extremely good insulators. It has recently been shown that for very thin films (<1000 Å) however sufficient charge carriers are produced during the ESCA experiment such that the sample is in electrical contact with a conducting substrate and thus the spectrometer.[88] For thicker samples or samples mounted on 'Scotch' tape (i.e. electrically isolated from the spectrometer) the process of photoejection of electrons causes the sample to become positively charged. This phenomenon is

termed sample charging and is of considerable interest in its own right,[88,138] as will become apparent from Chapter Four and subsequent chapters. Sample charging however causes a shift in the energy scale and some form of referencing back to the Fermi level is therefore necessary.[1] This is most readily accomplished by depositing a thin film (fractional monolayer) of a suitable reference material onto the surface, (e.g. hydrocarbon C_{1s} at 285.0 eV or gold Au_{4f} at 84.0 eV) and monitoring the core levels of both the sample and the reference. The disadvantages of using gold as a reference for polymers has been pointed out in the literature[84] therefore the preferred reference in this laboratory is the extraneous hydrocarbon which builds up on the sample surface to detectable levels when it has been left in the sample chamber for a period of hours. To put matters in perspective however, it should be emphasised that with most commercial spectrometers (based on unmonochromatized X-ray sources and retarding lens system, double focussing hemispherical electrostatic analysers and associated slit systems), sample charging is not too serious a problem and at worst involves only a few eV correction to the energy scale. With slitless designs and a monochromatized X-ray source as conventionally applied in dispersion compensation, sample charging can however reach serious proportions involving shifts in the energy scale of tens of eV for insulating samples. The problem can be alleviated to some extent by use of low energy electron flood guns or ultraviolet photoemission from the sample chamber walls[88] as is described in Chapter Four.

Figure 2.1 ullustrates the method of energy referencing employed throughout this thesis, the example being polytetra-

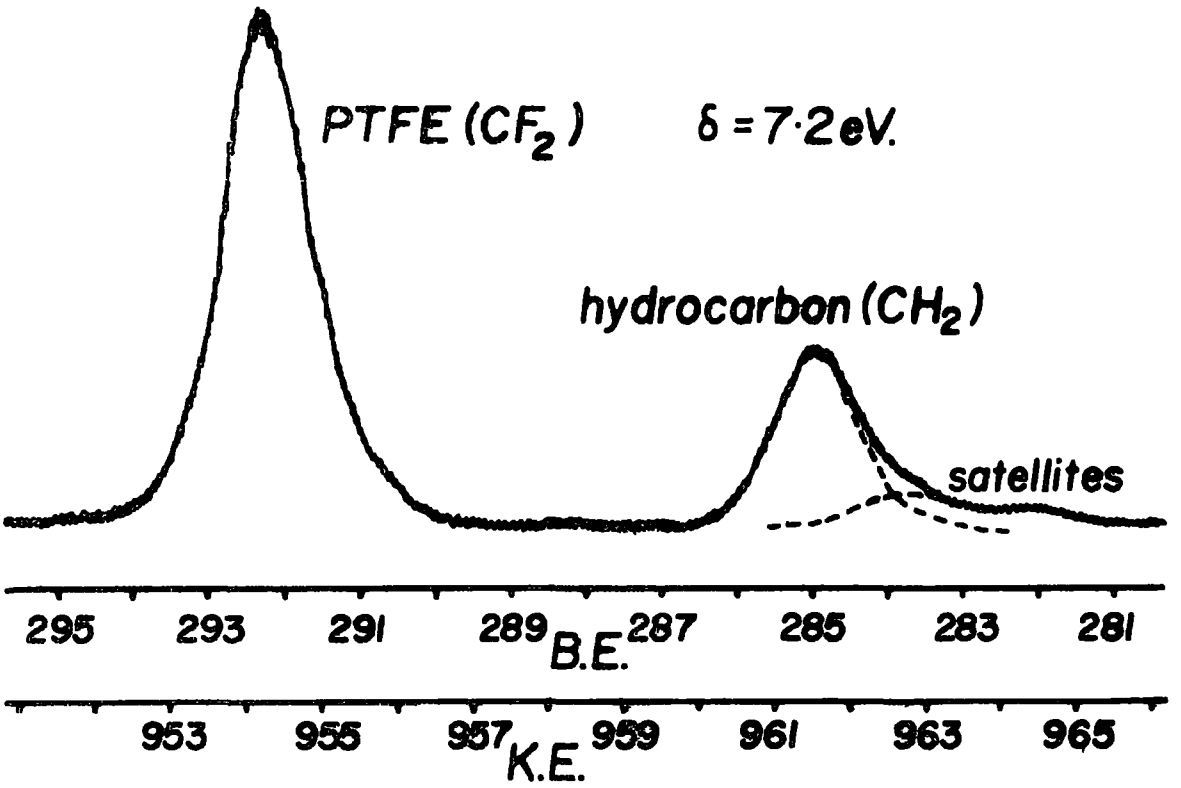

Figure 2.1. Energy referencing of polytetrafluoroethylene.

fluoroethylene. The spectra were obtained using a $Mg_{K\alpha_{1,2}}$ photon source of energy 1253.7 eV. The kinetic energy scale is taken directly from the output of the spectrometer scanning electronics. The binding energy scale is drawn so that the hydrocarbon signal falls at 285.0 eV. The sample charging is then the difference between the sum of the kinetic energy and binding energy at any point, and the photon energy.

4. Information Available from ESCA

Over the past six years ESCA has been applied to the study of structure and bonding across a broad front encompassing organic, inorganic and polymeric systems.[1,21,52,114-118]. These

studies together with complementary theoretical analysis have demonstrated that ESCA is an extremely powerful tool for investigations of structure and bonding with an information content per spectrum unsurpassed by any other spectroscopic technique. This distinctive attribute confers upon ESCA wide ranging applicability and versatility in respect of studies on polymeric systems. It will become apparent that there are areas in which the required information can only at present be derived from ESCA studies, whilst in others the technique nicely complements the more established spectroscopic tools. In general, however, ESCA provides data at a much coarser level and information pertaining for example to conformational effects may only be inferred rather indirectly. In many areas ESCA does not compare favourably in terms of resolution, sensitivity, etc. with the more conventional tools. The fact remains however that this is more than compensated by the great range of information available from a single ESCA experiment such that in the future one can envisage ESCA to be the technique of choice for any initial investigation of a polymer sample. Much of the information gained in the latter chapters of this thesis is attributable to the unique surface sensitivity of ESCA (sampling depth ~ 50 Å) and is not obtainable by any other technique.

A detailed account of the information levels available in ESCA was given in Chapter One. However it is worthwhile to briefly summarize again the levels used most frequently in the experimental sections of this work (Table 2.1).

Table 2.1. Information levels in ESCA

Primary information levels:

(i) Absolute and relative binding energies.

(ii) Relative peak intensities.

Secondary information levels:

(i) Shake up structure.

(ii) Angular dependence of peak intensities.

(iii) Sample charging.

5. Linear Polymers

5.1 Homopolymers

The simplest systems to start with are the high molecular weight homopolymers of the fluoroethylenes,[114,119] for which complications due to branching, end groups, etc. are minimal. The carbon-1s spectra for polyethylene (high density), polyvinyl fluoride, polyvinylidene fluoride, polyvinylene fluoride, polytrifluoroethylene, and polytetrafluoroethylene are presented in figure 2.2.

The C_{1s} spectrum of polyvinyl fluoride shows two partially resolved peaks of equal area corresponding to $\underline{C}HF$ and $\underline{C}H_2$ carbons whilst for polyvinylene fluoride in addition to the main peak corresponding to $\underline{C}HF$ carbons and hydrocarbon calibration peak, there is a weak peak at 292.0 eV. This in fact corresponds to $\underline{C}F_2$ type carbon arising from contamination from the fluorocarbon soap ($H(CF_2)_8COO^-NH_4^+$) used in the emulsion polymerization. For polyvinylidene fluoride well resolved peaks of equal area corresponding to $\underline{C}F_2$ and $\underline{C}H_2$ carbons are evident and for polytrifluoroethylene partially resolved peaks of equal area corresponding to $\underline{C}F_2$ and $\underline{C}FH$ carbons.

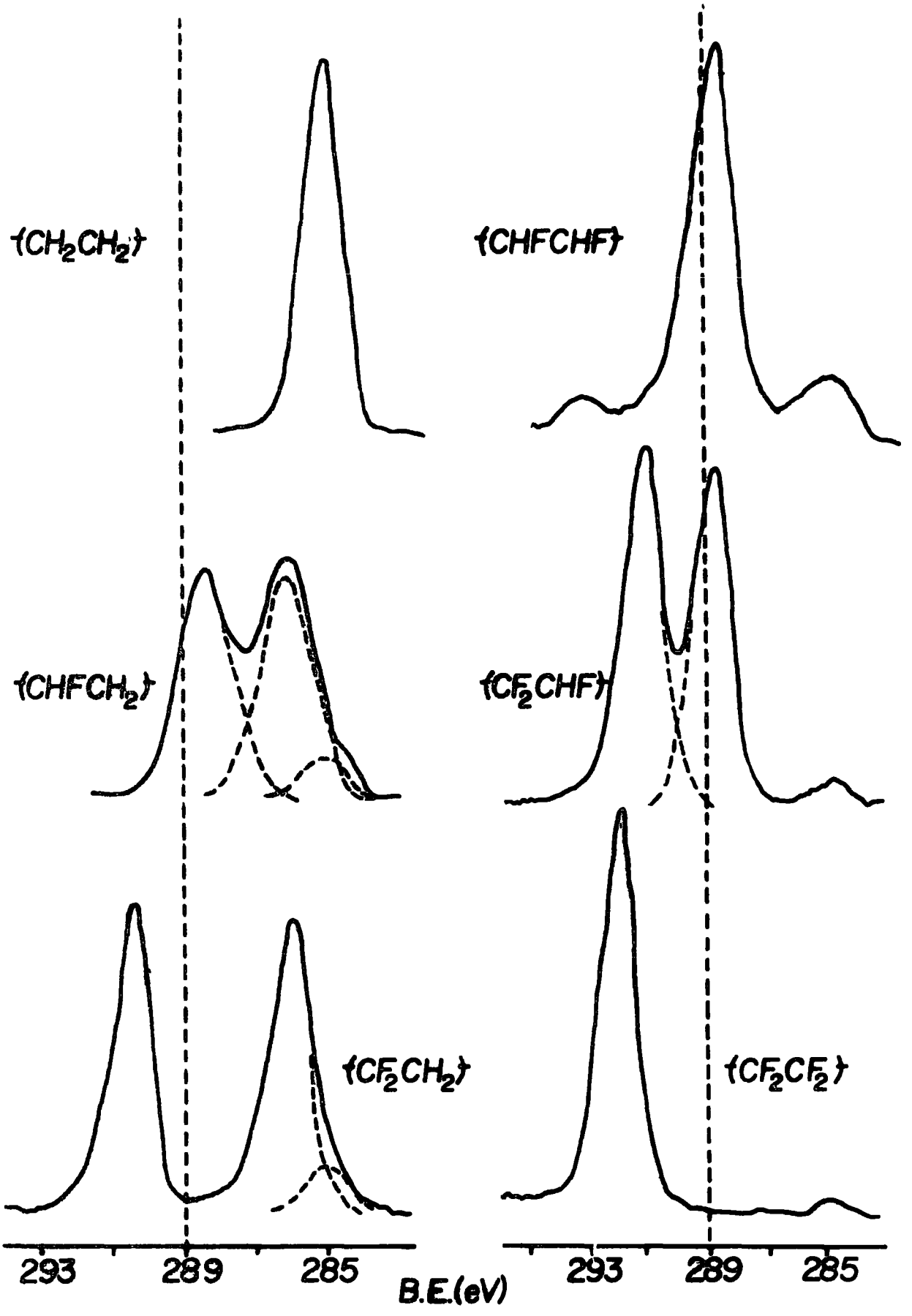

Figure 2.2. C_{1s} spectra of the homopolymers of ethylene and the fluoroethylenes.

The data pertaining to these homopolymers are collected in Table 2.2, the assignment of peaks arising from $\underline{C}F_2$, $\underline{C}FH$ and $\underline{C}H_2$ structural units is straightforward. By taking appropriate pairs of polymers it is possible to qualitatively investigate both primary and secondary effects of replacing hydrogen, Tables 2.3 and 2.4. The average primary (2.9 eV) and secondary (0.7 eV) substituent effects are in excellent agreement with those found for monomer systems and their relative constancy emphasizes the characteristic nature of substituent effects.

The rapid fall off in effect of the fluorine substituent provides a crude but immediate manifestation of the sigma inductive effect exerted by fluorine.

Although alpha and beta substituent effects provide a convenient starting point for the estimation of chemical shifts, it must be emphasized that more sophisticated methods are necessary to obtain accurate interpretations.

Calculated binding energies, within the CNDO/2 SCF MO formalism and Madelung charge potential model are also included in Table 2.2, clearly demonstrating the adequacy of this type of calculation for C_{1s} binding energies in these and related systems. The inability of ESCA to distinguish between the structurally isomeric systems is also evident from these calculations.

More recently similar data accumulation has been made on a series of more than one hundred standard polymers which has extended the 'reference bank' to include polymers containing oxygen, nitrogen, silicon, sulphur, chlorine and bromine.[127] A comprehensive review of this material[125-127] would

Table 2.2. Binding energies of the homopolymers of ethylene and the fluoroethylenes.

Polymer	Function	C_{1s} binding energy (eV)	ΔC_{1s}	F_{1s} binding energy (eV)	ΔF_{1s}	Calc.C_{1s} binding energy (head-head)	(head-tail)
Polyethylene	CH_2	285.0	(0)	-	-	284.9	
Polyvinylfluoride	CHF	288.0	3.0	689.3	(0)	288.0	288.1
	CH_2	285.9	0.9	-	-	285.6	285.4
Polyvinylenefluoride	CHF	288.4	3.4	689.3	0.0	288.6	
Polyvinylidenefluoride	CF_2	290.8	5.8	689.6	0.3	291.0	291.0
	CH_2	286.3	1.3	-	-	286.3	286.1
Polytrifluoroethylene	CF_2	291.6	6.6	690.1	0.8	291.7	291.8
	CHF	289.3	4.3	690.1	0.8	289.4	289.3
Polytetrafluoroethylene	CF_2	292.2	7.2	690.2	0.9	292.6	

Table 2.3. Primary Substituent Effects

Polymer pairs	Shift in C_{1s} binding energy on replacing H by F.(eV).
$(\underline{C}HFCH_2)_n$, $(\underline{C}H_2CH_2)_n$	3.0
$(\underline{C}F_2CH_2)_n$, $(\underline{C}HFCH_2)_n$	2.8
$(CHF\underline{C}HF)_n$, $(CHF\underline{C}H_2)_n$	2.5
$(CF_2\underline{C}HF)_n$ $(CF_2\underline{C}H_2)_n$	3.0
$(CF_2\underline{C}F_2)_n$, $(CF_2\underline{C}HF)_n$	2.9
$(\underline{C}F_2CHF)_n$, $(\underline{C}HFCHF)_n$	3.2
AVERAGE	2.9

Table 2.4. Secondary Substituent Effects

Polymer pairs	Shift in C_{1s} binding energy on replacing H by F.(eV). (per substituent)
$(CHF\underline{C}H_2)_n$, $(CH_2\underline{C}H_2)_n$	0.9
$(\underline{C}HFCHF)_n$, $(\underline{C}HFCH_2)_n$	0.4
$(CF_2\underline{C}H_2)_n$, $(CH_2\underline{C}H_2)_n$	0.7
$(\underline{C}F_2CHF)_n$, $(\underline{C}F_2CH_2)_n$	0.8
$(CF_2\underline{C}HF)_n$, $(CHF\underline{C}HF)_n$	0.9
$(\underline{C}F_2CF_2)_n$, $(\underline{C}F_2CHF)_n$	0.6
AVERAGE	0.7

require an extended discussion, however the salient features of relevance to this work may readily be summarized. An example of oxygen containing polymers is given by the study of a series of twelve polyalkylacrylates of general formula $(CH_2CH(CO.OR))_n$, where R is an alkyl group ranging from methyl to octadecyl.[125] Polyacrylic acid is included, as well as a range of small model compounds for comparison purposes.

Figure 2.3 shows the O_{1s} and C_{1s} core level spectra for four representative polyacrylates and polyacrylic acid. The similarity of these polymers is clearly reflected in their ESCA spectra. In each case the most intense component of the C_{1s} spectrum (lowest binding energy) coincides with the extraneous hydrocarbon peak which appears after the sample has been left in the spectrometer for several hours. It's binding energy is therefore assigned 285.0 eV. The measured binding energy of 285.0 eV for this component suggest that it be attributed to the carbon atoms of the polymer which are not directly attached to oxygen. It is clear that the shift in binding energy for a given carbon atom is highly characteristic of its chemical environment. For carbon atoms singly bonded to one oxygen atom the binding energy is found to be 286.6 $\pm$ 0.1 eV whilst for carbon atoms bonded to two oxygen atoms in an acid or ester group the binding energy is 289.1 $\pm$ 0.2 eV. It is worth including here that the binding energy for a ketonic carbon (in acetone) is 287.9 $\pm$ 0.2 eV[125] and for a carbon singly bonded to two oxygen atoms (in polymethylene oxide) is 287.8 $\pm$ 0.2 eV.[127]

The O_{1s} spectra show a two component structure with binding energies of 532.8 $\pm$ 0.2 eV and 534.3 $\pm$ 0.2 eV corresponding to doubly and singly bonded oxygen respectively. The

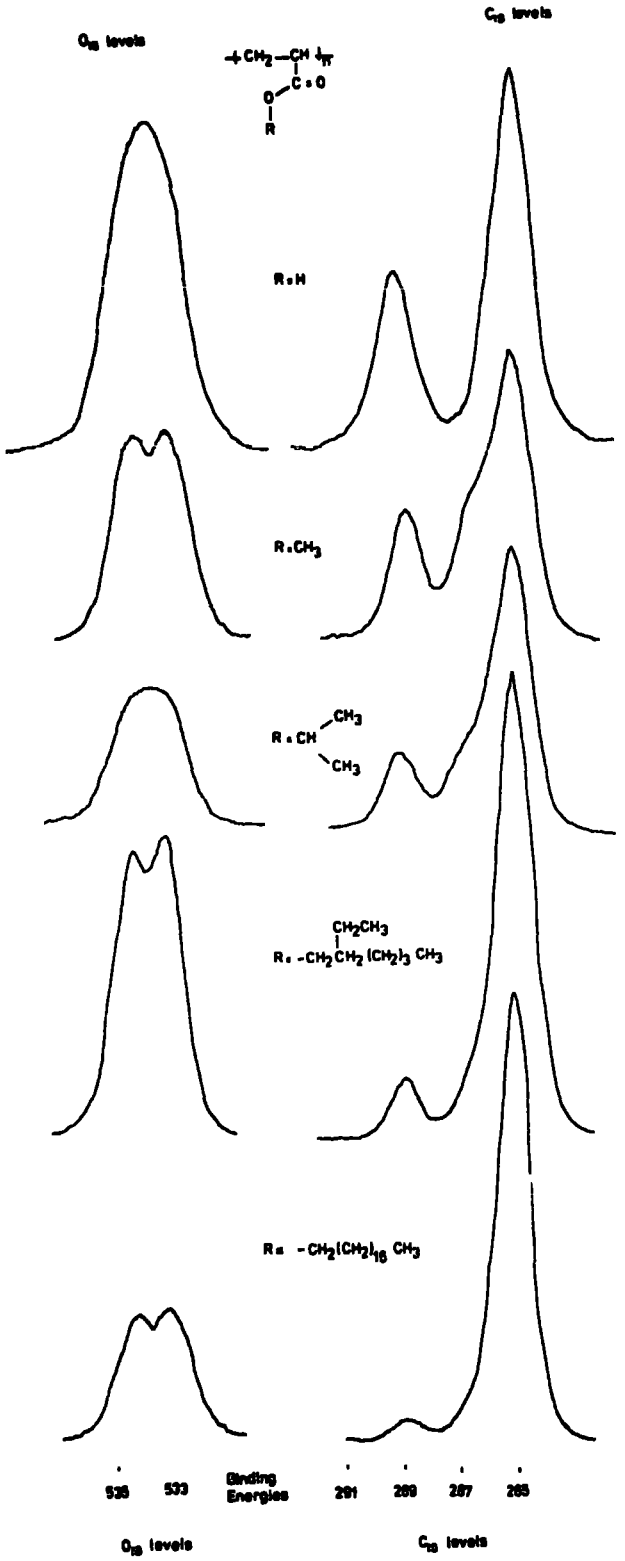

Figure 2.3. O_{1s} and C_{1s} spectra of a series of polyalkylacrylates and polyacrylic acid.

hydrogen bonding in polyacrylic acid is evidenced by a broadening of the signals.

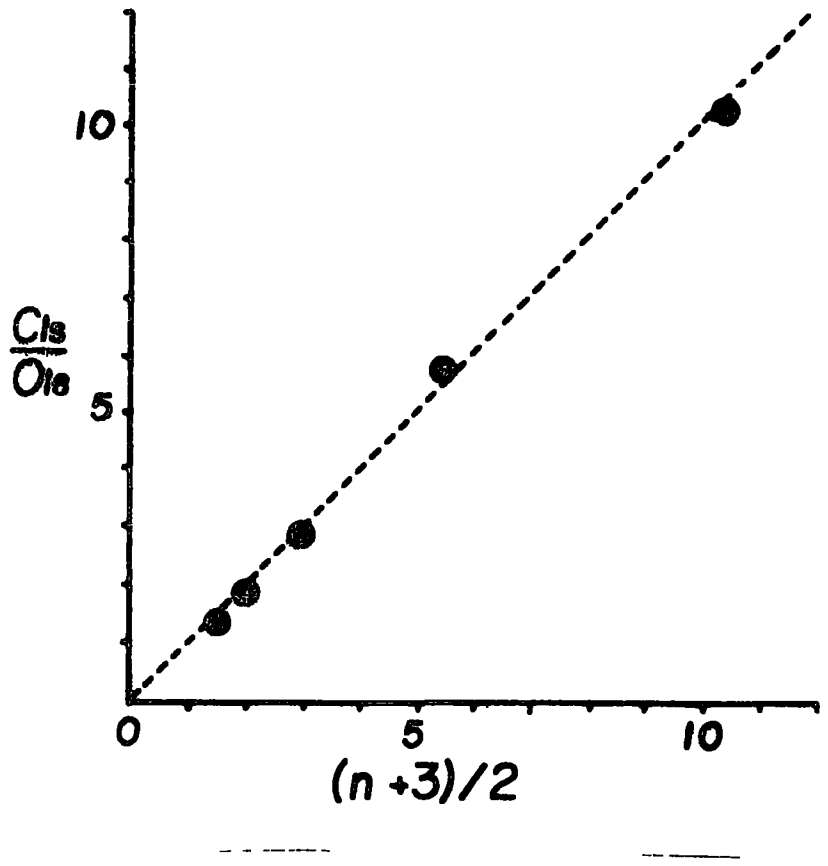

Figure 2.4. Total C_{1s} to O_{1s} area ratios versus the alkyl chain size.

Figure 2.4 shows the total integrated intensity of the C_{1s} spectrum ratioed to that for the O_{1s} spectrum plotted against the alkyl chain length for the polyacrylates (the C_{1s}/O_{1s} ratio is corrected for relative sensitivities). It is clear that the intensity of a signal is directly proportional to the number of atoms giving rise to it. Furthermore the closeness of the slope of the line to unity reflects the homogeneity of the samples on the ESCA depth scale.

This investigation, as with that of the fluoropolymers, was closely accompanied by detailed theoretical calculations on model systems and excellent agreement was found between theory and experiment. Again configurational, conformational and structural isomers were found not to differ more than the experimental error.

The observation of low energy shake-up satellites in homopolymers is often very useful as an extra level of information[55,56,128,129] reflecting the unsaturation or otherwise of the material and for purely hydrocarbon polymers provides the only source of information which is currently interpretable.[127,128] This aspect of ESCA will be dealt with in some detail in Chapter Three.

So far only information derived from the study of core levels has been discussed. Structure and bonding has then been largely inferred from shifts in core binding energies which reflect differences in valence electron distributions. Of obvious interest is the direct investigation of the valence levels of polymers. ESCA has two distinct disadvantages compared with the corresponding UPS measurements. Firstly, cross sections for photoionization are generally lower than for the longer wavelength photon sources used in UPS, and secondly the resolution is much poorer, (i.e. photon linewidths are $\sim$5meV for He(I) and $\sim$700meV for $Mg_{K\alpha_{1,2}}$). These disadvantages are considerably offset when studying involatile materials (see Chapter One, section 5).

To date, the study of valence levels of polymers by ESCA has been largely with respect to a 'fingerprint technique' rather than specific orbital assignment.[114,125,126]

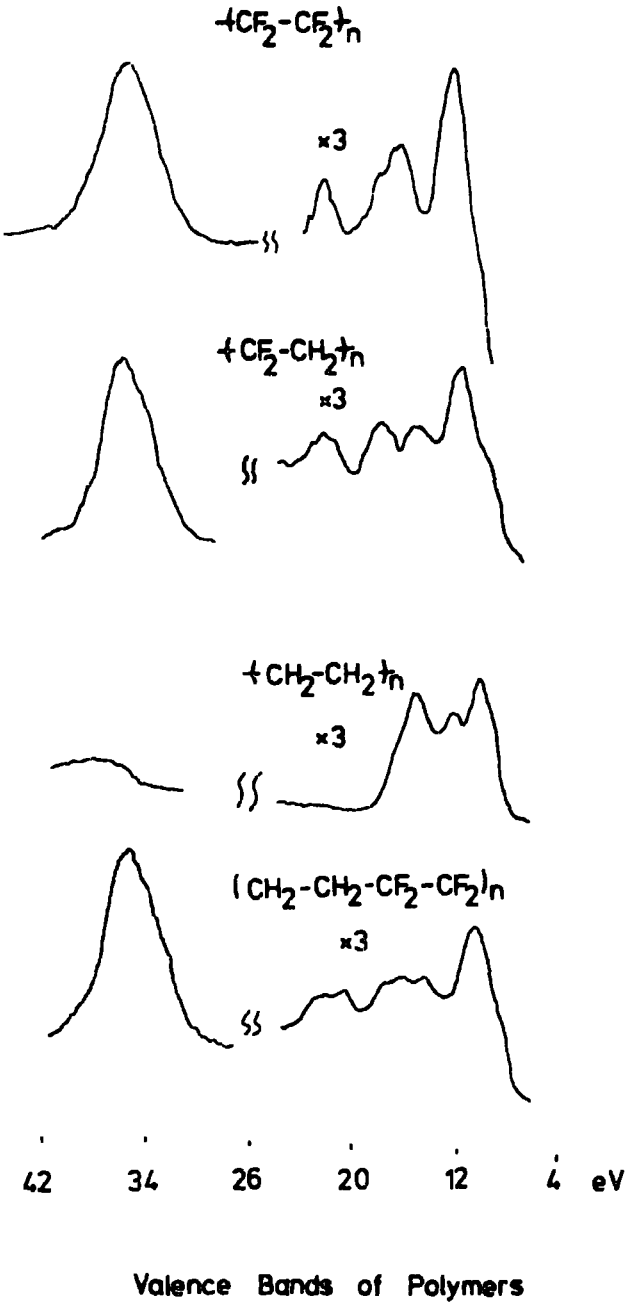

Figure 2.5. Valence band spectra of polytetrafluoroethylene, polyvinylidene fluoride, polyethylene and an ethylene-tetrafluoroethylene copolymer (52% T.F.E.).

Typical of the data which may be obtained is that shown in figure 2.5 for PTFE, polyvinylidene fluoride, and polyethylene.[114] The theoretical interpretation of the valence band structure[139-141] is not as straightforward as that of core levels.[1,18,19] For the spectra shown in figure 2.5

a reasonable assignment can be made as follows. The large peak at highest binding energy clearly evident in the fluorinated polymers arises from molecular orbitals essentially F_{2s} in character. The prominent peak at lowest binding energy for PTFE which is also clearly evident in polyvinylidene fluoride is assigned to M.O.'s corresponding essentially to fluorine 2p lone pairs. The shoulder at lower binding energy in polyvinylidene fluoride which has its counterpart in polyethylene may then be assigned to carbon-hydrogen bonding orbitals (essentially C_{2p} H_{1s}). The assignments for the remaining peaks are then essentially C-F and C-C (2s) bonding orbitals.[114] With an appropriate correction for work function (~5 eV) the binding energies correspond quite nicely to those obtained from UPS studies of simple systems containing the essential structural features.[82]

For comparison purposes the valence band for an ethylene-tetrafluoro-ethylene copolymer of composition close to 50-50 is also included. This bears a striking resemblance to that for polyvinylidene fluoride as one might expect on the basis of its largely alternating structure (discussed in the next section).

Valence band spectra have also been exploited to resolve ambiguities in structural isomerism in polybutylacrylates.[125]

5.2 Copolymers

It is evident from the previous section that substituent effects on core level binding energies in polymers can be understood both qualitatively and quantitatively on the same basis as those for simple monomeric systems.[114] With this knowledge it is possible to proceed to more complex systems

such as copolymers. The application of ESCA to this area has proved to be extremely useful in terms of monomer composition,[120,121] monomer sequences[121] (block, random or alternating) and domain structure in block copolymers.[122]

The work of Clark and coworkers[121] on a series of ethylene-tetrafluoroethylene copolymers provides an excellent example of the capabilities of ESCA in this field. The F_{1s} and C_{1s} spectra of a series of ethylene-tetrafluoroethylene copolymers are shown in figure 2.6. From the ESCA data the copolymer compositions may be calculated in two independent ways. Firstly, from the relative ratios of the high to low binding energy peaks in the C_{1s} spectrum attributable to $\underline{C}F_2$ and $\underline{C}H_2$ type environments respectively. Secondly, from the overall C_{1s}/F_{1s} intensity ratios taken in conjunction with the relative intensity ratio established previously for the homopolymers.[114,119] The results of these two analyses from ESCA data and those derived from conventional microanalysis for carbon and fluorine are compared in Table 2.5.

Table 2.5. Copolymer compositions (mole % C_2F_4)

Sample	From carbon analysis	From fluorine analysis	From $C_{1s}:F_{1s}$ area ratio	From $\underline{C}H_2:\underline{C}F_2$ area ratio
1	61	61	63	62
2	52	54	52	52
3	49	48	47	46
4	47	45	44	45
5	41	40	42	40
6	-	-	32	31

The agreement between the two sets of ESCA data demonstrates the uniformity (within the outermost $\sim 50\text{Å}$) of the

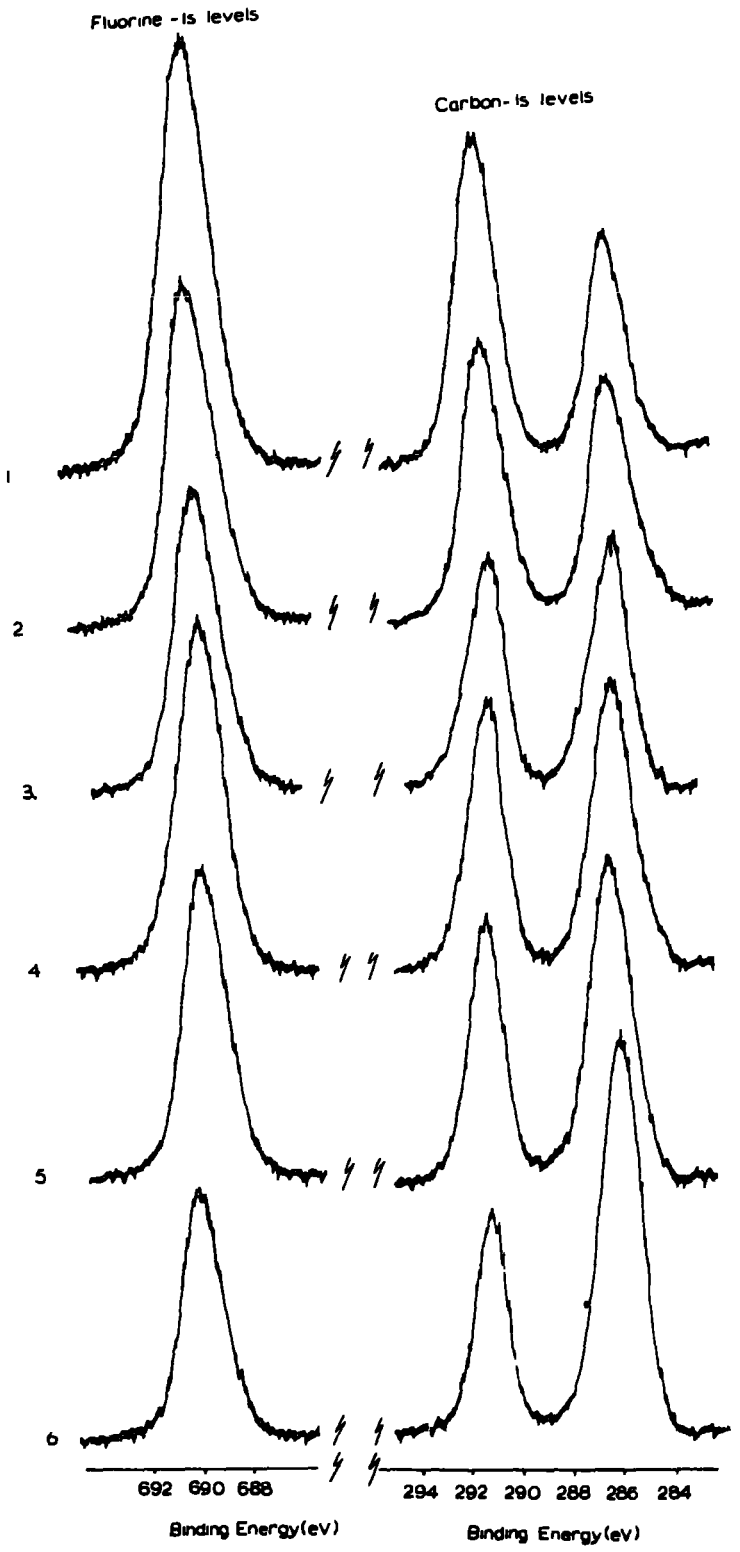

Figure 2.6. F_{1s} and C_{1s} spectra of a series of ethylene-tetrafluoroethylene copolymers.

copolymer since the mean free paths for electrons photoemitted from the F_{1s} and C_{1s} levels are significantly different. This is indicative of a largely alternating structure for the copolymers since the PTFE domains of a block copolymer would be expected (on the basis of their lower free energy) to predominate at the surface. In this hypothetical case, estimates of TFE incorporation based on either ESCA method would be unlikely to agree and both procedures would give values higher than those computed from elemental analysis of bulk samples. Comparison of the ESCA data with classical techniques corresponding to bulk analyses reveals overall good agreement and also demonstrates that for these systems ESCA is competitive with microanalytical techniques in terms of accuracy and reproducability with the added advantage of being nondestructive and much faster.

The previous studies of the homopolymers of the fluoroethylenes revealed that structural information is most readily derived from absolute binding energies and shifts in the C_{1s} core levels.[114,119] The shifts can be understood both qualitatively (in terms of simple substituent effects) and quantitatively, (in terms of the charge potential model and SCF MO computed charge distribution for appropriate models), and lead to a clear cut distinction between the two extremes of essentially block or alternating structure. Thus the C_{1s} binding energies to be expected for block sequences of ethylene and tetrafluoroethylene are the same as those measured for the respective homopolymers, viz. 285.0 eV and 292.2 eV.[114] By contrast, for an alternating structure, the C_{1s} binding energies are expected to be 286.3 eV and 291.0 eV, on the basis of (i) the experimentally observed values for polyvinylidene fluoride,[114] (ii) predicted values based on substituent effects

and (iii) theoretical calculations for the model compound shown below.

$$HCF_2CH_2CH_2CF_2\underline{C}F_2\text{-}\underline{C}H_2CH_2CF_2CF_2CH_3$$

291.0 286.3 (eV)

A clear distinction should therefore be evident if either of these features predominate both in terms of the predicted shifts (7.2 eV for the block and 4.7 eV for the alternating cases respectively) and absolute binding energies for the two major components.

A consideration of the shifts between the two component peaks in the C_{1s} spectra, figure 2.6 illustrates this quite strikingly. The measured shifts in all cases are ~5 eV, which establishes that the predominant structural feature is alternation. However, a close examination of the spectra reveals two features of importance to a complete interpretation of the data. In the first place the total linewidths (FWHM) are commonly greater than 2 eV compared with typical linewidths for individual core levels in homopolymers of ~1.3 ± 0.1 eV. Secondly, the peak shapes are distinctly assymmetric; indeed the observed shape varies with copolymer composition. Both these observations indicate that the experimentally observed spectra are the envelopes of numbers of overlapping peaks arising from different molecular environments. With a background knowledge of the binding energies of carbon environments which might be expected to be present in these copolymers (i.e. from the study of the series of homofluoropolymers) along with theoretical simulations it is possible to obtain a unique solution to the overall envelope by line shape analysis for each sample. The results of this are presented in Table 2.6.

Table 2.6. Experimental deconvolution of the ethylene-tetrafluoroethylene copolymers

	Binding energies (area ratios)						
Sample No.	a	b	c	d	e	f	g
1	292.1(25)	291.2(31)	290.4(5)	287.8(3)	286.3(30)	285.7(5)	285.0(1)
2	292.1(12)	291.0(33)	290.2(7)	287.6(4)	286.3(32)	285.7(6)	285.0(6)
3	292.3(4)	291.0(37)	290.1(5)	287.7(5)	286.4(36)	285.7(9)	285.0(4)
4	292.4(6)	291.1(35)	290.4(4)	287.7(4)	286.3(35)	285.7(9)	285.0(7)
5	292.2(2)	291.0(35)	289.4(3)	287.8(4)	286.4(34)	285.6(17)	285.0(5)
6	292.1(3)	291.1(27)	289.5(1)	287.3(3)	286.4(26)	285.7(30)	285.0(10)

For comparison a complete theoretical treatment was also carried out for these copolymers. The most likely monomer sequences and their relative abundancies were calculated from a knowledge of reactivity ratios for the free radical polymerization and feedstock ratios of the comonomers and the copolymer compositions derived from the ESCA data. Pentad sequences were chosen as the simplest suitable distributions to compute for direct comparison with experimental data, since they are large enough units to accommodate all important short range interactions for the central triads and thus allow a direct comparison between theory and experiment. Table 2.7 shows the most probable pentad sequences for these copolymers and Table 2.8 compares the experimental and theoretically derived intensities of the various components of the C_{1s} envelope.

The remarkable measure of agreement between the two sets of data in Table 2.8 is most encouraging. Thus the sequence distributions computed from the reactivity ratios show the marked degree of alternation inferred qualitatively from the raw ESCA data.

In the discussion of the ethylene/tetrafluoroethylene copolymers it was mentioned that the agreement between the various analyses for copolymer composition was evidence against a block structure, since PTFE blocks would be expected to segregate at the surface and hence be over estimated by a surface sensitive technique like ESCA. In a more general sense the differing sampling depths for photoemitted electrons from core levels corresponding to differing kinetic energies makes ESCA a very useful tool for studying domain structure

Table 2.7. Assignment of triads for most probable pentad sequences for the C_{1s} core levels

Sequence	
ABAAA	$-CF_2CF_2(\underset{e}{CH_2}\underset{e}{CH_2}\underset{b}{CF_2}\underset{a}{CF_2}\underset{a}{CF_2}\underset{a}{CF_2})\ CF_2CF_2-$
ABAAB	$-CF_2CF_2(\underset{e}{CH_2}\underset{e}{CH_2}\underset{b}{CF_2}\underset{a}{CF_2}\underset{a}{CF_2}\underset{b}{CF_2})\ CH_2CH_2-$
ABABA	$-CF_2CF_2(\underset{e}{CH_2}\underset{e}{CH_2}\underset{b}{CF_2}\underset{b}{CF_2}\underset{e}{CH_2}\underset{e}{CH_2})\ CF_2CF_2-$
BBABA	$-CH_2CH_2(\underset{f}{CH_2}\underset{e}{CH_2}\underset{c}{CF_2}\underset{b}{CF_2}\underset{e}{CH_2}\underset{e}{CH_2})\ CF_2CF_2-$
BABAA	$-CH_2CH_2(\underset{b}{CF_2}\underset{b}{CF_2}\underset{e}{CH_2}\underset{e}{CH_2}\underset{b}{CF_2}\underset{a}{CF_2})\ CF_2CF_2-$
BABAB	$-CH_2CH_2(\underset{b}{CF_2}\underset{b}{CF_2}\underset{e}{CH_2}\underset{e}{CH_2}\underset{b}{CF_2}\underset{b}{CF_2})\ CH_2CH_2-$
ABBAB	$-CF_2CF_2(\underset{e}{CH_2}\underset{f}{CH_2}\underset{f}{CH_2}\underset{e}{CH_2}\underset{c}{CF_2}\underset{b}{CF_2})\ CH_2CH_2-$
BBBAB	$-CH_2CH_2(\underset{g}{CH_2}\underset{g}{CH_2}\underset{f}{CH_2}\underset{e}{CH_2}\underset{c}{CF_2}\underset{c}{CF_2})\ CH_2CH_2-$

Table 2.8. Comparison of experimental and theoretical peak intensities.

Sample		Peak Designation*					
		a	b	c	e	f	g
1	Experiment	25	31	5	30	5	1
	Theory	26	37	-	37	-	-
2	Experiment	12	33	7	32	6	6
	Theory	8	43	1	45	1	-
3,4	Experiment	5	37	5	37	9	4
	Theory	4	46	2	46	3	1
5	Experiment	2	35	3	34	17	5
	Theory	1	39	6	42	10	3
6	Experiment	3	27	1	26	30	10
	Theory	-	24	10	31	23	12

* Peak d is assigned to carbonyl features consequent upon a small amount of oxidation.

of block copolymers.[122] A simple illustration of this is provided by a consideration of two block copolymers of polydimethylsiloxane with polystyrene.[122] Two samples were examined as films cast from cyclohexane, their characteristics are listed in Table 2.9.

Table 2.9. Polydimethylsiloxane - Polystyrene Block Copolymers

Sample	% PDMS	% PS	$\bar{M}_n$
1	77	23	121,000
2	41	59	124,000

Considering firstly sample 1, electron microscopy indicated that PDMS formed the continuous phase, the discrete phase being of PS the domains being of the order of 300 Å in dimension. Contact angle measurements suggested that the surface

of the samples were essentially PDMS. ESCA provides a means of investigating this directly.

From studies of simple model systems overall intensity ratios for homogeneous samples were established for the principle core levels pertinent to the copolymer system (viz. I_∞ values for O_{1s}, C_{1s}, Si_{2s}, Si_{2p} core levels). For the block copolymer, comparison of the intensity ratios showed that essentially only the polydimethylsiloxane component was observed. This is an important result for two reasons. Firstly it demonstrates that ESCA is potentially a very valuable technique for identifying the domain structure at the surfaces of block copolymers. Secondly since on the ESCA scale the sample appears to be homogeneously polydimethylsiloxane a knowledge of escape depth dependencies may be used to put a lower limit on the dimension of the domains. A reasonable estimate in this particular case would be >100 Å. For sample 2 again ESCA reveals that the surface is essentially PDMS which is only explicable in terms of a continuous phase of PDMS and discrete phase of PS. This conclusion is further emphasized by the fact that no low energy shake-up satellite is observed in the C_{1s} spectra of either sample, which would have been observed, had the polystyrene component been present at the surface, due to its unsaturated structure.[129] The utility of studying shake up phenomena for copolymers, particularly for purely hydrocarbon systems is expanded in some detail in Chapter Three.

6. Crosslinked Polymers

Due to the insolubility of crosslinked (network) polymers, the investigation of such systems is usually confined

to the solid phase. The major source of information concerning their bulk structure derives from infra-red spectroscopy for a few appropriate cases since other techniques (i.e. differential scanning calorimetry, thermal gravimetric analysis) are largely featureless.[130] Within the past year or so however ESCA has greatly extended the range of crosslinked polymers which may be studied due to the minimal amount of sample preparation necessary. Although the information derived from ESCA pertains strictly to the surface layers of the polymer the structure of the bulk material can be largely inferred when the information is taken in conjunction with complementary experiments (e.g. microanalysis, infra-red spectroscopy) or by sectioning the sample.

Recently a great interest has been shown in polymers produced by glow discharge techniques.[100,130,131,142-145] Although polymers of a specific structure or physical properties cannot as yet be prepared by these techniques the method is particularly appealing for a variety of reasons.[130,142] The advantages for preparing pore free, uniform films of superior physical, chemical, electrical and mechanical properties were recognized at an early stage. The one step preparation is cost effective and the choice of monomer is virtually unlimited. The product of this type of polymerization is almost invariably highly crosslinked. Due to the great range of information available from a single experiment ESCA has recently proved to be the most powerful tool available for the study of structure and bonding in these materials.[130,131,144,145]

As an example of the potential of ESCA in this area it is appropriate here to draw on the work of Clark and Shuttleworth carried out in these laboratories, over the past year.[52,100,131]

The application of ESCA to the elaboration of chemical composition in the case of fluorocarbon based systems for which the span in binding energies for the C_{1s} levels is particularly favourable consequent upon a large electronic effect of replacing hydrogen by fluorine is well established.[114] For this reason the predominant emphasis has been on glow discharge polymers based on fluorocarbon precursors.

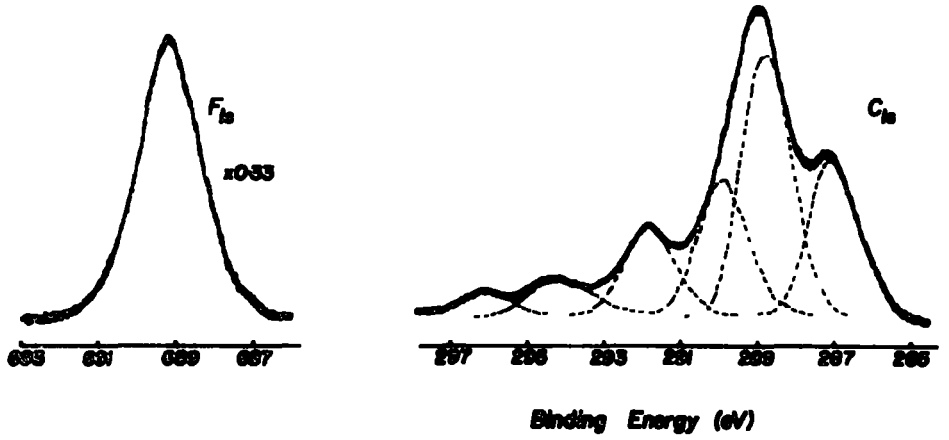

Figure 2.7. F_{1s} and C_{1s} spectra of a polymer produced in a radio frequency glow discharge excited in perfluorobenzene.

Figure 2.7 shows the core level spectra for a polymer film produced by a radio frequency glow discharge excited in perfluorobenzene as monomer. The complex nature of the C_{1s}

spectrum with components of binding energy appropriate to $\underline{C}F_3$, $\underline{C}F_2$ and $\underline{C}F$ sites as well as carbon atoms not directly attached to fluorine is evidence of the rearrangements occurring in the monomeric species prior to polymerization. The stoichiometry may be calculated from the relative integrated intensities of the C_{1s} components and for homogeneous samples independently from the relative intensity of the F_{1s} to the total C_{1s} signal. Comparison with micro analytical data strongly indicates that the samples are indeed homogeneous and that the surface as seen by ESCA is representative of the bulk polymer.[52,100,131] It is also interesting to note that a shoulder in the C_{1s} levels centred at $\sim$ 296.5 eV is too high in binding energy to be associated with a C_{1s} level shifted by fluorine substituents. It arises in fact from $\pi^* \leftarrow \pi$ shake up transitions accompanying photoionization of C_{1s} levels associated with $\underline{C}F$ structural features thus showing that the polymer structure encompasses unsaturated components involving vinylic $\underline{C}F$ environments. Such polymer films have been utilized to measure mean free paths of electrons as a function of kinetic energy in polymers.[100]

As an extension figure 2.8 shows the F_{1s}, C_{1s} and Au_{4f} core level spectra of a series of films polymerized onto gold substrates from perfluorobenzene, perfluorocyclohexa - 1,4 and 1,3 dienes, perfluorocyclohexene and perfluorocyclohexane.[130,131] In all cases the discharge parameters were the same (0.1 torr, 1.0 watts for 60 seconds). Several trends are clearly discernible. From the relative intensities of the Au_{4f} signals arising from the substrate it is evident that the film thickness decreases along the series from perfluorobenzene to perfluorocyclohexane reflecting the increase in reactivity as a

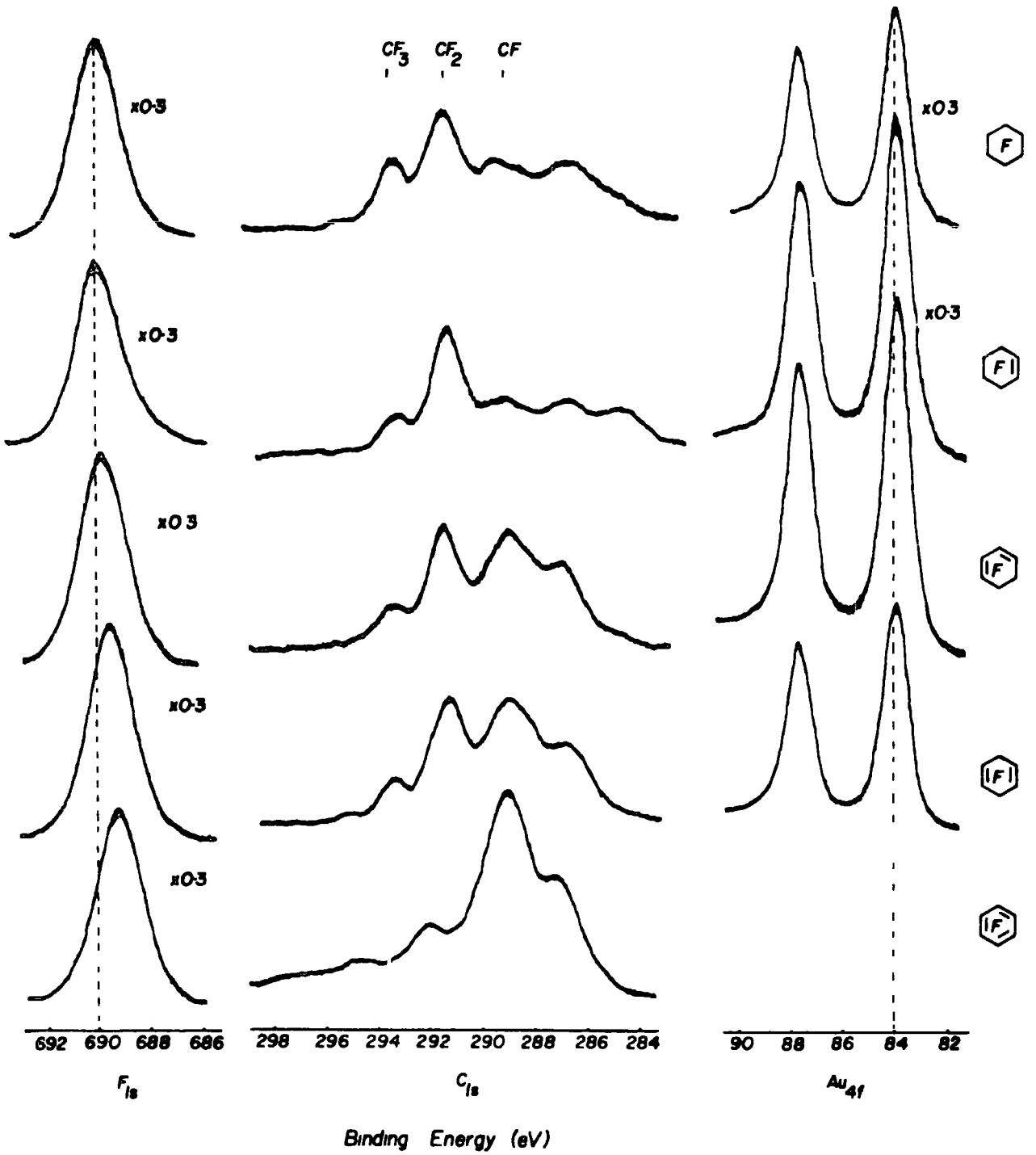

Figure 2.8. F_{1s}, C_{1s} and Au_{4f} spectra of polymers deposited onto gold substrates in radio frequency glow discharges excited in perfluorobenzene, perfluorocyclohexa 1,4 and 1,3 dienes, perfluorocyclohexene and perfluorocyclohexane.

function of unsaturation of the monomer. The structural information may be briefly summarized as follows. In going from the benzene to the cyclohexane derivative the $\underline{C}F_3$ signal increases, the $\underline{C}F_2$ signal is approximately constant and the $\underline{C}F$ signal decreases. The overall trend is reflected also in a distinct shift in the centroid of the F_{1s} signal.[114,119] It is readily apparent from these observations that the polymer structure is a stronger function of the monomer structure than previously suggested and that many features of the monomer are either retained or altered predominantly by the addition or subtraction of one fluorine atom. In this connection it is clear that the isomeric 1,3 and 1,4 cyclohexadiene derivatives produce essentially the same polymer although their rate of production is not the same. Figure 2.9 shows a similar set of core level spectra for the series 1,2 trans and cis difluoroethylene and 1,1 difluoroethylene.[130,131] The two 1,2 isomers give rise to essentially the same polymer whereas the 1,1 isomer produces a polymer of much lower $\underline{C}F$ content. The rates of polymerization as evidenced by the Au_{4f} signal intensity are in the order 1,2 cis > 1,2 trans > 1,1 suggesting that for the first two the effective elimination of HF is important and that trans elimination is preferred. For the 1,1 isomer however a different less favourable mechanism must be involved.

7. Surface Modified Polymers

Since solids communicate with the rest of the universe by way of their surfaces it is clear that any degradative process which depends intimately on the chemical, physical, electrical and mechanical properties of the surface regions is in principle directly amenable to investigation by ESCA.[132] If degradation

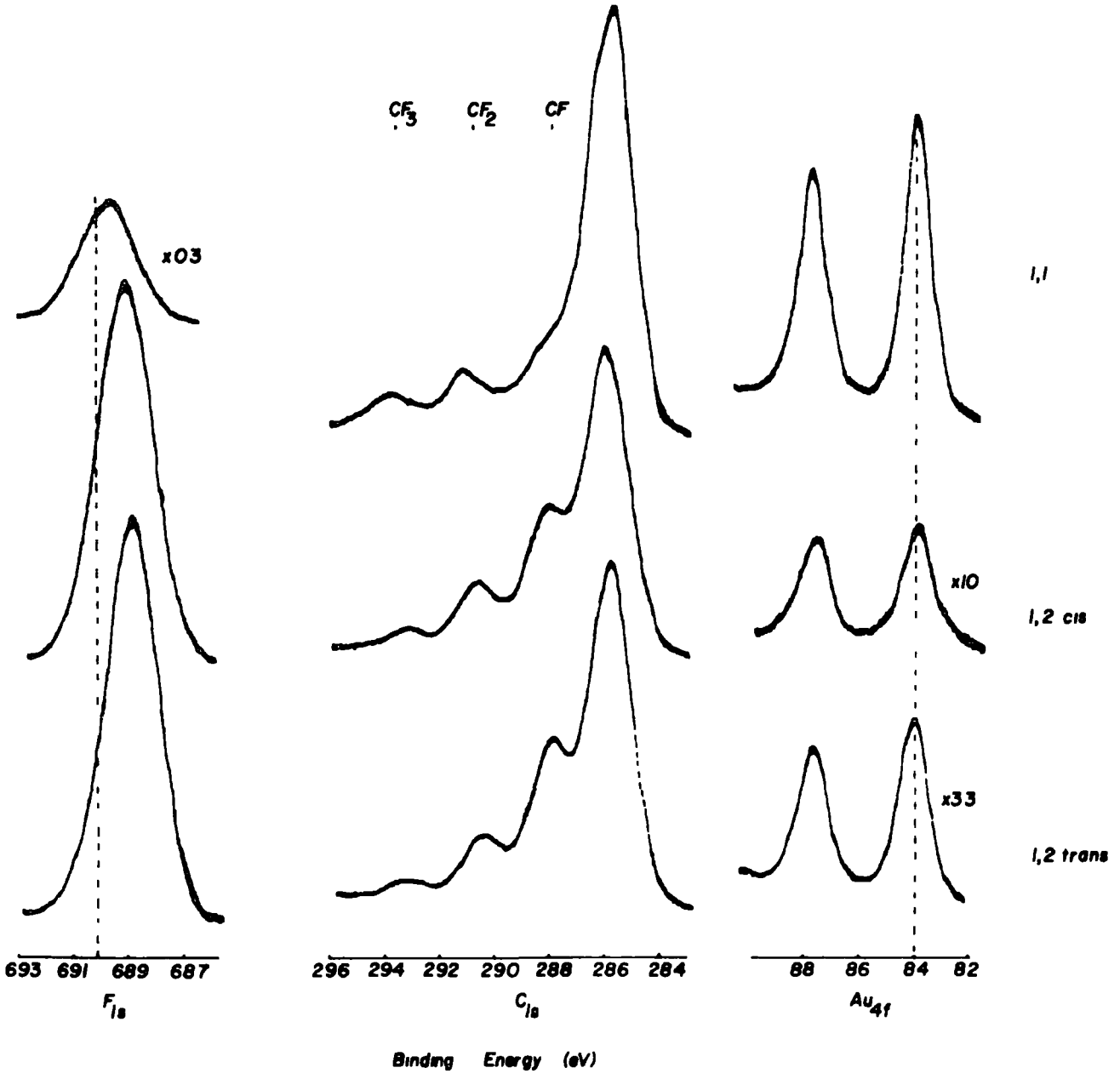

Figure 2.9. F_{1s}, C_{1s} and Au_{4f} spectra of polymers deposited onto gold substrates in radio frequency glow discharges excited in 1,2 trans and cis difluoroethylene and 1,1 difluoroethylene.

is construed as any process which alters the chemical, physical, electrical or mechanical properties of a polymer it should be evident that the surface of the polymer plays a central role. The surface modification of polymers may be roughly split into two categories; the first being undesirable processes such as weathering and ageing; the second being modifications specifically to improve the surface properties of the material. For example surface modifications effected by Corona discharge treatments and flame treatments extensively used for improving adhesive bonding, printability, etc. would be encompassed by this second category. Mechanical degradation of polymers also represents an important area in which surface studies are mandatory for any definitive study and may be put into the first category.

The essence of surface modification is a change in structure and bonding which may permeate through surface, subsurface and bulk but usually gives rise to inhomogeneities in these regions. Prior to the advent of ESCA the important question as to whether the surface composition of a polymer is the same as that of the bulk and if not, in what way it differs could only be inferred indirectly in favourable cases whilst the specific differentiation of surface from subsurface and bulk in inhomogeneous samples could not be encompassed. Clearly ESCA has a great potential in the field of surface modification of polymers and the succeeding sections consider how ESCA may be addressed to these problems, through a few examples.

7.1 Chemical Modification

The application of ESCA to the investigation of chemical modification of polymers is illustrated by reference to two

examples; the surface oxidation of polyalkylacrylates[125] and the surface fluorination of polyethylene,[123,124]

The spectra of several polyalkylacrylates have been discussed in section 5.1, where it was noted that the relative intensities of the O_{1s} and C_{1s} levels and the components of these levels suggest that the outermost few tens of Angstroms of cast films of the polymers have identical compositions to that of the bulk. By contrast the series of polyalkylacrylates shown in figure 2.10 do not conform to a simple picture.[125] Thus it is immediately obvious that the components of the O_{1s} levels are not of equal intensity. (The higher binding energy component corresponds to the singly bonded and the lower binding energy component the doubly bonded oxygen). The two components are unequal in a sense which suggests that the samples contain excess carbonyl features in the surface regions. Furthermore, the intensity ratio of the O_{1s} signal to the essentially core like O_{2s} signal is found to be higher than that derived from standard pure samples, and considering the widely differing mean free paths for electrons photoemitted from these levels this observation is consistent with oxidation confined to the outermost surface regions.[125] It should also be emphasized that by conventional techniques (multiple attenuated total internal reflectance spectroscopy or double beam transmission infrared spectroscopy) these samples show no evidence for oxidation.[125]

A particularly apposite example of the detailed investigation which becomes possible by means of ESCA, of a surface modification of a polymer is provided by the study of the surface fluorination of polyethylene.[123,124] The sensitivity of

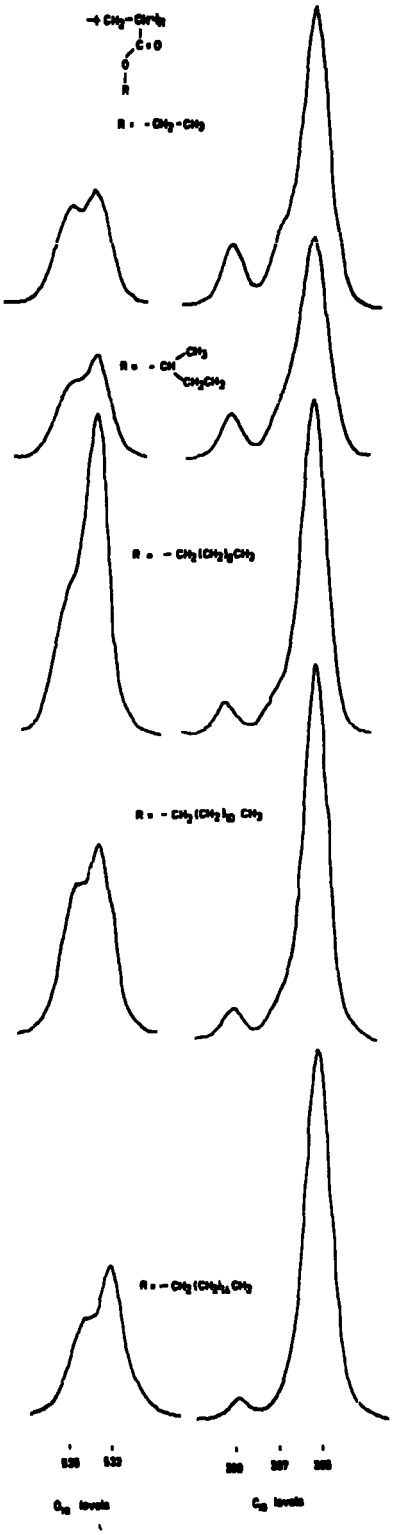

Figure 2.10. O_{1s} and C_{1s} spectra of a series of oxidized polyalkylacrylates.

of the technique is shown by the form of the core level spectra of samples of high density polyethylene which have been exposed to 10% fluorine with nitrogen as diluent for ½ sec. and 30 secs. respectively (figure 2.11).

The C_{1s} levels for the initial sample corresponds to a single peak centred at a binding energy of ∿285 eV. After ½ sec. exposure however a F_{1s} peak appropriate in binding energy to CF structural features is evident and the band profile for the C_{1s} levels also reveals the presence of CF environments with components appropriate to carbon directly bonded to fluorine and beta to fluorine substituents. From a complete analysis of the data it is possible to show that after ½ second exposure fluorination has proceeded to the first monolayer stage and that the composition of the latter corresponds quite closely to that appropriate to polyvinylfluoride (viz. after ½ second exposure the composite structure corresponds essentially to a monolayer of polyvinyl fluoride on polyethylene). After 30 seconds exposure the lineshape for the C_{1s} levels becomes extremely complex, extending to higher binding energies appropriate to CF_2 structural features. By reference to model systems it is possible to analyse the lineshape and this taken in conjunction with the relevant area ratios for the F_{1s} and F_{2s} levels leads to a straightforward analysis which shows that fluorination extends to a depth of ∿ 30Å with the overall stoichiometry in this region being ∿ $C_1F_{1.2}$. In this region however the surface will be more highly fluorinated than subsurface and bulk. It is possible to unravel the complexities of such a situation and it may be shown that the composition of the first monolayer at this stage

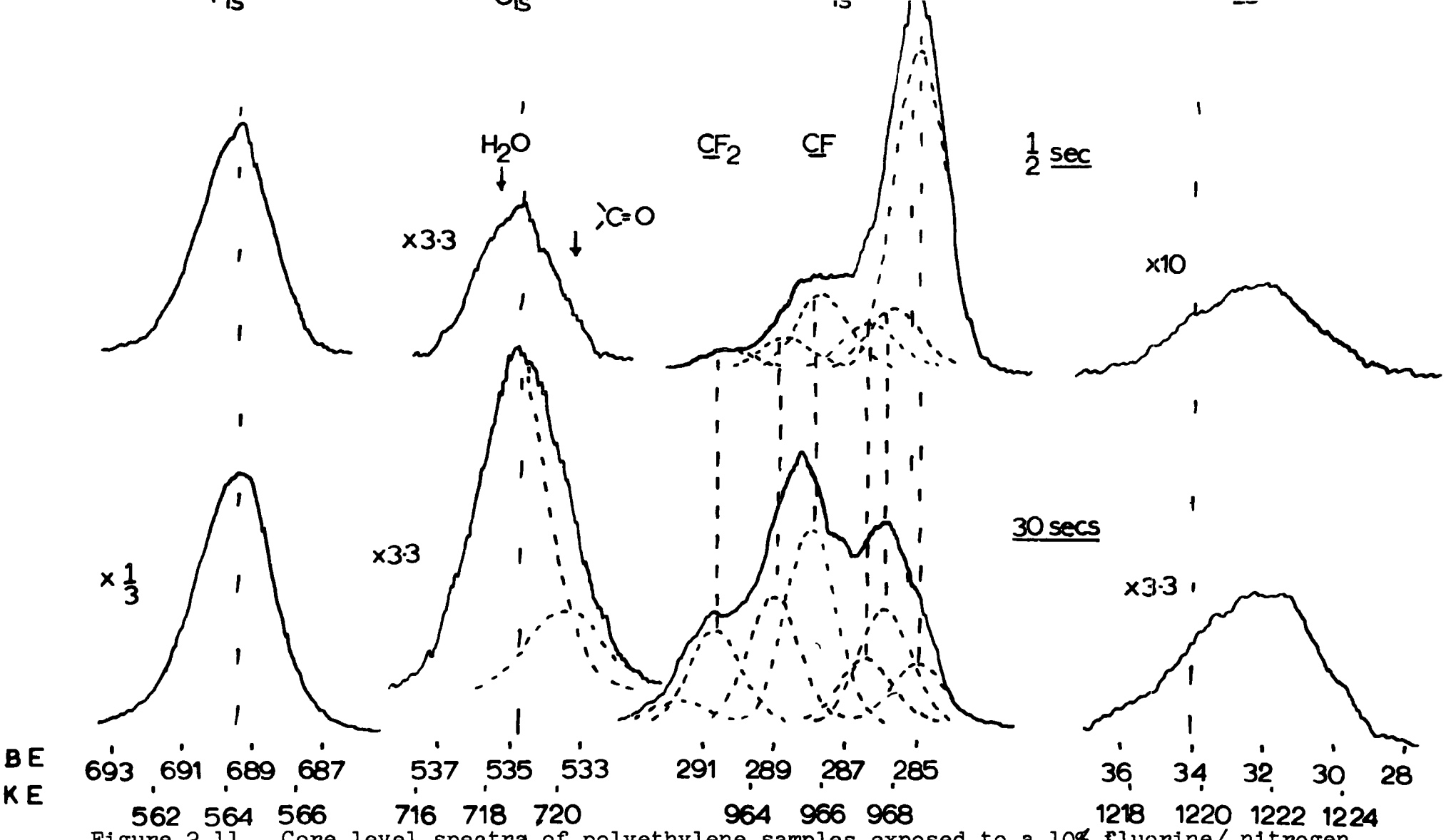

Figure 2.11. Core level spectra of polyethylene samples exposed to a 10% fluorine/ nitrogen mixture for $\frac{1}{2}$ sec. and 30 secs. respectively.

approaches that appropriate to polytrifluoroethylene.[123]

Although it is not appropriate to discuss this investigation in any greater detail here it should be evident from this that the time dependence of the chemical modification of polymers particularly in the initial stages may readily be followed by ESCA.

7.2 Modification by Plasmas and Discharges

The interaction of polymers with plasmas and with discharges in general forms the basis for several processes of industrial importance. Argon ion bombardment for example forms the basis for the CASING[146] process for improving adhesive bonding, whilst Corona discharge treatments in air which are tailor-made for rapid throughput are widely used for improving printability, wettability, adhesive bonding,etc.[147] The surface and bulk modification of polymers by interaction with plasmas excited in inert gases has also received considerable attention as has the oxidative degradation or ashing of polymers by means of plasmas excited in oxygen.[148] An important area which has received an increasing amount of attention is in surface grafting and surface modification in general of fibres particularly with regard to improvements in shrink, soil and flame-proofing.[149-151] Examples of the application of ESCA in these areas is presented in the ensuing discussion.

The degradation by ablatement of metal/metal oxide surfaces and of semi-conductor surfaces by interaction with argon ions is a widely used technique for effecting analytical depth profiles in such systems for ESCA or Auger investigation. Under normal operating conditions (high voltages, relatively

high beam currents) argon ion sputtering of polymers is extremely rapid and indeed provides a convenient 'sledge hammer' technique for removing polymeric films from metals or semi-conductors which sputter at a much lower rate. By using low voltages and beam currents however polymer surfaces may be cross-linked at convenient rates and under appropriate conditions such processes involve relatively modest levels of ablatement.

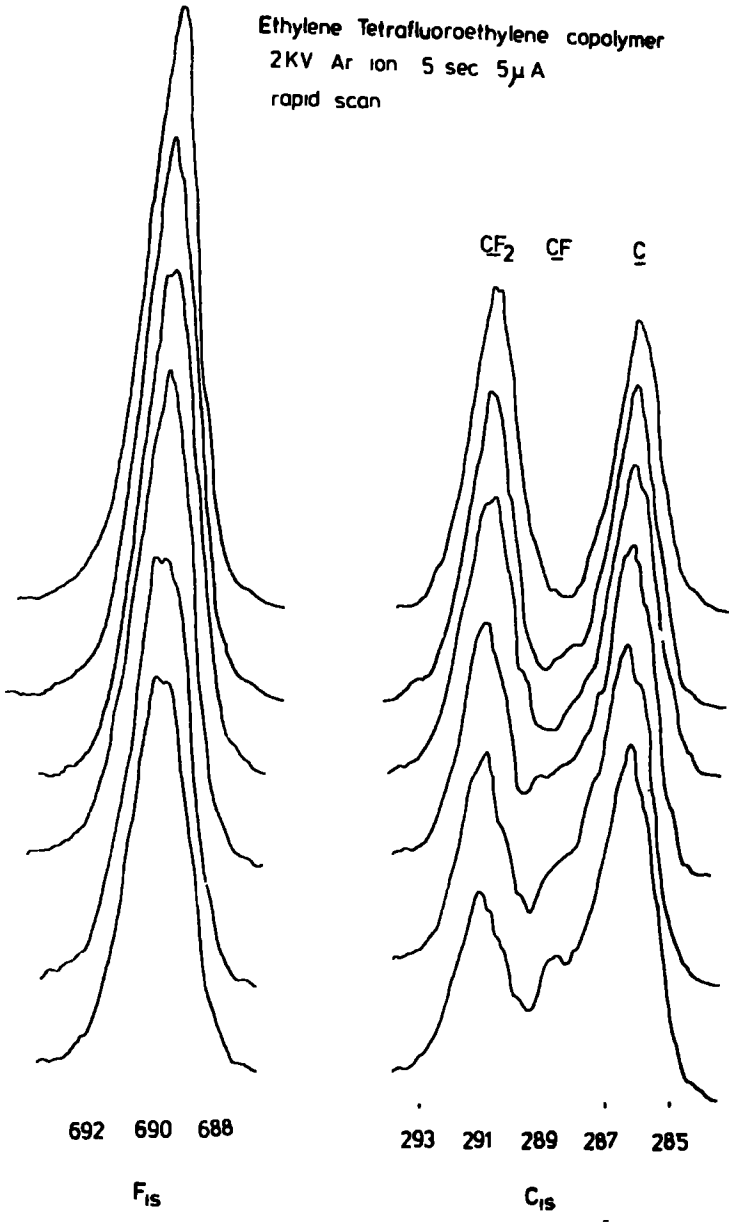

Figure 2.12. F_{1s} and C_{1s} spectra of an ethylene-tetrafluoroethylene copolymer (52% T.F.E.) before treatment and after successive 5 sec. treatments from an Argon ion gun.

Indeed the argon ion bombardment of polymer surfaces forms the basis of the process designated as CASING[146] (Cross-linking by Activated Species of Inert Gases) for improving adhesive bonding.

Figure 2.12 shows the F_{1s} and C_{1s} spectra of a largely alternating ethylene-tetrafluoroethylene copolymer (52% TFE) after irradiation with a low energy (2 kV) beam of argon ions having a beam current of 5μA, for successive periods of 5 seconds.[114] The results are quite striking and it is clear that argon ion bombardment causes extensive modification within the ESCA sampling depth ($\sim 50\text{Å}$ for the C_{1s} levels using $Mg_{K\alpha_{1,2}}$ radiation). The main features are as follows. The F_{1s} signal decreases as does the high binding energy component of the C_{1s} levels due to $\underline{C}F_2$ structural features with a concomitant increase in intensity of a component of intermediate binding energy in the C_{1s} spectrum due largely to $\underline{C}F$ type environments. These preliminary observations are entirely consistent with a crosslinking mechanism in which $\underline{C}H_2$ and $\underline{C}F_2$ features are converted to $\underline{C}H$ and $\underline{C}F$ respectively. From figure 2.12 it is possible, with a knowledge of previously published evidence to tentatively assign a mechanism to the reaction, in terms of cross-linking with the effective elinination of HF.[114]

The Corona discharge treatment of polymeric materials is one of the most widely used techniques for surface modification which essentially entails selective degradation of the surface. ESCA has been used by Millard and co-workers to investigate aspects of some surface treatments of wool fibres.[152-154] Corona discharge and low temperature discharge treatment of wool have been examined as methods of improving surface pro-

perties and shrink resistance. Examination of the S_{2p} levels of the materials before and after treatment indicate that before treatment there is predominantly one kind of sulphur environment (binding energy ∿164 eV) which can be assigned to cystine, together with a minor contributor (binding energy ∿ 169 eV). After treatment the higher binding energy peak is considerably increased at the expense of the cystine sulphur peak. The high binding energy peak corresponds with that observed for toluene sulphonic acid and is evidence for oxidation of cystine sulphur to sulphur(VI). Examination of the N_{1s} levels indicated that no oxidation of amine function had occurred in either process. Further evidence for the surface nature of the oxidation was obtained by re-examining the material after it had been laundered about 70 times, when the high binding energy S_{2p} peak had disappeared.[152]

Plasma polymerization and grafting at surfaces is an area in which ESCA is particularly applicable due to the insoluble nature of the polymers produced. The treatment of wool with a variety of both volatile[149] and non-volatile[150] monomers has resulted in considerable success in shrink, soil and flame-proofing of the fibre whilst not altering the bulk properties of the material. The advent of ESCA has allowed for the direct study of structure and bonding of both the substrate and grafted materials. It is important to distinguish between processes in which the polymer is merely deposited onto the surface of the fabric and actual chemical bonding of monomers to the substrate which greatly extends the life of the coating. These distinct situations have been observed for the example of polypropylene and wool exposed to plasmas excited in hexa-

fluoroethane and tetrafluoroethylene.[149] The spectrum of the polypropylene sample after exposure to the fluorocarbon discharge shows five signals in the C_{1s} region corresponding to $\underline{C}F_3$, $\underline{C}F_2$, $\underline{C}$=O, ($\underline{C}$F and $\underline{C}$-O) and $\underline{C}H_2$ structural features. A similar spectrum is exhibited by the wool sample after a similar treatment although the overall ratio of $\underline{C}H_2$ to C attached to fluorine is greater due to a lower incorporation of fluorocarbon species. The distinguishing feature between these two experiments however is that several of the signals due to carbon attached to fluorine on the wool substrate are ∿ 1 eV lower in binding energy than the corresponding signals of the thicker fluoropolymer film on the polypropylene. This is strongly indicative that the particular structural features are directly bonded to the wool substrate since the lowering of the binding energy is due to the lack of beta fluorine substituent effects[114] as are observed in the fluorocarbon polymer.

An extension of this work has been in the grafting of non-volatile species onto the fabric by exposing impregnated samples to r.f. glow discharges.[150] Although the percentage incorporation of monomers can be determined crudely by conventional techniques the use of ESCA has enabled accurate determinations to be made at the outermost surface of the material and moreover has detected degradation of the monomers themselves (i.e. depletion of bromine from tetrabromophthalic anhydride and tribromomethanilic acid monomers).

The latter part of this thesis is concerned with a detailed investigation of the surface modification of polymers by exposure to r.f. glow discharges excited in a variety of inert gases and oxygen. It will become apparent from this

work that ESCA has indeed a great potential in this field. The unique capabilities of the technique in respect of elaborating details of structure and bonding in samples which are inhomogeneous in the surface regions implies that for definitive studies of the initial stages of polymer degradation ESCA investigations will often be mandatory.

7.3 Mechanical Modifications

The simplest degradative change that can be envisaged is the direct contamination of a polymer surface arising from mass transfer. The utility of ESCA in this area is illustrated by two simple examples.

The first concerns surface degradation associated with the production of pressed polymer films.[114,123] The ESCA spectra of PTFE for sample films which are prepared by pressing PTFE powder between sheets of clean aluminium foil at the minimum temperature necessary for coalescence of the powder particles in a hand press ($\sim 200^{\circ}C$), indicate a surface stoichoimetry exactly corresponding to the bulk with no evidence for extraneous contamination. When the procedure is repeated using a higher temperature ($> 300^{\circ}$) films are produced which visually, bulk chemically and by transmission infrared(TIR) and multiple attenuated total reflectance (MATR) measurements, appear to be the same as those produced at lower temperatures.[114] The wide scan ESCA spectra of such films however are immediately revealing. It is clear from the appearance of peaks associated with the core levels of both oxygen and aluminium that in the higher temperature pressing process a contaminant surface layer of alumina Al_2O_3 is deposited on the PTFE. The thickness of the layer is almost certainly $< 10\text{Å}$. A more

common degradation of polymer surfaces of this genre is that encountered from handling or storing polymer samples in contact with one another. In the former case the usual manifestation is the detection of a low binding energy (~285 eV) component in the C_{1s} spectra and of O_{1s} signals originating from hydrocarbon material and surface hydrogen bonded water respectively.[114] However the latter situations are many faceted. One of the most important facets of contacting polymer surfaces relates to the phenomenon of triboelectric charging.[155] Contacting polymer films from opposite ends of the so-called triboelectric series results in charge transfer such that there is a considerable build up of static charge on each component of the contacting pair. Such charge transfer could conceivably occur via electron transfer from the material of low to that of higher work function thus equalizing the fermi levels or alternatively by mass transfer (transfer of ions) between the two components of the contacting pair. Even more likely is that both processes are of importance however the two possible mechanisms are not entirely separable since the propensity for adsorption of ions at the surface of a given polymer will undoubtedly be a subtle function of its electronic structure as will the work function. It is known that triboelectro-phenomena in general are explicable in terms of a charge density of the order of 1 in 10^4 of surface sites which is probably an order of magnitude lower than can currently be detected by ESCA. Nonetheless it is of interest to see if in contacting polymer samples there is mass transfer or not between the components.[155] If mass transfer is observed it certainly does not resolve the problem of how charging occurs but it certainly allows one to say that mass

transfer cannot be ruled out as a possible mechanism.

The surfaces of a variety of polymer films both before and after contacting events have therefore been investigated.[155]

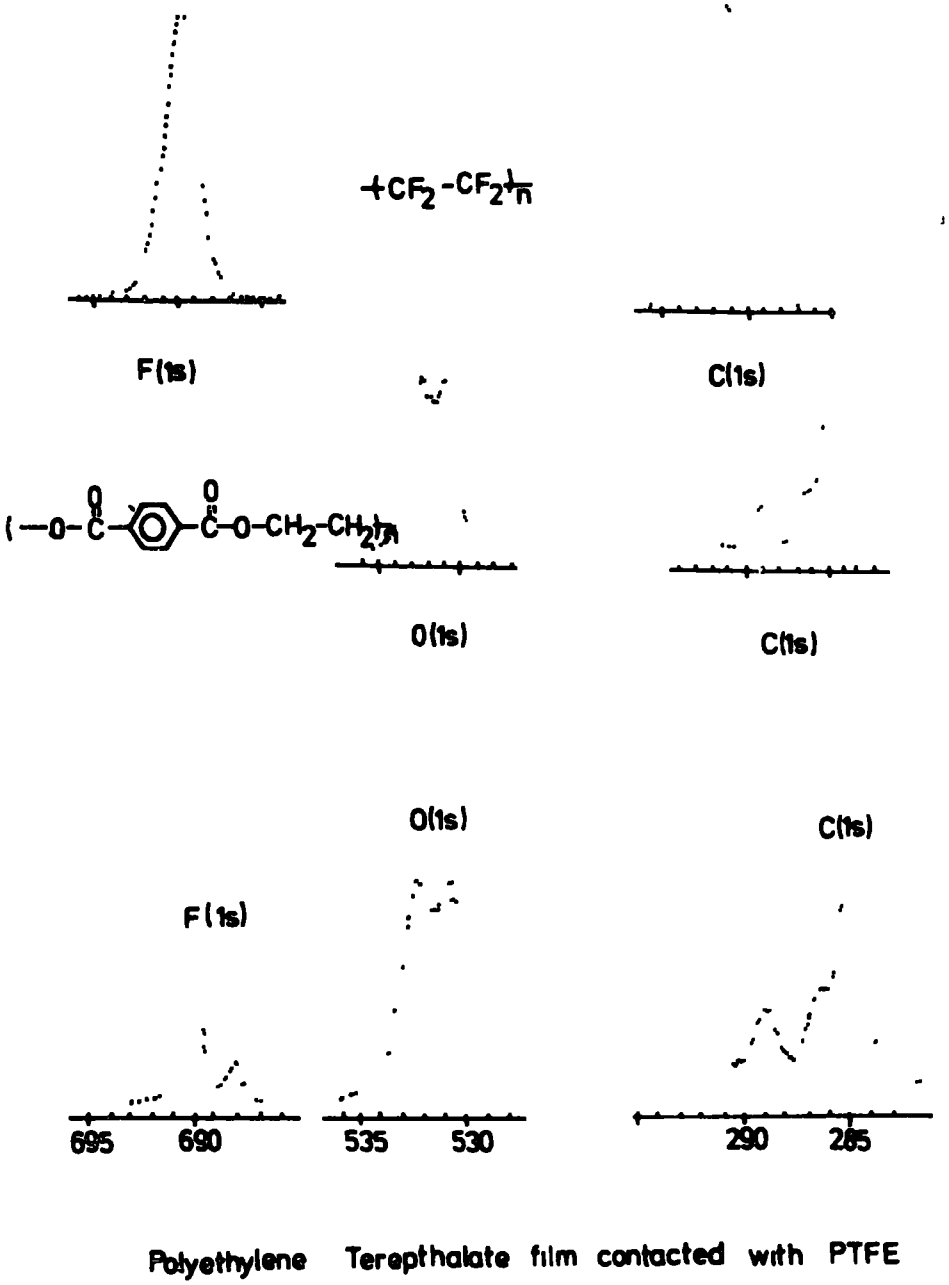

Figure 2.13. Core level spectra of polytetrafluoroethylene, polyethyleneterephthalate and a polyethylene-terephthalate film after being 'contacted' with polytetrafluoroethylene.

The great advantage of such an investigation by means of ESCA is the ability to look at both halves of contacting pair. As one example figure 2.13 shows the core level spectra for PTFE, and PET films, which are highly characteristic for each polymer. In addition there is also shown the core level spectra for the polyethylene terephthalate component after lightly contacting the PTFE film. Since the polymers are from the opposite ends of the triboelectric series the films show a strong tendency to adhere to one another, even on a light contact. The observation of the high binding energy component in the C_{1s} spectrum and the observation of the F_{1s} level shows that some PTFE transfers to the PET surface. It may be estimated that this represents fractional monolayer coverage. Of particular interest is the fact that in the F_{1s} peak in addition to the major high binding energy component associated with covalent $\underline{C}F_2$ linkages there is a lower binding energy peak attributable to fluoride ion thus providing evidence for bond cleavage accompanying the mass transfer. Examination of the other half of the component namely PTFE shows the presence of PET as evidenced by the characteristic O_{1s} and C_{1s} levels. These simple experiments illustrate the utility of ESCA in this area.

CHAPTER THREE

Shake up Phenomena in Polymers

1. Introduction

For a complete study, by ESCA, of any polymeric system, whether homogeneous or otherwise it is important to be familiar with and have at hand means of interpreting all of the available information levels. The hierarchy of information levels in the ESCA experiment has previously been discussed in Chapter One, and listed in Table 1.1. This chapter describes work pioneering the use of Shake-up phenomena to elucidate fine details of structure and bonding in polymer systems,[55,56,128,129] which are not directly attainable from the primary sources of information (absolute and relative binding energies and relative peak intensities).[55,56,128,129,156] The study of shake up structure has already proved to add a new dimension to ESCA studies of structure and bonding pertaining to transition-metal complexes.[157]

A detailed introduction to shake up phenomena has already been given in Chapter One, (Section 2.4) and it will suffice here therefore to reiterate the main points. The removal of a core electron, which is almost completely screening as far as the valence electrons are concerned leads to substantial electronic reorganization accompanying the core ionization. This provides a sufficiently strong perturbation for there to be a finite probability for simultaneous excitation of an electron from a higher occupied to a lower unoccupied valence level (shake up) and in the limit leads to a doubly ionized state (shake off). It may be shown theoretically[57] that the weighted average over the energies of the direct photoionization, and associated shake up and shake off peaks, is equal to the binding energy appropriate to the un-

relaxed system as would be obtained from Koopmans' Theorem.[43] Extensive theoretical studies, both in this and other laboratories have shown that although relaxation energies (given as the energy difference between the computed binding energies, including relaxation, and Koopmans' Theorem) depend significantly on the local electronic environment, they nonetheless fall within a narrow range[42] (e.g. for C_{1s} levels typically 12 ± 2 eV). It may be inferred from this, therefore, that shake up and shake off processes are perfectly general. However, our extensive studies of polymer systems to date[52,127,129] suggest that it is only in systems which have either an unsaturated backbone or pendant group that shake up peaks of considerable intensity and at energies much lower than the typical relaxation energies are observed. In studying solids by ESCA it is worthwhile emphasizing, however, that low-intensity transitions arising from shake up or shake off processes of energy >10 eV are largely masked by the tail arising from inelastic scattering events. Figure 3.1 shows the C_{1s} spectra for high density polyethylene and polystyrene. For the latter, the well developed shake up structure due to $\pi^* \leftarrow \pi$ transitions is clearly evident.

In order to apply the observation of shake up phenomena to further the scope of ESCA in studying structure and bonding in polymers it is important to identify the electronic transitions involved and also to establish how the shake up satellites vary, in terms of lineshapes, peak positions and peak intensities, as a function of structure and substituent effects in the polymer. / In this chapter a detailed experimental and theoretical investigation of shake up structure is described for a broad range of unsaturated polymers. Partic-

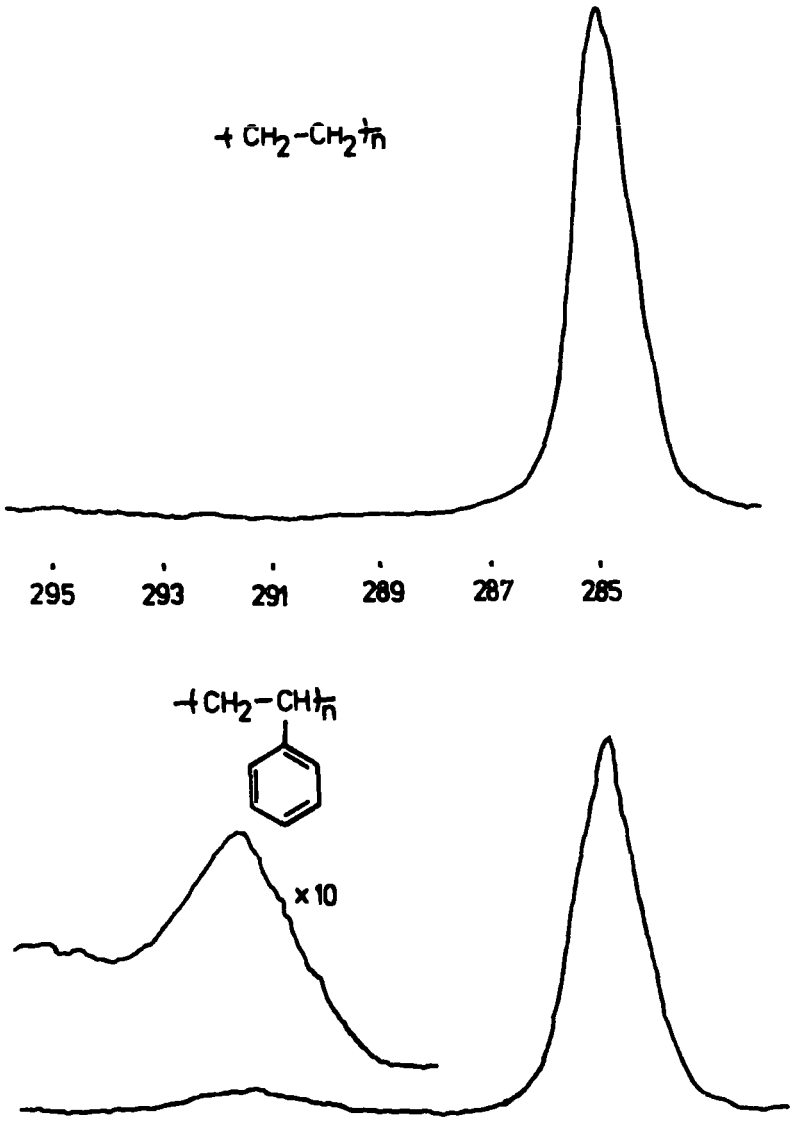

Figure 3.1. C_{1s} spectra of polyethylene and polystyrene.

ular emphasis is placed on the study of a series of poly (para-substituted) styrenes[55,129] as prototype systems to investigate the effects of substituents on the shake up structure. The application of shake up phenomena to the study of structure and bonding in polymers is extended to copolymer systems, in Section 6 revealing the potential of shake up

observations in the determination of comonomer compositions and indirectly to an understanding of surface morphology.[55,128]

2. Experimental

2.1 Samples

The homopolymer samples used in this investigation were obtained from Cellomer Associates, Webster, New York. Those received as powders were studies as received, mounted onto the ESCA probe tip by means of double sided Scotch tape, and complete coverage was monitored by means of the O_{1s} and Si_{2p} levels. Samples received as large granules were difficult to powder and were therefore studied as solvent cast films evaporated onto a clean gold substrate which in turn was mounted onto the probe tip. Table 3.1 lists the polymers used and the form in which they were studied. For the solvent cast films the solvent is also indicated.

Table 3.1. Sample Preparation

Polymer	Form	Solvent
Polystyrene	powder	
Poly(para-t-butyl-styrene)	powder	
Poly(para-methyl-styrene)	powder	
Poly(para-chloro-styrene)	powder	
Poly(para-bromo-styrene)	powder	
Poly(para-methoxy-styrene)	powder	
Poly(para-amino-styrene)	powder	
Poly-4-vinyl-pyridine	cast film	ethanol
Poly-2-vinyl-pyridine	cast film	chloroform
Poly-1-vinyl-naphthalene	powder	
Poly-2-vinyl-naphthalene	powder	
Polyacenaphthalene	powder	

Polymer	Form	Solvent
Polyvinylcarbazole	powder	
Polydiphenyl-siloxane	cast film	benzene
Polydimethyl-siloxane	cast film	benzene
Polyethylene	extruded film	

For comparison purposes spectra were also recorded for toluene, para-t-butyl-toluene, para-chloro-toluene, para-tolualdehyde and para-toluic-acid. Para-toluic-acid was studied as a powder on a cooled probe tip and the remaining samples were studied as thin films condensed onto a cold (-150°C) probe tip from a directed beam of vapour in the spectrometer source at a pressure of $\sim 10^{-7}$ torr. Under such conditions a random orientation of the substituted toluene molecules in the solid phase would seem to be most probable.

The alkane-styrene copolymers discussed in section 6 were kindly donated by Dr. D.H. Richards, ERDE, Waltham Abbey, England and the method of synthesis has previously been described.[158] The samples were studied as received, either in the form of powders (alkane chain length = 1,3,5) or in the case of the low Tg materials (alkane chain length = 6,10) as films smeared onto gold foil. A short investigation was also made on films cast from cyclohexane, benzene, toluene and bromobenzene.

2.2 ESCA Spectra

Spectra were recorded on an AEI ES200AA/B spectrometer using $Mg_{K\alpha_{1,2}}$ radiation and under the conditions employed in this investigation the $Au_{4f_{7/2}}$ level at 84.0 eV binding energy used for calibration purposes, had a FWHM of 1.15 eV. Deconvolution and integration of spectra was achieved by means of

a Du Pont 310 Curve Resolver. In all cases the measured energies are quoted with a precision of ± 0.2 eV and area ratios ± 5%.

The first and second derivatives of several of the shake up spectra were calculated manually by measuring the tangent to the spectrum as a function of energy. The accuracy of such a technique is necessarily poor due to the sacrifice of signal to noise statistics as the price for increased resolution.

2.3 U.V./visible Spectra

U.V./visible spectra were recorded on a Unicam SP800 spectrometer for the poly(para-substituted) styrenes using spectroscopic chloroform and for poly-4-vinyl pyridine using spectroscopic ethanol as solvent. In the particular case of the para-amino derivative the sample was discoloured and this taken together with the fact that it was essentially insoluble suggest oxidation and cross linking. It should be emphasized however that a relatively low degree of oxidative degradation and cross linking would be sufficient to account for these observations and would not necessarily seriously interfere with the ESCA studies. Thus the ESCA data falls into line with that for the other materials, and the fact that the surface is not extensively oxidized is readily confirmed by the spectra recorded for the O_{1s}, N_{1s} and C_{1s} core levels.

U.V./visible spectra were recorded for the alkane-styrene copolymers using spectroscopic chloroform as solvent in all cases.

3. Theoretical

The experimental investigations have been closely accompanied by theoretical calculations on model systems. The theoretical interpretation of the data pertaining to the intensity of the low energy shake up satellites has been within the sudden approximation, equivalent cores concept and CNDO SCF MO formalism. Within this approximation the probability of observing a transition from an occupied orbital Ψi corresponding to an unrelaxed valence electron in the hole state to a virtual orbital Ψf for the hole state (which follows monopole selection rules)[159] is proportional to $\langle \Psi i | \Psi f \rangle^2$. In partial justification for this simplistic single electron excitation approach, configuration interaction (CI) calculations have also been carried out to provide data on state mixing and the relative energies of the various excited states involved.

The model systems for the poly(para-substituted)styrenes, for which the justification will become apparent in the ensuing discussion, were chosen as simple substituted toluenes. Similarly the model systems for the remaining polymers were constructed by replacing the polymer backbone by a methyl group.[56] Holestate species were approximated by the appropriate equivalent cores system. The choice of simple molecules is intuitively appealing since a vast body of experimental and theoretical data is available on the excited states of these systems.[160-162]

In addition to the use of the standard CNDO/2 program calculations were also undertaken using a variable parameter version of CNDO which was originally developed[163] for interpreting various aspects of the excited states of molecules for

which the standard CNDO/2 parametrization[67] is inappropriate. One centre one electron integrals were derived from those given by Sichel and Whitehead[164] as were the one centre two electron integrals. Two centre one electron integrals were calculated using a Wolfsberg Helmholtz[165] relationship with a scaling constant of 0.7 which had previously been shown to provide an adequate account of the excited states of simple unsaturated systems.[163,166] Best atom exponents of Clementi and Raimonde were employed,[167] and two centre two electron integrals computed from a refined Mataga relationship.[168] Configuration interaction calculations were carried out considering all singly excited states generated from the two highest occupied and lowest unoccupied pi orbitals and calculations were also carried out in which configurations arising from excitations involving the totally symmetric pi orbital of the benzene ring system and the corresponding virtual orbital were considered.

The geometries for the model compounds used in the theoretical investigations were calculated from standard bond lengths and bond angles.[169] The computations were carried out on an IBM 360/67 computer and for a typical convergence limit of 10^{-5} a.u. in the total energy calculations the total c.p.u. time required was typically 100-400 secs.

The eigenvectors calculated from the CNDO package[67,163] describe the molecular orbitals in terms of basis functions consisting of the atomic valence orbitals.

That is:

$$\psi_i = \sum_{u=1}^{n} Cui\ \phi u \qquad (3.1)$$

$$\psi_f' = \sum_{v=1}^{n} KvF\ \phi' v \qquad (3.2)$$

where Ψ_i and Ψ_f' are the appropriate orbitals for the initial and final state, with Cui and Kvf being the weighting coefficients for the atomic orbitals i.e. $\emptyset u$ and $\emptyset' v$. This is a linear combination of atomic orbitals (LCAO).

Hence the shake up probability may be computed in the simplistic framework of a one electron transition as:

$$P_{f \leftarrow i} = N \left| \sum_{u=1}^{n} Kuf\ Cui \langle \emptyset' u | \emptyset u \rangle \right|^2 \qquad (3.3)$$

since $\langle \emptyset' i \mid \emptyset j \rangle = 0$ when $i \neq j$.

Furthermore, $\langle \emptyset u' \emptyset u \rangle$ is closely approximated by 1 and therefore:

$$P_{f \leftarrow i} \propto \left| \sum_{u=1}^{n} Kuf\ Cui \right|^2 \qquad (3.4)$$

Equation (3.4) reduces the calculation of shake up probabilities to a simple summation of the products of the corresponding weighting coefficients for the initial and final state wavefunctions and squaring the result.

4. Shake up Phenomena in Poly(para-substituted)Styrenes

4.1 Core Level Spectra

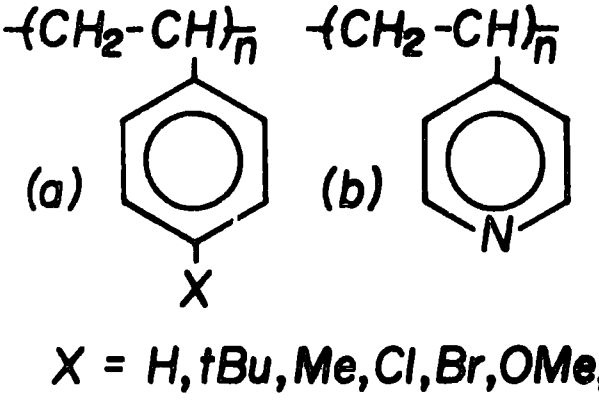

Figure 3.2. General formula of the poly(para-substituted) styrenes and poly-4-vinylpyridine.

The series of polymers described in this section[129] have the general formula shown in Figure 3.2.

The core level spectra for the series of poly(para-substituted)styrenes are shown in Figures 3.3 - 3.6. In each

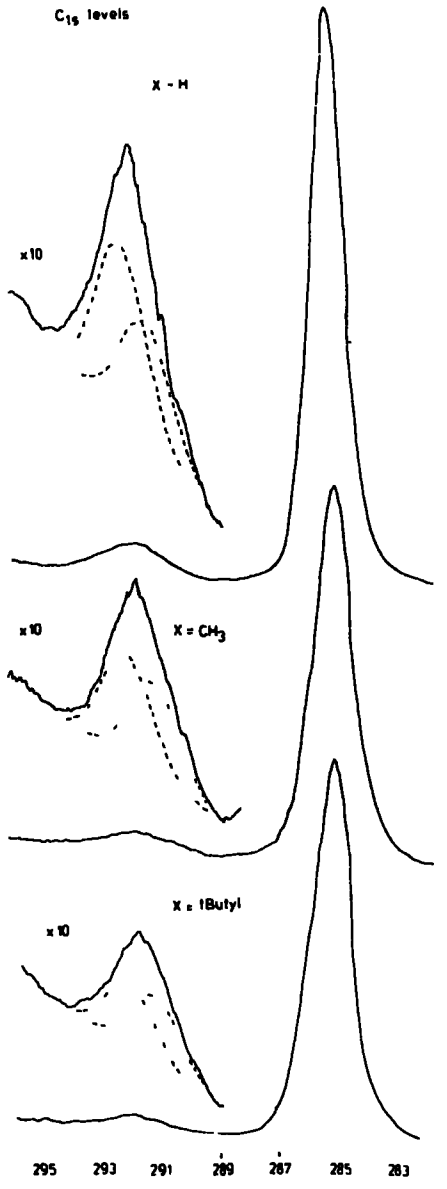

Figure 3.3. C_{1s} spectra of polystyrene, polyparamethylstyrene and polypara-t-butylstyrene.

case well developed satellites are clearly apparent to the low kinetic energy side of the direct photoionization peaks

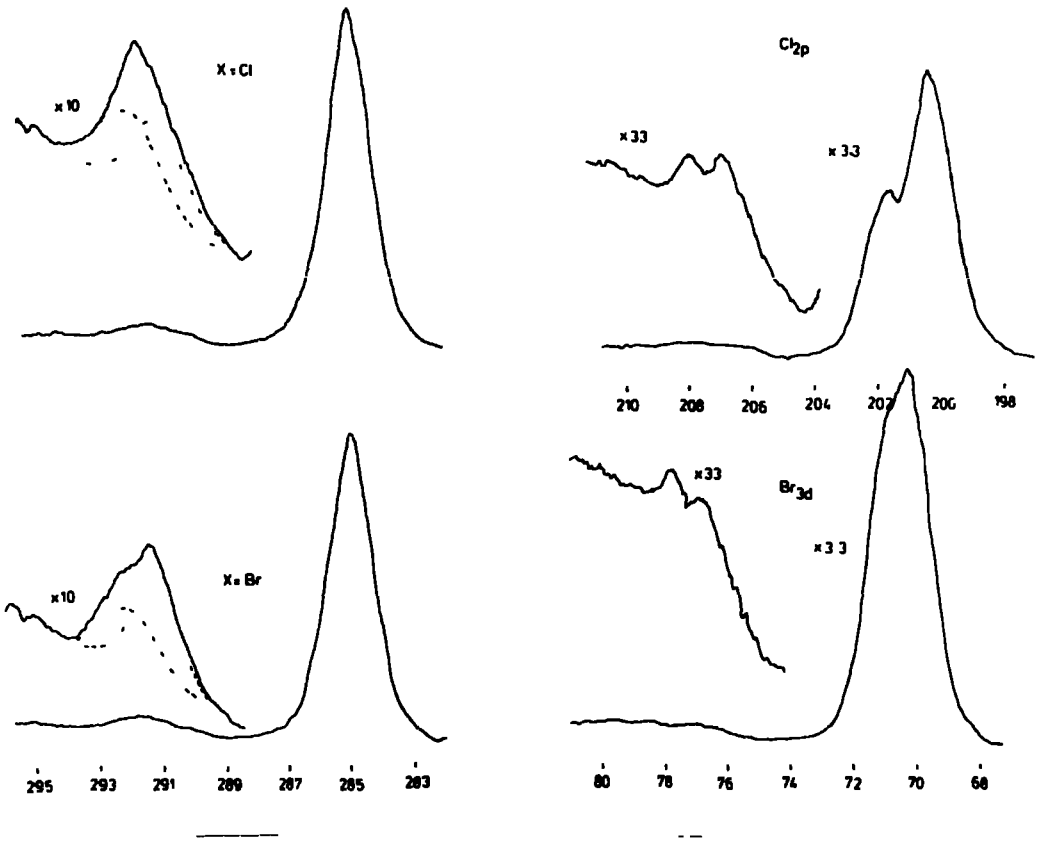

Figure 3.4. C_{1s} and Cl_{2p} spectra of polyparachlorostyrene and the C_{1s} and Br_{3d} spectra of polyparabromostyrene.

for both the C_{1s} levels and the core levels of the substituent. It is clear that in terms of the overall intensity and band profile these satellites are markedly dependent on the substituent. Before considering these satellites however we may briefly consider the data pertaining to direct photoionization of the relevant core levels. In each case the centroids of the C_{1s} levels other than for carbons directly bonded to the substituent are at 285.0 eV and analysis of the shoulder evident to the higher binding energy side of the main photoionization peak yields substituent effects of 1.3 eV, 1.2 eV, 1.7 eV, 1.3 eV and 0.9 eV for Cl, Br, OCH_3, NH_2 and (N) (Table 3.2). These are in good agreement with previously published

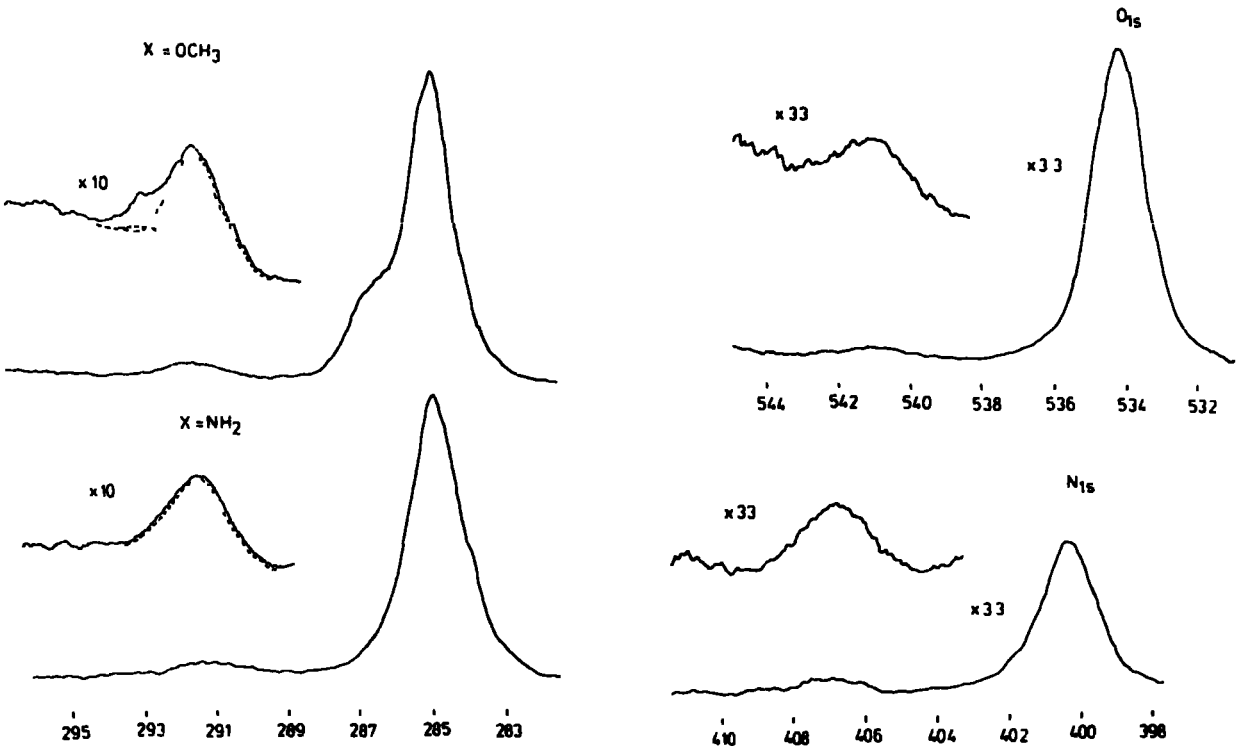

Figure 3.5. O_{1s} and C_{1s} spectra of polyparamethoxystyrene and the N_{1s} and C_{1s} spectra of polyparaaminostyrene.

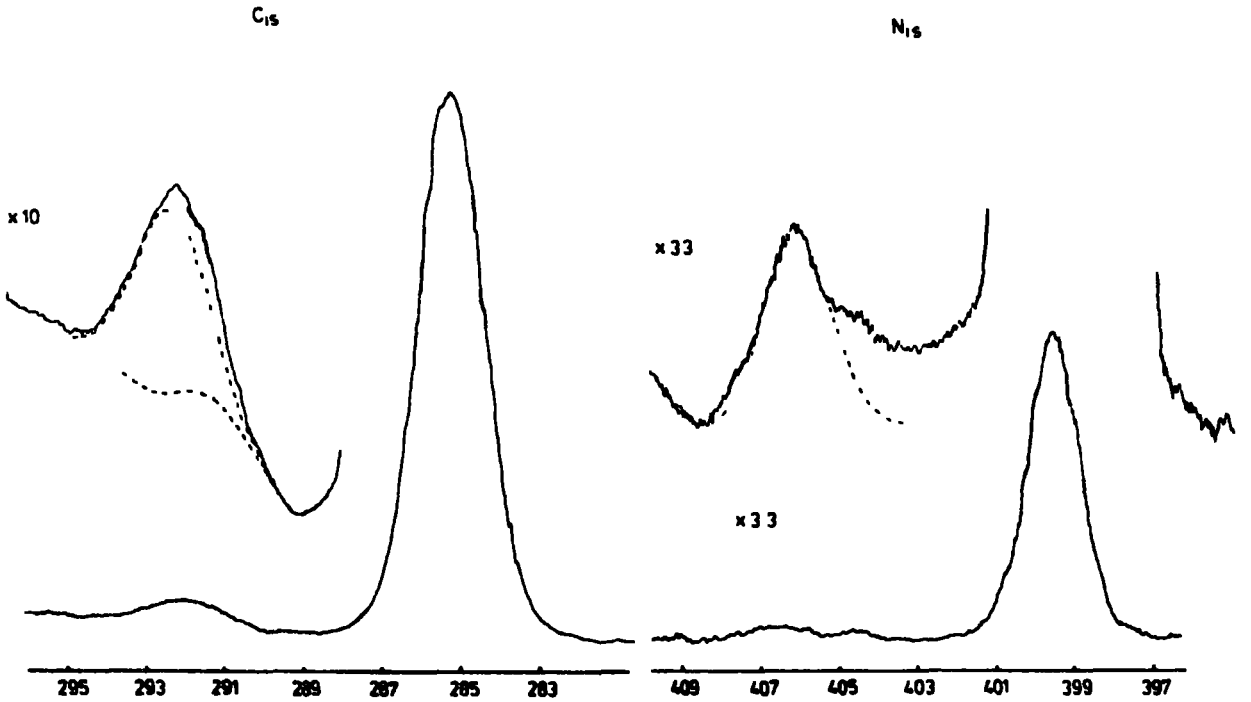

Figure 3.6. N_{1s} and C_{1s} spectra of poly-4-vinylpyridine.

data on simple model systems.[170-172] For the substituents the absolute binding energies are also in excellent agreement with those previously reported for simple model systems and in particular it is interesting to note that the shift of ~0.9 eV for the pyridine type versus the amino type nitrogen is also consistent in this respect.[173] This provides strong evidence that the extent of oxidation is sufficiently small such that the ESCA data essentially corresponds to the polymer formulation given in figure 3.2.

Measurement of relative area ratios for the core levels of the substituent with respect to the C_{1s} levels for the series of polymers confirmed by comparison with model systems that in each case the repeat units were statistically sampled.

4.2 Shake up Spectra

In considering the overall band profiles, energy separations and relative intensities for the low energy satellite structures a few general conclusions are self evident. Firstly for the parent system the marked asymmetry of the satellite strongly suggests that at least two transitions are involved. This conclusion is reinforced on consideration of the data pertaining to the para substituted derivatives in which the substituent is either a strong pi electron acceptor or pi electron donor (viz. (N), Fig. 3.2b versus NH_2, Fig.3.2a); the asymmetries of the overall band profiles being in the opposite sense for the two extremes in electronic demands of the substituents. The centroids for the satellite structures increase in energy separation with respect to the direct photoionization peaks as the para substituent changes from being an overall pi electron donor to a pi electron acceptor.

Table 3.2. Shake up data for the poly(para-substituted)styrenes

Substituent X	Core Level	Binding Energies[†] (eV)	Mean Shake Up Energy (eV)[††]	Total Shake Up Intensity (%)[†††]	FWHM Ratio[††††] (satellite/main peak)
(N)	C_{1s}	285.0 285.9	7.1	5.8	1.37
H	C_{1s}	285.0	6.6	8.1	1.85
tBu	C_{1s}	285.0	6.5	7.5	1.50
Me	C_{1s}	285.0	6.5	7.0	1.50
Cl	C_{1s}	285.0 286.3	6.7	6.3	1.50
Br	C_{1s}	285.0 286.2	6.6	5.9	1.51
OCH_3	C_{1s}	285.0 286.7	6.7	3.7	1.29
NH_2	C_{1s}	285.0 286.3	6.4	3.3	1.25
(N)	N_{1s}	399.5	6.5	7.1 (7.3)	1.25
Cl	Cl_{2p}	200.5 201.9	6.5	2.7 (3.0)	1.00
Br	Br_{3d}	69.8 70.9	6.8	1.9 (2.3)	1.27
OCH_3	O_{1s}	534.2	6.6	2.0 (3.8)	1.26
NH_2	N_{1s}	400.4	6.4	5.8 (12.3)	1.24

† Binding energies relative to hydrocarbon at 285.0 eV

†† Measured to centroids of asymmetric satellite peaks

††† Intensities expressed as a percentage of the total intensity due to the core level from atoms in the ring and directly attached to the ring. Figures in brackets refer to the relative substituent/carbon shake up intensity for equal numbers of atoms.

†††† Measured for undeconvoluted shake up satellites

The most striking feature however is the strong dependence (on the substituent) of the overall intensity of the shake up satellites, with respect to the direct photoionization peak. Table 3.2 shows the relevant data. It is clear that the overall shake up intensity for the C_{1s} levels decreases with increasing pi electron donating or accepting power of the para substituent. The trend for the shake up satellites associated with the core levels of the substituent on the other hand exhibit a clear trend in the opposite sense. This becomes more evident on consideration of the ratio corrected for equal numbers of atoms. The intensity ratio for the methoxy derivative is almost certainly a lower limit since there is some evidence from the O_{1s} spectrum that there is a small amount of water and/or oxidation at the surface (i.e. the core level area ratios indicate a stoichiometry somewhat higher in oxygen content than for that indicated in figure 3.2a).

Figures 3.7 and 3.8 show the core level spectra for toluene, para-t-butyl toluene and para-chlorotoluene for comparison and it is clear that the shake up structures are closely similar to the related polymer system in terms of both peak intensity and band profile.

It is appropriate at this point to include also the spectra of para-tolualdehyde and para-toluic-acid (figure 3.9) the para substituents in this case being pi electron acceptors.

Table 3.3 summarizes the integrated intensities of the shake up satellites relative to the direct photoionization peak for the toluene derivatives and again it is clear that the shake up intensity decreases with either increasing electron accepting or donating character of the substituent (cf Table 3.2).

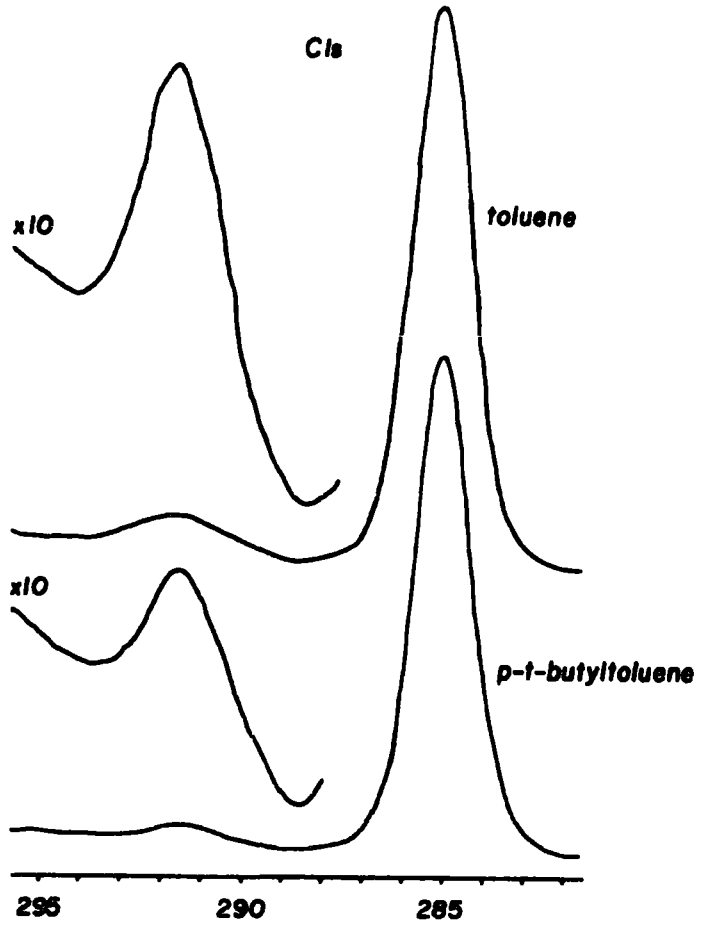

Figure 3.7. C_{1s} spectra of toluene and para-t-butyltoluene.

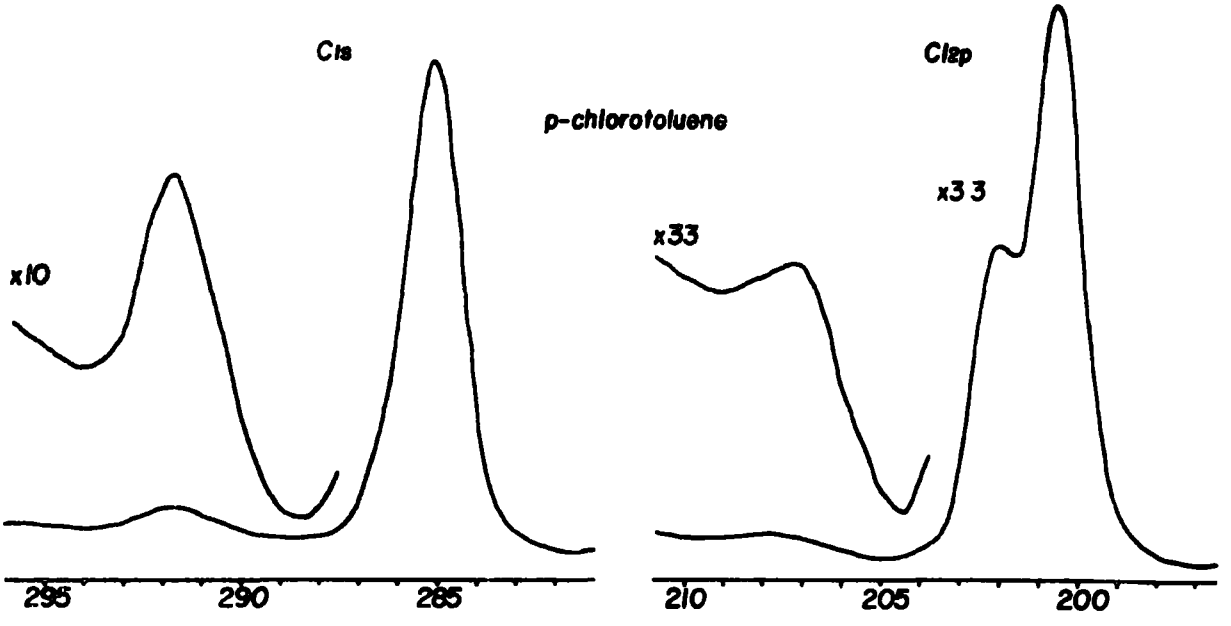

Figure 3.8. C_{1s} and Cl_{2p} spectra of parachlorotoluene.

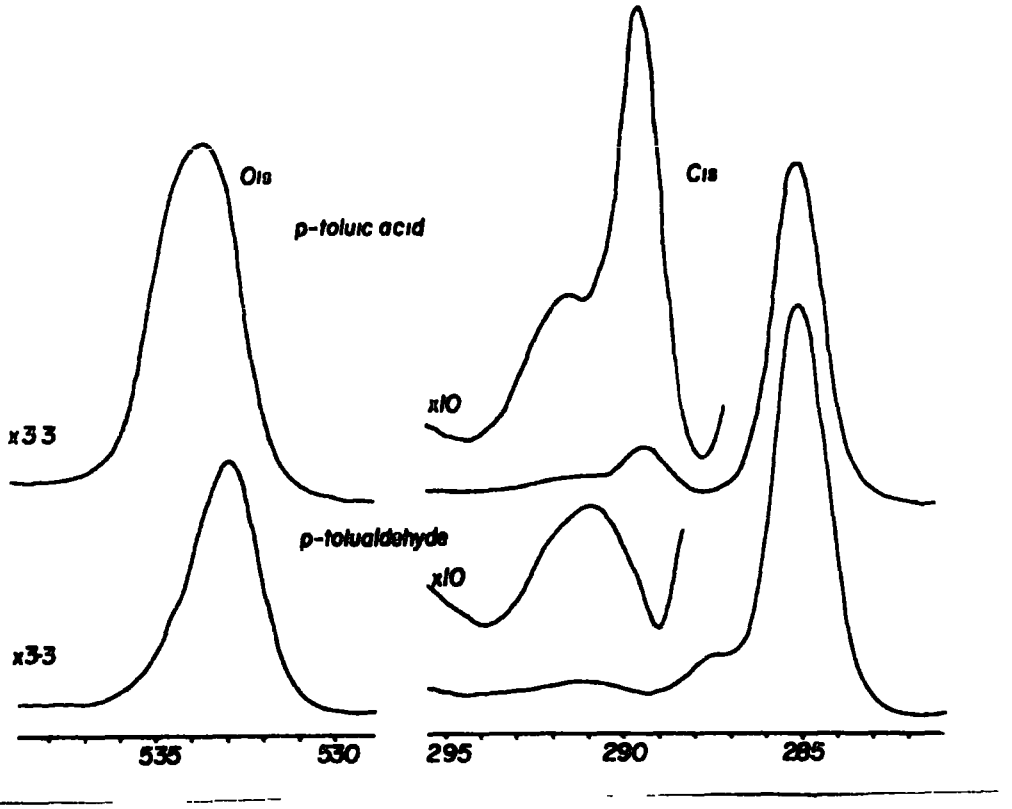

Figure 3.9. O_{1s} and C_{1s} spectra of paratolualdehyde and paratoluic acid.

Table 3.3. Shake up intensities of the parasubstituted toluenes

Para substituent	Intensity (%) †
- H	7.6
- t Bu	7.0
- Cl	6.3
- CHO	6.2
- COOH	7.3

† Intensities expressed as a percentage of the total intensity due to the core level from atoms in the ring and directly attached to the ring.

Since as has been previously described in section 2.1 the toluene derivatives were studied as thin films condensed onto a cold probe tip such that randon orientation of the molecules would seem to be most probable, the close similarity of the shake up structure of these systems (Figures 3.7 and 3.8) to those of the related polymers in terms of both band profile and intensity, (statistically corrected for differing numbers of carbon atoms) emphasizes two important points. Firstly, the poly(parasubstituted)styrene repeat units are effectively statistically sampled by ESCA, an observation previously noted for the core level spectra. This is the usual situation for polymers of short repeat units but not necessarily the case for longer repeat units,[128] (see section 6). Secondly, the similarity of the shake up spectra strongly emphasizes that the shake up transitions, following monopole selection rules,[159] are effectively localized within a given pendant group of the polymer. The para-substituted toluenes therefore might be expected to be good model systems for the poly(parasubstituted) styrenes and it will be seen in section 4.4 that calculations on the parasubstituted toluene systems provide a sound basis for the theoretical interpretation of the shake up data pertaining to the polymers.

Two parameters are commonly used in relation to substituent effects on the low lying $\pi^* \leftarrow \pi$ dipole excited states of substituted benzenes.[160,161] The first, Platt's spectroscopic moment[160,174] relates to the intensity change on substitution of the benzene 2600Å band and is given by the square root of the increase in maximum extinction coefficient on substitution. The second, the coulomb integral of a given substituent[161] derives from a localized orbital description of the dipole excited

states of substituted alternants and non alternants and is a measure of the change in potential of an electron in a 2pz orbital on an adjacent carbon atom. This may be derived experimentally by analysing the first order inductive shift in non alternants and second order shift in alternants.

The u.v. spectroscopic parameters, Platt's spectroscopic moment and Coulomb integral of the substituent are well defined for the mono-substituted benzene systems in the literature.[160,161] Figure 3.10 shows the correlation of the shake up intensity with Platt's spectroscopic moment and with the coulomb integral of the substituent. The correlations with the data pertaining

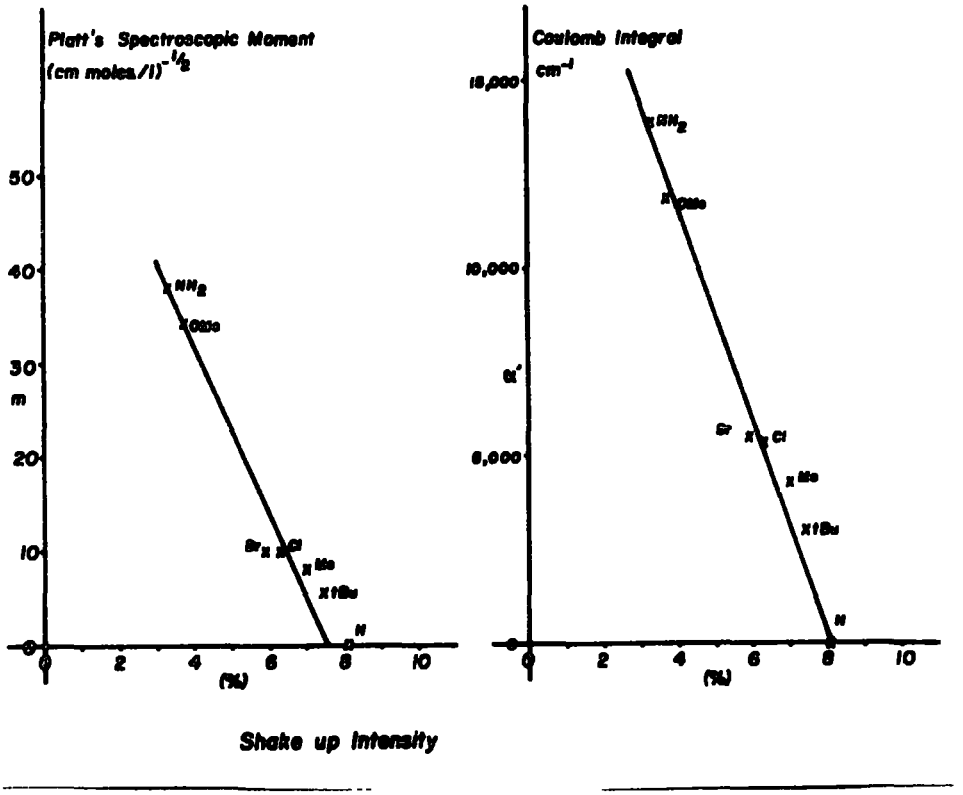

Figure 3.10. Shake up intensity versus Platt's spectroscopic moment and the coulomb integral of the substituent.

to the corresponding transitions for the neutral molecule (which of course follow dipole as opposed to monopole selection rules) are quite striking and leave little room for doubt that the satellites are in fact due to $\pi^* \leftarrow \pi$ transitions. Comparison of gas phase[175] with condensed phase data for substituted benzenes has suggested unambiguously that there is little contribution to these low energy satellites by discrete energy loss processes in the solid. This is also apparent from the study of thin unsaturated polymer films deposited onto gold foil, since similar structure is not observed for the Au_{4f} levels, as would be the case if discrete energy losses occurred in the polymer film.

The final column in Table 3.2 is the ratio of the FWHM for the shake up satellite and the direct photoionization peak. The considerable range of these values, along the distinct asymmetry of some of the shake up satellites strongly indicates that more than one transition is involved. To obtain a more complete understanding of the components involved in the shake up processes, it is of considerable interest to theoretically calculate the relevant transition probabilities. It will become apparent from section 4.4 that with the aid of the calculations a unique deconvolution of the shake up satellites is possible.

4.3 U.V./visible Spectra

As a prerequisite to the theoretical interpretation of shake up phenomena in polymers it is necessary to choose model systems which may be accommodated by the CNDO/2 computer program. Preliminary evidence for the suitability of related toluene systems has been given by the close similarity of their shake up spectra with those of the polymers. However, a more

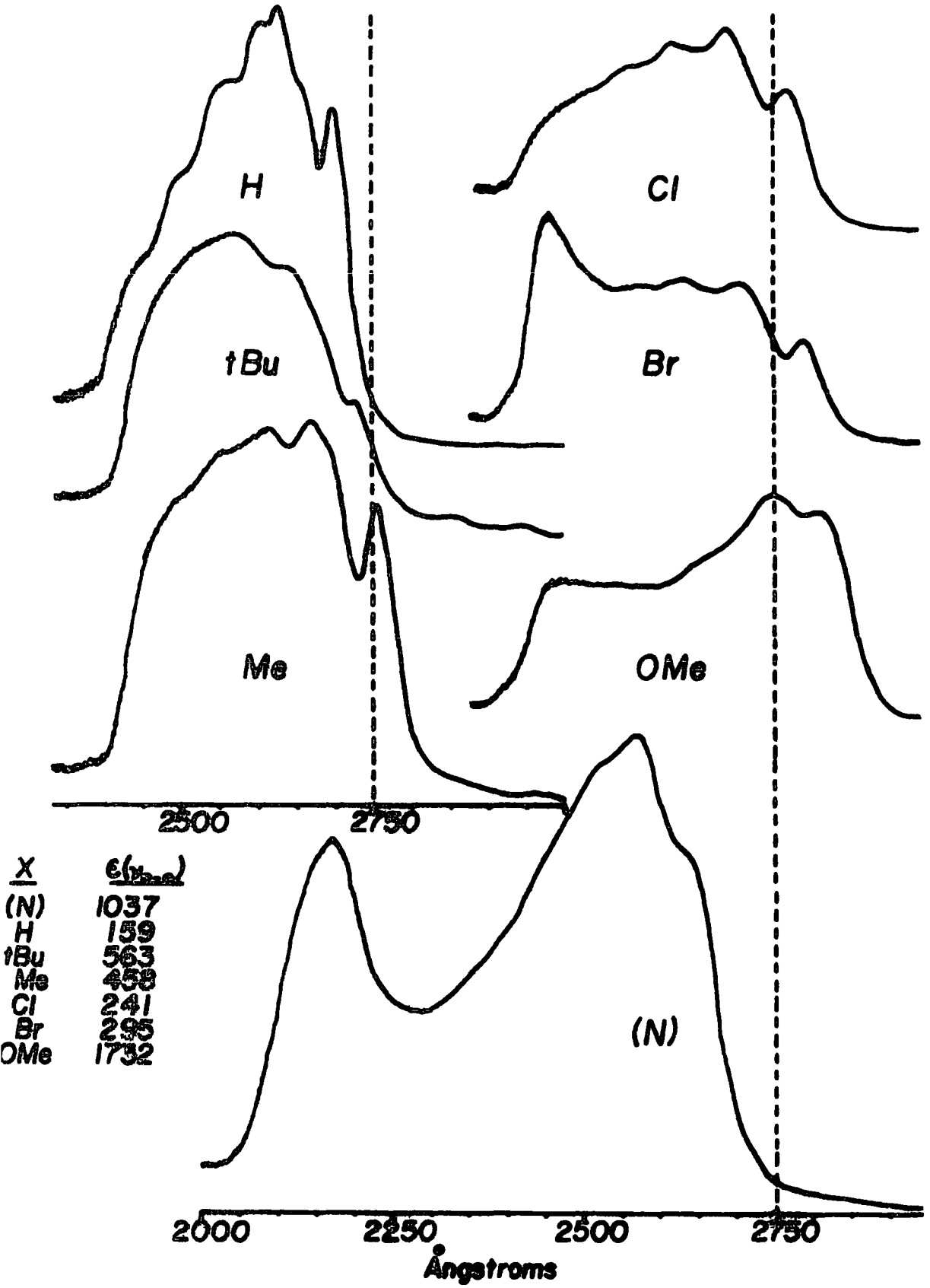

Figure 3.11. Ultraviolet spectra in the 2600Å region for the series of poly(parasubstituted) styrenes and poly-4-vinyl pyridine.

sensitive comparison is likely to be via their ultraviolet spectra. Figure 3.11 shows the ultraviolet spectra, in the 2600Å region, of the series of polymers, excluding poly(para-amino)styrene for reasons discussed in Section 2.3.

The u.v. spectrum of polystyrene in the 2600Å region is closely related to that of toluene,[176] in terms of both extinction coefficients and vibronic fine structure. The effect of para substituents is most conveniently characterized by the shift in the band corresponding to the υ_{0-0} transition[162] as shown in figure 3.12. With the single exception of the

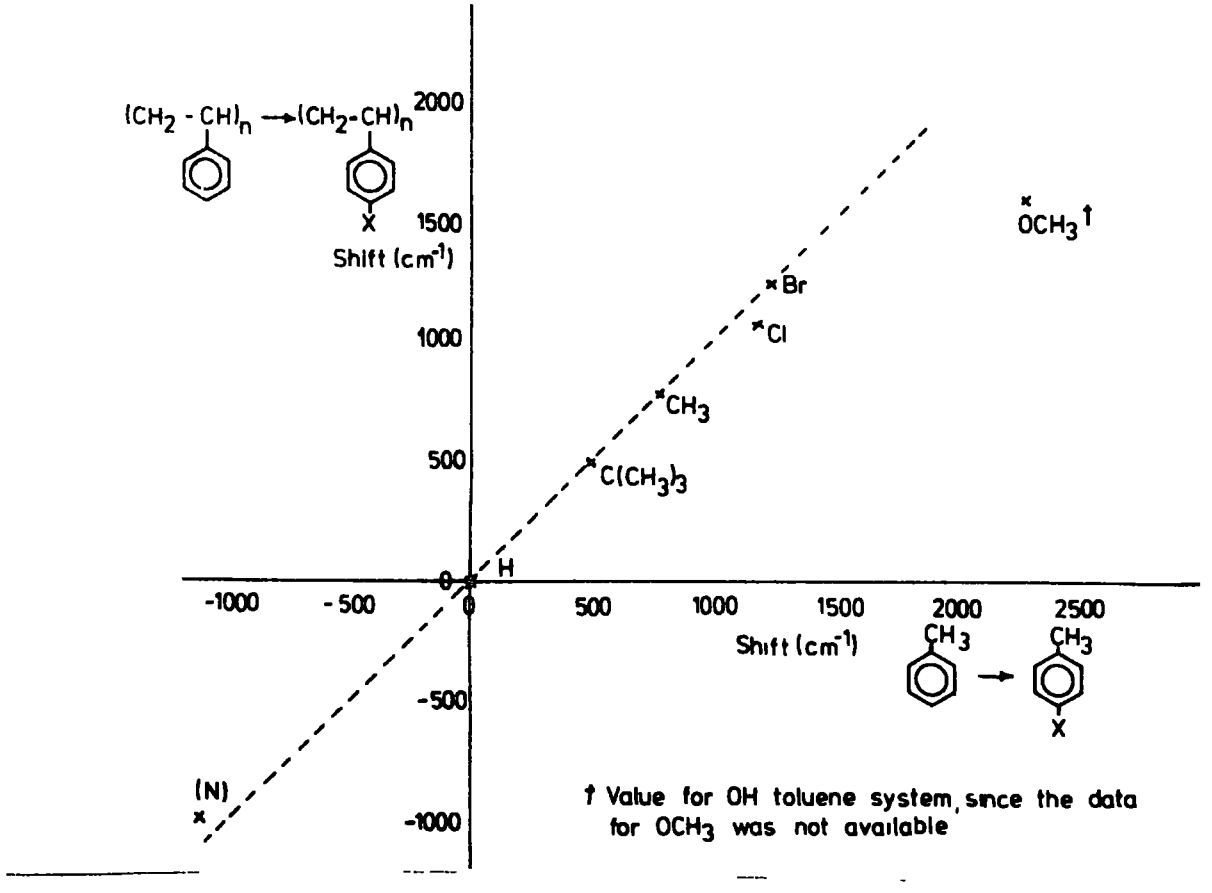

Figure 3.12. Plot of the shift on substitution of the υ_{0-0} band of polystyrene versus that of toluene.

methoxy substituent† the correlation between the experimental data for the para-substituted toluenes and poly(parasubstituted) styrenes in terms of the frequency shift of the long wavelength electronic transition closely follows the dotted line of unit slope. Such a correlation would only be expected if the $\pi^* \leftarrow \pi$ transitions were effectively localized within a given pendant group of the polymer system.

It should be apparent at this stage that all of the available data points to the fact that the para-substituted toluenes form excellent model systems for the poly(parasubstituted)styrenes as far as shake up probabilities are concerned, and we can summarize this as follows: (i) their core level and shake up spectra are closely similar; (ii) the shake up intensities can be correlated to m and α' derived from substituted benzenes; and (iii) the ultraviolet spectra in the 2600Å region show striking similarities.

4.4 Theoretical Interpretation of the Shake up Spectra

From the distinct asymmetry and broadness of the shake up satellites it is clear that at least two transitions must be involved in the shake up processes. Before a detailed interpretation of the shake up spectra is possible it is necessary to gain sufficient background information regarding the number and origin of the excitations and their relative probabilities. The theoretical interpretation of the low energy shake up satellites has been within the sudden approximation, equivalent cores concept and CNDO SCF MO formalism. Within this approx-

---

† The small discrepancy with respect to the methoxy substituent may partly be attributed to the small extent of oxidation previously noted from the study of relative intensities of the core levels. The implication from this is that the oxidation, however small, extends throughout the bulk.

imation, the probability of observing a transition from an occupied orbital ψ_i corresponding to an unrelaxed valence electron in the hole state to a virtual orbital ψ'_f for the hole state is proportional to $\langle \psi_i | \psi'_f \rangle^2$.

Considering firstly a discussion based on states described by a single electron excitation, figure 3.13 shows the four one electron transitions which could conceivably be involved in the low energy shake up satellites. It is convenient in discussing the results to classify transitions in terms of orbital excitations with symmetries designated with respect to the approximate local C_{2v} symmetry of the pi systems for the parent model.

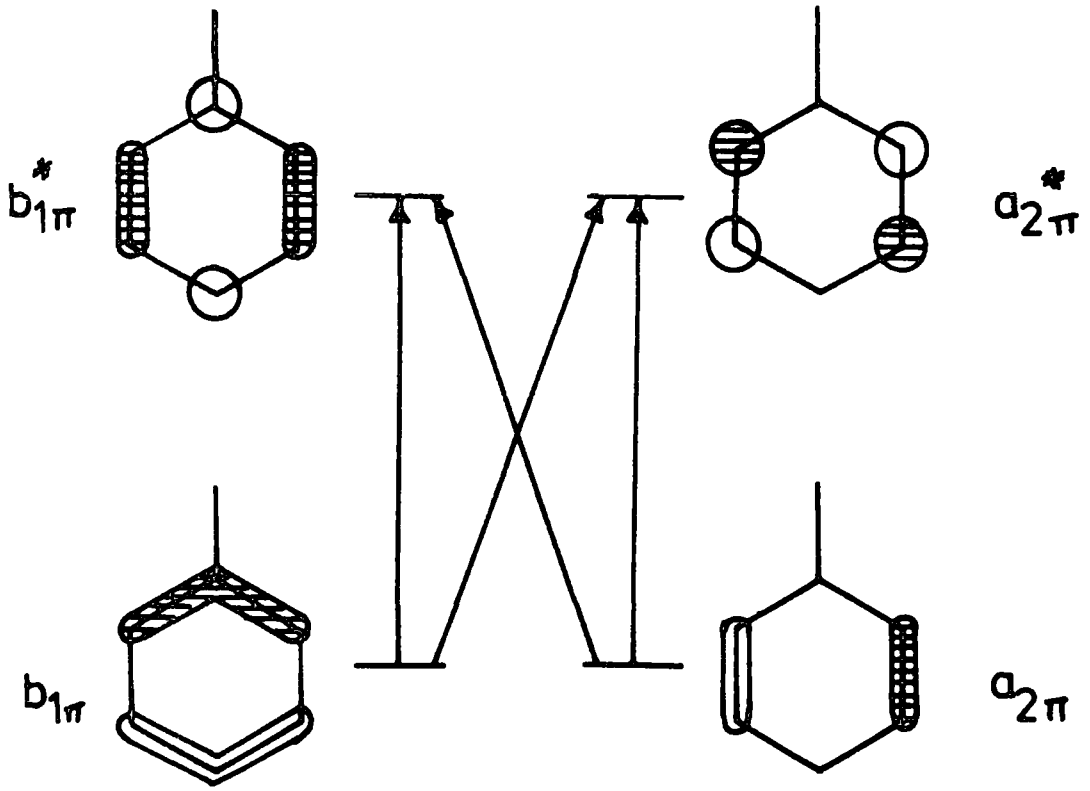

Figure 3.13. Four one electron transitions.

Before discussing the results it should be pointed out that the electronic reorganizations accompanying core ionizations are substantial and involve both the sigma and pi systems as has been demonstrated in a non-empirical LCAO MO SCF investigation of the core hole states of pyridine and series of small polyatomic molecules.[42,51,177] This being the case it would seem that any discussion of shake up phenomena should accommodate this by employing models in which sigma-pi interactions are taken explicitly into account. Figure 3.14 for example shows the changes in sigma and pi charges as a function of core hole generated for toluene, 4-methyl pyridine and

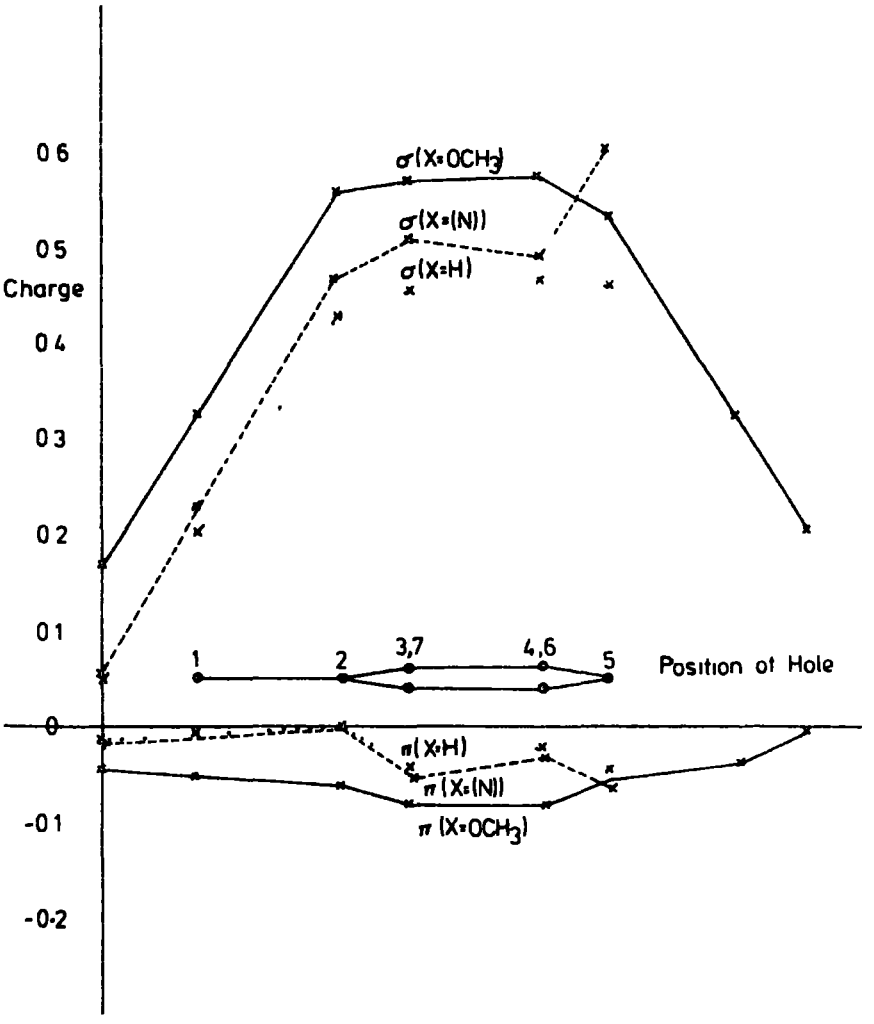

Figure 3.14. Total sigma and pi charge versus hole position for paramethoxy-toluene, toluene and 4-methyl-pyridine.

para-methoxy toluene. It is clear that substantial electronic migrations arise in response to core ionization for both the sigma and pi systems. It seems doubtful therefore if a pi electron only treatment neglecting the mutual interaction with the sigma system would form the basis for a detailed discussion of the shake up data.[175]

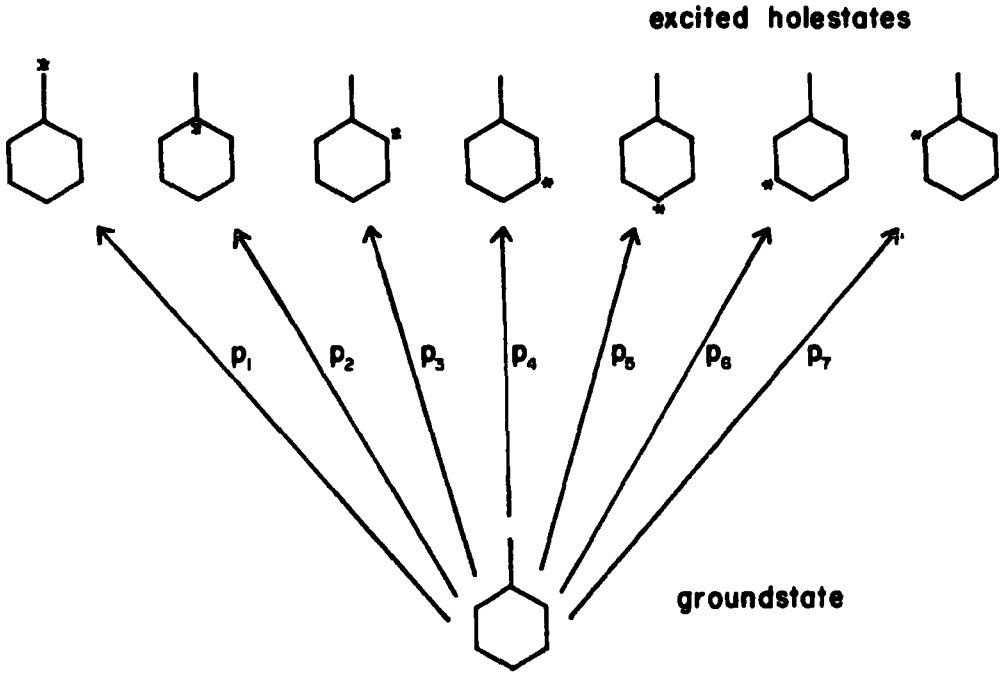

Figure 3.15. Seven holestates of toluene.

Figure 3.15 shows the possible holestates available for toluene, for example. Shake up probability calculations were carried out for all of the possible holestates and the total shake up intensity as observed must be the average value.

The shake up probabilities for toluene and p-methoxy toluene from CNDO SCF variable parameter calculations are shown

Table 3.4. Theoretical data for toluene and paramethoxy toluene

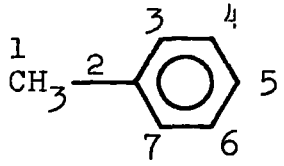

Transition	Atom	% Shake Up 1	2	3	4	5	6	7	8	9	Total C_{1s}	Total O_{1s}
$b^*_{1\pi} \leftarrow b_{1\pi}$		0.90	9.13	3.40	2.23	9.61	2.23	3.40	-	-	4.41	-
$a^*_{2\pi} \leftarrow b_{1\pi}$		0	0	0.06	0	0	0	0.06	-	-	0.02	-
$b^*_{1\pi} \leftarrow a_{2\pi}$		0	0	5.81	6.80	0	6.80	5.81	-	-	3.60	-
$a^*_{2\pi} \leftarrow a_{2\pi}$		0.11	0.01	0	0	0.02	0	0	-	-	0.02	-

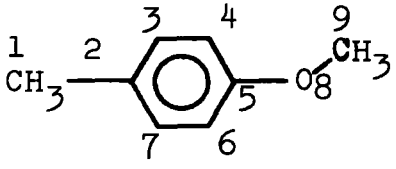

$b^*_{1\pi} \leftarrow b_{1\pi}$		1.15	10.20	3.02	4.07	10.24	3.59	4.08	1.39	0.45	4.60	1.39
$a^*_{2\pi} \leftarrow b_{1\pi}$		0	0	0.06	0.10	0	0.10	0.06	0.48	0.71	0.13	0.48
$b^*_{1\pi} \leftarrow a_{2\pi}$		0	0	6.06	4.84	0	5.36	4.72	0.05	0	2.62	0.05
$a^*_{2\pi} \leftarrow a_{2\pi}$		0.10	0.04	0	0	0.07	0	0	0.03	0.10	0.04	0.03

in Table 3.4. Of the four transitions (shown in Figure 3.13) those arising from $b^*_{1\pi} \leftarrow a_{2\pi}$ and $a^*_{2\pi} \leftarrow b_{1\pi}$ excitation are formally monopole forbidden. However the strong perturbation consequent upon removal of a core electron from an atom off the C_2 axis (i.e. C3, C4, C6, C7), effectively removes the symmetry restriction. This is apparent from Table 3.4.

The intensity of the low energy shake up satellites to the direct photoionization peak for the C_{1s} core levels. largely derives from two transitions: $b^*_{1\pi} \leftarrow b_{1\pi}$ and $b^*_{1\pi} \leftarrow a_{2\pi}$. When hydrogen is replaced by a pi electron donating substituent, whilst the intensity of the $b^*_{1\pi} \leftarrow b_{1\pi}$ transition is predicted to remain essentially the same, that for the $b^*_{1\pi} \leftarrow a_{2\pi}$ transition is predicted to decrease. The computed net overall decrease in shake up intensity of the models is therefore in qualitative agreement with experiment.

In this connection it should be noted that in addition to the relatively high intensity low energy shake up satellite structures observed experimentally for the polymer systems, there is also evidence for higher energy satellites of relatively low intensity. Such satellites almost certainly arise from states involving excitation of the totally symmetric pi orbital and the corresponding virtual orbital.

The trends in the low energy shake up probabilities are more clearly apparent when the data for the series of para substituted toluenes are taken as a whole. This is most readily achieved by a graphical representation of the results as in figure 3.16 in which both CNDO/2 and CNDO SCF variable parameter data are shown. For convenience the horizontal axis is taken as the coulomb integral, which is an experimentally determined parameter.[161] Although these plots have an overall

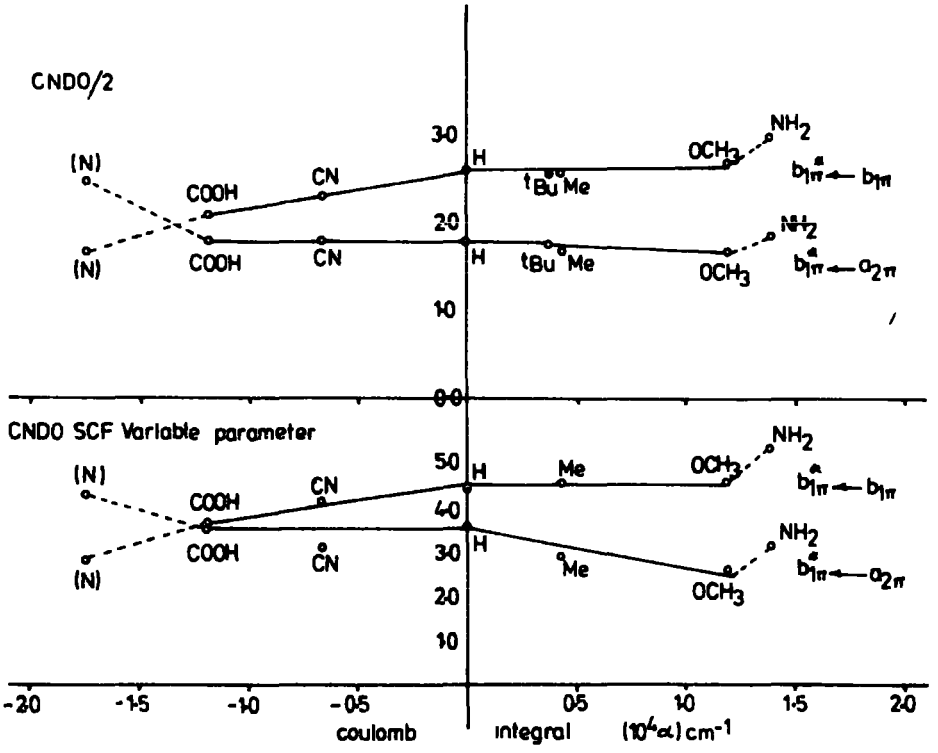

Figure 3.16. Transition probabilities derived from CNDO/2 and variable parameter CNDO calculations versus the coulomb integral of the substituent.

similar appearance, quantitative agreement with experiment is not obtained. On an absolute scale the probabilities from the CNDO/2 parametrization are somewhat smaller than experimentally determined and those from the CNDO SCF variable parameter calculations are larger. This is to some extent, at least, a function of the parametrization, particularly for the equivalent cores species and agreement could no doubt be improved by judicious optimization of parameters. Since the main concern has been to qualitatively understand the data no attempt has been made to improve matters in this direction.

The qualitative agreement in terms of the overall trends is satisfactory particularly with regard to the results from the CNDO parametrization appropriate to the discussion of excited states. The simplistic model is clearly at its worst with substituents representing the extremes in terms of electronic perturbations (N) and NH_2.

It is of interest in this connection to consider the results of the CI calculations. The CI calculations were restricted to toluene as the parent system together with 4-methyl pyridine and 4-methoxy toluene as representatives of substituted systems, with electron attracting and donating substituents respectively. For the methoxy derivative calculations were carried out on two conformers corresponding to the methoxy substituent being in the plane of, or at right angles to the benzene skeleton. Not unexpectedly the calculations revealed that conformational preference significantly affects overall intensities for shake up transitions and indeed it may be envisaged that such an effect could have some potential for studying some aspects of conformational processes by means of ESCA. The results to be presented here however are for the energetically preferred planar arrangement.

Considering firstly the 4-methyl pyridine system the CI calculations including the two highest occupied and two lowest unoccupied pi orbitals confirm the assignment of transition energies in the order $b_{1\pi}^{*} \leftarrow b_{1\pi} < b_{1\pi}^{*} \leftarrow a_{2\pi}$. For core holes which maintain the local C_{2v} symmetry inspection of the state mixing coefficients reveal that the coefficients corresponding to the configurations generated by $b_{1\pi}^{*} \leftarrow b_{1\pi}$ excitations are in the range 0.82 - 0.90. Including all configurations arising from promotion of an electron from an occupied pi orbital to a virtual

pi orbital reinforces this conclusion and the coefficients are then in the range 0.92 - 0.94. For core holes which lower the overall local symmetry of the pi system and which have been discussed in terms of $b_{1\pi}^{*} \leftarrow b_{1\pi}$ and $b_{1\pi}^{*} \leftarrow a_{2\pi}$ transitions the CI calculations again provide a firm basis for this simplistic analysis. State mixing coefficients of $\sim$0.90 and $\sim$0.80 were obtained for the contributions from the configurations arising from single electron excitations corresponding to the $b_{1\pi}^{*} \leftarrow b_{1\pi}$ and $b_{1\pi}^{*} \leftarrow a_{2\pi}$ transitions for the neutral system. The CI calculations including all pi orbitals gave somewhat larger state mixing coefficients than those involving simply the two highest and two lowest unoccupied MO's.

At the other extreme, involving the pi electron donating methoxy substituent, a closely similar pattern emerges and it is interesting to note that the calculated energy separation between the two dominant transitions is calculated to be $\sim$1.0 eV in good agreement with that inferred from the experimental data. The fact that the calculated energy separation is virtually the same for the parent toluene model system and for the substituted derivatives (involving both electron attracting and donating groups) also provides a firm basis for the validity of the analysis.

This theoretical background then provides the necessary information to allow the shake up spectra to be analysed into two main components, conveniently assigned according to the local C_{2v} symmetry of the pendant group, as $b_{1\pi}^{*} \leftarrow b_{1\pi}$ and $b_{1\pi}^{*} \leftarrow a_{2\pi}$. The latter is formally monopole forbidden and is expected to have zero probability when the core ionization it is associated with occurs along the local C_{2v} axis. The shake up satellites

of the substituent core levels, therefore, must only have one component, due to the symmetric $b^{*}_{1\pi} \leftarrow b_{1\pi}$ transition. This is reflected in the constant value of the FWHM ratio of ∿1.25 within experimental error (Table 3.2). The overall trends depicted by the theoretical analysis for the C_{1s} shake up may be applied to the experimental data since it can be justifiably assumed, (Figure 3.16), that the intensity of the $b^{*}_{1\pi} \leftarrow b_{1\pi}$ shake up transition, relative to that of the direct photoionization peak (statistically corrected such that only carbon atoms in the ring and directly attached to the ring are considered) is constant for pi electron donating substituents in the para position (coulomb integral positive); and that the intensity of the $b^{*}_{1\pi} \leftarrow a_{2\pi}$ shake up transition is constant for pi electron accepting substituents in the para position (coulomb integral negative). With this assumption it is clear that the intensity of the $b^{*}_{1\pi} \leftarrow a_{2\pi}$ shake up transition decreases with increasing pi electron donating power of the substituent. Now, the FWHM ratio for the C_{1s} levels of poly (para-aminostyrene) in Table 3.2 is 1.25. This indicates that the large perturbation caused by the amino group reduces the intensity of the $b^{*}_{1\pi} \leftarrow a_{2\pi}$ transition to zero, the satellite having only a $b^{*}_{1\pi} \leftarrow b_{1\pi}$ transition component of intensity 3.3%. Using this value for all the polymers with pi electron donating substituents and the value of 4.8% obtained for the $b^{*}_{1\pi} \leftarrow a_{2\pi}$ transition in polystyrene, for the polymer with a pi electron accepting substituent, yields the overall analysis in terms of components given in Table 3.5. The values of the transition energies, shown in Table 3.5, which increase slightly as the coulomb integral of the substituent becomes a high positive or negative value, indicates that this deconvolution of the C_{1s} shake up satellites

Table 3.5. Deconvolution of the shake up data for the poly(parasubstituted)styrenes

Substituent X	$b^*_{1\pi} \leftarrow b_{1\pi}$ Intensity (%) ††	Transition † Energy (eV)†††	$b^*_{1\pi} \leftarrow a_{2\pi}$ Intensity (%) ††	Transition † Energy (eV)†††	FWHM Ratio†††† (One component/ main peak)
(N)	1.0	6.6	4.8	7.4	1.25
H	3.3	6.2	4.8	7.0	1.48
tBu	3.3	6.2	4.2	7.0	1.25
Me	3.3	6.2	3.7	7.0	1.25
Cl	3.3	6.2	3.0	7.0	1.25
Br	3.3	6.4	2.6	7.2	1.25
OCH_3	3.3	6.6	0.4	7.4	1.21
NH_2	3.3	6.4	0.0	-	1.25

† Symmetries designated as described in text

†† Intensities relative to the signal due to atoms in and attached to the ring

††† Energies measured as the shift of the satellite component from the main peak

†††† Measured for the deconvoluted shake up component

is consistent.† The final column in Table 3.5 shows the ratio of the FWHM for one component of the shake up satellite and the direct photoionization peak. The value of ∿ 1.25 for the substituted derivatives is again consistent, however the parent systems shows a somewhat higher value. This may be more apparent than real since the binding energy range spanned by the chemically equivalent core levels is somewhat less for the parent than for the derivatives. It has been previously noted that shake up satellites typically have a larger FWHM than for the direct photoionization peaks with line width ratios being in the range 1.2 - 1.5.[54] The large FWHM for shake up satellites as compared to the direct photoionization peaks could arise from several sources the most likely of which are unresolved multiplet effects and/or vibrational fine structure, since in general we may expect larger changes in equilibrium geometry in going from the ground state to excited state of the hole state than in going from the ground state of the neutral system to the ground state of the core ionized species. Vibrational broadening would seem to be the most likely explanation for these systems since in the light of recent theoretical work[178,179] it would appear that the multiplet components of shake up satellites differ in energy by a substantial amount. It seems more probable therefore that the satellite peaks of high intensity observed in this work

---

†The available experimental data on the $\pi^* \leftarrow \pi$ excited states of model systems[160,161] shows that substituent effects are typically in the range ± 0.2 eV for the $^1B_{2u}$ (2600Å) band ± 0.5 eV for the $^1B_{1u}$ (2050Å) band and ± 0.4 eV for the $^1E_{1u}$ (1850Å) band. It is not therefore unreasonable that the energies of the $\pi^* \leftarrow \pi$ shake up states should appear to be relatively insensitive to substituent effects with the typical resolution and reproducibility involved in this work.

derive from the multiplet component of the $\pi^* \leftarrow \pi$ excited states of 'singlet' parentage. The corresponding components of 'triplet' parentage are almost certainly of much lower intensity and are probably located in the unresolved region between the direct photoionization peak and the stronger satellite peaks. Analysis of the bond overlap populations in going from the neutral molecule to the equivalent cores species and to the $\pi^* \leftarrow \pi$ excited states reveals a consistent pattern with respect to the likely changes in equilibrium geometries and supports the proposal that the dominant contribution to the increased linewidth of the shake up components arises from vibrational fine structure.

Further evidence for the overall validity of the broad outlines of this interpretation is given by a comparison of the experimental data for the poly(2-vinyl pyridine) with that previously discussed for the 4-substituted isomer. On the basis of the analysis, the lowering of the local symmetry of the pi-system should manifest itself in both shake up transitions being observed for the N_{1s} level. The experimental data clearly provides strong confirmation of this. The observed shake up intensity for poly(2-vinyl pyridine) is 6.4% of the total intensity due to the N_{1s} core level, the FWHM ratio being 1.40 relative to the direct photoionization peak, compared to a value of 1.25 for poly(4-vinyl pyridine). The increased value for the ratio of FWHM for the 2 as compared with the 4 substituted derivative suggests that more than one transition is involved.

Figure 3.17 shows, graphically, the results of the experimentally determined shake up intensities (cf Table 3.5 and figure 3.16).

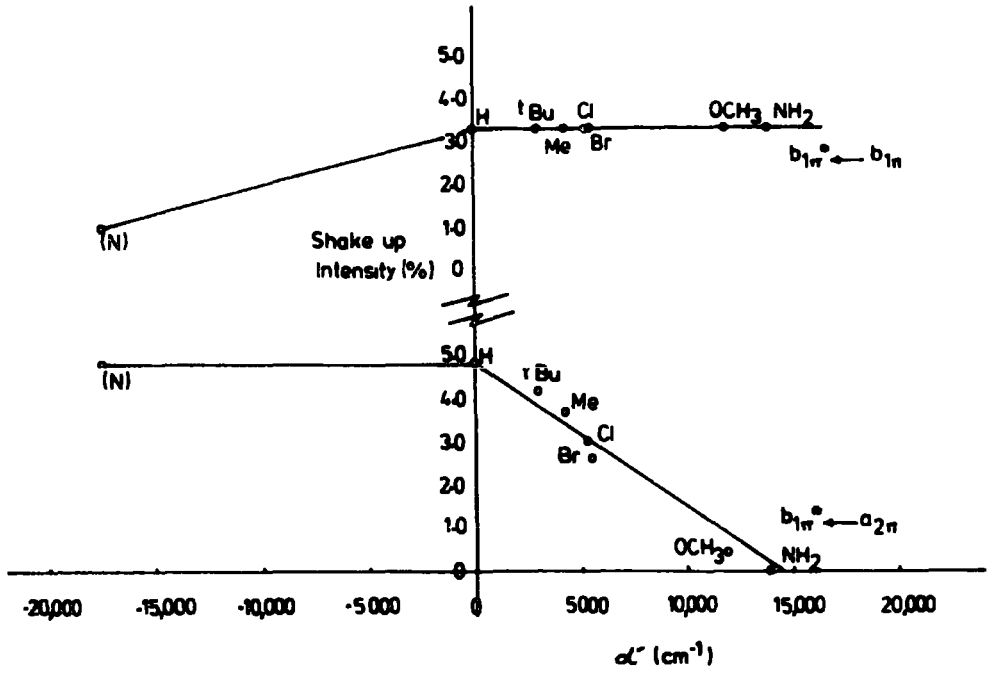

Figure 3.17. Transition probabilities derived from the deconvolution of the experimental data versus the coulomb integral of the substituent.

4.5 Derivative Spectra

So far in the discussion little verification of the transition energies has been possible. In Table 3.5 the component peak positions resulted from treating this parameter as a variable in the deconvolution of the shake up spectra. Furthermore the theoretical calculations used throughout this chapter are not parameterized to reproduce the transition energies. Further information concerning the transition energies should be available, from the application of derivative spectroscopy to the shake up profiles. It must be understood from the outset, however that the enhanced resolution gained from differentiating the spectra is at the expense of the statistical accuracy of the result. It will become apparent from the discussion that despite this drawback the exercise is worthwhile. Figure 3.18 shows the smoothed shake up spectra and the 2nd derivatives. It is immediately clear that very little or no information is readily attainable concerning the relative

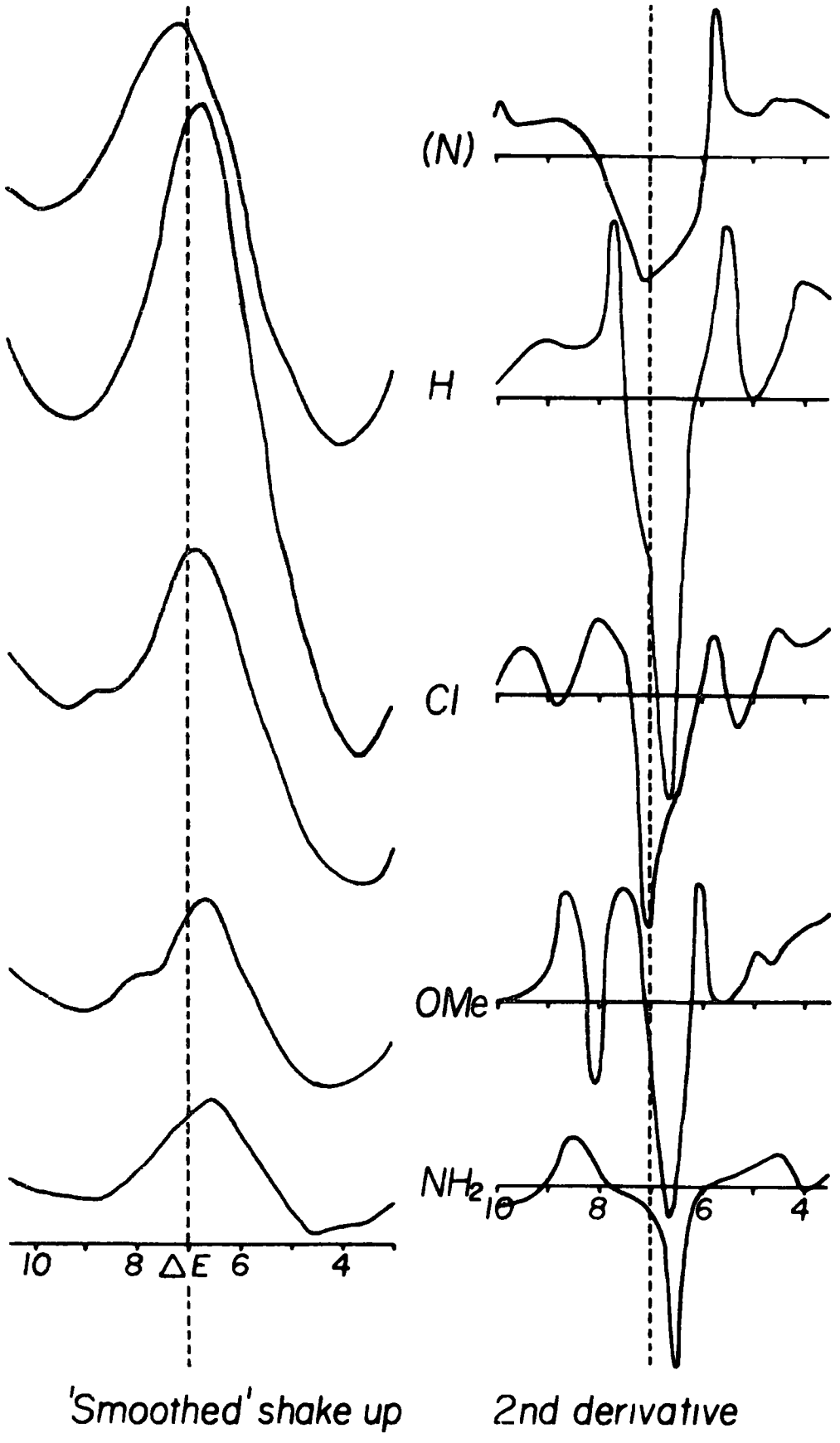

Figure 3.18. Derivative shake-up spectra for the series of poly(para substituted)styrenes.

intensities of the component transitions. Closer inspection however reveals that although the 2nd derivative does not completely resolve the component signals, each spectrum, with the exception of the amino derivative, shows a definite two component structure. This is entirely consistent with the previous conclusions. Furthermore the degree of agreement of the transition energies (obtained by line shape analysis of the derivative spectra) with those listed in Table 3.5 is remarkable and provides strong confirmatory evidence that the overall analysis of the data is internally self consistent.

It should be noted here that the possibility of using analytical curve fitting techniques to obtain derivative spectra of these systems was explored in some detail. It was found however that such methods became very unstable when differentiated to an order greater than one.

5. Shake up Phenomena in Homopolymers

5.1 Core level and Shake up Spectra

Figure 3.19 shows the core level spectra of high density polyethylene, polystyrene, polydimethylsiloxane and polydiphenyl siloxane. While it is clear that the direct photoionization peaks for each of the two pairs are closely similar the replacement of a pendant hydrogen or alkyl group by an aromatic system gives rise to low energy satellite structures of substantial intensity. In the light of the previous data these may be assigned to shake up transitions involving the pi electron systems of the pendant aromatic groups. Such satellite structures could conceivably arise from characteristic energy loss processes; however as has been previously noted the available data would indicate that the contribution

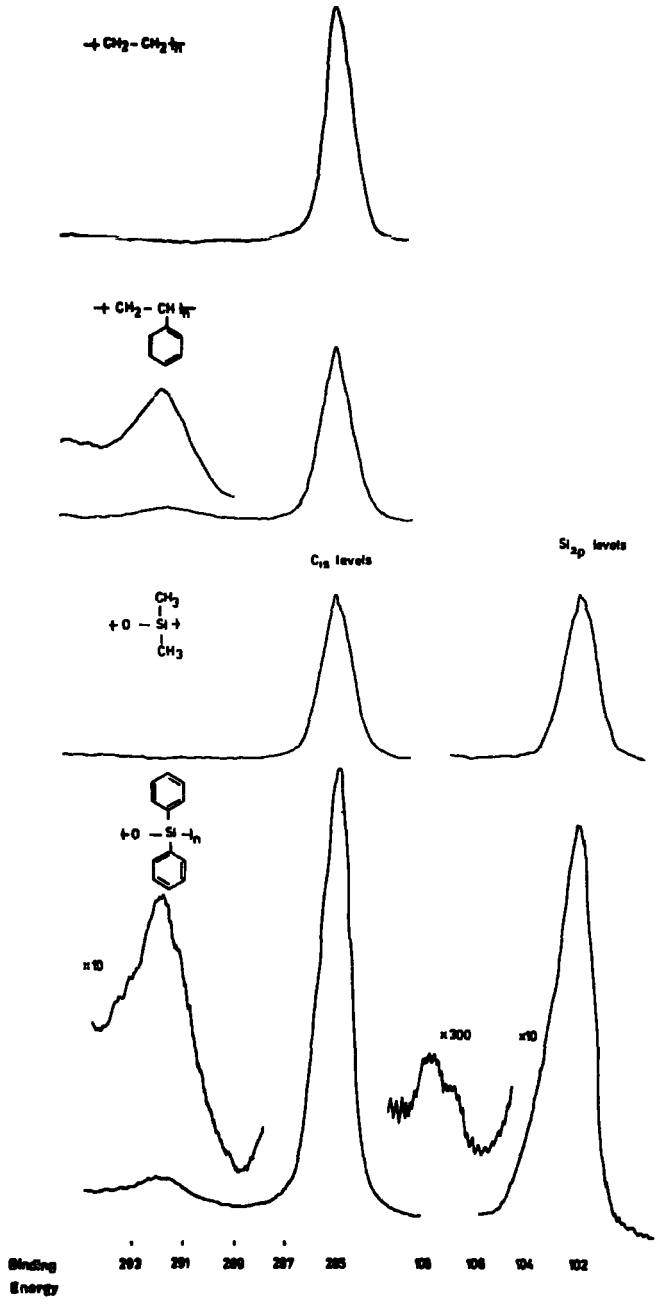

Figure 3.19. Core level spectra of polyethylene, polystyrene, polydimethylsiloxane and polydiphenylsiloxane.

from such a mechanism must be relatively unimportant.[54,175,180] Thus a comparison of satellite structures for simple model systems studied in both the gas and solid phases shows them to be very similar and whilst the interpretation of the gross

features of the overall band profiles and relative intensities for such satellites are well described in terms of an assignment based on shake up phenomena, in general an interpretation in terms of characteristic energy losses would be difficult to sustain.

Figure 3.20 shows the core level spectra for poly-1-and -2-vinylnaphthalenes, polyacenaphthalene and polyvinylcarbazole.

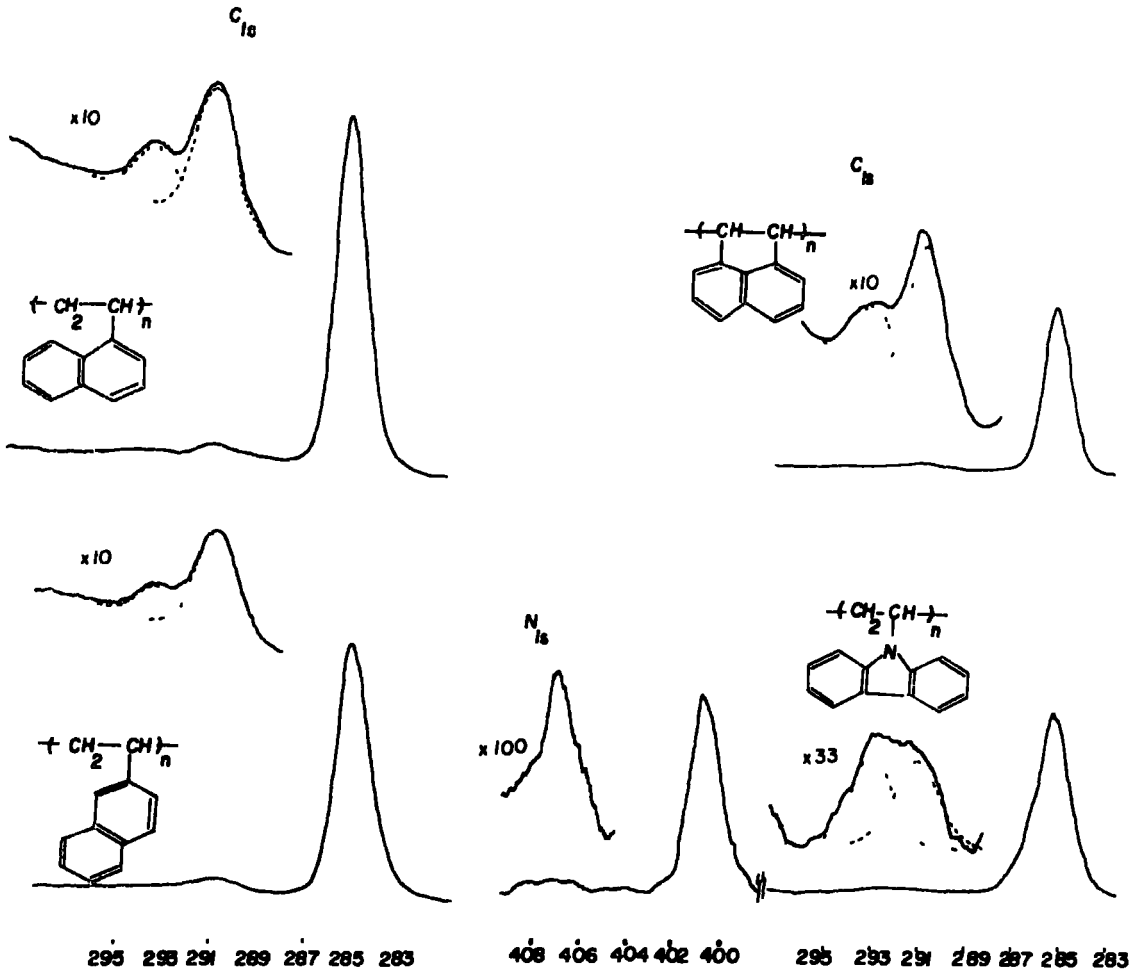

Figure 3.20. Core level spectra of poly-1-and-2-vinylnaphthalene, polyacenaphthalene and polyvinylcarbazole.

As the complexity of the conjugated pi system of the pendant group increases, the band profiles, full width at half maximum

and energy gap with respect to the direct photoionization peak all show substantial changes. A striking feature clearly evident from these data is, that the band profiles and FWHM for the direct photoionization peaks for the C_{1s} levels are closely similar for these systems (since the shift range is so small). By contrast the satellite structures are highly characteristic of the particular pendant group. It is clear from the data in figure 3.20 that for the poly-1-and-2-vinylnaphthalenes and polyacenaphthalene at least two shake up transitions must be involved and it has been shown in the previous sections that a similar situation obtains for polystyrene. The much larger FWHM for the low energy satellite of polyvinylcarbazole compared with the direct photoionization peak suggests that a similar situation obtains for this system as well. We have seen that the typical ratio of FWHM for a shake up satellite with respect to the direct photoionization peak is in the range 1.2-1.4.[54,129,180] The analysis presented in this and the subsequent section is consistent with this and an interpretation in terms of two low energy shake up transitions accompanying core ionizations of the C_{1s} levels is clearly justified by the theoretical treatment. The analysis of the experimental data in terms of two components is in each case straightforward and yields linewidth ratios which are internally self consistent. The relevant data is given in Table 3.6 to facilitate direct comparison with the theoretical analysis in the next section.

5.2 Theoretical Interpretation of the Shake up Spectra

The great complexity of these systems dictates that even within a CNDO/2 SCF MO framework some simplifications are still required. Thus for the pendant naphthyl groups in poly-1-

Table 3.6. Experimental Data for Homopolymer Systems

Polymer system	Core level	Binding Energy	FWHM	ΔE	Intensity (%)	FWHM	FWHM sat. / FWHM level
$-(CH_2-CH_2)_{\bar{n}}$	C_{1s}	285.0	1.2				
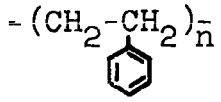	C_{1s}	285.0	1.4	6.2	3.3	1.9	1.4
				7.0	4.8	2.0	1.4
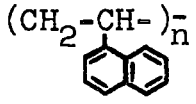	C_{1s}	285.0	1.6	5.7$_5$	5.0	2.0	1.3
				8.3$_5$	1.9$_5$	2.1	1.3
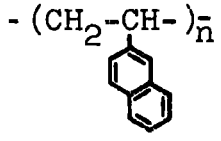	C_{1s}	285.0	1.7	5.8	5.0	2.1	1.2
				8.3	1.7	2.2	1.3
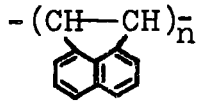	C_{1s}	285.0	1.4	5.7	3.8	1.9	1.4
				7.9	1.9	2.0	1.4
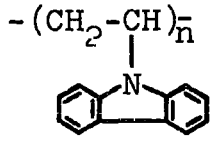	C_{1s}	285.0	1.7	5.8	2.7	2.1	1.2
				7.9	2.7	2.2	1.3
	N_{1s}	400.7	1.6	6.1	10.0	1.9	1.2
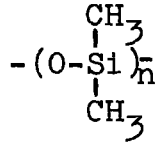	C_{1s}	285.0	1.3$_5$				
	Si_{2p}	102.0	1.5				
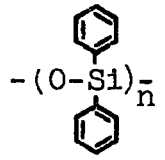	C_{1s}	285.0	1.4	6.4	3.8	1.8	1.3
				7.5	2.7	1.8	
	Si_{2p}	102.0	1.7	6.5	3.8	2.3	1.4

and-2-vinylnaphthalenes there are no less than 10 C_{1s} hole states to be simulated within the equivalent cores model. Separate experiments with toluene as a model system showed that in terms of the intensities and overall band profiles ESCA spectra of thin films gave results within experimental error the same as those derived from polystyrene. This strongly suggests that both the core hole states and their associated shake up states are effectively localized within a given pendant group and hence that the theoretical analysis can be based straightforwardly on a model of the appropriate repeat unit. The model systems which have therefore been investigated are toluene, diphenyl-di-siloxyl silane, 1- and 2-methylnaphthalenes and N-methylcarbazole. Shake up probabilities were calculated for transitions involving orbitals with Fock eigenvalues in the range > -22 eV for the ground state molecule (occupied orbitals) and < 3 eV for the equivalent cores species (virtual orbitals). As a typical example for the methylnaphthalene systems this involved a matrix of 14 occupied and 8 virtual orbitals. In all cases the transitions calculated to have the largest probabilities arose from $\pi^* \leftarrow \pi$ transitions involving the few highest occupied and lowest unoccupied orbitals. Although the systems studied do not all have either strict sigma-pi separability or the overall symmetries of the parent ring systems of the pendant groups it is nonetheless convenient to designate the transitions in terms of the local symmetries of the parent pi electron systems. In each case inspection of the relevant eigenvectors shows this to be a reasonable approximation. This is most readily apparent when a graph is drawn of orbital energies as a function of the hole state. The correlation with the relevant orbitals of the

neutral system may then readily be drawn on the basis of the overall symmetry characteristics of the orbital and the predicted change in orbital energy consequent on replacement of carbon by the equivalent cores species, this correlation being straightforwardly related to the magnitude of the $2p_z$ coefficient at the atom on which the core hole is located.

The complete theoretical analysis in terms of the model systems is too extensive to be presented straightforwardly here; however inspection clearly reveals that in all cases the lowest energy satellites should arise from excitations involving the two highest occupied pi orbitals of the neutral system and the lowest unoccupied "virtual" orbital of the corresponding equivalent cores species. The relevant data are given in Table 3.7.

Considering firstly the transition energies, no serious attempt to specifically parametrize the calculations has been made to reproduce the experimentally determined shake up energies, since the prime interest is in employing the standard CNDO/2 parametrization to discuss the overall shake up intensities. Only a qualitative discussion is therefore presented. The final column of Table 3.7 records the difference in orbital energies and in each case the differences in eigenvalues were taken as averages over the relevant holes for the orbitals concerned; in no case did the deviation from the average for a given transition exceed $\sim$0.3 eV. Since the transition energies depend not only on differences in orbital energies but also summations of electron repulsion terms it might be expected that only qualitative agreement between the calculated differences in $\Delta\varepsilon$ and the separation of the two components of the

Table 3.7. Calculated Shake up Intensities and Energies

Molecule	Hole State	Transition probability		(%)	Δε
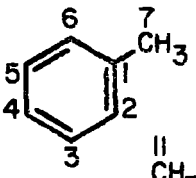	C_{1s}	LUMO-HOMO	$(b_{1\pi}^* \leftarrow b_{1\pi})$	2.6	8.2
		LUMO-SHOMO	$(b_{1\pi}^* \leftarrow a_{2\pi})$	1.8	9.0
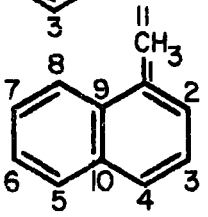	C_{1s}	LUMO-HOMO	$(a_{2\pi}^* \leftarrow a_{2\pi})$	3.6	5.4
		LUMO-SHOMO	$(a_{2\pi}^* \leftarrow b_{1\pi})$	1.6	8.2
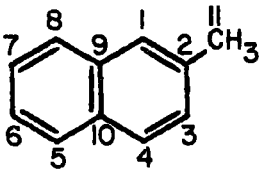	C_{1s}	LUMO-HOMO	$(a_{2\pi}^* \leftarrow a_{2\pi})$	3.5	5.7
		LUMO-SHOMO	$(a_{2\pi}^* \leftarrow b_{1\pi})$	1.6	8.2
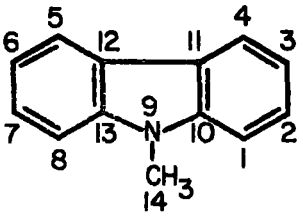	C_{1s}	LUMO-HOMO	$(b_{1\pi}^* \leftarrow b_{1\pi})$	1.9	6.5
		LUMO-SHOMO	$(b_{1\pi}^* \leftarrow a_{2\pi})$	1.5	7.1
	N_{1s}	LUMO-HOMO	$(b_{1\pi}^* \leftarrow b_{1\pi})$	3.4	-
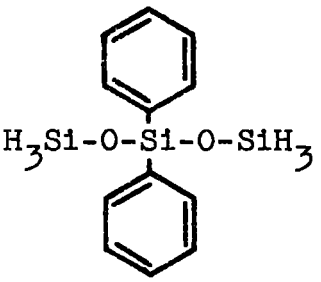	C_{1s}[a]		$(b_{1\pi}^* \leftarrow b_{1\pi})$	2.2	
			$(b_{1\pi}^* \leftarrow a_{2\pi})$	1.9	
	Si_{2p}[a]		$(b_{1\pi}^* \leftarrow b_{1\pi})$	4.3	

[a] Since there is considerable interaction between π systems of the phenyl substituents, the relevant transitions have been merely grouped together on the basis of the local symmetry of the π systems.

shake up peaks. With the exception of N-methyl carbazole however, the agreement is fortuitously good. Δ ($\Delta\epsilon$) has values of 0.8 eV, 2.8 eV, 2.5 eV and 0.6 eV for the models for polystyrene, poly-1- and -2-vinylnaphthalenes and polyvinylcarbazole respectively, compared with the experimental values of 0.8 eV, 2.6 eV, 2.5 eV and 2.3 eV.

Turning now to the calculated transition probabilities the data in Table 3.7 refer to weighted averages over all the relevant hole states. Before a comparison is drawn with the experimental data a few generalizations can be outlined. For toluene as a model for polystyrene the calculations indicate that the shake up intensity for the highest occupied molecular orbital to lowest unoccupied molecular orbital, (HOMO-LUMO) transitions derives largely from the C1 and C4 holes (numbering as in table 3.7) in which the local C_{2v} symmetry is retained, whilst the second highest occupied molecular orbital to lowest unoccupied molecular orbital (SHOMO-LUMO) transitions derive exclusively from the C2(C6) and C3(C5) holes (since the retention of the overall symmetry of the system for the C1 and C4 holes ensures that the corresponding transition is monopole forbidden). For the 1- and 2-methylnaphthalenes as models for the corresponding polyvinylnaphthalenes the HOMO-LUMO transitions of highest intensity derive from the beta carbons. For both systems the bridgehead carbons are calculated to contribute very little intensity to either transition and this also applies to the pendant methyl groups. For N-methylcarbazole as a model for polyvinylcarbazole the situation is somewhat more complex. Thus the HOMO-LUMO transition derives intensity largely from the C1(C8) and C3(C6) holes whilst the SHOMO-LUMO transition arises predominantly from C4(C5) and C10(C13).

From a consideration of the effect of para-substituents in the polystyrene system, previously shown, the band profile for the low-energy shake up satellites can be described in terms of the two component transitions which have differing responses to the change in electronic demands of the substituent. For the parent system the theoretical calculations predict that the HOMO-LUMO transitions should provide greater intensities than the SHOMO-LUMO transition, which is not in agreement with the experimental data. The calculated transition probabilities are also too small, however this lack of quantitative agreement does not detract from the overall success of the simple model in for example successfully reproducing semi-quantitatively the substituent effects on the overall band profiles which gives some measure of confidence in the interpretation. Comparison of theory with experiment reveals a similar situation for the more complicated ring system. Thus the model reproduces the trends in the total intensities for the low energy shake up satellites in going along the series from polystyrene to polyvinylcarbazole and although the calculated intensity ratios for the HOMO-LUMO/SHOMO-LUMO transitions are consistently underestimated the trends along the series are successfully reproduced. Further evidence for the validity of this interpretation comes from the low energy satellite for the N_{1s} levels of polyvinylcarbazole. Although the calculations again underestimate the intensity of the satellite, the theory suggests that only the HOMO-LUMO transition is involved, and in agreement with this the FWHM for the satellite is only slightly greater than for the direct photoionization peak. Further the transition energy of 6.1 eV is approximately the same as that for the corresponding transitions derived

from the analysis of the C_{1s} spectra (5.8 eV).

Finally we may consider polydiphenylsiloxane which forms an interesting comparison with polystyrene, since it allows a distinction to be drawn between shake up phenomena involving the pi system of the pendant phenyl groups and that for the polymer chains. The spectra shown in figure 3.19 clearly reveal the close similarities in the low-energy shake up satellites for the polymer systems and the experimental data are included in Table 3.6. The theoretical calculations also show the close similarities with respect to the overall band profile for the satellite accompanying direct photoionization of the C_{1s} levels. The calculations slightly overestimate the shake up intensity for the Si_{2p} core levels and both theory and experiment are in agreement in that the intensity of any low-energy shake up satellite for the O_{1s} core levels is extremely small. These results therefore form a consistent overall picture in that the shake up intensity largely derives from the pendant groups, the contribution for the atom to which the group is attached being relatively small and the contribution for the remainder of the chain being negligible. For comparison purposes the shake up intensity arising from the methyl carbon in toluene is calculated to be $\sim 0.2\%$ - considerably smaller than that for silicon in the polydiphenylsiloxane model system. This is not unexpected in terms of (i) the greater delocalization in the latter system arising from the presence of the two phenyl groups per repeat unit and (ii) the availability of 3d orbitals on silicon which have significant coefficients for the virtual orbitals. This receives further support from the fact that the overall and relative intensities for the 1- and 2-polyvinylnaphthalene systems and for polyacenanaphthylene are very similar.

6. Shake up Phenomena in Copolymers

It may be wrongly concluded from the foregone discussions that the study of shake up phenomena in polymers must closely be accompanied by detailed theoretical computations. This is not the case however since the greatest potential of shake up studies, when related to the synthesis and surface modification of polymers, is as a means of establishing the degree of unsaturation in the material[52,100,137,157] both qualitatively and semi-quantitatively. Indeed an example of this type of application has already been seen for the plasma polymerization of perfluorobenzene[52,100] in Chapter Two, section 6. On these same lines it should also be possible in appropriate cases to determine comonomer compositions in a copolymer on shake up data alone as long as one component is unsaturated.[128] As an example of this we may now consider shake up phenomena in a series of alkane-styrene copolymers[128,158] of general formula shown in figure 3.21.

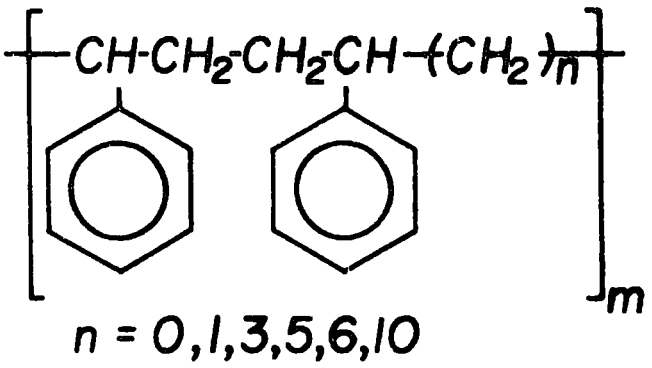

Figure 3.21. General formula of the alkane-styrene copolymers

It will be seen from the ensuing discussion that not only can comonomer compositions be determined by shake up intensities but also some aspects of surface morphology.

Figure 3.1 shows the C_{1s} spectra for high-density polyethylene and polystyrene. For the latter, the well-developed shake up structure arising from $\pi^* \leftarrow \pi$ transitions is clearly evident. Model calculations within the sudden approximation by using the CNDO/2 SCF MO formalism and the equivalent cores model suggest that the shake up structure arises predominantly from $b^*_{1\pi} \leftarrow b_{1\pi}$ and $b^*_{1\pi} \leftarrow a_{2\pi}$ transitions (C_{2v} local symmetry) and the distinct asymmetry of the peak would tend to confirm that more than one transition is involved. We have previously seen that shake up structure is a function of the substituents and also that the shake up structure in terms of band profile, intensity and energy relative to the main photoionization peak is characteristic of the pendant group for polymers of a given general structure.[56]

The straightforward observation of shake up peaks therefore greatly extends the scope of ESCA in studying polymers, since as has been already noted the shift range within C_{1s} levels for hydrocarbon-based systems is often too small. It is clear from figure 3.1 (apart from slight differences in line width), that the profile for the direct photoionization peaks of polyethylene and polystyrene are closely similar.

The spectra reproduced in figure 3.1 correspond to uncontaminated samples both in respect of surface oxidation and extraneous hydrocarbon contamination. Detailed studies have been made of polystyrene samples covering a large range in molecular weight and in method of preparation. In general,

while the powdered samples show a very small O_{1s} signal arising from surface oxidation features and are completely reproducible as far as the shake up structure is concerned, solvent-cast films show varying degrees of contamination which are readily detected by monitoring the O_{1s} core levels and the C_{1s} shake up satellite. This is not unreasonable, since it might be expected that traces of impurity distributed throughout the bulk of a sample would segregate specifically at the surface.

6.1 U.V./Visible Spectra

Spectra of the series of copolymers of general formula given in figure 3.21 were recorded at several concentrations of the polymer in chloroform typically ranging from 10^{-4} to 10^{-3} moles/litre. The Beer-Lambert law was obeyed and in all cases the vibronic fine structure was the same and extinction coefficients calculated for peak maxima were within $\pm 5\%$. The only exception noted was for n=1, for which the extinction coefficients calculated assuming the empirical formula were consistently (and reproducibly) high. The vibronic fine structure also differed and in addition there was a pronounced tail to the long wavelength region. The spectra are shown in figure 3.22 and the relevant data are collected in Table 3.8.

Table 3.8. Ultraviolet Data for the Alkane-Styrene Copolymers

	ε, l/cm-mole[a]						
n	λ = 244.5 nm[b]	λ = 250.0 nm[b]	λ = 256.0 nm[b]	λ = 260.0 nm[b]	λ = 262.5 nm[b]	λ = 265.5 nm[b]	λ = 270.0 nm[b]
0	215	300	410	460	462	400	340
1	-	699	783	811	788	670	594
3	219	311	400	455	455	367	343
5	254	293	376	425	426	344	322
6	217	306	390	441	444	356	337
10	204	296	383	435	437	353	332

a The extinction coefficients are expressed in terms of the repeat unit.

b λ refers to the peak maxima of the vibronic fine structure

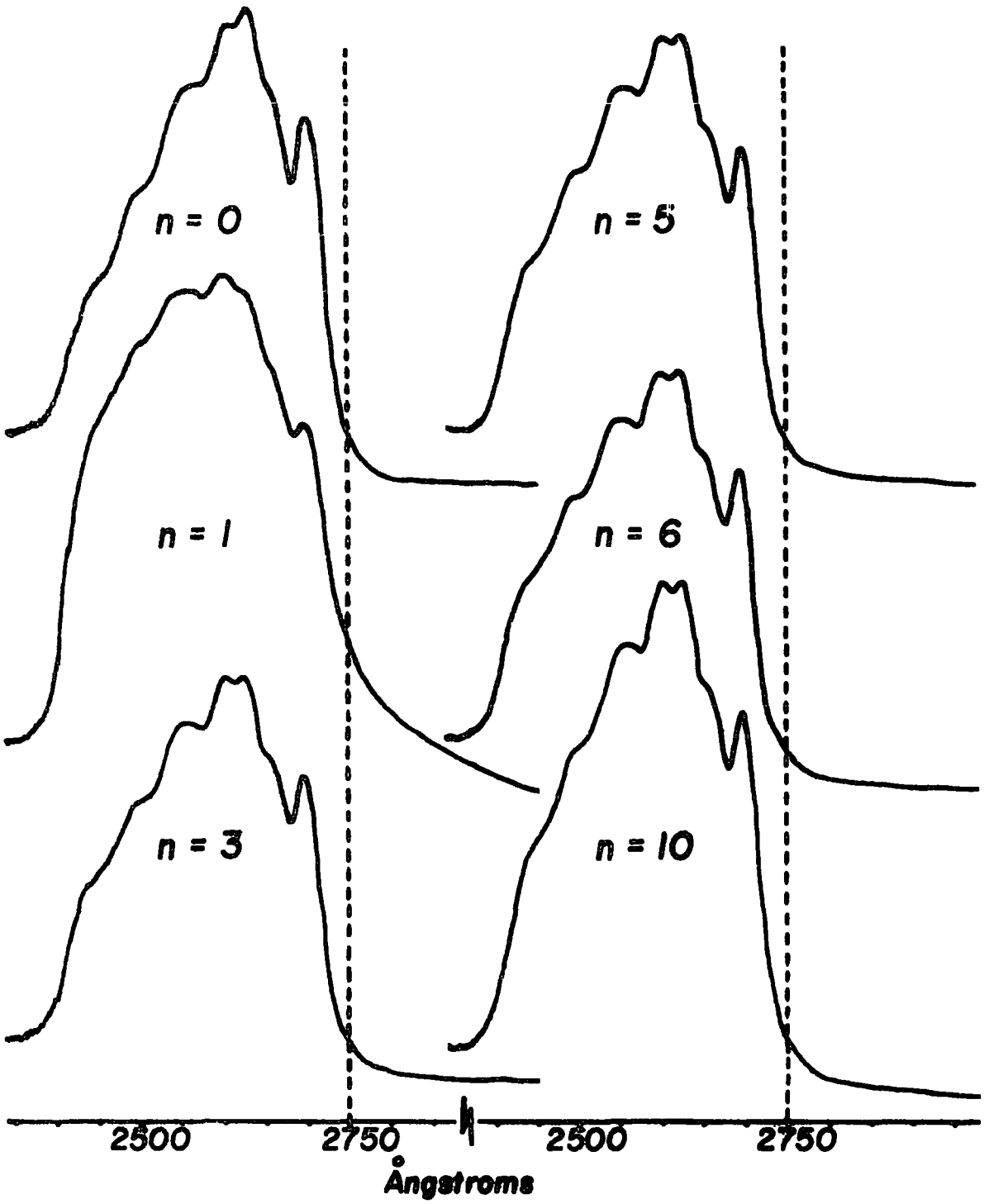

Figure 3.22. Ultraviolet spectra in the 2600Å region for the series of alkane-styrene copolymers.

These solution-phase electronic spectra of the alkane-styrene copolymers suggest that there is little electronic interaction between the phenyl groups disposed along the polymer backbone. On the basis of appropriate molecular models and theoretical calculations on model systems this is readily understandable, since both through-bond and through-space interactions are predicted to be small. The sole exception is perhaps the n=1 copolymer which, as has been previously noted, does not compare directly with the other members of the series in terms of wavelengths and extinction coefficients. The reason for this is unclear, since it is difficult to envisage any specific long-range interaction for this polymer which is not also open to some other members of the series. It will become apparent, however, that with respect to the shake up structure this copolymer falls into line with the data for the other members of the series. This being the case, shake up phenomena arising from $\pi^* \leftarrow \pi$ transitions accompanying core ionizations in the pendant phenyl groups might be expected to be additive in the absence of any specific chain-orientation effects.

6.2 Shake up Spectra

Figure 3.23 shows the measured C_{1s} levels and shake up satellites for the alkane-styrene copolymers for n = 0,1,3,5, 6 and 10. Several spectra of separate preparations of each sample were recorded, and in some cases these revealed evidence of surface contamination arising from silicone-type material. The data in figure 3.23, however, refer to samples which were essentially uncontaminated. It should be emphasized, however, that ESCA is such a surface-sensitive technique that the levels of contamination are extremely small and almost certainly would go undetected by other techniques.

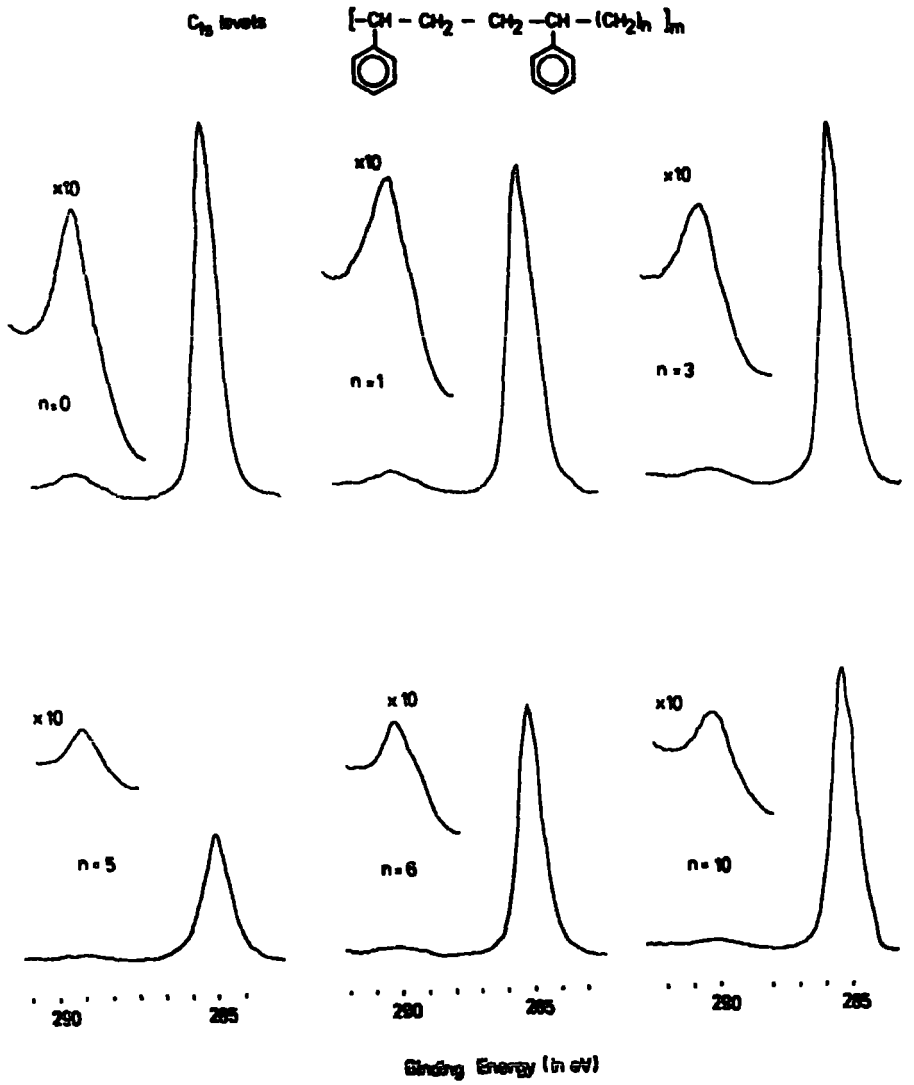

Figure 3.23. C_{1s} spectra of the alkane-styrene copolymers.

It is evident by visual inspection of figure 3.23 that the relative intensities of the shake up satellites with respect to the main photoionization peaks decrease with increasing chain length of the alkane component. The measured intensities and energy separations are given in Table 3.9, where the data refer to the samples studied directly as solids (data corresponding to the solution cast films are discussed in a later section).

It is evident from a cursory examination of these data

Table 3.9. ESCA Data for the Alkane-Styrene Copolymers

	Binding Energies, (eV)			Area ratios (C_{1s}/C_{1s}^{s})	
n	C_{1s}	C_{1s}	Δ†	As received	Solvent-cast film ††
0	285.0	291.6	6.6	13.4	13.8
1	285.0	291.6	6.6	14.5	14.7
3	285.0	291.6	6.6	18.5	18.4
5	285.0	291.6	6.6	22.7	19.1
6	285.0	291.6	6.6	23.8	29.8
10	285.0	291.6	6.6	32.3	32.6

† Shake up energy with respect to centroid of shake up peak

†† Average value of casting from cyclohexane, benzene, toluene and bromobenzene.

that a trend exists between shake up intensity and the chain length of the alkane component. It is also clear that the structure of the shake up satellites and the energy separations remain essentially constant, as might be expected if the shake up transitions were effectively localized within a given pendant group. A least-squares plot of this data (intensity ratio of direct photoionization peak to shake up satellites versus n, the chain length of the alkane component) gives a correlation coefficient of 0.997, the slope being 1.91 and intercept 12.91 The latter may be compared with the measured value of 13.1 for the parent system (i.e. polystyrene). Taking the measured shake up intensities for polystyrene and the repeat unit for a given copolymer, the calculated slope assuming an additive model is 0.90. (see figure 3.24).

The fact that an additive model applies to the experimental data but with a much larger dependence of intensity on n than predicted theoretically would strongly suggest that

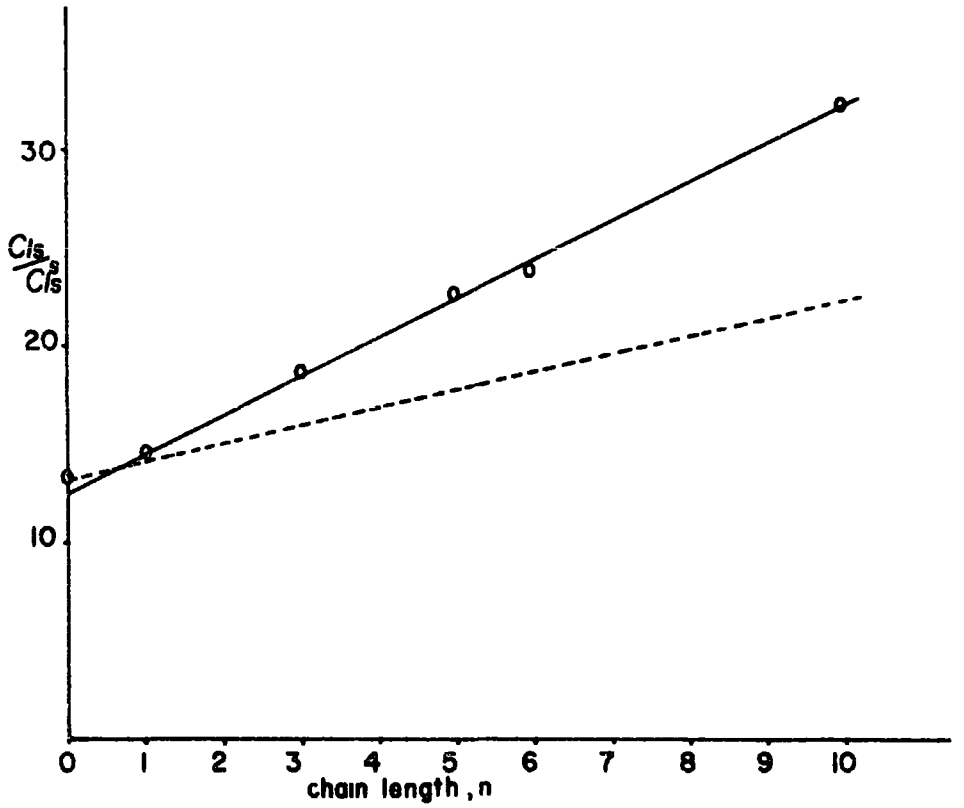

Figure 3.24. C_{1s}/C_{1s}^{s} versus the alkane chain length,

there are specific orientation effects of the polymer chains in the topmost 100 Å. Unfortunately, data pertaining to the surface morphology of these polymers are conspicuously absent in the literature, so that we may only put forward logical suggestions as to the reason for this deviation from the theoretically predicted correlation. As a first step it is useful to consider the shake up structure in toluene as a model system. As has previously been described samples were studied as thin films condensed at a pressure of $\sim 10^{-7}$ torr. Under such conditions, a random orientation of toluene molecules in the solid phase would seem to be most probable. The experimentally determined ratio of direct photoionization to

shake up satellites for such films is 12.2. If the outermost few tens of angstroms of the polystyrene samples are such that ESCA effectively statistically samples the repeat units, then the calculated shake up intensity based on the toluene data would be 13.9, in good agreement with the experimentally determined value 13.4. † The fact that a good linear correlation is obtained for the copolymers with a slope which suggests that the decrease in shake up intensity as a function of n is greater than predicted theoretically on the basis of a random structure would strongly suggest some degree of ordering common to all of these copolymers. In this respect, the data corresponding to n=1 are such that within experimental error they may also be fitted to a linear correlation with the theoretical slope.

In the absence of detailed information on the surface structure of these systems we may only speculate as to the possibilities which might give rise to an attenuation of the shake up intensity. Since the mean free path for the photoemitted electrons is of the order of ~10 Å,[99,100,123] (implying that 50% of the elastic peak corresponding to direct photoionization and detection of the photo-ejected electrons without

---

† By statistically sample we simply imply that the surface structure is such that for the sampling depth appropriate to photoionization from the C_{1s} levels (mean free path ~10 Å) the signals arising from the chemically distinct carbon atoms are representative of the repeat unit. This could, of course, arise from a completely random arrangement as well as a well-ordered surface structure. In fact, molecular models would seem to indicate that it would be difficult to envisage a structure in which statistical averaging on the ESCA depth scale did not obtain. For the alkane-styrene copolymers, however, with n >1 this is not necessarily the case.

energy loss derives from the topmost ~ 7 Å of sample), short segments of the polymer chains may be considered. Two extreme possibilities suggest themselves from such a consideration.

The possibilities are illustrated in figure 3.25. In figure 3.25(a) the folded chain structure has the alkane component oriented specifically at the surface with the pendant phenyl groups being some distance below. The net effect of

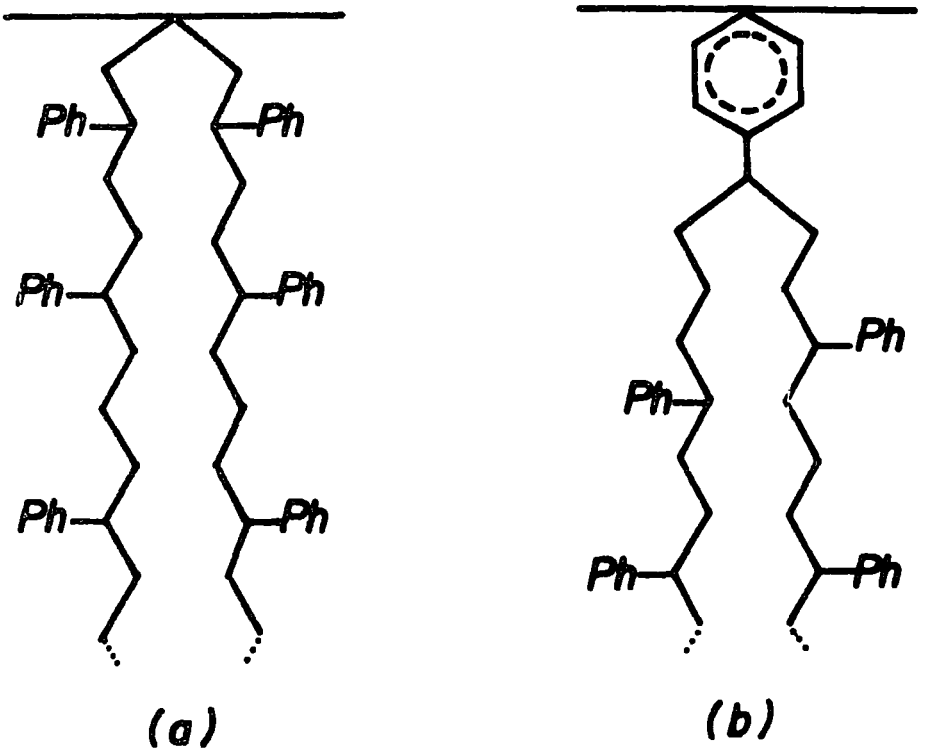

Figure 3.25. Folded chain models for the case where n = 3.

this arrangement would be an apparent attenuation of the shake up intensity as is observed. The alternative (b) again corresponds to a folded chain structure with a phenyl group specifically oriented at the surface. Both of these models are such that a statistical averaging over the repeat unit does not obtain. Taking typical bond lengths and angles and

calculating the ratio of the intensities of the main photoionization peak to the shake up satellite suggests that the models qualitatively follow the observed trend with a tendency for the structure of (a) to provide a closer approximation to the observed attenuation in shake up intensities. The results are therefore qualitatively understandable in terms of some such model. An alternative possibilitity is that the observed attenuation arises from hydrocarbon type contamination at the surface. This possibility has been considered in some detail and it would appear that the results cannot be readily rationalised in this manner. Two possibilities have been considered. Firstly, from the observed attenuation of shake up intensity a hypothetical surface depth of contamination may be calculated, d. (see Table 3.10).

Table 3.10. Hydrocarbon Contamination Possibility.

n	d	x
1	0.34	0.086
3	1.34	0.318
5	2.42	0.547
6	2.36	0.535
10	3.69	0.785

In all cases this comes out to be significantly less than that appropriate to monolayer coverage and would therefore imply that, if hydrocarbon type contamination is present, then it must correspond to a fraction of a monolayer coverage, (x).The data were therefore reanalysed on this basis. However a rationalization in terms of such a model requires an order of magnitude span in fractional monolayer coverage across the series which seems most improbable in terms of both the method of preparation and the reproducibility of the experimental intensity ratios.

Some independent evidence that hydrocarbon type contamination is unlikely to be responsible for the observed attenuation is also available from the solvent-cast films. As we have previously pointed out, negligible traces of silicone contamination (probably arising from vacuum grease picked up during the synthesis) were observed by ESCA for the powders. (It should be emphasized that by conventional methods of analysis the polymers are of very high purity, i.e. bulk analysis by AAS revealed negligible quantities of silicone in the bulk). Since ESCA is such a surface-sensitive technique, however, it is not unexpected that specific segregation during the casting process gives sufficiently high silicone coverage at the surface to be readily detected by ESCA. If hydrocarbon contamination were also present in trace amounts in the bulk, then solvent casting might again be expected to lead to specific segregation of the contaminant at the surface. For the solvent-cast films uncontaminated by silicone, however, the shake up intensities are the same within experimental error as those measured for the polymer samples studied directly (n = 0, 1,3,10). (Table 3.9).

In general the spectra obtained from solvent cast films were irreproducible within acceptable error limits, emphasizing the care which must be taken when using this method of sample preparation. However in this connection it is worthwhile noting that surface contamination caused by the casting processes is readily monitored by the shake up satellite intensity. This is particularly useful when studying purely hydrocarbon systems.

7. Conclusions

It should be readily appreciated that shake up structure

in terms of band profile, intensity and energy separation from the direct photoionization peak is a sensitive function of the electronic structure of the polymer system to which it pertains, with respect to both substituent effects and the overall structure of the conjugated pi system. The interpretation of shake up phenomena is greatly aided by theoretical treatments on model systems within a semi-empirical CNDO framework. The greatest potential of shake up phenomena with respect to surface analysis of polymers however is on a lower level of sophistication, involving the determination of the degree of unsaturation, providing a valuable source of extra information particularly in the study of purely hydrocarbon systems for which little information can be derived from the primary sources.

CHAPTER FOUR

Sample Charging Phenomena in Polymers

1. Introduction

The problems associated with sample charging in the ESCA examination of thick insulating samples were recognized and diagnosed at an early stage of the development of the technique by Siegbahn and coworkers.[18] The irradiation of a solid sample with X-rays causes ar emission of photo-, Auger-, Compton- and secondary electrons. These processes tend to leave the surfaco regions of the sample electron deficient. This deficiency is at least partially compensated by a current of electrons into the sample originating from similar processes occurring in the window of the X-ray source and surrounding components of the sample chamber, which are also irradiated by the X-rays, and by conduction through the sample.[18,22,23,181-184] This is illustrated schematically in figure 4.1

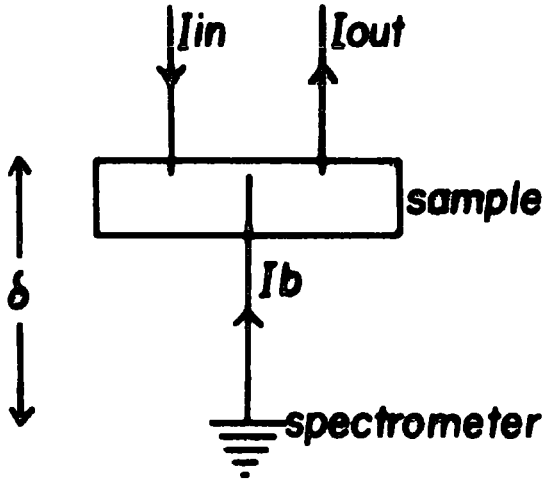

Figure 4.1. Currents involved in sample charging.

Photoelectrons either lost from the sample or gained from the sample surroundings generally have relatively large kinetic energies so that the number leaving or arriving at the sample will be relatively insensitive to the charge on the

sample. On the other hand the secondary electron flux entering or leaving the sample, which accounts for the greater proportion of the total number of electrons,[23] has a significant number with energies sufficiently low that the number arriving at or leaving the sample depends to a great extent on the electrical potential of the sample. These 'vacuum' currents are usually summed to produce I in and I out as shown in figure 4.1. A further factor determining the overall charge on the sample concerns the electrical conductivity and capacitance of the sample/sample holder system (under conditions of X-ray irradiation) giving rise to a current I_b into the surface regions of the sample. This source of electrons is enhanced by the X-ray irradiation and photoionization process itself which produce charge carriers within the sample. For conducting samples, such as metals I_b is such that the sample surface is maintained in electrical contact with the spectrometer and their Fermi levels are the same. In this situation the kinetic energies of the photo-emitted electrons will follow a bias applied to the reverse side of the sample precisely. An intermediate situation is obtained for resistive samples since I_b is limited by the resistance of the sample. This situation is readily detected since the kinetic energies of the photoemitted electrons will only partially follow an applied bias, and asymmetries in the core level signals as seen by ESCA may be induced by applying potential gradients across the surface of the sample.[185] For samples electrically isolated from the spectrometer, as may be defined by $I_b=0$ an equilibrium between I in and I out is reached when the surface of the sample acquires a certain floating potential relative to the spectrometer. This potential, namely the equilibrium

sample charge δ, is usually positive although in certain cases may be negative (for example when I in is increased by the introduction of an electron flood gun[87] into the sample chamber or when I out is reduced by shielding the sample from the X-ray source,[23] when, of course, no spectrum is observed) and manifests itself in a shift in the kinetic energy scale of the photoelectron spectrum.[18] A bias applied to the reverse side of the sample produces no effect on the spectrum. Many classes of materials fall into this last category including thick films of organic polymers which by their very nature are extremely good insulators. Figure 4.2 illustrates the energy components involved.

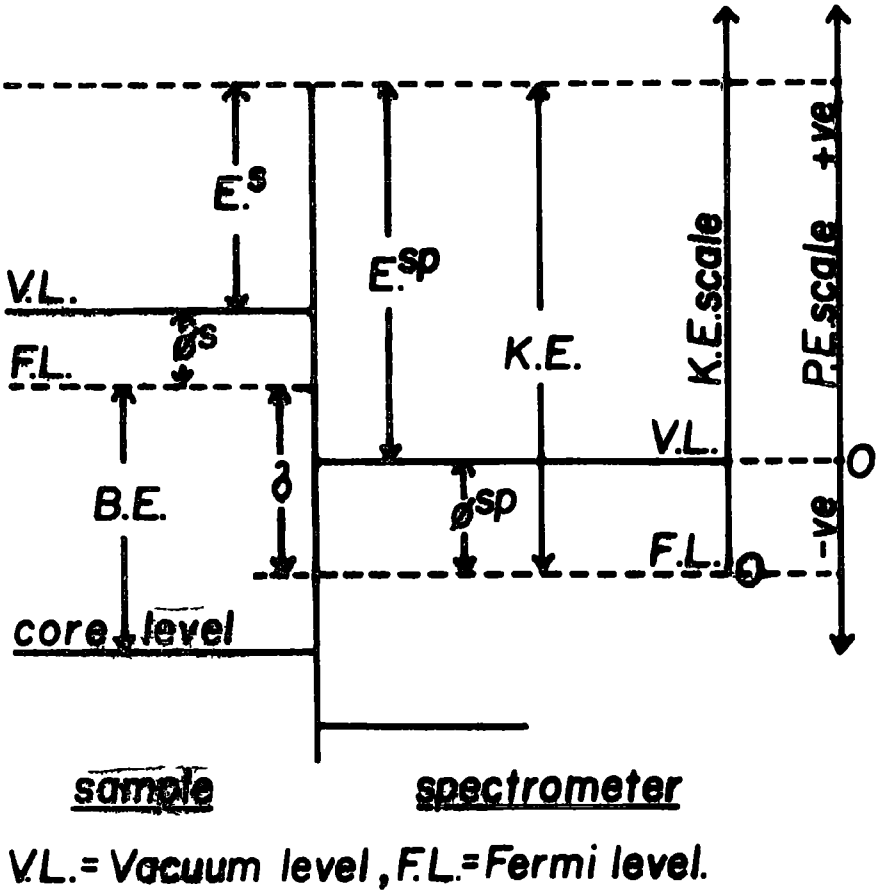

Figure 4.2. Energy components for an insulating sample.

It is clear from figure 4.2 that the Fermi levels of the sample and spectrometer are not the same and a direct measurement of the binding energies of the various core levels of the sample is not possible without a knowledge of the magnitude of the sample charge. As a recent ASTM report affirms,[186] sample charging and its correction is still a source of error in attempting to set up calibration standards for insulators and indeed the prevailing climate would seem to be that the phenomena encompassed by sample charging is a nuisance which practising spectroscopists must learn to live with. To put matters into perspective however, for the majority of insulator systems the problems caused by sample charging phenomena may be circumvented by the use of reference materials and the suggested use of the characteristic signal arising from contaminant hydrocarbon species originating in the extraneous atmosphere of the spectrometer as a convenient energy reference derives from the pioneering work of Siegbahn and coworkers[18] and to this date offers with due care and attention a convenient and reliable means of correcting for sample charging.[18,115] It will become apparent from the remainder of this chapter that sample charging, far from being a nuisance, is a potential source of valuable information which has largely been overlooked in the past.[52,133]

The experiments described in this work fall into two main categories. The first category (Section 3) involves the use of a $Mg_{K\alpha_{1,2}}$ X-ray gun which is not monochromatized. The X-ray spectrum derived from such a source consists of the characteristic line spectrum of the magnesium anode superimposed onto a continuum of white X-rays or bremsstrahlung.[108] This, coupled with the fact that, as will be elaborated upon in the experimental section, the aluminium foil window of the gun is $\sim$0.5 cms

from the sample, produces an intense flux of secondary electrons at the sample surface. (I in is large). The magnitude of the sample charging for such a situation is typically < 15 eV.

The second category of experiments (Section 4) involves the use of a monochromatic $Al_{K\alpha_{1,2}}$ X-ray source which is remote from the sample. The band profile of the X-ray spectrum derived here consists of essentially the pure $K\alpha_{1,2}$ lines with a virtually zero background. Furthermore the beam size is ∿ 1mm square (compared to ∿ 1cm square for the $Mg_{K\alpha_{1,2}}$ source) and hence the production of electrons from anywhere but the sample is small (I in ∿0) and the sample charging may be of the order of tens of volts for insulating samples. Section 4 also includes an investigation of the use of a low pressure mercury lamp as an alternative to an electron flood gun as a means of increasing I in and decreasing the sample charge.

2. Experimental

2.1 Samples

The polymers used in this work are listed in Table 4.1.

The ethylene-tetrafluoroethylene copolymer (E-TE) included here has previously been the subject of an ESCA investigation.[121] The structure of the copolymer (52% tetrafluoroethylene) is known to be largely alternating and, therefore, is closely similar in composition to polyvinylidene fluoride (PVF_2). The rationale behind the inclusion of this copolymer is that it is used extensively in the study of surface modification of polymers by inert gas plasmas, described in Chapters Five and Six. It is therefore of considerable interest to gain a knowledge of its charging characteristics.

Table 4.1. List of materials and their physical form studied in this work.

Material	Abbreviation	Form
Polyethylene (high density)	PE	F
Polyvinylfluoride	PVF	F, P
Polyvinylidenefluoride	PVF_2	F
Polytetrafluoroethylene	PTFE	F, P
Polyhexafluoropropylene	PHFP	P
Ethylene-tetrafluoroethylene copolymer	E-TE	F
Poly-n-butylmethacrylate	PBMA	F, P
Polyethyleneterephthalate	PET	F
Polycaprolactam (Nylon 6)	N6	F
Polyvinylchloride	PVC	P
Gold	Au	F

F = film, P = powder

The remaining polymers were obtained from Cellomer Associates, Inc., Webster, New York 14580 and were used as received as either fine powders (P) coated onto double-sided 'Scotch' tape (3M Company, Tape No. 75 a thermosetting silicone based adhesive on polyester film) directly attached to the spectrometer probe tip, or as films (F) attached by either of two methods. (1) Films mounted in what is referred to as 'intimate contact' were attached directly to the probe tip with double-sided 'Scotch' tape, and pressed in place. (2) Films mounted in what is referred to as 'spotted contact' were wrapped over the probe tip and taped to the opposite side. These two methods of attaching the films to the probe tip provided two distinct situations. The first being a composite of conductor (probe tip at ground potential)/dielectric ('Scotch'tape)/and film

sample; the second being a conductor/vacuum and point contact of film and probe tip.

Gold has also been included in this investigation both because of its chemical inertness (and hence reproducible character of the surface) and for its high cross section for photoionization. In addition gold still serves as a primary standard for the energy referencing of spectrometers.[1,18] The gold foil used in this study was obtained from Johnson Matthey Chemicals Ltd., London and was Grade 1 purity. The samples could either be mounted insulated from the spectrometer by means of 'Scotch' tape or in electrical contact with the spectrometer by bolting directly to the sample probe tip. Gold samples were also used to investigate the effect of an electrical bias on the hydrocarbon contamination of samples. The experimental procedure was as follows. Two samples were mounted side-by-side on double sided tape where one sample was in electrical contact with the spectrometer (grounded) and one sample connected to a D.C. supply, variable from +20 to -20 Volts. Under these experimental conditions two peaks are observed in the spectra of the particular core levels being investigated associated with the two samples, separated by the applied bias.

Composite samples of gold/polymer were prepared by mounting the gold and polymer side by side on the probe tip with 'Scotch' tape such that the core levels of both samples could be monitored simultaneously.

Thin polymer films were deposited onto gold substrates by polymerization of paraxylylene precursors generated in a pyrolysis flow system, the direct measurement of film thicknesses being accomplished by means of a quartz deposition monitor. The experimental details of this technique may be found else-

where,[99] and it will suffice to say here that this method provides a convenient, clean method for building up polyparaxylylene films of increasing thickness, by the use of a pretreatment chamber bolted directly onto the insert port of the spectrometer, allowing sample charging to be monitored as a function of film thickness.

In all cases the total sample size was 18mm x 7mm.

2.2 Instrumentation

Figure 4.3 shows the general arrangement of the sample region in the AEI ES 200B spectrometer used in this investigation, which is equipped with two X-ray sources. The $Mg_{K\alpha_{1,2}}$ source is non-monochromatic and the aluminium foil window, which prevents electrons from passing into the sample chamber from the filament, is ∿0.5cm from the sample. The $Al_{K\alpha_{1,2}}$ source is monochromatic and remote from the sample. The sample region is separated from the monochromator by a thin polyester window. Both X-ray guns are of the 'hidden filament or Henke' type design[92] in which the filament is not directly in front of the target. The power source consists of a Marconi-Elliott Type GX5 high voltage generator which may be operated in the vacuum region of $< 10^{-5}$ torr. The target can be operated at a power of up to 300 watts and both voltage and current supplies are stabilized to 0.1% which produces photon fluxes in the region of ∿0.1 millirad per second. Both voltage and current are dial up facilities in which integral values in the range 2-15 kV and 2-20 mA were available. Typical operating conditions for the Al and Mg X-ray guns were 15 kV, 38 mA and 12 kV, 15 mA respectively, and the pressure in the sample region 10^{-8} torr. Under the experimental conditions employed the gold $4f_{7/2}$ level at 84 eV used for calibration of the

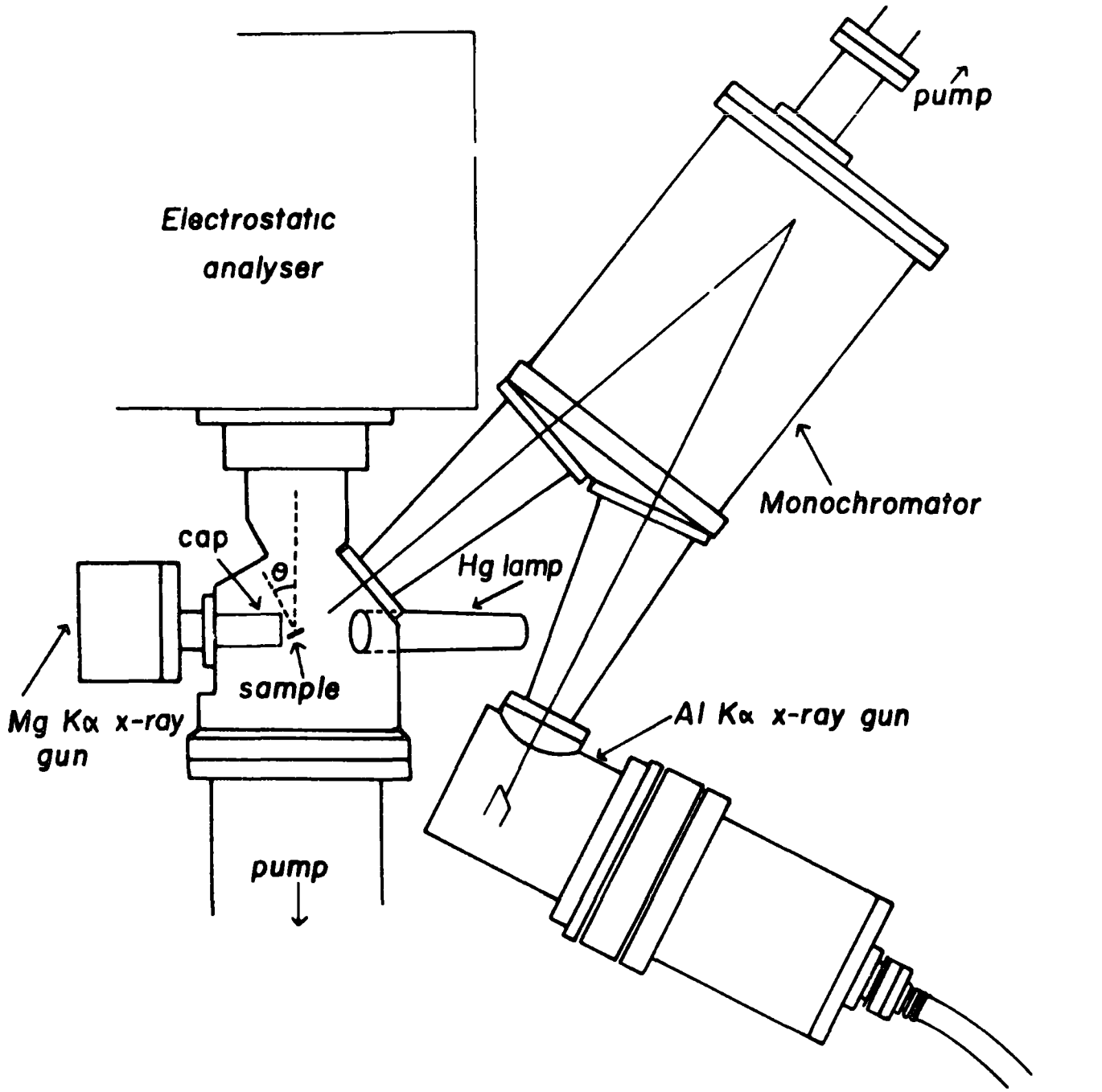

Figure 4.3. AEI ES 200B X-ray photoelectron spectrometer.

energy scale had a full width at half maximum of 0.9 and 1.2 eV respectively for the Al and Mg photon sources.

The angle between the analyser entrance slit and the Al and Mg X-ray sources is fixed at 55^{o} and 90^{o} respectively whilst the angle of the sample with respect to the analyser entrance slit is continuously variable through 360^{o}. (θ is the angle between the normal to the sample surface and a line drawn between the sample and the analyser slit). This angle is referred to as the electron take off angle since it implies the direction in which the electrons leaving the sample are analysed.

The low pressure mercury lamp is operational between 0.8 and 5.0 watts and is manufactured by Engelhard Hanovia Lamps, Slough, Buckinghamshire. The 184.9nm radiation is directed into the spectrometer sample chamber via a quartz viewing port. The whole system is enclosed in an opaque casing and purged with dry nitrogen.

No evidence was obtained for radiation damage either by ultraviolet or X-ray sources during the typical time scale involved in the recording of data. Spectra were recorded at an electron take of angle of 45^{o} unless otherwise stated.

2.3 Sample Charge and Time Dependent Studies

The charge on the sample was determined as the difference between the measured kinetic energy of a photoemitted electron from a specific core level and the kinetic energy appropriate to a sample ideally in electrical contact with the spectrometer. The latter is taken as the kinetic energy appropriate to the absolute binding energy as previously determined for these systems, on the same calibration scale.[127]

It was observed for all of the samples in this investigation that the charge was time dependent, therefore, spectra were

recorded immediately upon irradiation (taken as T=0) and subsequently every five minutes. The equilibrium charge is taken as the maximum observable shift obtained from a contamination free sample.

For the particular cases of polytetrafluoroethylene and gold the equilibrium sample charge was measured as a function of the applied potential and the filament emission current of the X-ray photon source.

3. Charging Induced by a Non-monochromatized X-ray Source

The experiments described in this section fall into three main groups. In the first a series of polymer films and gold were mounted on the sample probe such that they were effectively electrically isolated, although in 'intimate contact' with the probe tip. Measurements were then made of the static equilibrium charge for each sample as evidenced by the shift in core level spectra from the binding energies appropriate to samples ideally in electrical contact with the spectrometer. The second series of experiments involved the monitoring of the time dependent nature of the sample charging under a given set of experimental conditions as a function of hydrocarbon contamination which was allowed to accumulate on the sample surfaces. The final series of experiments consisted in attaching polymer films ($\sim$ 50 μ thick) to the spectrometer probe such that only 'spotted contact' was made, and monitoring the time dependence of the initial charging phenomena as well as that associated with deliberate hydrocarbon contamination.

3.1 Equilibrium Charging of Polymers

Over a period of years it has become increasingly evident from extensive investigations in these laboratories of a wide

range of polymeric materials,[1,52,114-118] that sample charging is dependent on electronic structure. The initial experiments in this work, therefore, involved a systematic investigation of the sample charging characteristic of a series of polymers (∿50 μ in thickness) studied under identical instrumental conditions (unmonochromatized $Mg_{K\alpha_{1,2}}$ X-ray source 12 kV, 15 mA with a fixed electron take off angle of 45°). In these initial experiments samples were mounted in 'intimate contact' with the copper probe tip (spectrometer probe grounded) by means of double sided 'Scotch' tape as outlined above. With this configuration it was found that the equilibrium shift in kinetic energy scale arising from sample charging was rapidly established, at least as far as the typical time scale taken to record spectra is concerned . Repeat measurements established that the sample charging was typically reproducible to ± 10% even in comparing powdered samples with films.

That the shifts are characteristic of the polymer system is readily apparent considering the data for three typical samples viz. PE, PVF_2 and PHFP. The corresponding shifts in kinetic energy scale δ are ∿3.4 eV, ∿ 7.5 eV and ∿10 eV. It should be emphasized that these values pertain specifically to the experimental arrangement described above. To shed further light on the relationship between sample charging and electronic structure, investigations were also made of gold sheet (ultra high purity ∿ 0.3 mm. thick) mounted on double sided 'Scotch' tape. The equilibrium static charge in this case amounted to ∿13.5 eV.

Under identical instrumental conditions it seems evident that the surface charge acquired by a sample must be a function of the total photoionization cross section and to investigate

this in some detail we may consider appropriate relative theoretical cross sections for each material. As a starting point the recently published data of Schofield[94] have been employed to compute cross sections for both the gold and polymer surfaces and for convenience in discussing this data this has been normalized to a unit surface area. Knowing typical covalent radii for gold[187] and as a first approximation taking representative bond lengths and angles[169] for extended chains of the polymers together with appropriate interchain spacings,[188] it is possible to compute relative photoionization cross sections per unit area for the polymer and gold surfaces. The correlation between equilibrium charge, as measured as a shift δ in kinetic energy scale, and total theoretical cross section for photoionization is shown in figure 4.4. The exhibited trend of larger shift being associated with higher cross section is particularly striking and although the absolute magnitude of sample charging as such represents a convolution of many contributing factors such a correlation underscores the structural dependence of such phenomena. It is of particular interest to note that polyvinylidene fluoride (PVF_2) exhibits the same charging characteristics as an ethylene/tetrafluoroethylene copolymer (E-TE in figure 4.4) of essentially identical overall composition. This again illustrates the characteristic nature of sample charging phenomena since it is known that the structure of this copolymer is largely alternating and hence has a close correspondence with PVF_2.

It is appropriate at this point in the discussion to note the dependency of the sample charge on the geometry and orientation of the sample with respect to the components of the spectrometer. It may readily be demonstrated that the equil-

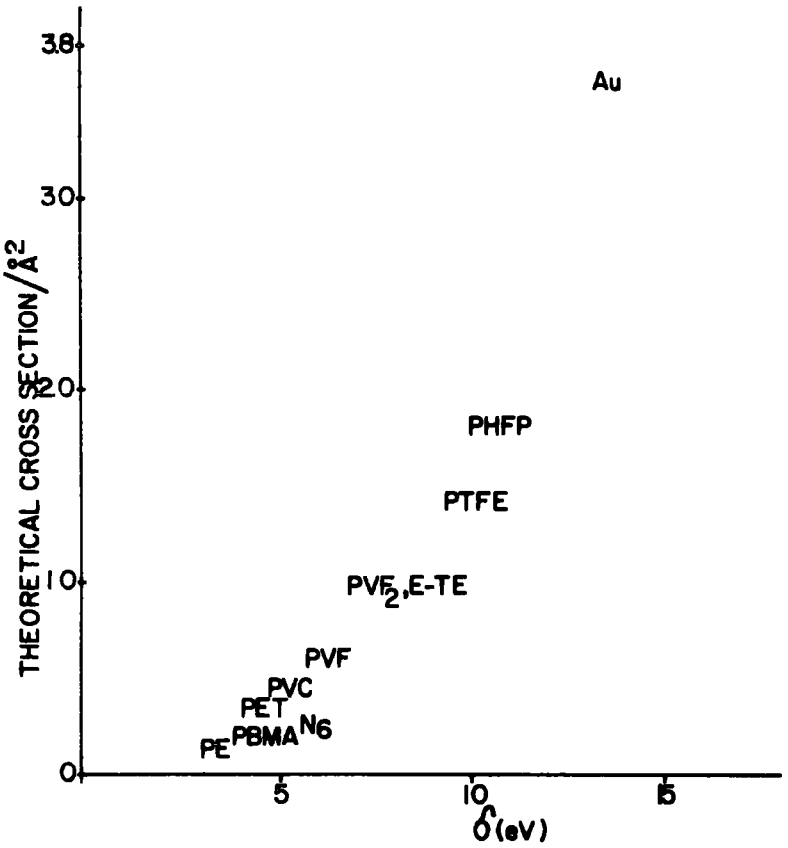

Figure 4.4. Calculated total theoretical cross sections for normalized unit areas versus the experimentally determined equilibrium sample charge for samples irradiated with a non-monochromatic magnesium X-ray source.

ibrium sample charge is a function of the sample size and its position in the sample chamber, as might be expected since the vacuum current, I in is not homogeneous and I out depends on the total X-ray flux impinging on the sample. A geometric variable of greater importance however is the rotation of the sample along its axis, since θ in figure 4.3 is readily within the control of the operator. Ascarelli and Missoni have previously measured the sample charge as a function of the angle by means of an electrometer attached to samples of gold and

aluminium.[23] Their work clearly demonstrates that when the samples were facing the X-ray source gold exhibited a higher positive charge than aluminium (as might be expected in the light of the foregone discussion). However, when the samples were turned away from the X-ray source both the gold and aluminium samples showed the same negative potential (-8 volts). This was rationalized[23] in terms of I out being equal to zero since no photoionization or related processes could occur in the sample shielded from the X-rays and both samples would therefore attain the same potential governed by I in, which might be expected to be essentially independent of the nature of the sample. In practise the sample charging effects are only observed for a small portion of the available angular variation, i.e. $\theta \approx 0$ to 90° in figure 4.3, since beyond these limits either no signal due to photoionization is produced ($\theta = 90^{\circ}$ to 270°) or is detectable ($\theta = 270^{\circ}$ to 360°). In this region the data of Ascarelli and Missoni[23] is not clearly presented, thus it is of interest to present such data here. Figure 4.5 shows the equilibrium sample charge on the ethylene-tetrafluoroethylene copolymer as a function of θ. Due to the number of parameters involved and the inhomogeneous nature of the vacuum currents in the spectrometer it is not possible to rationalize the trend depicted in figure 4.5 at the present time. However it is interesting to note that a similar trend has been observed for a variety of samples and this example serves to illustrate the importance of maintaining a standard geometry when comparing the charge on different samples.

A further point in this connection is derived from the study of composite samples of gold and polymer mounted side by side on the probe tip. The data are collected in Table 4.2 where $\theta = 45^{\circ}$.

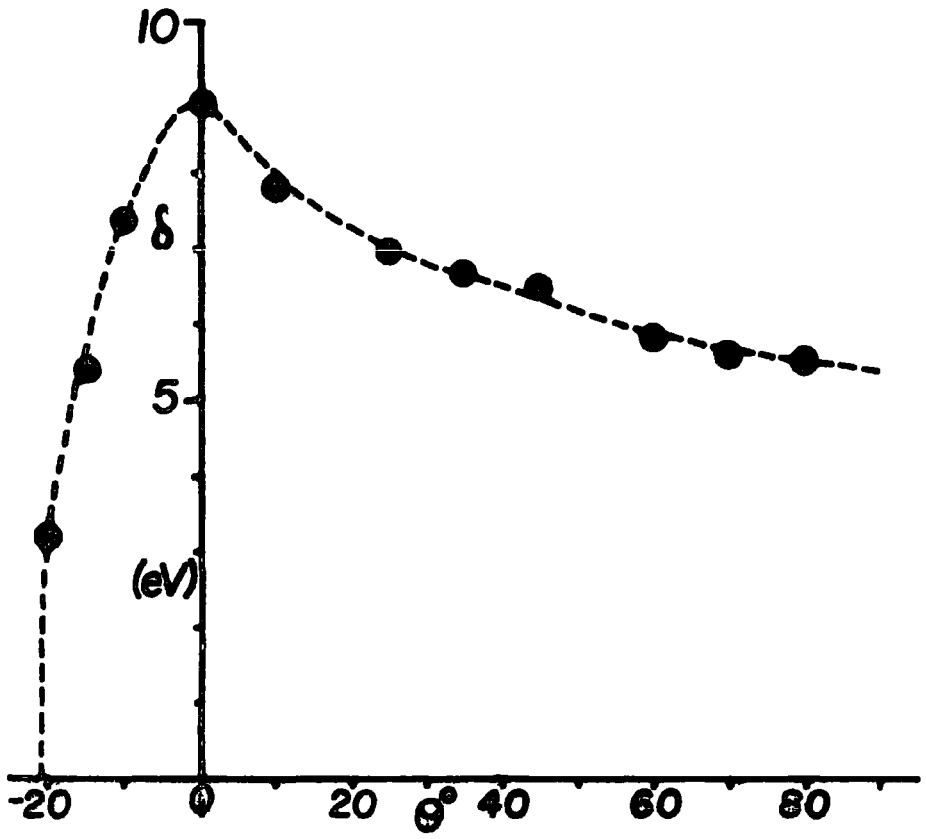

Figure 4.5. Sample charging of the ethylene-tetrafluoro-ethylene copolymer as a function of θ.

Table 4.2. Charging of Composite Samples

Sample	Charge on Gold (eV)	Charge on Polymer (eV)
Au	13.5	-
PE	-	3.4
E-TE	-	7.5
PTFE	-	10.0
Au/PE	11.4	7.6
Au/E-TE	10.2	9.1
Au/PTFE	13.5	13.5

This data suggest that for samples mounted in close proximity that the equilibrium charge on each is changed in a

direction towards that of the other. It should be apparent from these observations that sample charging can be a very useful source of information but due to its complex nature must be treated with due care and attention.

Having outlined the characteristic nature of the sample charging phenomena and having intimated that this depends strongly on structure and bonding in the surface regions the next section describes a series of experiments which amply demonstrate the surface sensitivity of the phenomena.

3.2 Surface Sensitivity of Sample Charging.

A recent publication from this laboratory has outlined a method which allows a convenient means of both obviating and selectively controlling hydrocarbon contamination of surfaces.[111] Therefore a systematic investigation of sample charging as a function of hydrocarbon contamination of the surface for both gold and the polymer samples has been carried out. The objective of this investigation is twofold; firstly to investigate the sensitivity of sample charging phenomena to surface contamination and secondly to provide a more detailed study than has hereto been available on the reliability of establishing absolute binding energies by reference to hydrocarbon contamination of samples.

Spectra were, therefore, recorded under conditions in which hydrocarbon contamination built up over a convenient time period of $\sim$100 minutes. Since the features which emerge from this investigation are common to all of the systems studied a detailed discussion will be confined to gold, PTFE and PVF_2 which together with PE encompass the spectrum of sample charging observed for the complete series. Considering firstly gold,

figure 4.6 shows plots of both the sample charge and the Au_{4f}: C_{1s} ratio as a function of time in the spectrometer. From the relative intensity ratios of the core level spectra it may readily be shown that the initial gold sample to which the equilibrium static charge in figure 4.4 pertains corresponds to a gold surface with hydrocarbon coverage corresponding to a monolayer (~ 5 Å).[99] The correlation between decrease

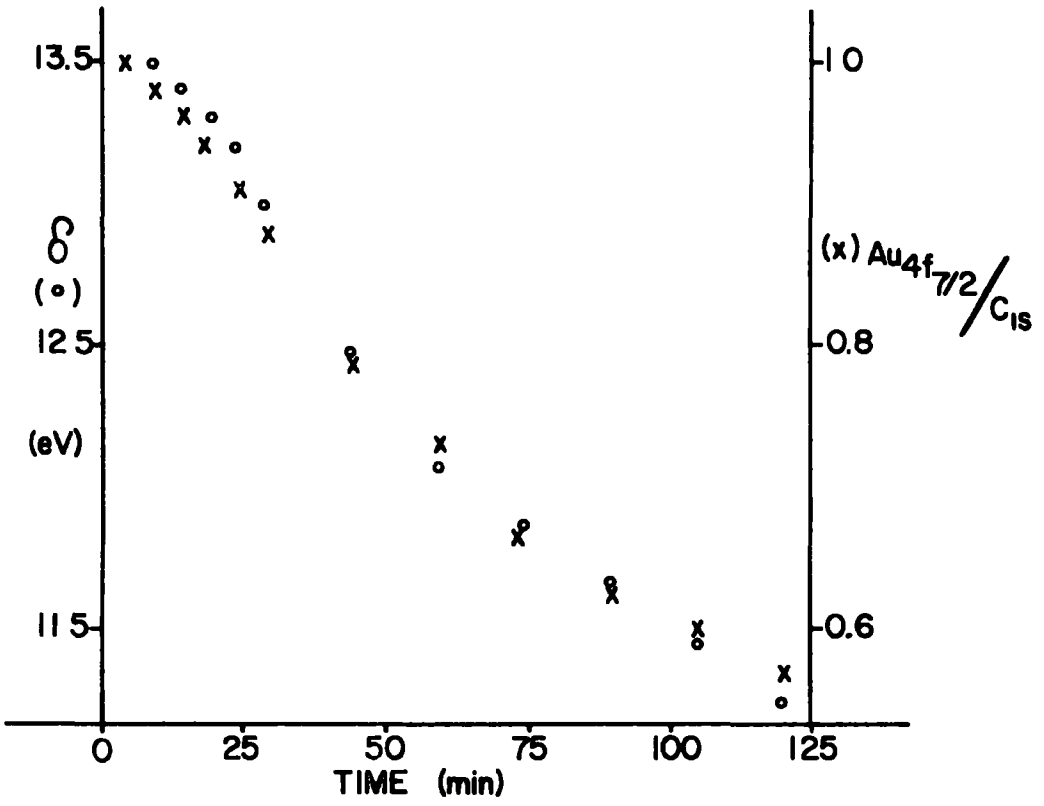

Figure 4.6. Sample charging and degree of hydrocarbon contamination (monitored by the $Au_{4f_{7/2}}$: C_{1s} ratio) versus time in the spectrometer for a gold sample.

in surface charging and increase in thickness of the hydrocarbon contaminant layer provides a straightforward pictorial representation of the surface sensitivity of sample charging.

With a knowledge of electron mean free paths as a function of kinetic energy it is a straightforward matter to estimate the thickness of the hydrocarbon film.[52,99] (In this connection it should be noted that the independent estimates based on the signal attenuations for the $Au_{4f_{7/2}}$ and C_{1s} levels give essentially the same result). For a decrease in sample charging of 2 eV the corresponding increase in thickness of the hydrocarbon overlayer is ~ 8 Å. The form of the curve relating sample charging to thickness of contaminant film would suggest that a completely clean surface studied under identical conditions would have a slightly larger shift (probably of the order of a few eV) the net effect being to displace the data point for gold indicated in figure 4.4 to the right. If for a sample of essentially zero total cross section the sample charging were zero the data points relating sample charge (δ) to cross section would then fit a smooth curve. These experiments, therefore, suggest that charging for samples which are insulated from the spectrometer probe depend on structure and bonding on a depth scale of the same order of magnitude as electron mean free paths.

The deliberate surface contamination of samples with hydrocarbon has been advocated as one of the most routinely reliable and reproducible means of establishing the energy reference for insulating samples.[1] In this connection, therefore, it is of interest to consider the shift in binding energy between the $Au_{4f_{7/2}}$ and C_{1s} levels as a function of overall sample charging. This is shown in figure 4.7. Considering the extremes, of zero sample charging (gold in electrical contact with spectrometer) and the maximum in sample charging (~ 13.5 eV), the shift in energy between the core levels of substrate (Au) and over-

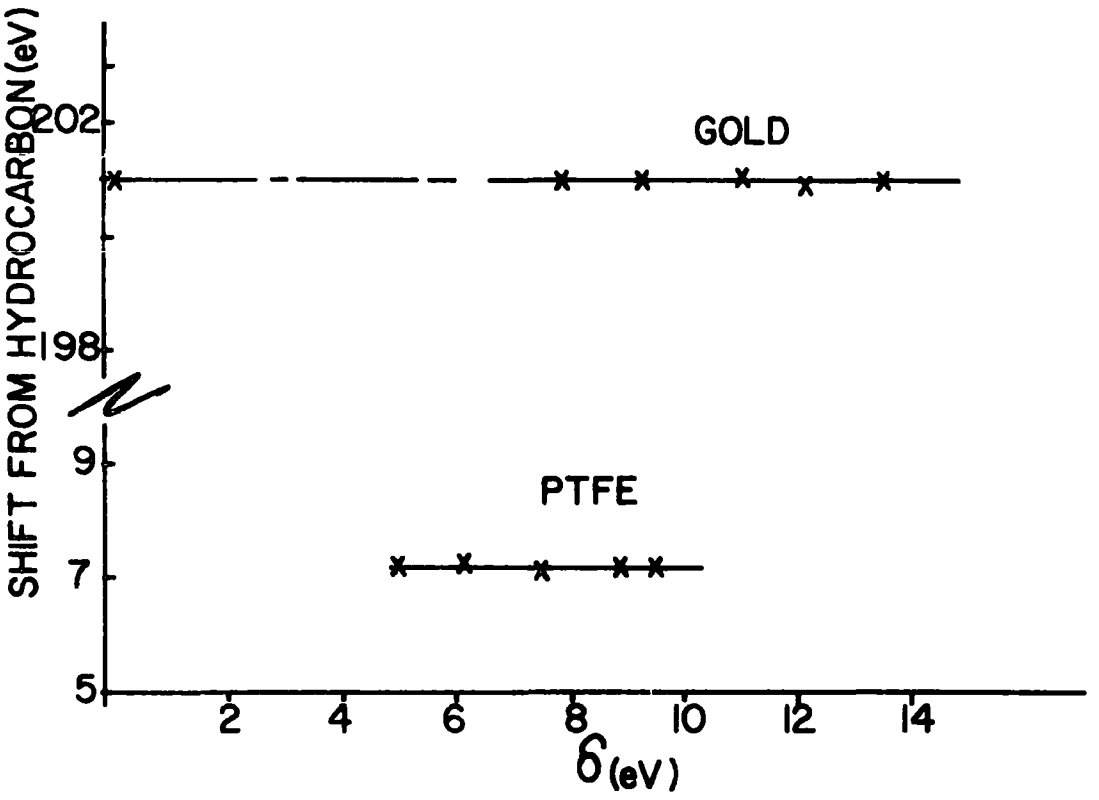

Figure 4.7. Shift in kinetic energy between the $Au_{4f_{7/2}}$ and C_{1s} core levels versus sample charge for gold and polytetrafluoroethylene.

layer (hydrocarbon) is exactly the same within very small error limits, ~ 0.1 eV. Since for most polymeric systems (for which we have previously advocated the use of this technique for energy calibration), the span in sample charging is substantially smaller, the accuracy of the method is extremely good.

The corresponding data for PTFE, PVF_2 and PE are shown in figure 4.8. The decrease in sample charging as a function of hydrocarbon deposited on the surface is clearly evident in the particular cases of PTFE and PVF_2. However, the closely similar chemical nature of the polymer surface and contaminant film ensure that for PE the sample charging remains essentially constant. Since the overall integrated intensity of the C_{1s}

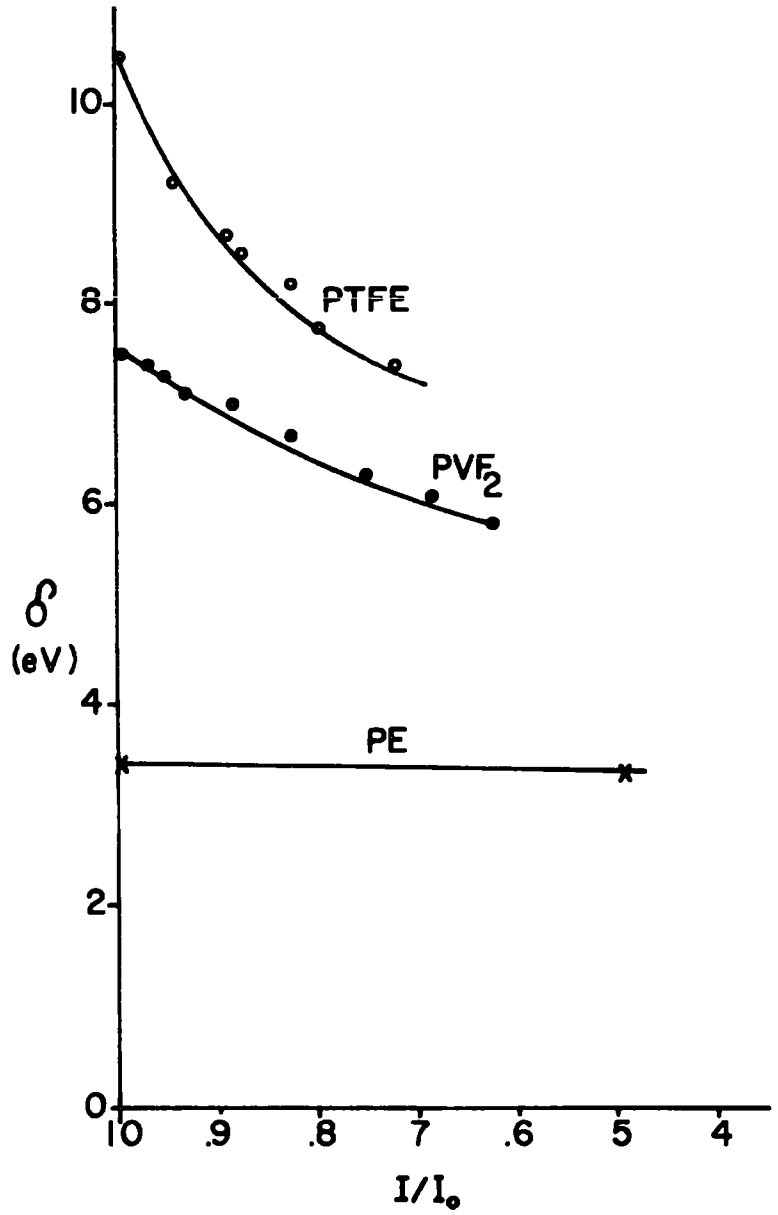

Figure 4.8. Sample charging as a function of hydrocarbon contamination. (Monitored by the decrease in intensity of a core level signal arising from the polymer relative to its intensity at the start).

levels for the latter do not change with time there is no direct evidence from this source alone that hydrocarbon contamination of PE itself occurs. The fact that it does, however, may readily be demonstrated by investigating samples with submonolayer extents of surface oxidation. Such low levels of oxidation do

not of themselves alter the overall sample charging, however, they do provide a valuable "marker" in the O_{1s} levels. By monitoring the decrease in intensity as a function of time it may thus be readily demonstrated that hydrocarbon contamination also occurs for PE.

The rate of build up of hydrocarbon is a convolution of several factors including the partial pressure of extraneous hydrocarbon in the vicinity of the sample surface. The single most important sample dependent factor will be the sticking probability for hydrocarbon at the polymer surface which will be related to surface free energy. On this basis it might be anticipated that under comparable experimental conditions rates of hydrocarbon contamination should reflect this. By monitoring the decrease in C_{1s} intensity, of appropriate characteristic peaks for PHFP, PTFE, PVF_2, E-TE and PVF, films, attributable to hydrocarbon contamination as a function of time this may readily be demonstrated. Thus the time taken for the signal to decrease by 1/eth of its original value in a particular series of experiments in which hydrocarbon contamination was deliberately accelerated was 280, 120, 84, 90 and 80 minutes respectively for PHFP, PTFE, PVF_2, E-TE and PVF. Since each polymer system has a characteristic equilibrium charging shift it might also be anticipated that the change in this shift as a function of surface contamination should also be characteristic of the sample. This may readily be shown by considering the change in equilibrium charging shift for PHFP, PTFE, PVF_2, E-TE and PVF when the contaminant film is such that the characteristic C_{1s} levels for these systems has again decreased by 1/eth of its original value. The corresponding shifts for this series of polymers are 3.5, 3.3, 1.5, 1.8 and 1.2 eV respectively.

It should be noted that in these experiments it is also possible to monitor the shift between the C_{1s} signal of the hydrocarbon contaminant and the peaks of characteristic binding energy for the fluoropolymers. As in the case of gold discussed above the shift is independent of sample charging within very narrow limits confirming the thesis that hydrocarbon contamination is an excellent technique for energy referencing. (The data for PTFE being a representative sample is shown in figure 4.7). In the particular case of PE the rate of build up of hydrocarbon may be monitored by following the decrease in intensity of the extraneous O_{1s} signal. For gold as we have previously noted the original sample has approximately a monolayer of hydrocarbon contamination already present and it might, therefore, be anticipated that the rate of build up of hydrocarbon contamination on both the PE and gold samples would be somewhat similar. That this is the case may readily be demonstrated by following the decrease in intensity of the gold 4f levels. When due allowance is taken of the differing electron mean free paths corresponding to electrons photoemitted from the O_{1s} and Au_{4f} levels the comparable rates put onto a similar basis as those of the other samples gives a time scale of $\sim$ 50 minutes which is entirely reasonable on the basis of the higher surface free energy.

One question which immediately springs to mind on the basis of the data presented this far is "do rates of hydrocarbon contamination themselves depend on the absolute magnitude of surface charge?" The crucial issue embodied in this question is whether sticking probabilities are in any way substantially altered compared with the neutral system if the sample carries a surface charge. To investigate this possibility experiments

were carried out in which gold samples either insulated from or in electrical contact with the spectrometer were studied simultaneously and the rates of hydrocarbon contamination monitored as a function of charging shift between them. Experiments corresponding to overall positive and negative charging shifts were carried out by means of biasing the samples and revealed that for shifts ranging from + 19V to - 19V the rates of hydrocarbon build up were identical to that of the gold sample in electrical contact with the spectrometer. The sticking probabilities under the conditions of these experiments, therefore, directly reflect structure and bonding of the sample surface.

To summarize the data presented to this point it is clear that sample charging under a given set of conditions is characteristic of a sample and depends on structure and bonding on a similar depth scale to that appropriate to typical electron mean free paths.

It will be seen from the chapters of this thesis concerned with surface modification of polymeric materials that the surface sensitivity of sample charging adds another 'string to the bow' in the use of ESCA for the investigation of structure, bonding and reactivity of the very outermost surface regions of a sample, particularly for fluorinated systems where the range of charging shifts may be large. (Cf figure 4.4).

3.3 Sample Charging as a Function of the Operating Parameters of the X-ray Source.

As a logical next stage in the investigation, sample charging has been studied as a function of the operating parameters of the X-ray source. As a reasonable overall compromise in terms of signal intensity, signal/background, signal/noise, time

scale for generating spectra, minimizing radiation damage etc., the most usual operating conditions using an unmonochromatized $Mg_{K_{\alpha 1,2}}$ X-ray source is 12 kV and 15 mA. To study the effects of varying these parameters sample charging for gold mounted insulated from the spectrometer probe has been investigated and the results are displayed in figure 4.9. Considering firstly sample charging as a function of current in the X-ray tube at

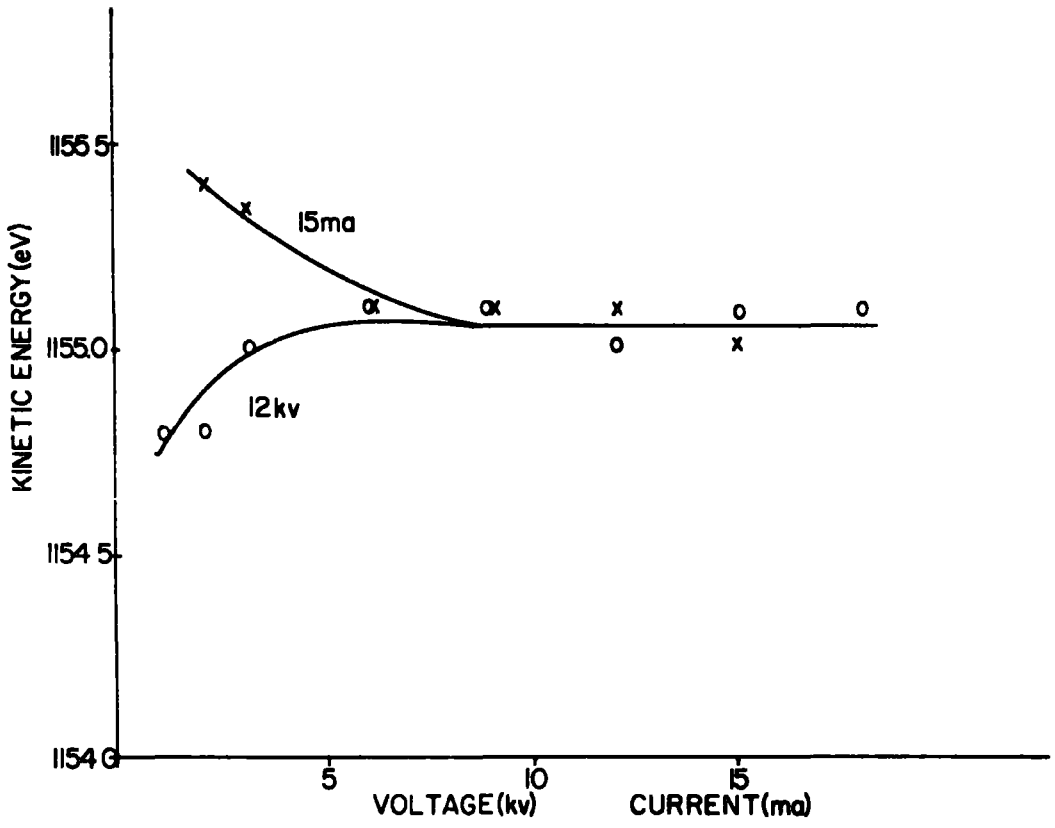

Figure 4.9. Sample charge as a function of a fixed voltage (12kV) and variable current (6-20mA) and a fixed current (15mA) and variable voltage (2-15kV) for a gold sample electrically isolated from the spectrometer.

fixed voltage (12kV) it is clear that in the range 6-20 mA sample charging remains essentially constant. Below 6 mA

there is a gradual increase such that at 2 mA the sample charge has changed by ∿ 0.2 eV (viz. ∿ 1.4% change in sample charging for an order of magnitude decrease in current). Also shown is the change in sample charging for a fixed operating current of 15 mA and varying the voltage in the range 2-15 kV. In the region 6-15 kV which spans the normal operating region for all commercially available spectrometers the sample charging is constant within very narrow limits. Below 6 kV there is a tendency for sample charging to decrease, however, the effect is again small such that at 2 kV the sample charging differs by only ∿ 0.3 eV from the equilibrium charge under normal operating conditions. These experiments, therefore, amply demonstrate that under the conditions employed in this work the equilibrium charge acquired by a sample is essentially constant over a wide range of operating conditions encompassing power loadings in the range 12 watts - 225 watts which is consistent with previous data.[183,184] Furthermore it may readily be shown that with samples directly mounted onto the probe with double sided 'Scotch' insulating tape that the time scale to establish equilibrium charge is rapid compared with the typical time scale required to record the data. Essentially identical data are therefore obtained if equilibrium charge is studied by successively increasing or decreasing either the voltage or current in the X-ray tube, viz. the data displayed in figure 4.9 exhibit no hysteresis effects. To demonstrate that the phenomena illustrated in figure 4.9 are entirely representative of samples in general comparable studies have also been carried out on PTFE and again in the operating range 6-15 kV and 4-20 mA the equilibrium charge remains constant.

3.4 Time Dependence of Sample Charging

Although as has been indicated for samples mounted on double sided 'Scotch' insulating tape the equilibrium charge for a given sample is rapidly established this is not generally the case for polymer films which are directly attached to the spectrometer probe either by locating screws or by insulating tape located on the reverse side of the probe tip. In the case of samples mounted on 'Scotch' tape the adhesive bonding at the tape/probe and polymer/tape interface ensures intimate contact and the composite, therefore, behaves as a capacitor of layered dielectric composition. For samples mounted directly on the probe, however, the polymer-probe contact on a macroscopic scale is "spotted" and the situation is much more complex.

In this section, therefore, is described the time dependence of sample charging phenomena for polymer films mounted directly in contact with the spectrometer probe.

Three systems were chosen for detailed investigation, namely PTFE, E-TE and PE. Considering firstly the data (figure 4.10) for PE the initially measured shift for the 50μ film (identical to that used for the investigation described in section 3.2) corresponds closely to that for films mounted on 'Scotch' tape, however, over a period of ∿ 25 minutes the charging shift increases until an equilibrium value of ∿ 5 eV is attained. Both PTFE and the E-TE copolymer exhibit similar but somewhat larger increases in sample charging with respect to the initial values which again correspond closely to those measured for samples mounted on insulating tape. The maximum in charging shift relative to that measured for samples mounted on tape increases in going from PE to PTFE. For PTFE and E-TE polymer films the

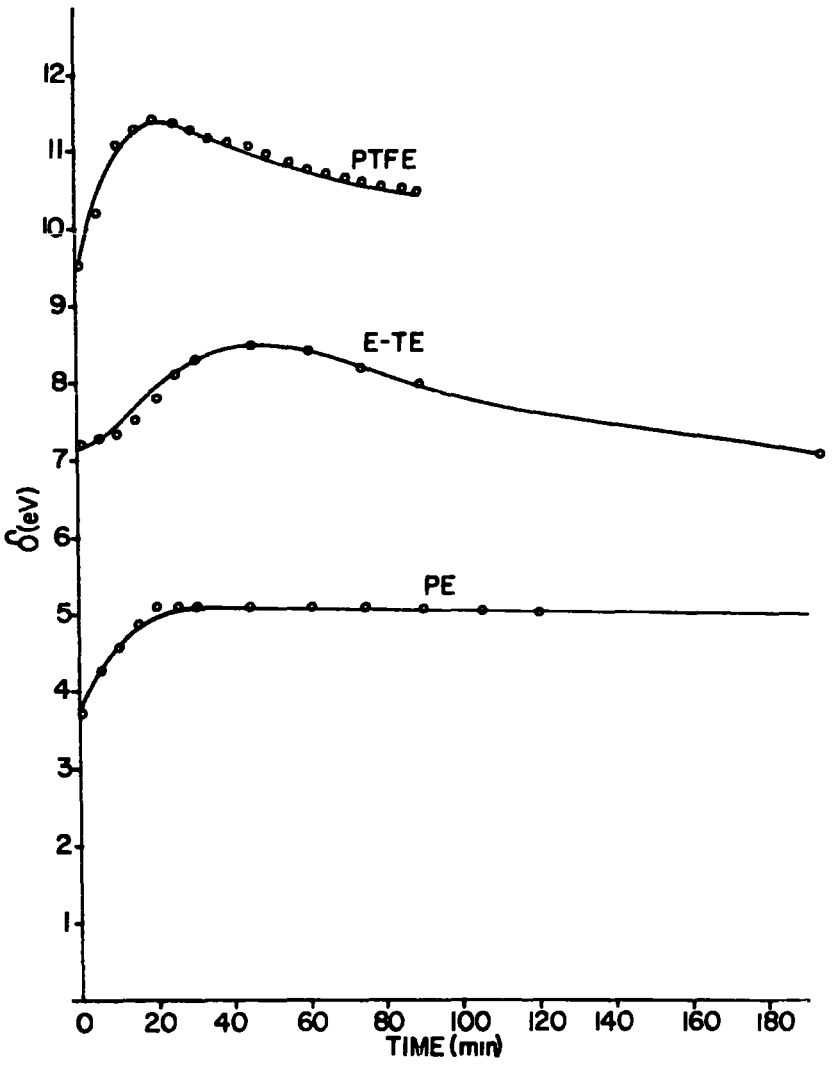

Figure 4.10. Sample charging of PTFE, E-TE and PE, mounted in 'spotted contact' with the probe tip, versus time.

decrease in sample charging is attributable to hydrocarbon contamination as is clearly evidenced by the core level spectra. Although the sticking probability for hydrocarbon on the PTFE surface is lower than for the E-TE copolymer the decrease in shift onsets after a shorter period since the difference in cross sections between a hydrocarbon overlayer and polymer are somewhat larger in the case of PTFE (cf. figure 4.4). The data displayed in figure 4.10 are representative of that obtained

for a number of repeat experiments. Since it is unlikely that the polymer-probe interface was exactly the same in this series of experiments, and since the extraneous hydrocarbon partial pressure was also allowed to vary it would not be expected to be able to exactly reproduce the data for a given sample. The broad features in each case, however, follow the trends discussed above. Namely that the initial charge showed a close similarity to that for samples mounted directly on 'Scotch' tape and that the shift first increased and then decreased as a function of time, the decrease being associated with hydrocarbon contamination. For films studied in this manner, therefore, (spotted contact) even in the absence of hydrocarbon contamination there is a distinctive time dependence for the sample charging and clearly the accurate measurement of absolute binding energies requires that such films be studied when equilibrium has been established. If measurements are being made over extensive energy ranges and which require considerable time spans then it becomes imperative to take such factors into account. Such a situation obtains in generating valence band spectra where the low photoionization cross sections for soft X-ray sources often entails experiments on an extended time scale.[125,136] Hydrocarbon contamination which needs to be taken into account in measuring absolute and relative binding energies must also be considered from the point of view of the shifts in sample charging which may arise consequent upon its build up at sample surface. Although, therefore, even for polymer samples mounted directly on to the spectrometer probe, sample charging is characteristic of the polymer, the convolution of factors contributing to the time dependence of such charging considerably complicates matters and in the extreme could lead to artificially

narrowed or broadened peaks, skewed line shapes and incorrect energy referencing. It is clear, therefore, that if use is to be made of the structural dependence of sample charging then samples must be studied under conditions in which the equilibrium charge is rapidly attained and hydrocarbon contamination (which provides an extremely convenient and reliable energy reference) must also be closely controlled.

4. Charging Induced by a Monochromatic X-ray Source

The use of an $Al_{K\alpha_{1,2}}$ monochromatized X-ray source greatly extends the scope of sample charging studies since the reduction in the vacuum current I in, consequent upon removal of the bremsstrahlung, narrowing of the X-ray beam and having the X-ray gun remote from the sample, results in greater charging effects and extended time dependencies. In general however many of the trends are expected to be similar to those observed for the unmonochromatized $Mg_{K\alpha_{1,2}}$ X-ray source. In this section, therefore, only features which form an extension to those already discussed are included. In particular the study of sample charge as a function of film thickness is discussed in detail.

A common method to control sample charging when using a monochromatic X-ray source and to reduce it to low levels, is by the inclusion of a low energy electron flood gun in the sample region.[87] Recently a more convenient method has been devised in this laboratory involving a low pressure mercury lamp ultraviolet source. A discussion of this is included in the next section.

4.1 Some Instrumental Dependent Factors Governing Sample Charging

In previous sections it has been shown that samples of gold specifically mounted on insulating films of 'Scotch' tape charge

in a characteristic manner. The absolute magnitude of the sample charging employing an unmonochromatized $Mg_{K\alpha_{1,2}}$ X-ray source (∿13.5 eV) is independent of the photon flux over a considerable range of operating powers, and the equilibrium charge is rapidly attained compared with the typical time required to obtain a spectrum. The importance of the spectral distribution of the X-ray source amongst the many parameters determining the sample charge is evidenced by the results of similar studies employing identical gold samples irradiated by a monochromatic $Al_{K\alpha_{1,2}}$ X-ray source. In this situation the sample charging is enhanced by almost an order of magnitude at comparable power loadings and exhibit a marked time dependence. Thus at 150 watts (15 kV, 10 mA) the equilibrium shift compared with a grounded gold sample amounts to ∿64 eV and the typical time scale to obtain equilibrium is 60 minutes. This typical average charging rate of ∿1 eV/minute complicates the direct monitoring of the core levels since the time scale to generate the relevant data is somewhat similar. In addition to exhibiting time dependence the equilibrium shift is also a strong function of the power supplied to the monochromatic X-ray source. In going from 150 watts to 450 watts the equilibrium shift increases by ∿32 eV. It is of course well documented that removal of the bremsstrahlung as a source of low energy secondary electrons enhances sample charging and this had led to the development of low energy electron flood guns.[87] Indeed the use of a flood gun often results in a negative charge on the sample. The use of low power, low pressure mercury lamps is an alternative.

With an appropriate quartz viewing port in the spectrometer sample chamber and nitrogen purging facilities a 5 watt lamp

provides sufficient output in the ultraviolet (∿184.9 nm or ∿ 6.7 eV) to produce a copious source of low energy electrons from direct photoemission from the spectrometer sample chamber such that sample charging is effectively neutralized. Indeed it may be readily shown that by varying the power to the lamp sample charging may effectively be tuned over a considerable energy scale. Figure 4.11 for example shows a plot of equilibrium shift in sample charging for a gold sample, mounted insulated from the spectrometer probe, as a function of the power supplied to the low pressure mercury lamp at 150 watts and 450 watts for the X-ray source.

The net effect of the electrons produced by the ultraviolet photoemission is two fold. Firstly the time scale for reaching equilibrium is considerably shortened, compared to the time required to record the spectrum (viz. the equilibrium charges displayed in figure 4.11 are attained virtually instantaneously). With the X-ray source operating at 150 watts sample charging is small and remains essentially constant over the range 1.7 - 5.0 watts input to the lamp. At the higher X-ray power the sample charging is constant over a much smaller range, 2.5 - 5.0 watts. At lower lamp input powers the sample charge rapidly increases such that at the lowest operating levels (∿ 0.8 watt) the difference in shift with respect to the asymtotic value at higher ultraviolet outputs amounts to∿ 11 eV and 25 eV for power loadings of 150 watts and 450 watts for the X-ray source respectively. As has been previously noted the equilibrium charge for the sample under conditions in which the lamp is not used, as a source of secondary electrons, is time dependent. The possibility of being able to effectively remove the time dependency by means of the lamp and of being able to tune the magnitude of the sample charging suggests considerable utility for this technique in

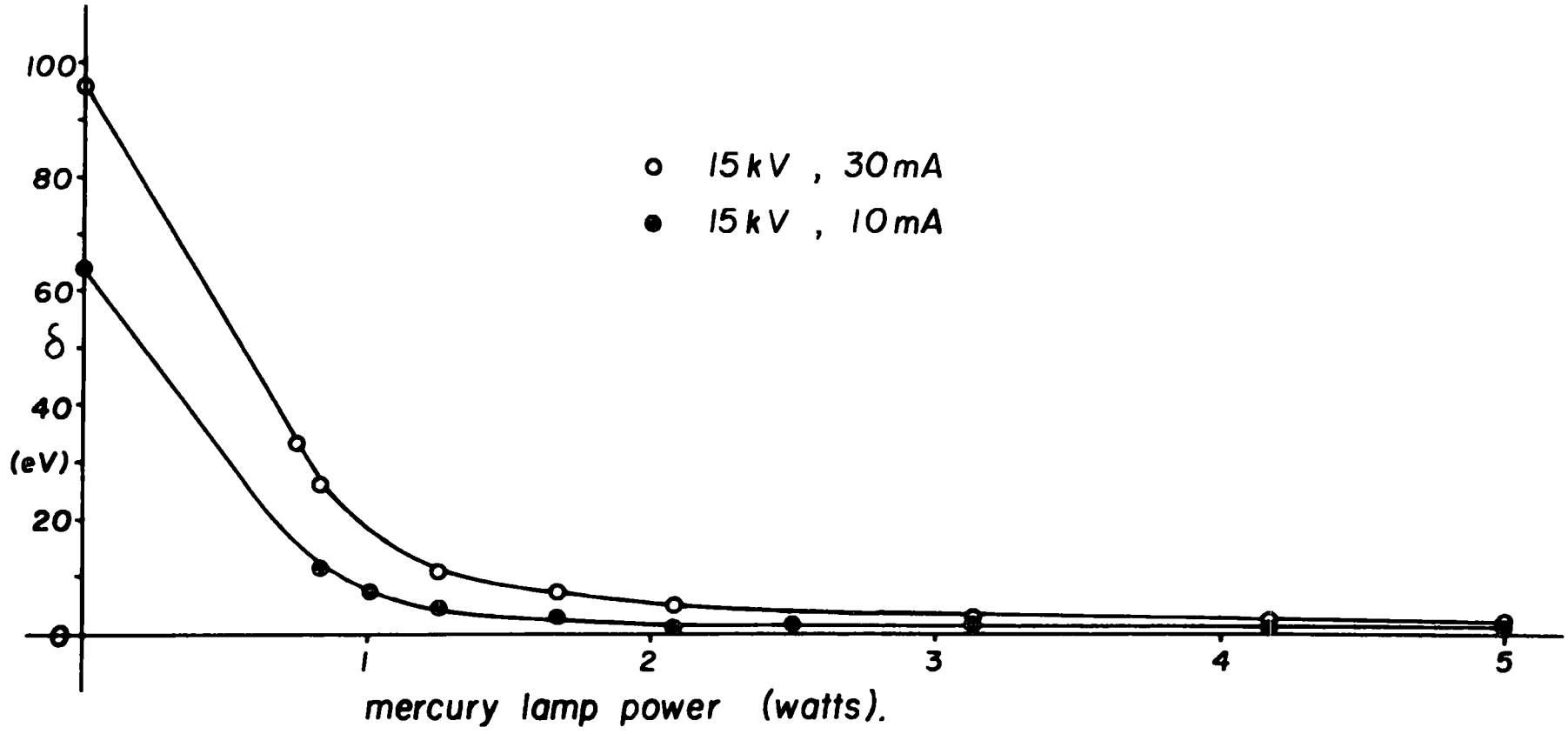

Figure 4.11. Sample charging of gold, at X-ray input powers of 150 and 450 watts, as a function of the power supplied to the mercury lamp.

studying sample charging in general. Furthermore, incorporation of modulation facilities into the lamp systems opens up the possibility of studying the time dependence of sample charging in far greater detail.

4.2 Sample Charging as a Function of Film Thickness

In previous sections the sample charging of thick samples has been rationalized in terms of, amongst other factors, the total photoionization cross-section of the material. The surface nature of the characteristic charge has been demonstrated by reference to thin films of extraneous hydrocarbon contamination deposited onto the surface of the samples. Due to the large charging shifts induced by a monochromatic X-ray source the investigation of sample charging as a function of film thickness may be greatly extended. Thus in this section is discussed an investigation into sample charging characteristics of polymer films in the thickness range 0-20μm deposited onto gold substrates which are in electrical contact with the spectrometer. Figure 4.12 shows a plot of the sample charge on a polyparaxylylene film, deposited onto a gold substrate in electrical contact with the spectrometer, on irradiation by the monochromatic $Al_{K\alpha_{1,2}}$ X-ray source (15 kV, 38 mA), versus the film thickness. For the thinner films the Au_{4f} core levels were also observed and of course showed no deviation from the kinetic energy appropriate to a binding energy of 84.0 eV. Under these conditions the polymer films of less than ∿1000 Å thick showed very little charge. This can be readily understood since for these samples the mean free path of the X-ray photons is such that they may penetrate through the sample to the gold, thus producing sufficient charge carriers to allow electrical conduction through the polymer. This is emphasized by the fact that the core level

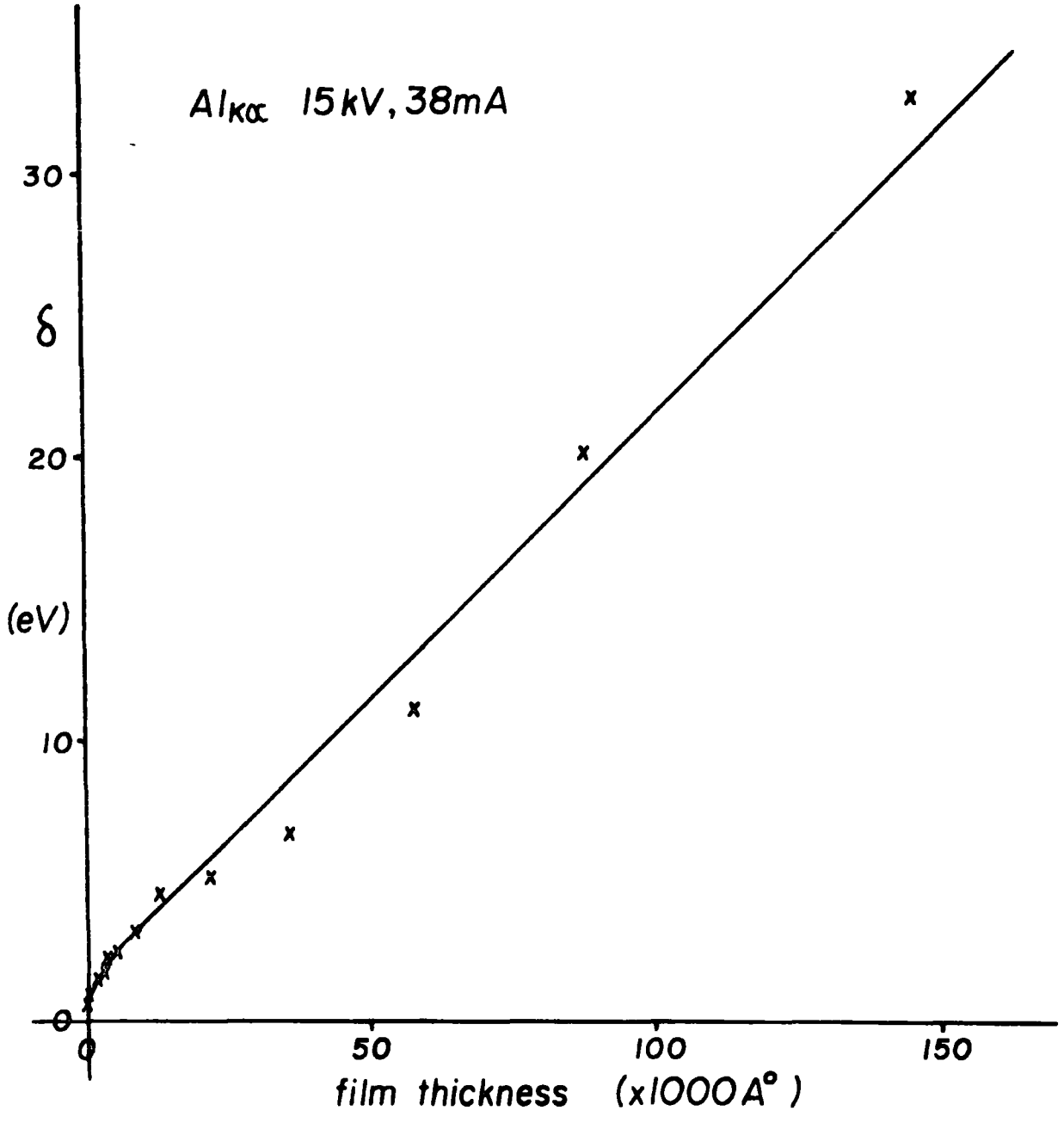

Figure 4.12. Sample charging of polyparaxylylene deposited onto a gold substrate in electrical contact with the spectrometer, versus film thickness.

signals from the polymer follow exactly a bias applied to the gold substrate. For thicker films however the sample charge shows a closely linear correlation with the film thickness and the equilibrium charge becomes increasingly more time dependent until above ~150,000 Å (15μm) the situation described previously

is obtained in which the charge varies on a time scale faster than that required to obtain a spectrum, hence no data is available for samples thicker than this. The effect of applying a bias to the gold substrate of these samples parallels the charging effects in that the time taken to follow the bias becomes very long for the thicker samples. The increased sample charge is also paralleled by the increasing inability to attain the shift appropriate to the magnitude of the applied bias, with increasing thickness of the film. The linear correlation exhibited between sample charge and film thickness suggest that there is almost an ohmic relationship between the currents passing through the sample, the sample thickness and the potential difference between the upper and lower polymer surfaces. It may even be envisaged that the phenomena described here might form the basis of a sensitive technique for the measurement of film thicknesses.

5. Conclusion

It should be clear from the discussion and examples presented in this chapter that in appropriate cases sample charging phenomena in polymers, contrary to being a nuisance, is potentially a valuable source of information pertaining both to the structure of the surface regions of the material and also to the physical parameters of the sample in terms of its geometry within the sample chamber, the method of mounting of the sample and the film thickness.

CHAPTER FIVE

Surface Modification of Polymers by Inert Gas Plasmas

Part I

1. Introduction

The plasma treatment of polymers and solids in general has been the subject of considerable research interest over the past decade.[148] Indeed the modification of polymer surfaces by electrical discharges (radiofrequency, microwave, corona) excited in a variety of gases is a technique widely used to increase the surface free energy or wettability of the material.[148,189-194] The major virtues of the technique are that it involves clean reactions which take only seconds to achieve the required results and is therefore ideally suited to a flow system, and whilst producing profounc changes in the surface properties of the material (permeability, bondability, printability, etc.) the overall bulk properties of the material, for which it was originally chosen remain unchanged, (electrical characteristics, tensile strength, etc.). The thickness of the modified layer has been estimated to be in the range of 0-10 μm[148] depending on the conditions of the discharge (pressure, power, gas, flow rate). However the surface properties of a polymer sample are determined solely by the composition of the outermost few monolayers, which makes it difficult to employ conventional techniques for understanding the processes involved. This and the following chapter describe a detailed ESCA investigation into the modification of polymers effected by inert gas plasmas whilst Chapter Seven is concerned with those caused by oxygen plasmas.

Symptomatic of the difficulties of employing conventional techniques which do not have specific surface sensitivity is the elaboration of the relative roles of direct and radiative energy transfer in effecting surface modification by inert gas

plasmas. Although no hard scientific evidence has been produced, the general concensus seems to be that the crosslinking at the very surface of a sample may be associated with either or both of direct energy transfer from species in the plasma and the ultraviolet component (wavelength <3800 Å and therefore encompassing the vacuum region) of the electromagnetic radiation emitted from the plasma. For the bulk however the evidence would appear to be in favour of a mechanism dominated by radiative energy transfer.

A plasma may be defined as a partially ionized gaseous state consisting of molecules, atoms and ions in both ground and excited states (including metastable states)and electrons such that the concentration of positively and negatively charge species result in close to overall electrical neutrality. De-excitation of excited states (electronic, vibrational and rotational) produces a wide range of electromagnetic radiation.

Figure 5.1 summarizes the various plasmas which may be found in nature and in the laboratory defined by their electron density and average electron energy. λD is the Debye length, a function of the square root of the electron energy to density ratio.[195] For the ionized gas produced in a discharge to be properly termed a plasma it must have approximate electrical neutrality, a criterion satisfied when the dimensions of the discharged gas volume are significantly larger than λD. The plasmas of particular interest to organic chemists have the characteristic feature that the Boltzmann temperature of the massive species is roughly ambient whilst the average electron energy is some two orders of magnitude greater.

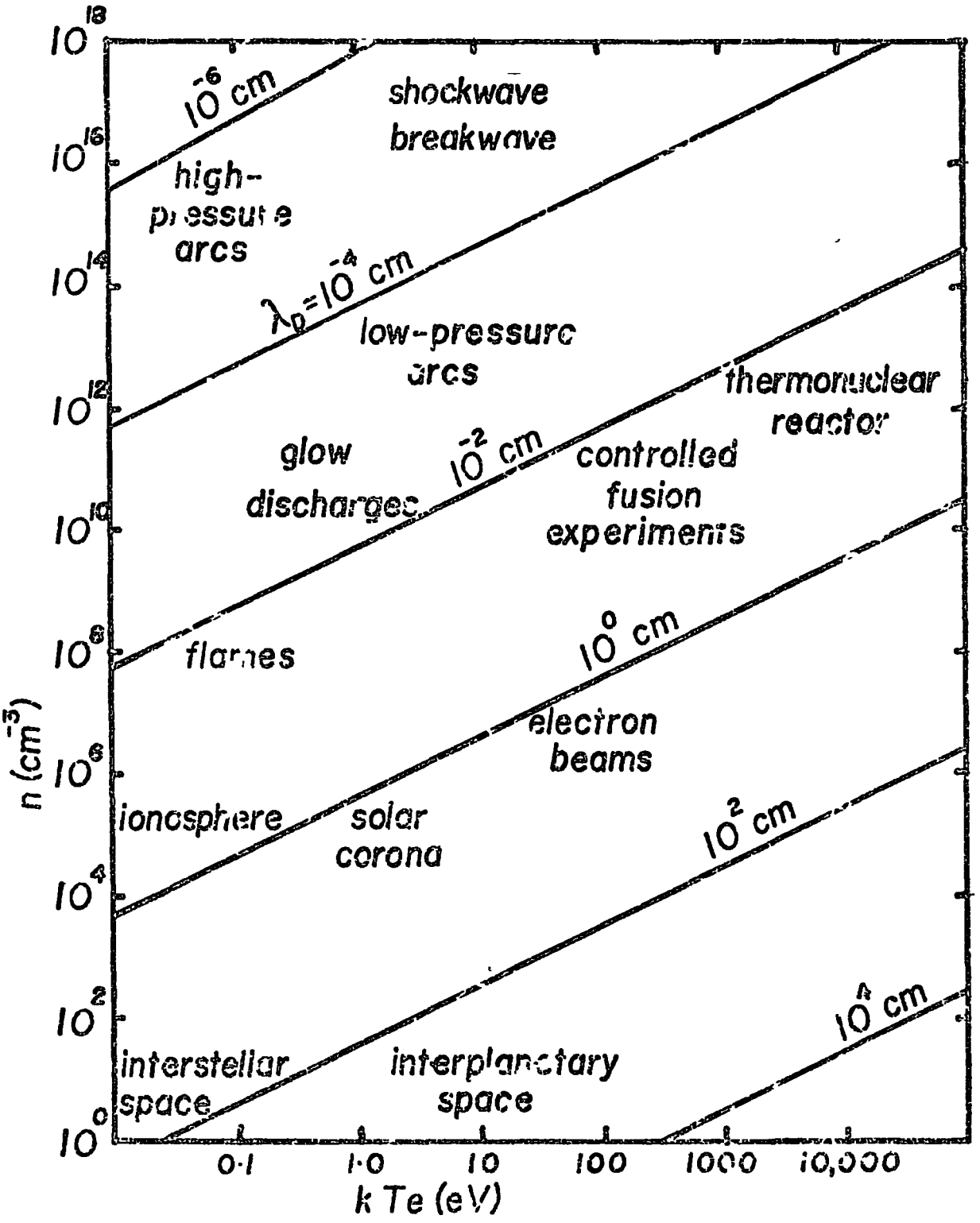

Figure 5.1. Plasmas found in nature and in the laboratory.

These plasmas are termed non-equilibrium or 'cold plasmas' and include glow discharges. By contrast 'hot plasmas' have a near equality between gas and electron temperatures and are usually employed as a high temperature source.

The production of a non-equilibrium, glow discharge may be achieved in many ways, the three major variables being the source of electrical power to sustain the plasma, the coupling mechanism, and what may loosely be termed the plasma environment. The combination selected for a given investigation is dependent on a number of factors such as cost, ease of construction, and convenience. Whilst most of the early work involved AC and DC electroded discharges the greater flexibility and closer control over operating parameters has in recent years shifted the emphasis towards the use of inductively coupled radiofrequency and microwave plasmas. Recent reviews provide a good background to much of the work.[130,148,194]

The choice of electrodeless inductively coupled radiofrequency glow discharges excited in inert gases for the study of surface modification of polymers, in this work, enables close consideration of all of the variables which are likely to be of importance and in addition allows considerable flexibility in terms of reactor design and configuration for introducing and removing samples. The nature of the experiment allows for example a wide range of pressures and flow rates to be investigated and provides a convenient means, since the power loading can be continuously varied, of performing kinetic studies as a function of power loading. In this work emphasis has been placed on the following primary points.

(1) Since plasmas are a copious source of electromagnetic

radiation extending from the vacuum ultraviolet to the visible[196] and on to the infra red and microwave, and since for the vacuum ultraviolet, cross sections can be very large even for saturated systems, it is clear that the surface reaction could also contain a significant contribution arising from radiative energy transfer from the plasma. A technique such as ESCA which allows one to differentiate the surface from the subsurface and bulk should in principle be capable of shedding light on the relative importance of direct and radiative energy transfer as far as the surface is concerned.

(2) For a given polymer system, how does the surface and subsurface reactions vary with the parameters involved (power, flow rate, pressure, sustaining gas) and what can this tell us indirectly about the plasma itself?

This chapter is exclusively concerned with radiofrequency glow discharges excited in argon. The observed trends might be expected to be similar for the two lighter and two heavier members of the inert gas series although absolute values will themselves form trends along the series. This aspect is investigated in Chapter Six which extends the work to include helium, neon, argon, krypton and xenon.

Although the interaction of radiofrequency glow discharges with solids in general has been an active area of research in both industrial and academic laboratories there have been few attempts to characterize the plasmas involved in terms of the energy distribution of electrons, ions and metastables. Indeed such information is only semi-quantitatively available for very simple systems although the broad theoretical framework is reasonably well understood.[195,197] Theoretically a

plasma may be characterized in terms of the average electron energy and the electron density within the system. For simple systems (e.g. inert gas plasmas) the solution to the Boltzmann equation, which need not be of direct concern here, leads to a Maxwellian distribution of electron energies. For more complex systems the average electron energies may be analysed by electrical probe measurements[198-199] and direct electron sampling.[133] (Some preliminary observations of the latter are presented in Chapter Six). Figure 5.2 illustrates the form of the Maxwellian distribution, which is a close approximation for the inert gas plasmas, for average electron

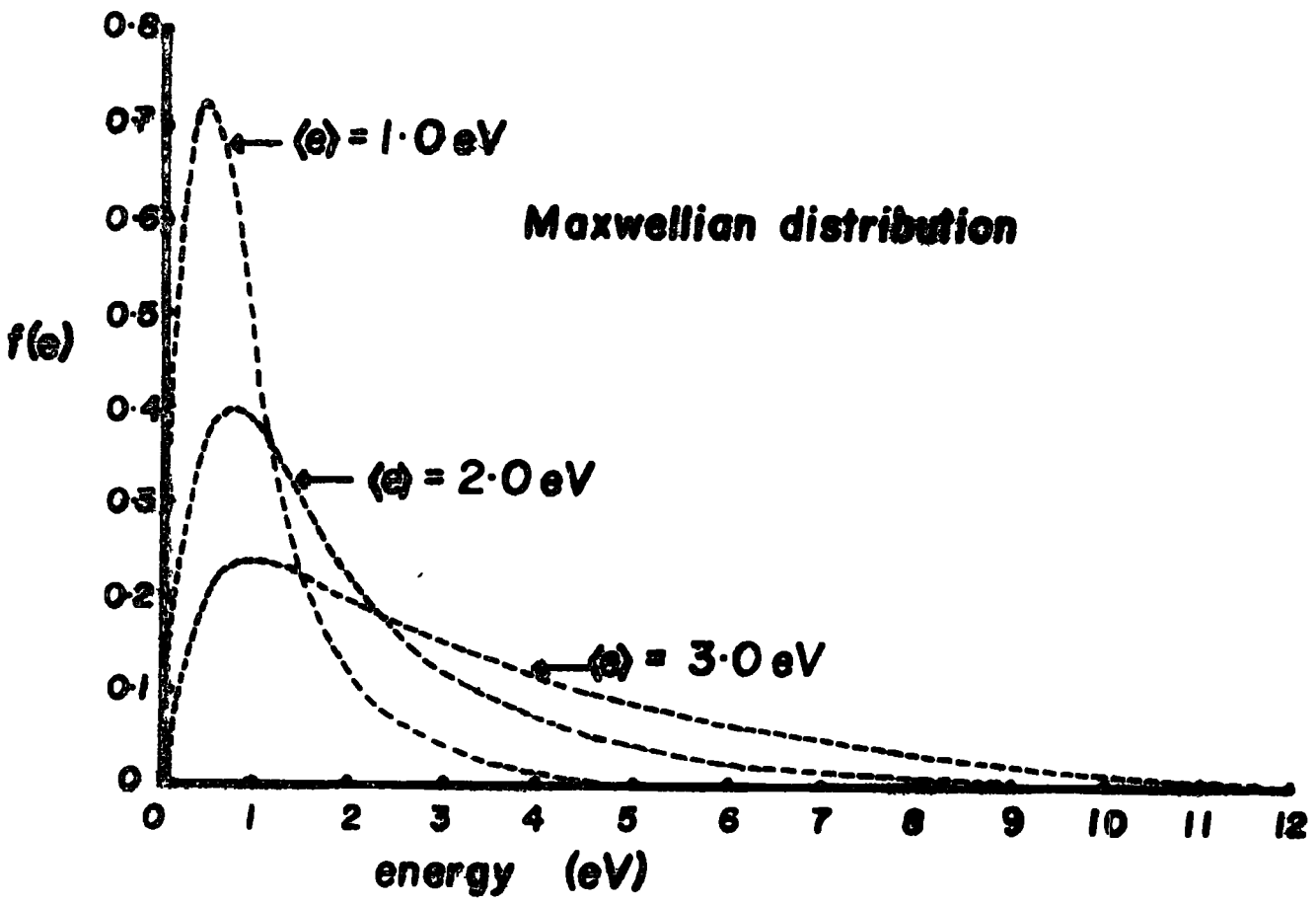

Figure 5.2. Energy distribution of electrons in an inert gas glow discharge.

energies of 1.0, 2.0 and 3.0 eV. In the pressure range 0.05 - 100 torr the distribution typically peaks in the energy range 0-10 eV. The average electron energy is a function of both the power loading and the pressure. Whilst electrons play a dominant role in the plasma itself, in the interaction with polymers it seems likely that their role will be secondary. Although there have been no definitive studies of the mean free paths of electrons in the energy range 0-10 eV in polymers, the generalized form of the mean free path as a function of kinetic energy[200] for the materials which have been studied in detail and the available data for polymers at much higher kinetic energies suggest mean free paths in the hundreds of Angstrom range for near zero kinetic energy electrons in polymers. This being the case direct energy transfer in the surface region is likely to be relatively small and dominated by phonon excitation.

The energy distributions for the neutral species and positive ions corresponds approximately to the ambient temperature. For plasmas excited in argon the important neutral species capable of undergoing energy transfer to a surface are the relatively long-lived metastable $^3P_{2,0}$ states, with electronic energies of 11.55 and 11.72 eV, for which the dominant energy transfer process may well be via Penning ionization processes.[201] The first ionization potential of argon $^2P_{3/2}$, 15.759 eV; $^2P_{1/2}$, 15.937 eV is also higher than for a typical polymer sample so electron transfer at the surface is likely to be of some importance. Indeed the interactior of argon ions with surfaces forms the basis for a sensitive spectroscopic technique developed by Hagstrum[202] (Ion Neutralization Spectroscopy). The mean free paths of argon ions and metast-

ables are likely to be of the order of a few monolayers[203] and they would therefore be expected to dominate the energy transfer processes to the surface, contrasting strongly with the situation previously described for electrons. This becomes even more apparent when recognition is made of the fact that the concentration of positively charged ions and electrons are approximately equal in a plasmas by definition, and that the concentration of metastables is also of the same magnitude.

The electromagnetic radiation associated with radiofrequency glow discharges excited in argon is predominantly in the vacuum ultraviolet with the Ar I (1048 Å, 1067 Å) and Ar II (920 Å, 932 Å) resonance lines being the most important features and to a lesser extent the high photon energy Ar I and Ar II series.[196,204] The continuum due to transitions from the Ar_2^* molecule is not observed at the relatively low pressures necessary for radiofrequency discharges. The vacuum ultraviolet output from the inert gas plasmas is dealt with in more detail in the following chapter. For photon energies in the range spanned by the vacuum region (>8eV) the total attenuation cross sections are undoubtedly dominated by the photoionization component. It is interesting to note that for the experimentally determined attenuation cross section for polyethylene in the corresponding photon energy region ($k = 2 \times 10^5$ cm^{-1} at 1300 Å) 10% of the light at that wavelength is absorbed in the top 50 Å.[205] The production of ions in the polymer lattice provides a variety of mechanisms for cross-linking which are considered in a later section. It is clear however that in addition to fragmentation and isomerization the neutralization of the polymer ions by low energy electrons yields highly energetic species

capable of further transformations.

In an extensive series of publications it has been shown how ESCA as a spectroscopic tool may be used to investigate various aspects of the structure, bonding and reactivity of polymeric systems.[52,114-118] (cf. Chapter Two). A particular feature arising from the strong dependence on kinetic energy of the mean free path for photoemitted electrons is the possibility of employing the technique for analytical depth profiling in which surface, subsurface and bulk may be differentiated. ESCA therefore provides a very powerful tool for the study of surface modification of polymers and indeed in previous works the surface fluorination of polyethylene[123,124] and the surface modification of an ethylene/tetrafluoroethylene copolymer initiated by argon ion bombardment[114] in a simulation of the casing procedure,[146] have been detailed. These preliminary investigations of the argon ion treatment[114] showed that the reactions were essentially confined to the surface regions. Since the light output from the DC discharge employed was essentially collimated and hence irradiation confined to a small fraction of the total surface area the results obtained represent prima facie evidence that ions and metastables in an inert gas plasma can initiate surface modifications.

2. Experimental

2.1 Samples

The system subjected to the most detailed scrutiny involves an ethylene/tetrafluoroethylene copolymer (52% TFE) for a variety of reasons, summarized as follows. Firstly the polymer has been the subject of an intensive ESCA investigation previously and the structure is known to be largely

alternating.[121] The shift in binding energy for the C_{1s} levels is sufficiently large that the signals arising from photoemission from the tetrafluoroethylene components are well resolved with respect to the ethylene components (shift $\sim$ 4.7 eV). It is therefore relatively easy to monitor changes in structure

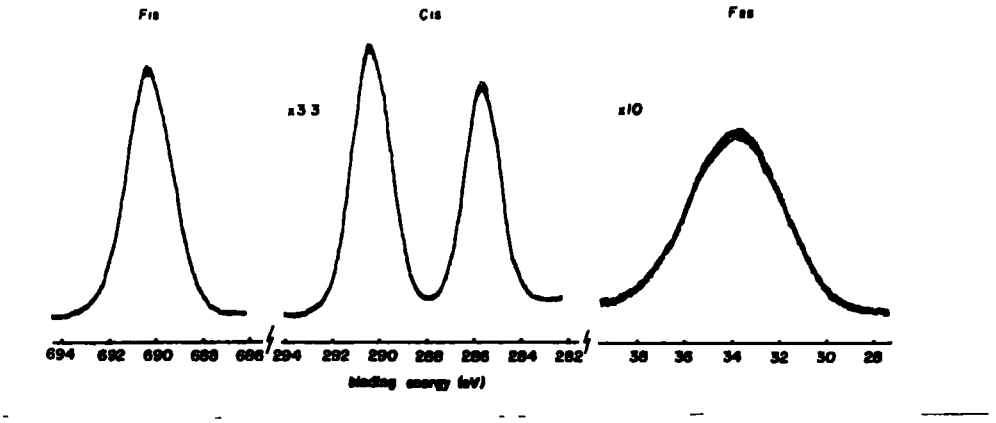

Figure 5.3. F_{1s}, C_{1s} and F_{2s} regions of the ethylene/tetrafluoroethylene copolymer ESCA spectrum.

arising from plasma treatment by monitoring the components of the C_{1s} levels and also the F_{1s} levels. The F_{1s} and F_{2s} levels span a substantial range in kinetic energy for the photoemitted electrons and the monitoring of these levels therefore provides a convenient means of establishing the homogeneity or otherwise of the surface regions of the sample.[123,124] The dominant features in the polymer structure of alternation provides a convenient mechanism for cross-linking arising from the effective elimination of HF and the system therefore provides a simple prototype for more complicated systems for which the number of information levels available from the ESCA experiment is considerably reduced.

For comparison purposes experiments have also been carried out using polystyrene and polyethyleneterephthalate films.

Gold foil has also been employed to study the possibility of sample contamination.

2.2 Instrumentation

Spectra of the plasma treated samples were recorded on the AEI ES 200B spectrometer using $Mg_{K\alpha_{1,2}}$ radiation as previously described. In all cases the measured binding energies are quoted with a precision of $\pm$ 0.15 eV and area ratios (determined by curve fitting procedures) $\pm$ 5%. although these may be slightly generous where the C_{1s} spectra exhibited fairly complex line shapes.

Plasmas were excited in all cases using a Tegal Corporation Radiofrequency Generator capable of delivering a power output from 0.05 - 100 watts, continuously variable. The system includes a pulsing facility which was employed on a microsecond timescale to give greater stability to the plasma at low average power loadings. Tuning of the radiofrequency power was achieved by an L-C matching network in an inductively coupled mode and monitored by the standing wave ratio using a Heathkit HM102 R.F. power meter.

2.3 Plasma Configurations

Three reactor designs have been used in this investigation. Reactors A and B, used for the preliminary investigations, are illustrated in figure 5.4 and were mounted in a greaseless vacuum system, pumped by a two stage rotary pump with a pumping speed rating of 50 $l.\,min.^{-1}$ Pressures were recorded using Pirani type vacuum gauges and the argon introduced via a leak valve. Reactor A consisted of a pyrex tube 52 cms. long and 9cms diameter, with 1" inlet and outlet tubes at its ends. The discharge was excited by a 2.5μH copper coil centred 10cms from

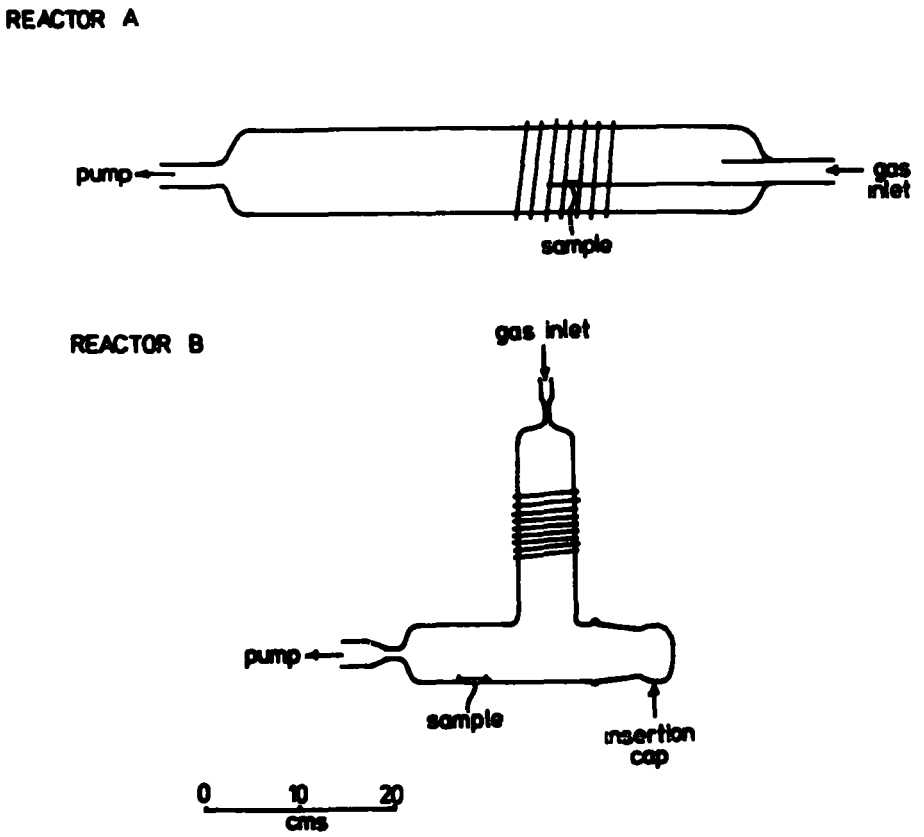

Figure 5.4. Reactor designs A and B.

the inlet tube. Samples were mounted on a glass platform positioned at the centre of the copper coil. Reactor B consisted of 6 cm. diameter pyrex tubing in an inverted 'T' shaped configuration. The overall dimensions were 28 cms. long and 27 cms. high with inlet and outlet tubes, $\frac{1}{4}$" and $\frac{1}{2}$" diameter respectively, the inlet being at the top. The discharge was excited in the vertical limb by a 3.5μH copper coil centred 13 cms. from the inlet tube. Samples were mounted in a stainless steel frame capable of holding two samples side by side with one covered by a quartz slide (1mm thick) for the investigation of the importance of the U.V./visible radiation (wavelength >1600 $\mathring{A}$) in effecting modification. The frame

was inserted into the reactor via a removable cap opposite the outlet tube. For ESCA analysis the samples were removed from reactor A or B and mounted onto the sample probe tip by means of double sided 'Scotch' tape.

The preliminary experiments using reactors A and B led to the development of a more sophisticated reactor design which bolted directly onto the ESCA spectrometer and allowed considerable flexibility in terms of sample handling and the investigations of the pressure and power dependence of the surface modifications. Figure 5.5 is a drawing of the reactor, designated reactor C. Reactor C consisted of a pyrex tube 16 cms. long

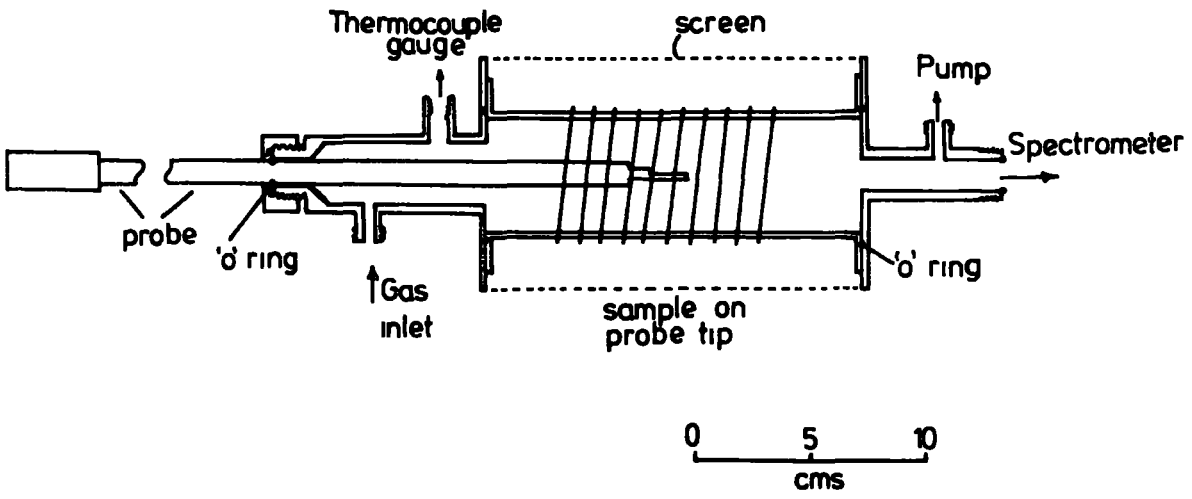

Figure 5.5. Reactor design C.

and 5 cms. diameter sandwiched between stainless steel flanges by viton 'O' ring seals and enclosed in a copper mesh screen, to prevent radiofrequency interference with the electronics of the spectrometer. The discharge was excited by a 4μH copper coil wound centrally on the pyrex tube. Samples were mounted on a ½" stainless steel probe, 60 cms. long, (by means of 'Scotch' tape) which was capable of passing through the reactor,

on viton 'O' ring seals and into the spectrometer for analysis of the samples without exposure to the atmosphere.

The reactor was connected to a two stage 50 l. $min.^{-1}$ rotary pump (Edwards ED50) by means of a spring loaded teflon seat isolation valve, 1 metre of $\frac{1}{4}$" nylon tube connected via $\sim$ 1 metre of $\frac{1}{2}$" copper tubing. This arrangement although not taking full advantage of the available pumping speed for the rotary pump nonetheless gave a convenient range of flow rates and pressures such that with relatively modest power loadings a convenient time scale was available for monitoring the overall reactions. Since this pumping arrangement corresponds to that normally employed in introducing samples into the spectrometer by means of insertion locks it becomes a relatively trivial operation to set the apparatus up for studying glow discharge modifications without interruption of the normal work load for the spectrometer. Pressures were recorded using a thermocouple vacuum gauge and are nominal rather than precise in all cases.

Research grade argon was used and purification achieved by a sorption train (Hydro-Purge, Coast Engineering Laboratories, California, and Dow Gas Purifier, Dow-Chemical Company, Michigan) which removed hydrocarbons, water, carbon dioxide and oxygen. Flow rates were measured by monitoring the initial rise in pressure as a function of time when the reactor was isolated from the pumping system.

2.4 Kinetic Studies

For each kinetic run described in this investigation the cycle of operation was the same. The probe was first inserted into the reactor without a sample so that the tip was at a fixed geometry with respect to the reactor. The pressure was adjusted

to that required for the particular run to be performed and the system allowed to purge for approximately half an hour before striking the glow and adjusting the power rating to that required. The probe was then withdrawn and two samples mounted, one on either side of the two sided probe tip by means of Scotch tape ensuring that no tape was exposed. On replacing the probe the pressure was readjusted before each discharge period and the system purged for half an hour before the first and 5 mins. before subsequent periods. The time intervals of the discharge periods were such that the total treatment time increased thus: 1 sec., 4 secs., 9 secs., 16 secs., ... 169 secs., 196 secs. This choice of time intervals gave convenient spacing of points on the graphical recording of the results. After each discharge the probe tip was advanced into the spectrometer via the 'O' ring seals and a gate valve for analysis of the sample on one side of the tip. Spectra were recorded as fast as possible (~3 mins.) to minimize hydrocarbon contamination in the spectrometer and a check on this was achieved by running the spectrum of the sample on the reverse side of the tip (which had not been previously exposed to the X-ray gun[†]) at the end of the experiment and comparing it to the sample which had been used for the kinetic study. In all cases no appreciable contamination was observed. The total time between discharge periods was typically 10 mins.

[†] A complete study of hydrocarbon contamination in the AEI ES200B spectrometer has been recently reported from this laboratory.[111] The main conclusion to be extracted here is that the majority of the contamination results from heating of the cap covering the X-ray gun. Samples kept out of line-of-sight of the cap experience little or no contamination.

The samples were exposed to the plasma for a total of 196 sec. for each kinetic run. Samples exposed to the plasma under identical conditions but for 196 secs. in one treatment interval showed ~ 20% less reaction presumably due to a build-up in the partial pressure of products of the reaction (e.g. H_2, HF) which would inhibit the overall crosslinking process. In the situation of the experiments described the products of the reaction are pumped away during sample analysis times, and the rate of rise and decay of the plasma after switching on or off is fast compared to the treatment time intervals.

3. Preliminary Observations on the Argon Glow Discharge Modification of Polymers

The preliminary experiments using reactors A and B enabled several important points to be established which are crucial to the detailed investigation of the surface modification of polymers by means of inert gas plasmas. The initial experiments were carried out in reactor A and quickly established that for an ethylene/tetrafluoroethylene copolymer sample which has been exposed to an argon plasma, the changes in the core level spectra are qualitatively and indeed semi-quantitatively similar to those previously reported for argon ion treatment. The reaction is extremely rapid and low power loadings were necessary to allow the reaction to proceed on a convenient time scale. For power loadings less than 5 watts pulsing the discharge on a microsecond timescale produced greater stability and experiments showed that for any given overall power, with the systems studied here, pulsing the plasma has little effect on the rate or extent of reaction of the polymer sample.

Figure 5.6 shows the C_{1s} and F_{1s} core level spectra for the initial copolymer and samples treated for increasing periods

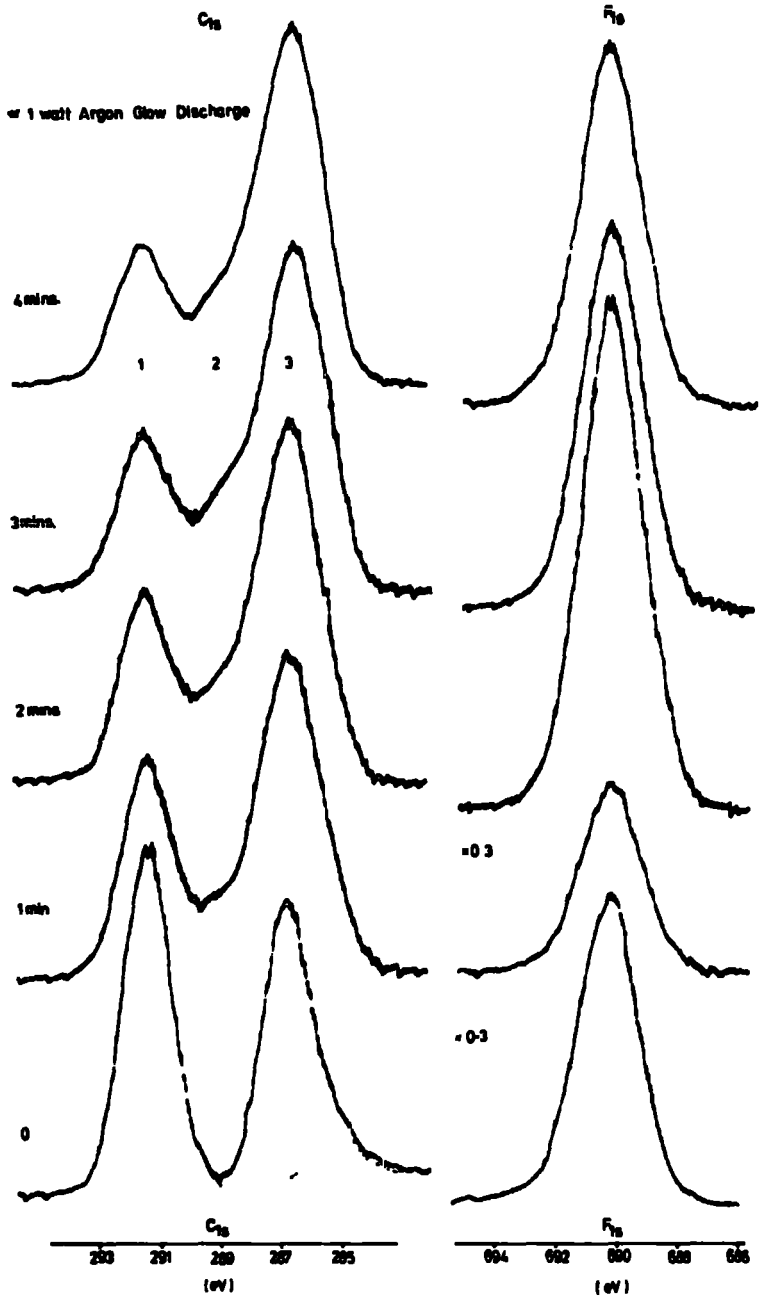

Figure 5.6. Core level spectra of the ethylene/tetrafluoroethylene copolymer and samples treated in an argon plasma in reactor A.

in an argon plasma (2.5×10^{-2} torr, 1.0 watt). The intensity of the $\underline{C}F_2$ component of the C_{1s} spectrum decreases as does the F_{1s} core levels, with a concomitant increase in intensity of signals at intermediate binding energy corresponding to CF and CH structural features. Figure 5.7 presents the relevant data for the C_{1s} components and figure 5.8 for the F_{1s} levels and the O_{1s} region of the spectrum. The smooth nature of the curves demonstrates the reproduceability of the plasma over the region which the samples were located although separate experiments indicated that the overall rate of reaction could be varied by locating the samples in differing positions with respect to the coil. This was particularly evident if samples

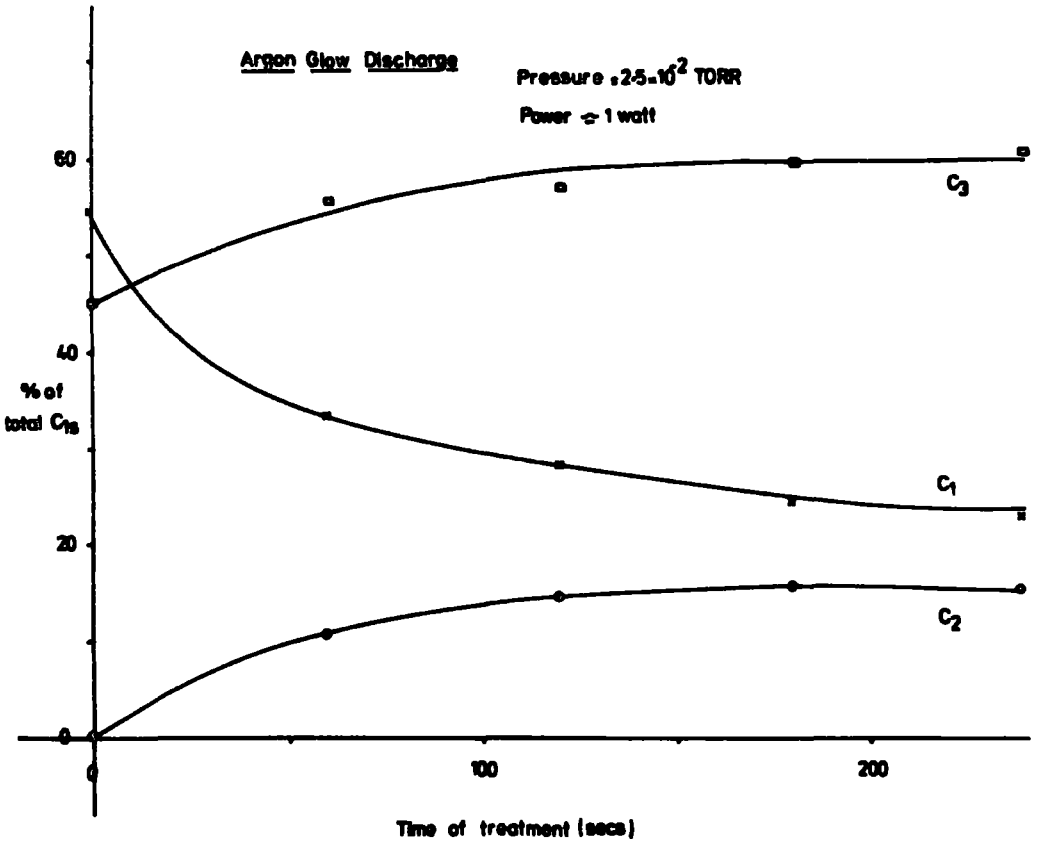

Figure 5.7. Relative intensities of the components of the C_{1s} spectrum as a function of reaction time.

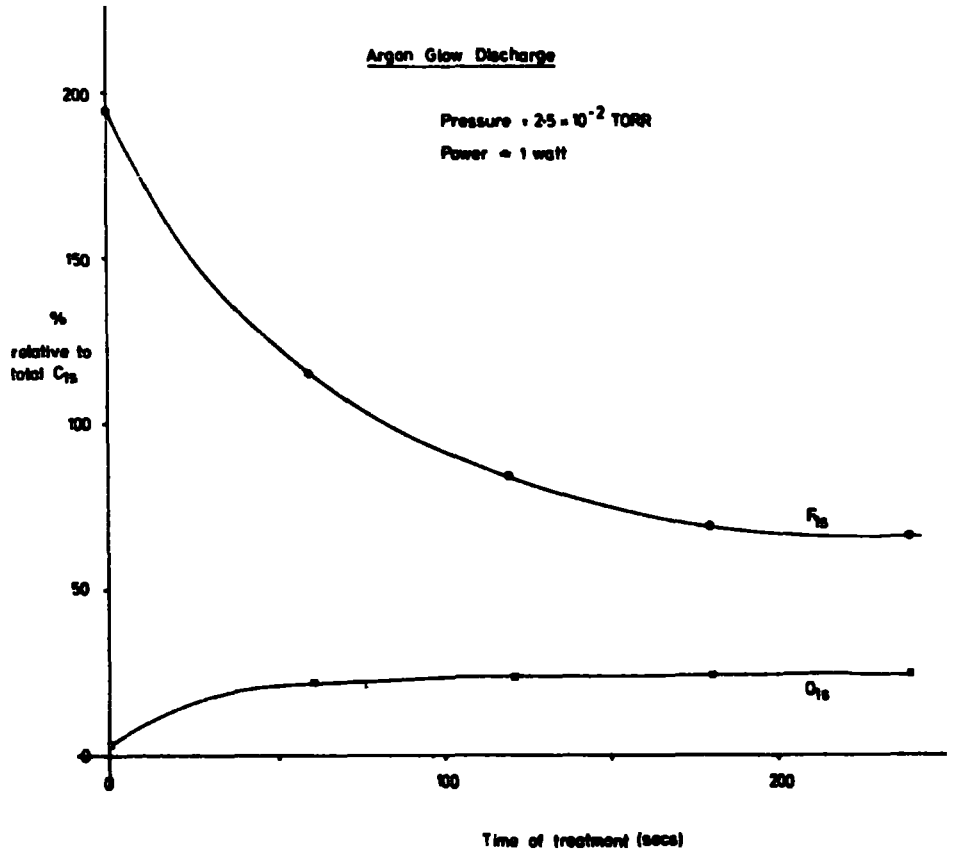

Figure 5.8. Intensities of the F_{1s} and O_{1s} signals as a function of reaction time.

were located not coaxially with the discharge tube but close to the reactor walls, which resulted in an increase in the rate.

The initial samples of the copolymer exhibited a low level of surface oxidation, as evidenced by a relatively weak signal for the O_{1s} levels (~2% of the intensity of the C_{1s} levels) at a binding energy appropriate to >C=O structural features. The treated samples even in a purified argon plasma also exhibited an extraneous oxygen signal which had a somewhat larger full width at half maximum than for the initial sample and with a centroid at somewhat higher binding energy suggestive of both singly and doubly bonded carbon oxygen environments. A plot

of signal intensity versus reaction time rapidly reaches a constant (reproducible) limiting value, for a given pressure and power loading with the oxygen signal typically reaching $\sim$10% of the intensity of the signal appropriate to the C_{1s} levels. This phenomenon has also been observed by other workers in the field.[206] The origin of the oxygen containing species is not altogether clear but three possibilities exist. The first being oxygen containing species desorbed from the reactor walls by the plasma, the second being oxygen containing species diffusing from the sample itself and the third is that minute traces of impurities may remain in the argon after purification since extremely low levels could account for the observation. Experiments were carried out in which the plasma was excited in the reactor for a prolonged period prior to the introduction of the sample under an argon atmosphere in an attempt to remove oxygen containing species from the walls of the reactor and in which the sample was stored at a pressure of $<10^{-7}$ torr for a period of several hours before exposure to the plasma to remove oxygen species from the sample. Both experiments resulted in a small reduction in the extent of oxidation of the sample. More recently however the observation of the vacuum ultraviolet radiation emitted from inert gas plasmas, under similar conditions to those employed in this work,[204] has revealed the presence of trace amounts of atomic oxygen, nitrogen, and hydrogen, even after careful purification. It is likely therefore that all of the three possibilities are involved to varying degrees. Nitrogen is also observed in the ESCA spectra of treated samples but to a lesser extent.

The surface nature of the crosslinking reaction is readily demonstrated by following the intensity ratios of the F_{1s}

and F_{2s} levels, since it is known that these levels span an appreciable difference in electron mean free path dependence. If the surface differs therefore from subsurface and bulk in terms of its chemical composition with the surface region being relatively lower in fluorine content, the larger mean free path for photo-emitted electrons from the essentially core like F_{2s} levels should lead to a decrease in the overall intensity ratio as is clearly apparent from the results displayed in figure 5.9.

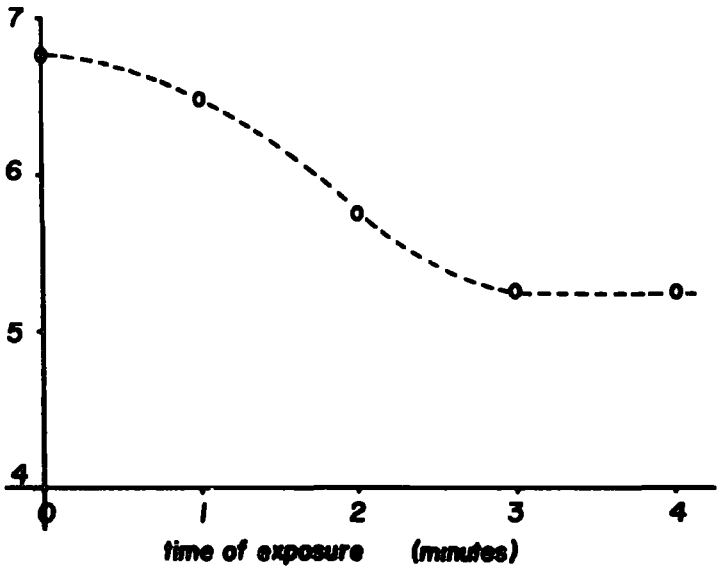

Figure 5.9. F_{1s}/F_{2s} intensity ratio as a function of reaction time.

Since the experiments suggested that even at relatively low power loadings side reactions, arising from species desorbed from the reactor walls, diffused from the bulk of the sample or in trace amounts in the purified inert gas, contributed to a small but significant extent to the overall reaction, the possibility arises that hydrocarbon contamination from desorbed species could contribute to the increase in intensity of the lower binding energy component of the C_{1s} levels. This

may readily be discounted however from further experiments which will now be described. A further point worthy of some consideration is the relative importance of surface ablation processes.

To investigate these points and also provide a more flexible design for mounting and removing samples the reactor configuration B was introduced. This also allows a straightforward rudimentary investigation of the relative importance of radiative and direct energy transfer processes.

To investigate the possibility of hydrocarbon contamination a sample of gold whose ESCA spectrum revealed slight hydrocarbon contamination of the surface was subjected to an argon plasma under similar conditions to those employed in the previously described work. Re-investigation of the core level spectra showed that after treatment for 60 seconds at a power loading of 1 watt the hydrocarbon contamination was in fact significantly reduced which provides some evidence that even at low powers low molecular weight material can be removed from surfaces.

A series of experiments were performed in which the reactor was coated by plasma polymerization of a pentafluoroethane monomer to a depth of ~ 3 - 4000 Å. Gold, silver and glass substrates were placed in the reactor during the polymerization so that the composition of the polymer could be determined by ESCA. The C_{1s} spectra were highly structured showing $\underline{C}$, $\underline{C}F$, $\underline{C}F_2$ and $\underline{C}F_3$ groups. A sample of polystyrene film was then treated in the coated reactor by an argon plasma at a power loading of 100 watts for 30 mins. (Polystyrene was chosen because of its relatively high reactivity towards oxygen

containing species in the plasma, as determined from previous work). Subsequent analysis of the ESCA spectrum of the treated film revealed a highly fluorinated system. The C_{1s} spectrum was again highly structured showing $\underline{C}$, $\underline{C}F$, $\underline{C}F_2$ and $\underline{C}F_3$ groups. The only reasonable mechanism for this is via ablation of low molecular weight fragments from the surface of the polymer coating and grafting of the fragments onto the polystyrene film.

This experiment demonstrates that ablation of the surface of a polymer can be achieved at high power loadings although at lower power levels the process would be expected to be relatively unimportant. Under the conditions of the previously described work ($\sim$1 watt) desorption of hydrocarbon and low molecular weight oxygen containing species might be expected to be the dominant processes as far as the internal surface of the reactor is concerned.

Hydrocarbon contamination of samples is therefore a severe problem in new reactors, and may be reduced by exciting a discharge in the reactor for a period of time before use. Furthermore, once hydrocarbon has been removed from the walls of the reactor it is less likely that it would be replaced before subsequent treatment of polymer films, compared with the oxygen containing species which are at a higher partial pressure in the laboratory atmosphere to which the reactor was exposed in loading samples.

The close similarity of the surface modified samples by means of either argon ion bombardment or low powered radio-frequency discharge in argon strongly suggests that at the outermost surface reaction is dominated by direct energy trans-

fer from charged and/or metastable species in the plasma.

Plasmas are however copious sources of electromagnetic radiation and there is an extensive body of literature on the modification of polymers initiated by U.V. radiation[207]. Indeed there has been considerable discussion in the literature on the relative importance of direct and radiative energy transfer processes, however the techniques which have previously been brought to bear on this problem have not enabled the initial stages of reactions involving the outermost few tens of Angstroms to be delineated.[148]

In the pressure range pertinent to this work and indeed most previous investigations the photon flux is highest in the vacuum ultraviolet, however there are significant outputs in the U.V. and visible regions.[196,204] For an ideal ethylene-tetrafluoroethylene copolymer the lowest excited states, corresponding to $n(F_{2p}) \rightarrow \sigma^*$ and $\sigma \rightarrow \sigma^*$ transitions, correspond to absorption in the vacuum U.V. and only end absorption would be available for the U.V. and visible regions. In a largely alternating ethylene/tetrafluoroethylene copolymer it is inevitable that elimination of HF occurs to a minute extent (not detectable by most conventional techniques) and the unsaturated centres so produced could give rise to absorption in the U.V. A similar possibility arises from surface oxidation features (>C=O) known to be present in submonolayer coverage in the polymer films studied.[121] Such features could conceivably be important if the oscillator strengths for the transitions were orders of magnitude larger than for absorption and photoionization processes occurring at much shorter wavelengths in the vacuum U.V. with the considerably more intense radiation from the plasmas in that region. The available data strongly

mitigates against this possibility since the total attenuation coefficients increase quite sharply in going from the U.V. to vacuum U.V. and at shorter wavelengths the total cross sections are dominated by Rydberg transitions converging on ionization limits and by direct photoionization processes.[205,208]

This situation may well be modified for polymer systems with chromophores with a large number of available excited states in the U.V./visible region.

The evidence is fairly conclusive therefore that short wavelength radiation can lead to modification of polymers and undoubtedly such processes compete with direct energy transfer from species in the plasma which because of their diffusion controlled nature would be expected to be of most importance for reactions at the immediate surface.

In order to elucidate the relative importance of surface reactions arising from direct and radiative energy transfer a special sample mount was developed which enabled polymer samples to be located in the plasma either directly in contact with the plasma or exposed only to the electromagnetic radiation from the plasma through a quartz window.

Using reactor configuration B, samples of the copolymer were located symmetrically with relation to the coil with one of the samples being covered by 1 mm. thick quartz slide. After a 60 second treatment at 1 watt the sample covered by quartz showed no reaction whilst that exposed to the plasma showed a distinct loss of CF_2 features. The cut off for quartz is ~ 1600 Å and for a slide ~1 mm. thick there will be some attenuation of longer wavelength radiation.[196] The experiment therefore suggests that the radiative energy transfer component

of the reaction is dominated by wavelengths < 1600 Å as might have been anticipated. To confirm this, experiments were carried out in which samples covered with a quartz slide were exposed to the electromagnetic radiation from plasmas run at full power (100 watts) for a period of 30 minutes. The C_{1s} spectra for these samples showed them to be completely unreacted. For comparison purposes experiments were also carried out with samples of polystyrene and polyethylene terephthalate both of which absorb strongly in the U.V. At high power and after substantial periods of irradiation both systems showed; some evidence of reaction in terms of a decrease in shake-up intensity (loss of unsaturation) and for polyethyleneterephthalate a decrease in overall O_{1s} to C_{1s} intensity. Indeed in this experiment the products from polyethyleneterephthalate were very similar when either exposed to the plasma or covered by the quartz slide.

The general conclusion from the experiments outlined above is that any radiative energy transfer component is likely to be dominated by radiation with wavelength < 1600 Å. The experiments described thus far, suggested the design of a reactor configuration (C) directly mounted on the ESCA spectrometer source which would enable detailed kinetic studies to be made on the same sample without exposure to the atmosphere between successive interactions with a given plasma. The pumping speed for reactor configuration C was considerably lower than for the previously described reactors (A and B). The convolution of factors involving geometry and gas flow characteristics resulted in a considerable increase in the rate of reaction in reactor C, for a given power and pressure, than for either A or B. In order to increase the time scale for convenient kinetic studies the total pressure of argon at which

the discharges were excited was increased to span 0.1 - 1.0 torr. The results of the kinetic studies are discussed in section 5.

4. Angular Dependence of Absolute and Relative Peak Intensities.

Before proceeding to the discussion of the kinetic studies it is important to consider the consequences of the electron take off angle at which the ESCA spectra are recorded. Indeed it will become apparent from this section that for inhomogeneous samples the angle, θ, (cf. Chapter Four, figure 4.3) must be kept carefully under control to obtain meaningful results, and furthermore treating θ as a variable provides a wealth of extra information concerning the vertical inhomogeneity of the surface regions of the sample.

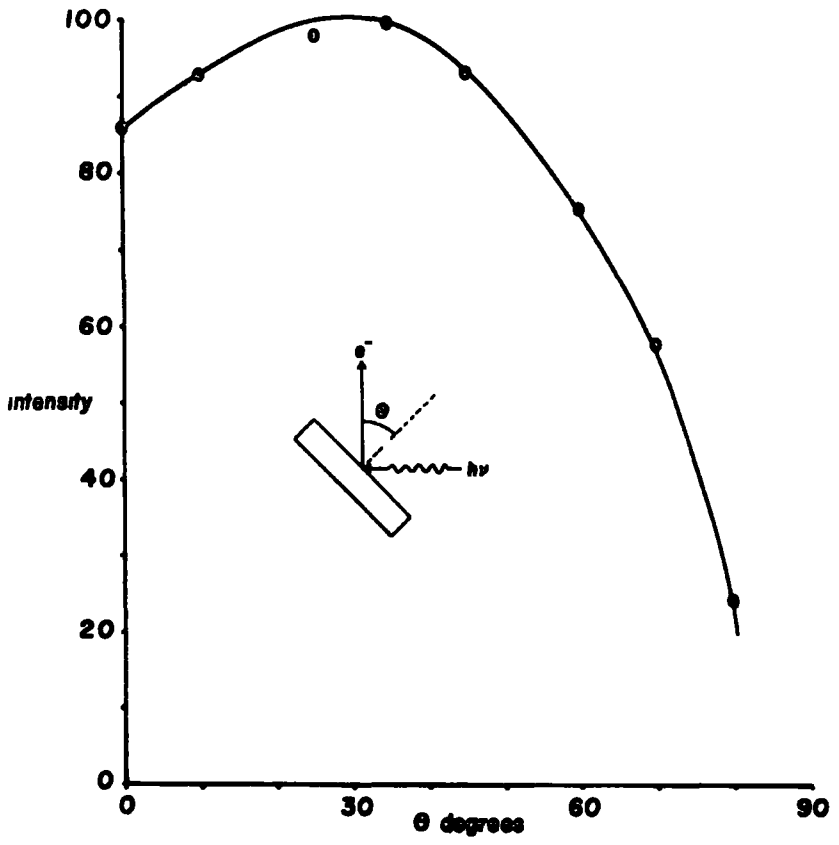

Figure 5.10. Total integrated intensity of the C_{1s} spectrum, of the ethylene/tetrafluoroethylene copolymer sample, plotted against θ.

In the spectrometer used in this study (AEI ES 200B) the angle between the incident X-rays and the analyser entrance slit is fixed at 90^{o}. The angle of sample surfaces relative to the analyser entrance slit is variable. Figure 5.10 shows how the absolute intensity of the total C_{1s} signal of an homogeneous ethylene/tetrafluoroethylene copolymer film varies as a function of the take off angle θ. (θ is the angle between a line drawn normal to the sample surface and a line drawn between the sample and the analyser slit). The shape of the curve can be described in terms of various instrument and geometric parameters, as functions of θ,[90] but for the purposes of this work it is sufficient to describe it simply by a function $f(\theta)$. The absolute intensity of the F_{1s} signal for the sample is also described by $f(\theta)$. The relative intensity ratios: $\underline{C}F_2/\underline{C}H_2$ and C_{1s}^{TOT}/F_{1s} are independent of θ.

By contrast for the treated samples, angular studies readily reveal the inhomogeneous nature of the surface regions from investigations of the C_{1s} levels alone or by comparison of C_{1s} and F_{1s} levels.

Figure 5.11 shows the C_{1s} levels for a sample of the copolymer which has been treated for 25 seconds in an argon plasma at 0.1 torr and 0.2 watts. The spectrum is shown at angles of θ at 18^{o} and 80^{o} respectively. The differences are quite striking. The decrease in fluorine content of the surface regions is revealed by the large relative decrease in intensity of the component arising from $\underline{C}F_2$ structural features and concomitant increase in the lower binding energy component associated with $\underline{C}F$. The integrated intensities of the component signals as a percentage of the total C_{1s} signal intensity are

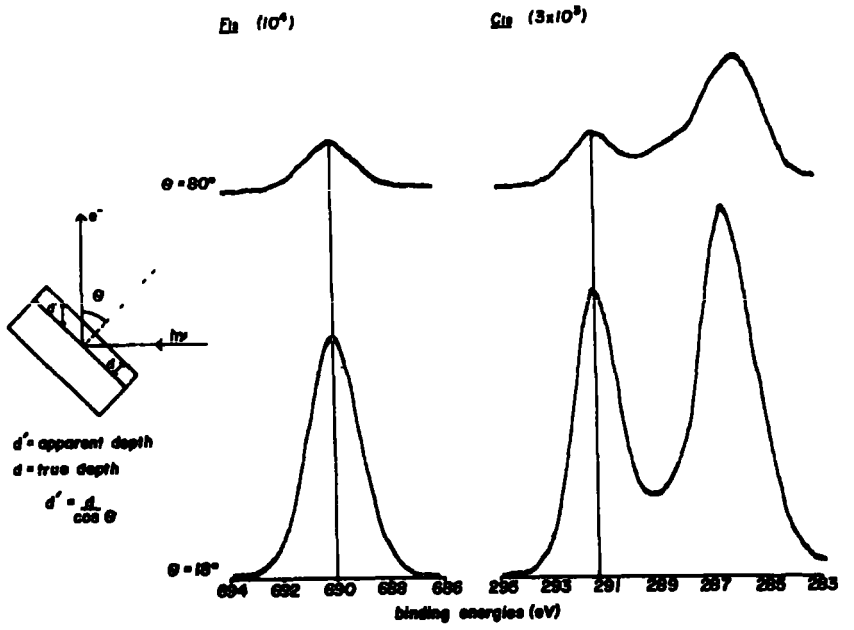

Figure 5.11. The C_{1s} spectrum, of a sample treated for 25 secs. in an argon plasma (0.1 torr, 0.2 watt), at electron take off angles of 18° and 80°.

$\underline{C}F_2$:$\underline{C}F$:$\underline{C}$ = 32.4:7.4:60.2 at θ = 18° and 20.1:17.7:62.2 at θ = 80°. These observations can be understood in terms of a substrate/overlayer type model. The $\underline{C}F_2$ structural features are contained in the 'substrate' which is the unreacted copolymer. The relative intensity decreases from θ = 18° to 80°. The $\underline{C}F$ structural features however are contained in the 'overlayer' which is the crosslinked polymer. The relative intensity increases from θ = 18° to 80°. The signal designated $\underline{C}$ (carbon not attached to fluorine) originates from CH_2 and CH features both in the 'substrate' and 'overlayer', and the relative intensity is much less dependent on θ. Clearly surface features are greatly enhanced at values of θ approaching 90° as might have been expected since the apparent thickness of the surface layer (Figure 5.11), d' increases with $1/\cos\theta$.

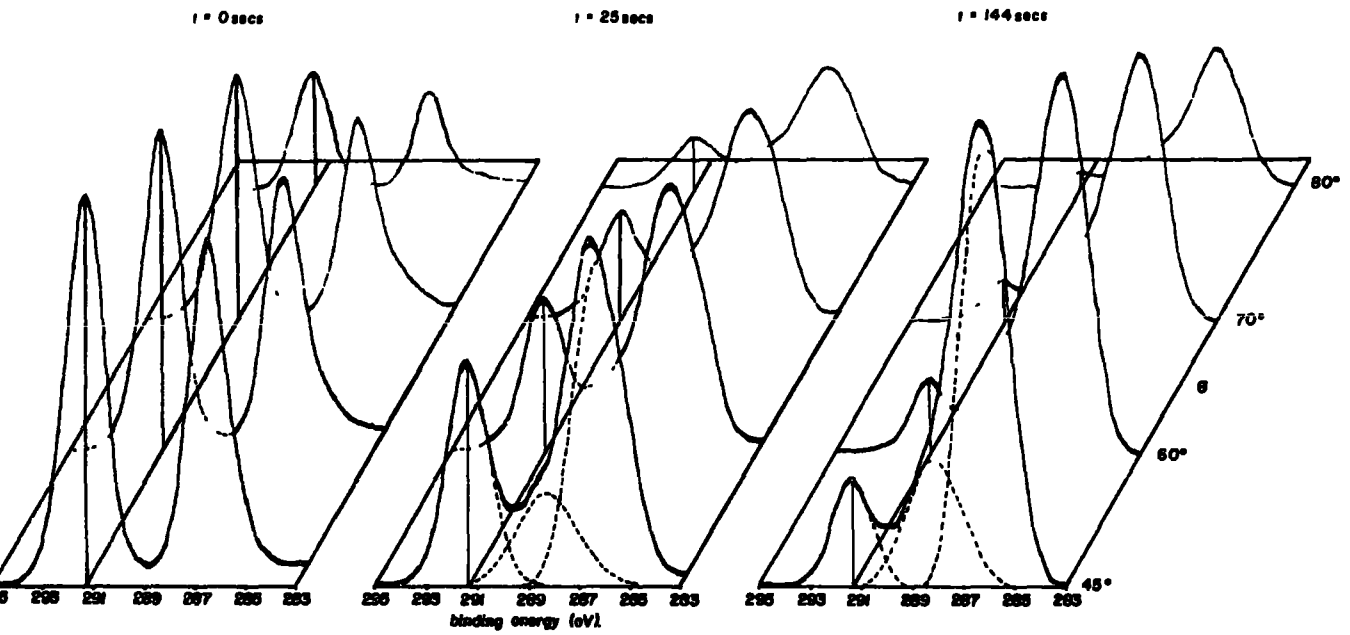

Figure 5.12. C_{1s} spectra at various angles for samples treated for 0, 25 and 144 secs. (0.1 torr, 0.2 watt).

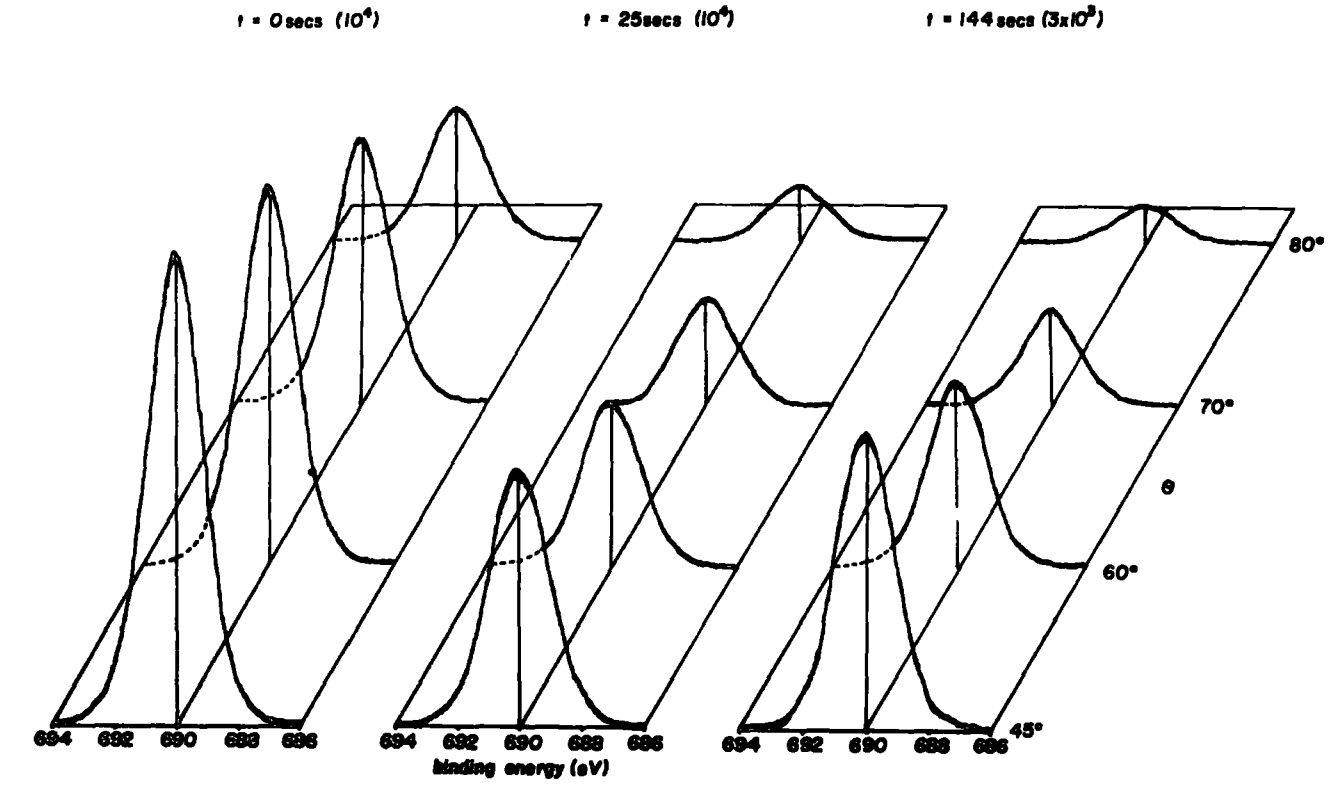

Figure 5.13. F_{1s} spectra at various angles for samples treated for 0, 25 and 144 secs. (0.1 torr, 0.2 watt).

Figures 5.12 and 5.13 show the angular dependence of the C_{1s} and F_{1s} signals respectively for the initial copolymer and samples treated for 25 and 144 seconds (0.1 torr, 0.2 watts) in an argon plasma. It is clear from these spectra that angular dependent studies considerably aid the investigation of inhomogeneous materials. For example in comparing the F_{1s} levels for which the mean free path for photoemitted electrons is rather short it is clear that whilst the instrumental and geometrical factors contributing to $f(\theta)$ give an overall decrease in F_{1s} signal for the initial copolymer of approximately 0.25, for the discharge treated sample, the decreasing fluorine content in the surface regions is evident from the fact that the corresponding decrease in going from $\theta = 45^{o}$ to $\theta = 80^{o}$ is by a factor of ~ 0.12.

The data is more clearly presented graphically as in figure 5.14 in which the absolute intensities of the C_{1s} components and F_{1s} signal are plotted against the electron take off angle, for the untreated sample and samples treated for 25 and 144 seconds. In each case the signal intensity due to $\underline{C}$ structural features closely follows $f(\theta)$, as do all the signals of the untreated sample. However, in all cases where the origin of the signal can be defined as dominantly in the 'substrate' or in the 'overlayer' the signal intensity does not follow $f(\theta)$. For signals originating dominantly in the 'substrate' ($\underline{C}F_2$ and $\underline{F}_{1s}$) as the depth of reaction, d, increases (i.e. longer treatment time) the angle θ_{max} giving a maximum absolute intensity decreases. The opposite is true for signals originating dominantly in the 'overlayer' ($\underline{C}F$). This effect can be rationalized simplistically in terms of two equations for the absolute intensities of 'substrate'

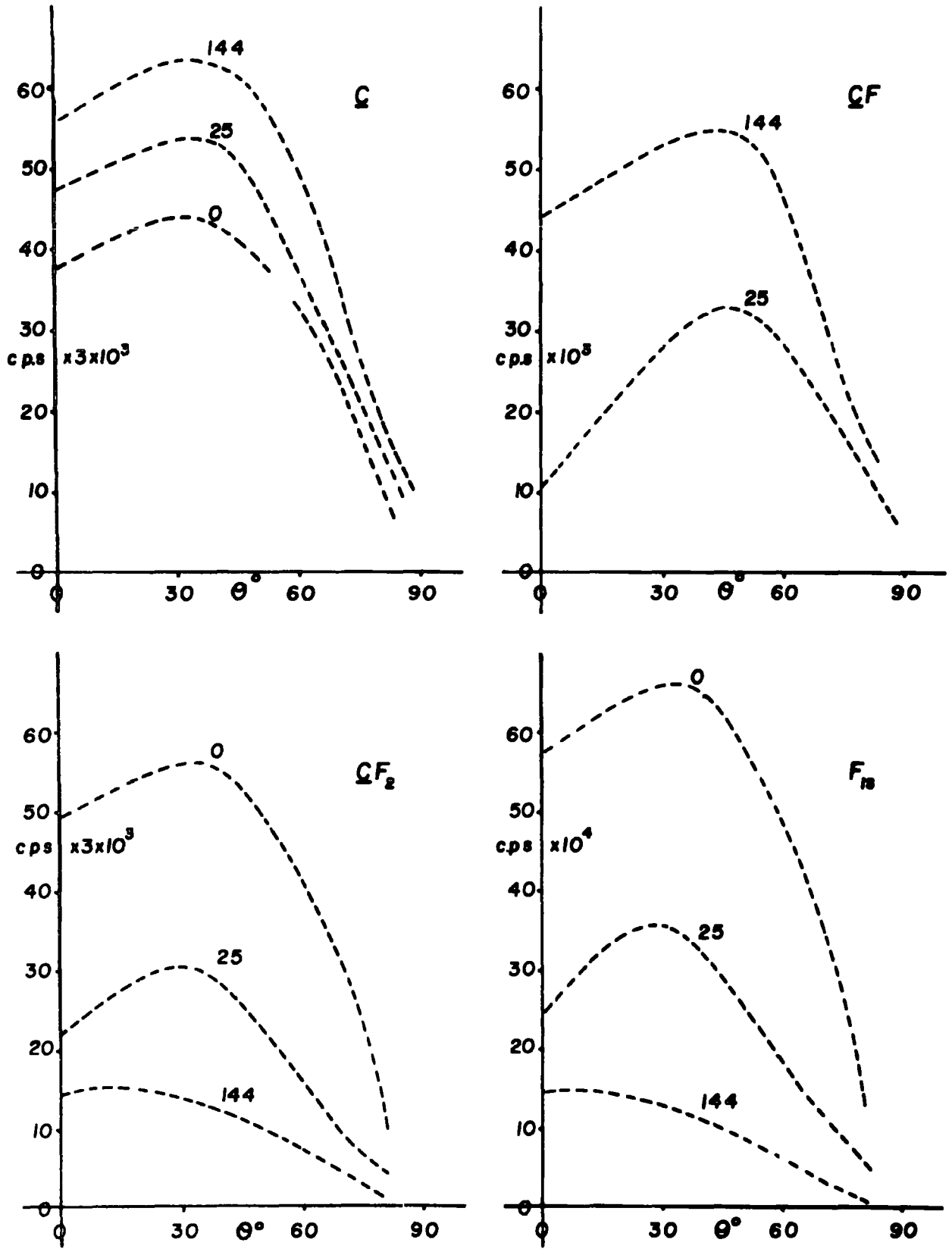

Figure 5.14. Integrated intensities of the components of the C_{1s} spectrum (i.e. C, CF and CF_2) and F_{1s} spectrum, for samples treated for 0, 25 and 144 secs. versus θ .

(bulk) and 'overlayer' (surface) core levels, I_b and I_s respectively:

$$I_b = f(\theta)\, F \alpha_b N_b K_b \lambda_b .\ e^{-d/\lambda_b \cos\theta} \qquad (5.1)$$

$$I_s = f(\theta)\, F \alpha_s N_s K_s \lambda_s .\ (1 - e^{-d/\lambda_s \cos\theta}) \qquad (5.2)$$

where, $f(\theta)$ is defined above, F is the X-ray flux, α is the cross section for photoionization, N is the number of atoms (on which the core level is localized) per unit volume, K is a spectrometer dependent factor and λ and d are the electron mean free path and film thickness respectively.

It is worthwhile to carry this analysis a stage further in order to properly appreciate the implications of equations 5.1 and 5.2. As has been discussed in Chapter One (section 7.3) $f(\theta)$ may be thought of in simple terms as a convolution of two factors. The first being the total X-ray flux incident on the sample which is a function of $\sin\theta$ for a parallel beam of X-rays and the second involves the projected area with respect to the analyser which varies as $\cos\theta$. For the ideal case therefore $f(\theta)$ may be equated to $\sin\theta \cos\theta$. Substituting this expression into equations 5.1 and 5.2 and setting their first differentials to zero defines the values of θ giving a maximum in signal intensity for the bulk and surface respectively.

For the bulk,

$$\frac{d}{\lambda_b} = \frac{\cos^3 \theta_{max}}{\sin^2 \theta_{max}} - \cos\theta_{max} \qquad (5.3)$$

and for the surface,

$$\frac{d}{\lambda_s} = \cos\theta_{max} \ln. \left[\frac{g(\theta_{max}) - d/\lambda_s}{g(\theta_{max})} \right] \qquad (5.4)$$

where,
$$g(\theta) = \frac{\cos^3\theta}{\sin^2\theta} - \cos\theta$$

Therefore, in principle, it is possible to determine film thicknesses by simply optimizing the angle to give a maximum intensity for a core level signal arising from either the bulk or the surface. Equation 5.3 gives the thickness relative to the electron mean free path directly, but an iterative procedure is necessary to solve equation 5.4.

Unfortunately, equations 5.3 and 5.4 apply to the ideal case involving a perfectly parallel beam of X-rays and this is not the situation in practice. However, this error may be overcome by approximating the ideal θmax from an empirically derived expression relating the ideal θmax to the experimentally observed value. For our particular spectrometer geometry equation 5.5 applies.

$$\theta_{\text{ideal}} \simeq \frac{9}{11}\theta_{\text{expt.}} + \frac{180}{11} \qquad (5.5)$$

It should be evident from this that a great deal of extra information pertaining to inhomogeneities in surface regions can be obtained, qualitatively and semi-quantitatively, by observing the angular dependence of the absolute and relative signal intensities of the components of the relevant core level spectra.

The prime motivation in this work is the elaboration of a kinetic model for the glow discharge modification of polymers and angular dependent studies will be seen from ensuing sections to be clearly important in this respect. For the elaboration of mechanistic and structural details of the processes involved such investigations are mandatory.

In the kinetic studies described in the next section a value of 34° was chosen as the take-off angle which corresponds in our instrumental arrangement to a maximum value of

$f(\theta)$ for our particular geometry. It may be noted however that in principle it should be possible to effectively isolate the contributions to the overall rate processes of reactions occurring specifically in the outermost monolayer or so of the surface by recording spectra at take-off angles approaching grazing exit for photoemitted electrons. Unfortunately $f(\theta)$ is such that the absolute signal intensities are substantially lower than for a take-off angle of $\sim 34^{o}$ and hence such studies are extremely time consuming. However work along these lines in included in the next Chapter.

5. Kinetic Studies of the Glow Discharge Modification of Polymers.

5.1 The Kinetic Model

The theoretical model developed to quantify the data is outlined in the schematic in figure 5.15, where processes occurring in the surface layer of thickness d are separated from the subsurface and bulk reaction. The starting hypothesis considers that, because of the diffusion controlled nature of processes involving M* (for which the dominant reaction should be associated with that from argon ions and metastables) reactions at the surface should have components from both direct and radiative energy transfer processes whilst for those in the subsurface and bulk the dominant process should be that associated with radiative energy transfer. As will become apparent the experimental results are entirely consistent with such a hypothesis.

There might appear to be a tautologous element to this analysis since the hypothesis starts with the premise that the reactions initiated by the radiative energy transfer are longer

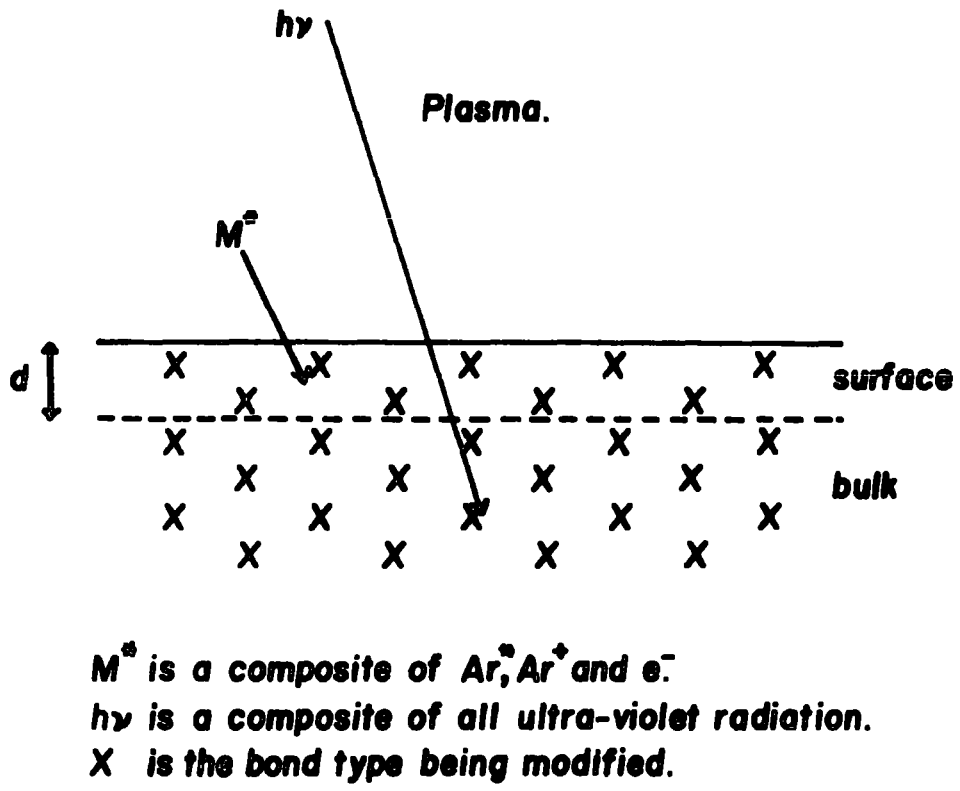

Figure 5.15. Theoretical Model.

range than from direct energy transfer and hence that the answer is prejudiced from the outset. It is clear however from the work on surface modification with a conventional argon ion gun and from published data on attenuation lengths for ions and electromagnetic radiation in a variety of materials that radiative energy transfer processes will undoubtedly be longer range than those arising from direct energy transfer processes involving ions and metastables. The crucial question to be answered therefore is whether even for the surface regions, processes involving direct energy transfer are competitive with those arising from radiative energy transfer. The possible outcome of the analysis is therefore either that the overall modification (surface, subsurface and bulk) is dominated by

radiative energy transfer or that in the surface regions direct energy transfer is a competitive process and that the results will only be explicable in terms of a convolution of surface modification with both direct and radiative energy components with bulk modification involving solely radiative energy transfer. In the event of the outcome being the latter case then the analysis should provide an indication of the relative importance in the surface region of the two components and also give an indication of the range involved.

If the concentration of structural features (designated X) is X_o^s for the surface layer, thickness d, of the polymer, (d is the depth to which reaction caused by direct energy transfer is important), then the rate of modification of such sites may be written as (with obvious notation)

$$\frac{dx^s}{dt} = K_M(X_o^s - X^s)M^* + K_L(X_o^s - X^s)I_o(1-e^{-kd}) \qquad (5.6)$$

where K_M is a composite rate constant for processes involving M^*, $I_o(1-e^{-kd})$ represents the fraction of electromagnetic radiation absorbed in the surface layer, with k representing a composite of attenuation coefficients for all the frequencies involved, and K_L is a composite rate constant for the radiative energy transfer processes; which may well be a function of both the wavelength and intensity distribution of the electromagnetic radiation.

Since the flux of M^* and electromagnetic radiation bombarding the sample surface is constant, for a given set of operating parameters for the plasma, we may recast equation 5.6 in a simplified integrated form in which rate processes involving the surface layer are encoded in the pseudo rate constant K_s as in equation 5.7

$$X_o^s - X^s = X_o^s . e^{-K_s t} \qquad (5.7)$$

where $$K_s = K_M M^* + K_L I_o (1-e^{-kd}) \qquad (5.8)$$

For the subsurface and bulk a parallel treatment gives equations 5.9 and 5.10.

$$\frac{dX^b}{dt} = K_L (X_o^b - X^b) I_o . e^{-kd} \qquad (5.9)$$

$$\therefore \quad X_o^b - X^b = X_o^b . e^{-K_b t} \qquad (5.10)$$

where $$K_b = K_L I_o . e^{-kd} \qquad (5.11)$$

Now the proportion of core level signal arising from the surface layer, d, for a given structural feature is given by $1-e^{-d/\lambda}$ where λ is the mean free path for photoemitted electrons of a given kinetic energy. Whilst for the subsurface and bulk the proportion of signal arising is modulated by a factor of $e^{-d/\lambda}$. The total integrated intensity for a core level monitoring a given structural feature as a function of time is therefore given by equation 5.12.

$$\frac{I^t}{I_o^{TOT}} = \frac{X^t}{X_o^{TOT}} = (1-e^{-d/\lambda}) e^{-K_s t} + e^{-d/\lambda} . e^{-K_b t} \qquad (5.12)$$

where I_o^{TOT} is the total integrated intensity for a given structural feature for the initial system and I^t the intensity at time t.

5.2 Glow Discharge Modification of an Ethylene/Tetrafluoroethylene Copolymer by Plasmas Excited in Argon.

The system subjected to the most detailed investigation involves an ethylene/tetrafluoroethylene copolymer (52% TFE) whose structure is known to be largely alternating. Its ESCA spectrum has been presented in figure 5.3. Figure 5.16 shows a typical set of spectra from a kinetic run at a pressure of 0.1

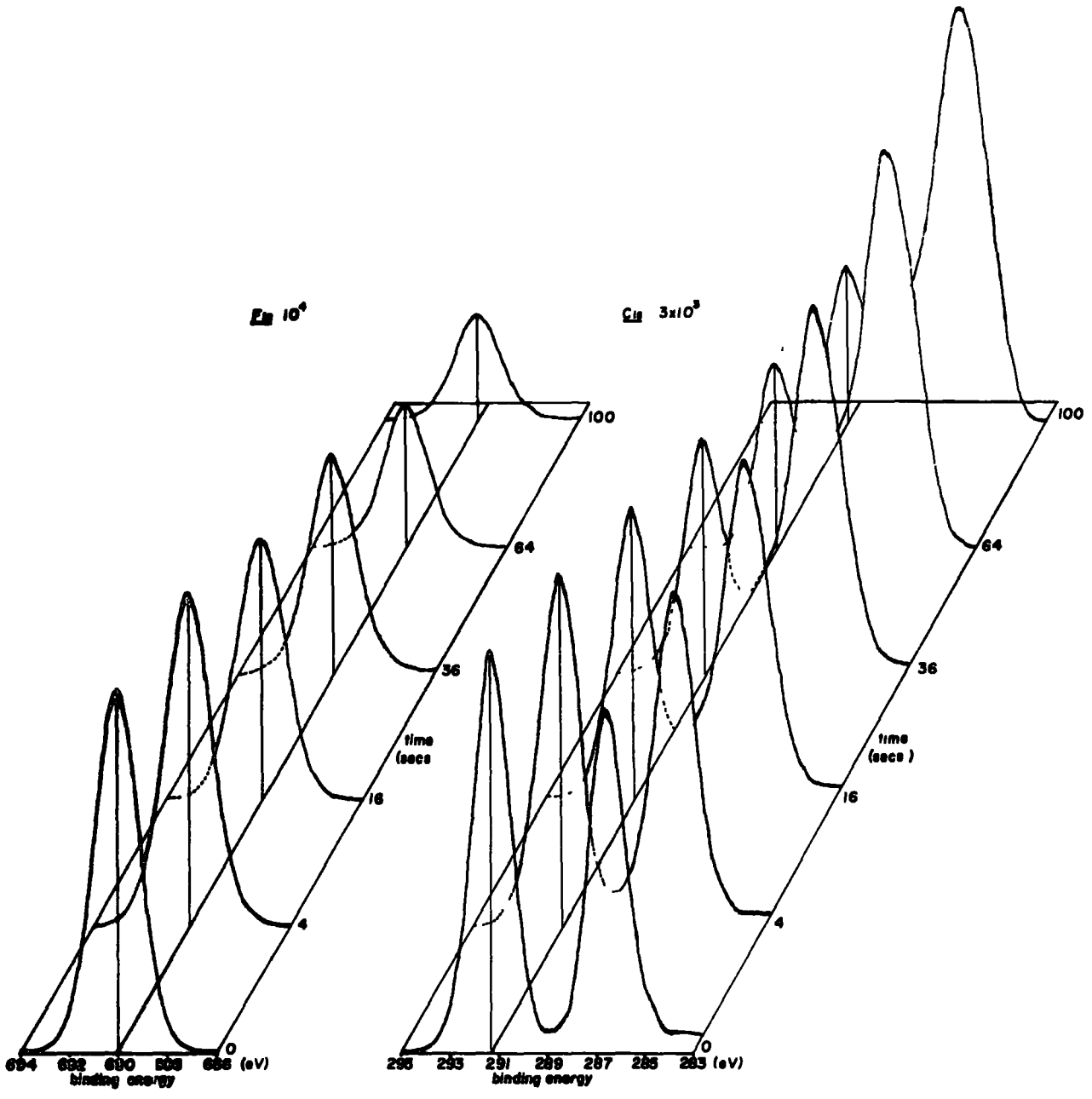

Figure 5.16. Core level spectra of a sample versus time of exposure to an argon plasma. (0.1 torr, 0.1 watt).

torr and power loading of 0.1 watt. The data was accumulated as described in section 2.4 and the time axis in figure 5.16 refers to the total time of exposure of the sample to the plasma before the spectrum was recorded.

It is clear from this data that convenient means of monitoring the rate processes involved are provided by the F_{1s} levels and $\underline{C}F_2$ component of the C_{1s} levels. The component signals in the C_{1s} spectrum relating to oxygen containing structural features should manifest themselves as higher binding energy components in the C_{1s} spectra in the region intermediate between that for the $\underline{CF_2}$ and $\underline{CH}$ structural features at binding energies of 291.2 eV and 286.5 eV respectively (cf. -$\underline{C}$OOH ~ 289.0 eV, $\geq\underline{C}$=O ~287.8 eV). The relatively low level of incorporation of oxygen however even for the samples treated for the full reaction time implies a small error in monitoring the overall rate processes from the $\underline{CF_2}$ component of the C_{1s} levels and from the F_{1s} signal intensities as a function of time. The effect of the introduction of oxygen containing species into the plasma would be expected to show up most dramatically in the initial stages of reaction since one mechanism for crosslinking which will be outlined in a subsequent section involves the introduction of double bonds into the polymer chain through effectively eliminating $\underline{HF}$. Such features would be particularly prone to oxidative degradation to produce carbonyl and carboxyl features. Figure 5.17 shows a logarithmic plot of the $\underline{CF_2}$ intensity relative to its value at t=0 and the corresponding plot for the F_{1s} levels is shown in figure 5.18. Both exhibit distinct curvature as might be expected for a two component system.

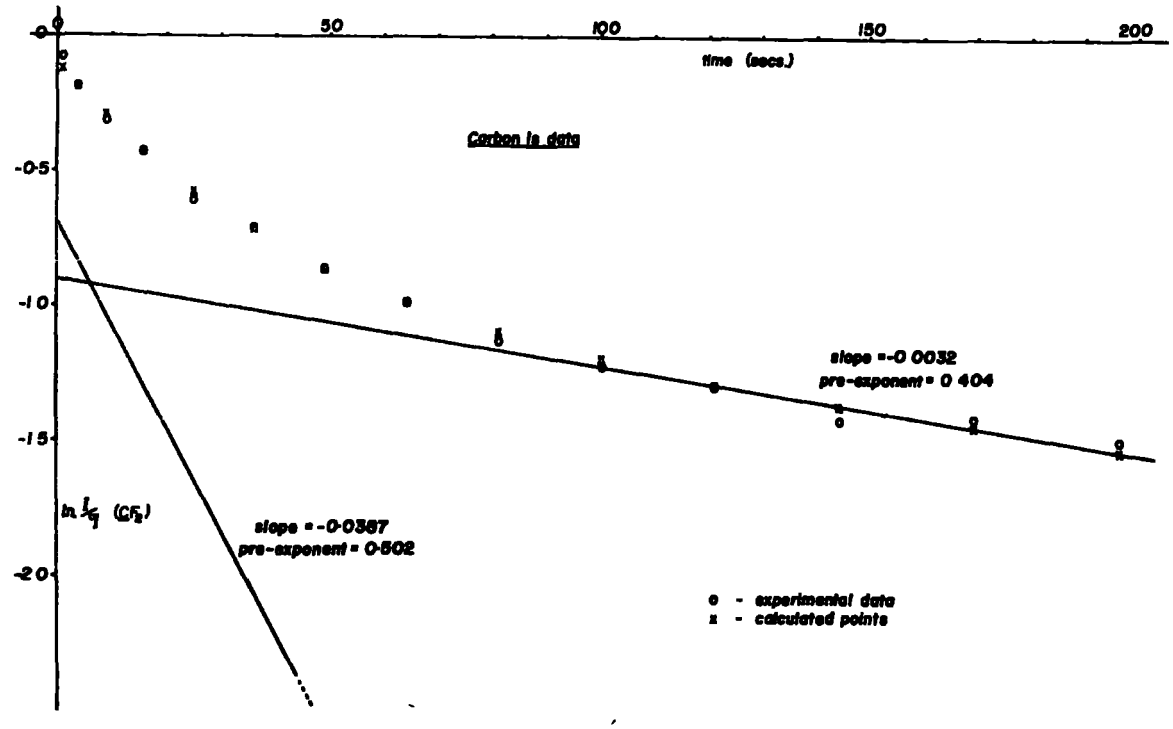

Figure 5.17. ln I/I_o for the $\underline{C}F_2$ levels, versus t.

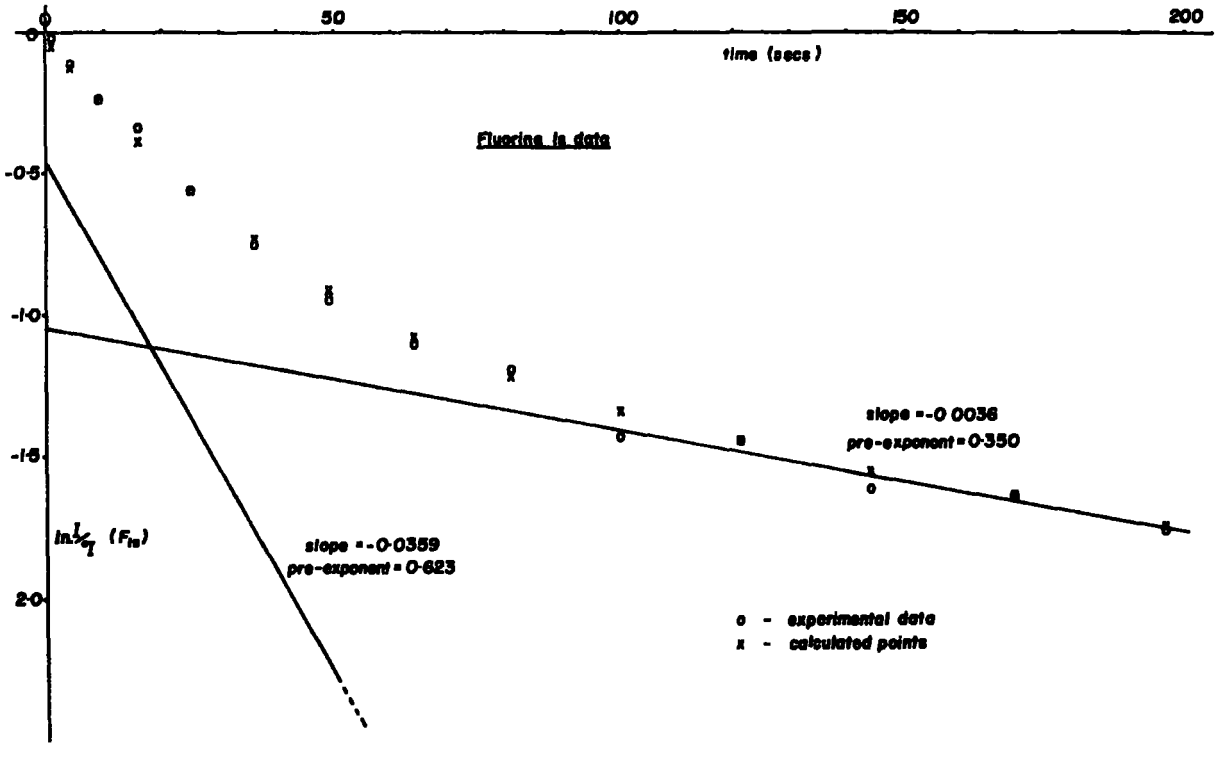

Figure 5.18. ln I/I_o for the F_{1s} levels, versus t.

The analysis in terms of a two component system is straightforward since it is clear from figures 5.17 and 5.18 that as t becomes large the dominant contribution is from the component of smaller exponent. A plot of $\ln \frac{I^t}{I^{TOT}_0}$ versus t should therefore approach linearity the absolute slope of the line being the composite rate constant for the slower process and the intercept at t=0 the exponent of the time independent term which relates to the depth information (i.e. $e^{-d/\lambda}$). Replotting the differences of the experimental data at small t, from the extrapolated section of this line yields a second straight line which provides the corresponding data for the faster of the two composite rate processes.

As a check on the overall correctness of this analysis it should also be pointed out that the sum of the terms relating to the depth information for the rate processes should equal unity. As will become apparent this is in fact closely the case. Considering firstly the data derived from an analysis of figure 5.17, the slopes and intercepts are -0.039 $sec.^{-1}$ and 0.50 for the fast component and -0.003 $sec.^{-1}$ and 0.40 for the slower component.

The surface components of the reactions must obviously be faster than for the subsurface and bulk (at least in the initial stages of reaction which we are considering here) since both direct and radiative energy transfer components are likely to be of importance and we may therefore assign the larger exponent to this surface component. It is interesting to note that the rate processes for the surface are an order of magnitude larger than for the subsurface reaction and since the attenuation coefficients for the electromagnetic radiation

are likely to be such that the radiation suffers relatively minor attenuation in passing through the surface the only consistent conclusion which may be drawn is that the surface reaction is dominated by reactions involving ions and metastables with only a minor contribution from radiative energy transfer whilst the latter dominates processes for the subsurface and bulk. As a check on the analysis of the data in terms of a two component system one may re-calculate the theoretical curve (crosses) and comparison with the original data (open circles) shows excellent agreement over the whole time scale. A similar analysis can be carried out on the F_{1s} levels (figure 5.18). This type of kinetic analysis was repeated over a wide variety of power and pressure settings and the complete set of results for all of the experiments is presented in Table 5.1 ($\underline{C}F_2$ levels) and Table 5.2 (F_{1s} levels). These results represent the best fits obtained by a computer least squares analysis of the data within the framework of the method of calculation described above.

For each set of data the extrapolation and difference procedures were performed on all reasonable combinations of N1 and N2 (where N1 is the number of data points at large t taken to calculate the first straight line and N2 the number of data points at small t taken to calculate the second straight line), and the best fit determined from the correlation coefficients which were typically in the range 0.97 to 0.99. The errors and accuracy quoted in Tables 5.1 and 5.2 pertain to the least squares calculations on the experimental data, although the true error in the composite rate constants is estimated to be $\sim \pm$ 10%. Subsequent least squares analyses of the theoretical curves, re-calculated from the data in Tables 5.1 and 5.2,

Table 5.1. Composite rate constants and pre-exponential terms derived from the Carbon 1_s data.

Pressure (Flow rate)*	Power (watts)	W/P	$(1-e^{-d}/\lambda\cos\theta)$	K_s† (sec.$^{-1}$)	$e^{-d}/\lambda\cos\theta$	K_b† (sec.$^{-1}$)	Σr^2††
0.1 torr	0.1	1	0.50	0.039(1)	0.40	0.003(0)	0.01
	0.4	4	0.55	0.062(1)	0.43	0.002(0)	0.01
(6.5 cm.^{3} sec.$^{-1}$)	1.0	10	0.57	0.101(4)	0.28	0.006(1)	0.02
	2.0	20	0.49	0.082(6)	0.34	0.004(1)	0.02
0.2 torr	0.2	1	0.45	0.038(1)	0.50	0.003(0)	0.01
	0.8	4	0.51	0.060(3)	0.38	0.005(0)	0.02
(7.0 cm.^{3} sec.$^{-1}$)	2.0	10	0.55	0.073(2)	0.38	0.003(0)	0.01
	4.0	20	0.50	0.087(5)	0.40	0.003(1)	0.01
0.5 torr	0.5	1	0.55	0.038(1)	0.40	0.001(0)	0.00
	2.0	4	0.65	0.061(2)	0.25	0.001(0)	0.02
(12.5 cm.^{3} sec.$^{-1}$)	5.0	10	0.49	0.084(9)	0.39	0.004(0)	0.02
	10.0	20	0.46	0.092(9)	0.33	0.002(0)	0.04
1.0 torr	1.0	1	0.52	0.042(2)	0.32	0.001(0)	0.02
	4.0	4	0.58	0.089(5)	0.34	0.002(0)	0.01
(25.0 cm.^{3} sec.$^{-1}$)	10.0	10	0.65	0.139(5)	0.33	0.001(0)	0.01
	20.0	20	0.64	0.216(17)	0.33	0.003(0)	0.00

† Figures in brackets refer to errors calculated in the least squares analysis.

†† Sum of the squares of the residuals of the experimental data and the re-calculated data.

* Flow rates refer to the pressure at which the experiment was carried out.

Table 5.2. Composite rate constants and pre-exponential terms derived from the Fluorine 1_s data.

Pressure (Flow rate)*	Power (watts)	W/P	$(1-e^{-d/\lambda\cos\theta})$	K_s † ($sec.^{-1}$)	$e^{-d/\lambda\cos\theta}$	K_b † ($sec.^{-1}$)	Σr^2 ††
0.1 torr	0.1	1	0.62	0.036(1)	0.35	0.004(1)	0.02
	0.4	4	0.57	0.063(4)	0.36	0.004(0)	0.02
($6.5\ cm.^3\ sec.^{-1}$)	1.0	10	0.71	0.100(2)	0.19	0.005(1)	0.01
	2.0	20	0.60	0.079(4)	0.24	0.003(1)	0.03
0.2 torr	0.2	1	0.50	0.032(1)	0.46	0.004(1)	0.02
	0.8	4	0.71	0.055(3)	0.26	0.005(0)	0.02
($7.0\ cm.^3\ sec.^{-1}$)	2.0	10	0.65	0.065(1)	0.29	0.003(1)	0.01
	4.0	20	0.61	0.082(5)	0.34	0.003(0)	0.01
0.5 torr	0.5	1	0.62	0.042(2)	0.44	0.004(0)	0.01
	2.0	4	0.57	0.047(2)	0.20	0.003(0)	0.05
($12.5\ cm.^3\ sec.^{-1}$)	5.0	10	0.65	0.080(3)	0.29	0.004(0)	0.02
	10.0	20	0.49	0.070(6)	0.27	0.002(0)	0.05
1.0 torr	1.0	1	0.060	0.047(2)	0.33	0.003(1)	0.01
	4.0	4	0.63	0.072(2)	0.28	0.003(0)	0.01
($25.0\ cm.^3\ sec.^{-1}$)	10.0	10	0.69	0.105(6)	0.25	0.001(1)	0.02
	20.0	20	0.57	0.167(17)	0.30	0.004(0)	0.01

† Figures in brackets refer to errors calculated in the least squares analysis

†† Sum of the squares of the residuals of the experimental data and the re-calculated data.

* Flow rates refer to the pressure at which the experiment was carried out.

versus the relevant experimental data typically gave correlation coefficients of the order of 0.99. Although the kinetic data over the whole range of pressure and power loadings presented here can be adequately rationalized in terms of a composite of two exponential terms, this is clearly a minimum, as it might be expected that comparable fits are likely to be obtained in terms of three or more exponential terms. However, this would result in a higher degree of complexity and ambiguities would almost certainly result since the analysis would be largely subjective. It is believed therefore that the overall analysis is the most logical based on the experimental data available and that the data may adequately be discussed in terms of two dominant rate processes.

The data in Tables 5.1 and 5.2 span an extensive range in pressure and power (0.1 to 1 torr and 0.1 to 20 watts). The small values of the sums of the squares of the residuals, of the experimental data and the related values obtained from the calculated curve, is a further indication of the close fit to the two component direct and radiative energy transfer model postulated, it is also gratifying to note that the sums of the pre-exponential terms are close to unity.

The data for the rate constants associated with the radiative energy transfer component occurring in the bulk, K_b, show an order of magnitude agreement over the whole range of power and pressure. The trends however are not immediately obvious probably due to factors concerning the competitive side reactions (i.e. oxidation and hydrocarbon contamination) which could conceivably have rates of the same order of magnitude. It is of interest, however, to attempt to improve the

statistical accuracy of the data in order to gain some insight into the overall gross features which may be encoded in this data, by 'grouping' the results. For example figure 5.19

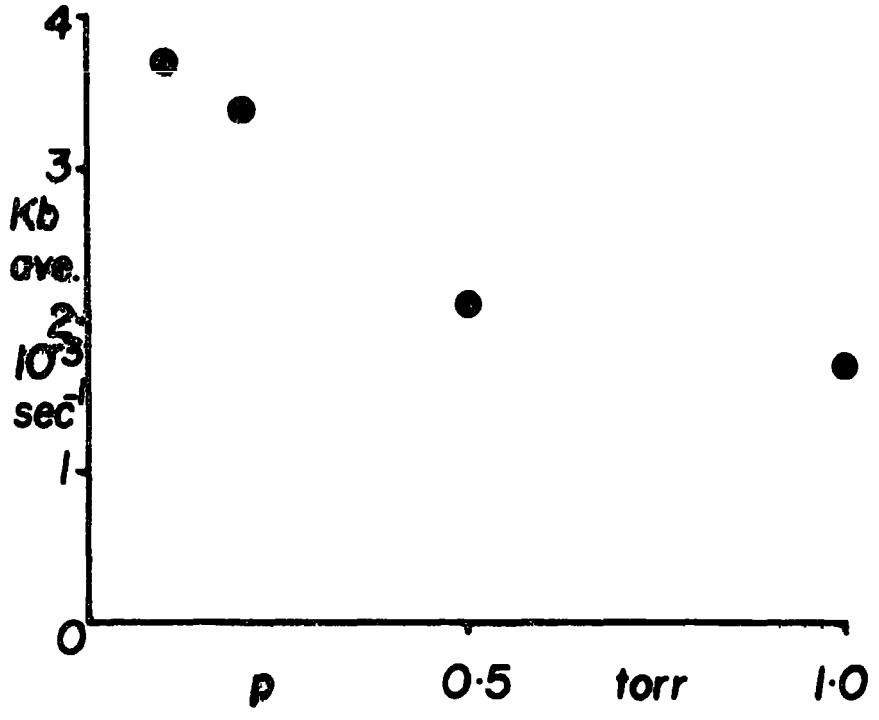

Figure 5.19. Average K_b (at a given pressure) versus pressure.

shows a plot of the average K_b (over the four power loadings) at a given pressure versus the pressure for the $\underline{C}F_2$ data. Since the average power loadings are 0.88, 1.75, 4.38 and 8.75 watts for 0.1, 0.2, 0.5 and 1.0 torr respectively the trend exhibited in figure 5.19 represents a lower limit to the differences, since the intensity of the vacuum ultraviolet radiation is known to increase with the power.[204] It is clear then in qualitative terms that the rate, K_b, decreases with increasing pressure. A similar treatment of the data is presented in figure 5.20. Here the average K_b (over the four pressures) at a given $^{W}/_{p}$ (power/pressure) is plotted against $^{W}/_{p}$ for the $\underline{C}F_2$ data. Hence, it may be tentatively suggested that the rate, K_b, under the conditions of these experiments, and in the range of $^{W}/_{p}$ from

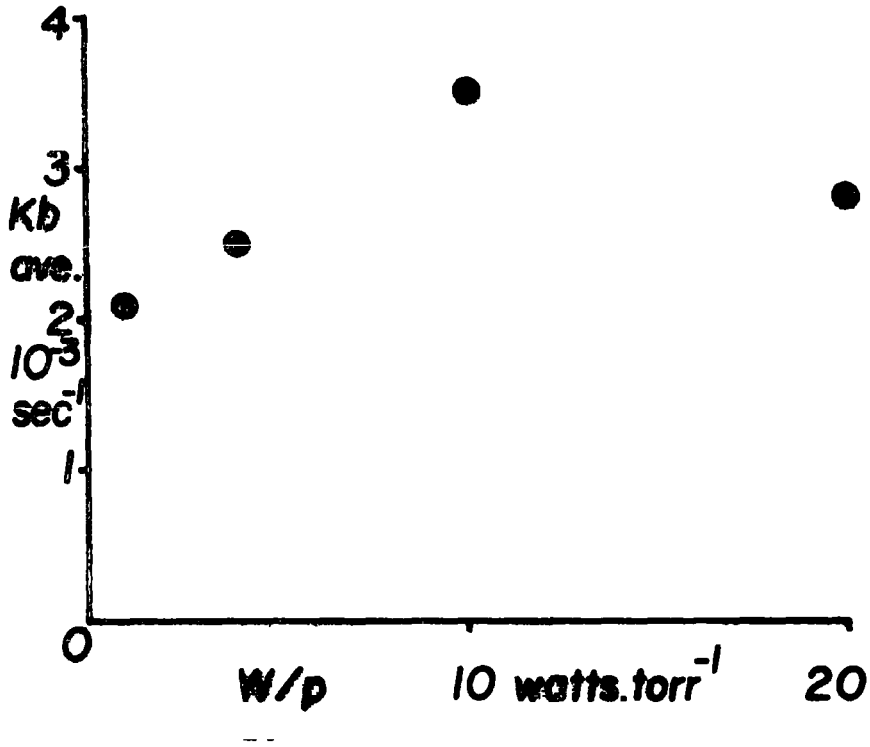

Figure 5.20. Average K_b (at a given $^{W}/_{p}$) versus $^{W}/_{p}$. 1 to 20 watts $torr^{-1}$ shows a maximum value.

It must be strongly emphasized that the data displayed in figures 5.19 and 5.20 is of unknown accuracy and cannot form the basis for any firm conclusions concerning the dependence of the rate for the radiative energy transfer processes, occurring in the subsurface and bulk of the sample, on the pressure and power loading of the plasma. However it is appropriate to present these data here such that they may be compared to the observations of the vacuum ultraviolet output from an argon plasma as a function of power and pressure presented in Chapter Six, section 3.3.

In contrast, the faster surface reaction is affected little by competitive side reactions and exhibits readily discernible trends. The most striking feature is the similarity of the

surface composite rate constants whether derived from either $\underline{C}F_2$ or F_{1s} data. This suggests that the surface reaction is dominated by $CF_2 \rightarrow CF$ with the CF sites undergoing little further reaction.

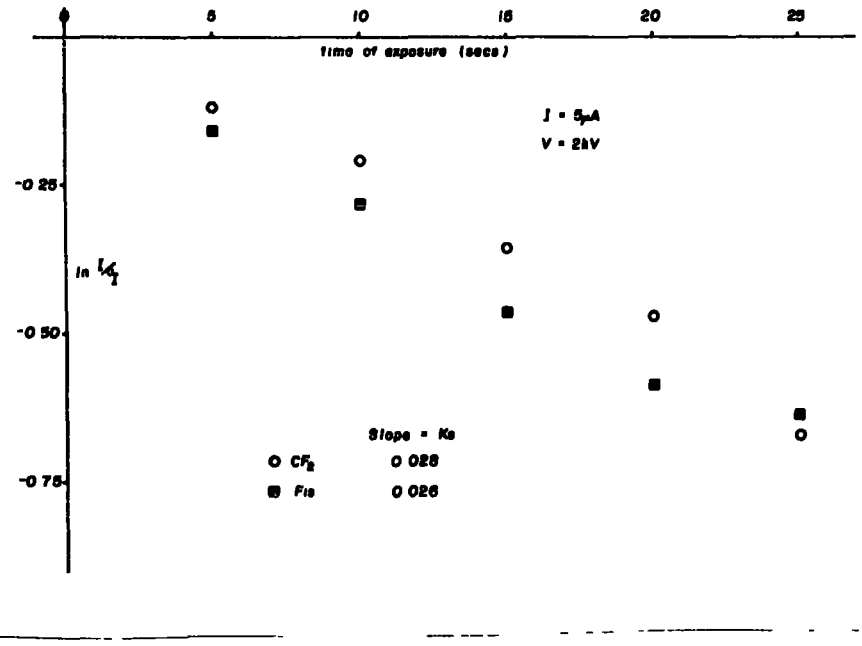

Figure 5.21. In I/I_o for the $\underline{C}F_2$ and F_{1s} levels, versus t, for data extracted from reference 114, involving the crosslinking of the copolymer by argon ion bombardment.

In this connection it is worthwhile, before discussing the trends in Ks, to consider data pertaining to direct energy transfer alone. Figure 5.21 shows plots of $\ln {}^{CF_2}/{}^{o}CF_2$ and $\ln {}^{F_{1s}}/{}^{o}F_{1s}$ versus t for an experiment in which the ethylene-tetrafluoroethylene copolymer was subjected to argon ion bombardment of kinetic energy 2 kV and a beam current of 5 μA. The light output from the D.C. discharge employed was essentially collimated and hence vacuum U.V. irradiation confined to a small fraction of the total surface area.

The main features are that the plots are good linear correlations as might be expected in terms of the kinetic model given by equation 5.13

$$\frac{X^t}{X_o^{TOT}} = e^{-K_s t} \qquad (5.13)$$

which is a particular case of equation 5.12, where d is large compared to the ESCA sampling depth scale and K_b is zero. The absolute slopes of the two straight lines correspond to K_s and it is clear that they are essentially the same. This is again indicative that the crosslinking initiated by direct energy transfer does not involve CF features being converted to C type environments.

The following discussion of the trends in K_s for argon plasma treated samples will therefore be confined to the $\underline{C}F_2$ data although the corresponding data derived from the F_{1s} levels show closely similar results.

Figure 5.22 shows a three dimensional simulation of a 'smooth fit' to the experimental data, for the C_{1s} levels, obtained by plotting the empirically derived expression $K_s = 0.041W^{(0.33p + 0.20)}/p^{0.24}$ where W is defined as the input power in watts and p the pressure in torr. The trends are readily understandable in terms of a fast surface reaction dominated by direct energy transfer since it is known that the concentrations of ions, electrons and metastables are directly related to the ratio of electric field and pressure in a given plasma.[209,210] For any given pressure/flow rate the rate increases with increasing power loadings, and for low power loadings (i.e. $<$ 10 watts) the rate decreases with increasing pressure and becomes relatively insensitive to the pressure above $\sim$0.2 torr. At higher power loadings and

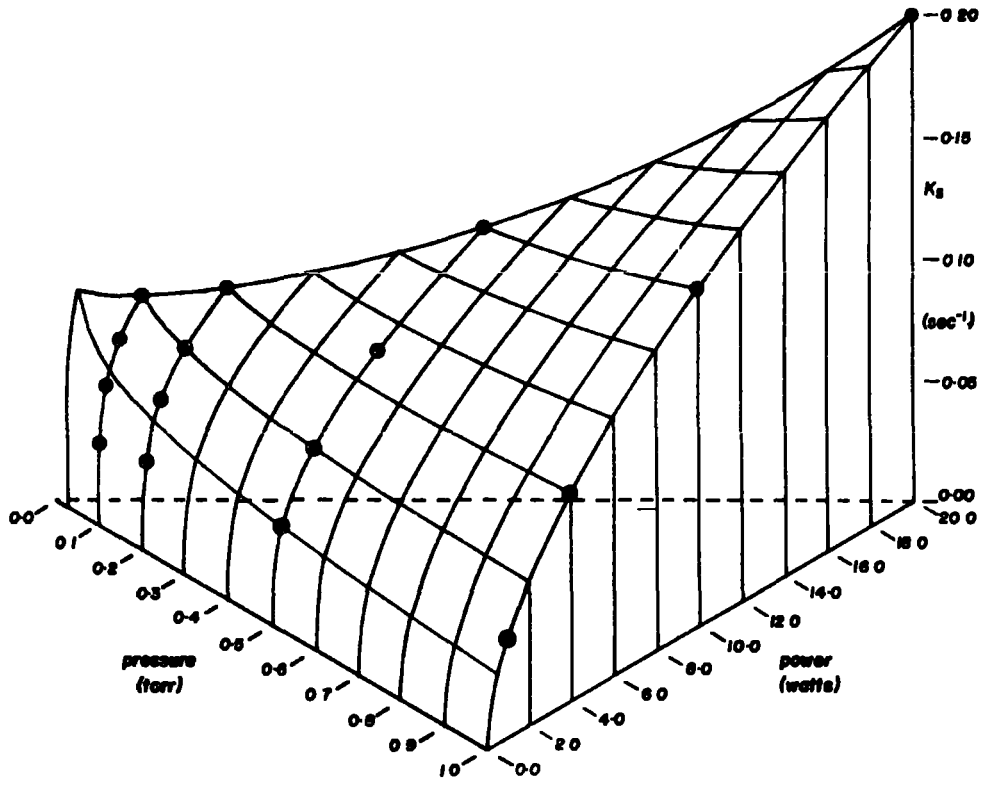

Figure 5.22. Three dimensional simulation of a plot of the surface composite rate constant, K_s, as a function of power and pressure, in the range of this investigation.

and higher pressure however, the rate increases with pressure. This phenomenon is understandable when the 'reverse' reaction is considered. If a sufficient partial pressure of the volatile products of the crosslinking process (H_2,HF) accumulates in the vicinity of the surface regions of the sample it is likely that they will undergo reaction with the sample and the apparent overall rate for the crosslinking process as monitored by the F_{1s} and CF_2 levels will be diminished. The magnitude of this 'reverse' reaction will be less at high pressures (i.e. $>$ 0.5 torr) since with the pumping system employed in this investigation the flow rate shows a steep rise resulting in quicker removal of volatile products.

Previous work in these laboratories have suggested that electron mean free paths for kinetic energies appropriate to photoemitted electrons from F_{1s} and C_{1s} core levels using $Mg_{K\alpha_{1,2}}$ radiation are in the order $\lambda_{C_{1s}} > \lambda_{F_{1s}}$.[100,123,124] This is also apparent from the data for the pre-exponential factors. The analysis of data on the surface fluorination of polyethylene[123,124] suggests typical mean free paths of 7Å and 10Å for the F_{1s} and C_{1s} levels respectively. For the direct investigation of polymer films (polyparaxylylene) of known thickness deposited onto a gold substrate a value of 14 ± 3Å was obtained for $\lambda_{C_{1s}}$.[99] The most recent determination involved the glow discharge polymerization of vinylidene fluoride onto gold substrates yielding values for $\lambda_{F_{1s}}$ and $\lambda_{C_{1s}}$ of 7 ± 3Å and 10 ± 2Å respectively.[100] With a knowledge of the electron mean free paths it is possible to compute a value for d, the depth to which direct energy transfer processes are important, from the pre-exponential factors containing the depth information. ($e^{-d/\lambda \cos\theta}$ and $1-e^{-d/\lambda \cos\theta}$ in Tables 5.1 and 5.2).

From the F_{1s} level data this analysis, using $\lambda_{F_{1s}} = 7$Å, gives a value of $\simeq 7$Å whilst for the $\underline{C}F_2$ levels, using $\lambda_{C_{1s}} = 10$ Å, a value of $\simeq 8$ Å is obtained. These are in good agreement considering the approximations inherent in the analysis and furthermore are close to the depth appropriate to one or two monolayers,[188] which is eminently reasonable in terms of the chemistry and the physics of the processes involved.

6. Mechanistic Aspects of the Plasma Modification of an Ethylene-Tetrafluoroethylene Copolymer Film

In this section possible mechanisms are briefly considered which would provide a basis for rationalizing the results.

Clearly the most that can be accomplished at this stage is a likely scenario for the processes involved and more detailed discussions must await the results of further experiments involving reactions of the same polymer system with plasmas excited in other inert gases and for a given inert gas plasma, studies of the variation of rate processes as a function of polymer structure. A key observation in addition to those relating to the relative changes in the intensities of the F_{1s} levels and the individual components of the C_{1s} levels, is that in all cases the total integrated signal intensity of the C_{1s} levels increases for the surface modified species (see figure 5.16). For example for reactions carried out at pressures of 0.1, 0.2 and 0.5 torr if one considers the total integrated intensity for the C_{1s} levels for a common reaction time of 100 secs, where the power loading is such that $W/_p$ is the same, (4), then the increase in intensities are 1.28, 1.25 and 1.23 respectively. These increases in signal intensity are most readily explicable in terms of cross linking processes occurring under the agency of the plasma and in which $\underline{CF_2}$ structural features are converted to $\underline{CF}$ environments, in the initial stages. (Throughout this discussion conversion of $\underline{CH_2} \rightarrow \underline{CH}$ is largely implicit since the direct observation of this process is not so readily achieved from the ESCA data). The signal due to $\underline{C}F$ structural features in the ESCA spectra of the modified copolymer is centred at $\sim$288.3 eV (cf. figure 5.11). However the substituent effect of fluorine ($\sim$2.9 eV shift to higher binding energy with respect to the unfluorinated system for C_{1s} levels of carbon directly attached to fluorine) has been exhaustively studied both theoretically and experimentally and the shift reported here is therefore only

explicable in terms of a further shift to higher binding energy originating from fluorine substituents in β positions.[114,119] Indeed from previous work the binding energy is entirely consistent with structural features such as

$$-CF_2-\underline{CF}-C- \quad \text{and} \quad \begin{matrix} & | \\ -CF-\underline{CF}- & \\ | & \end{matrix} C-$$

in which the $\underline{CF}$ groups are directly attached to $\underline{CF_2}$ or $\underline{CF}$ groups and carbons which do not carry fluorine substituents. The much larger full width at half maximum (FWHM) for the $\underline{CF}$ and $\underline{CH}$ structural features in going from the initial to plasma treated polymer samples suggests a variety of bonding environments also consistent with a cross linked formulation.

The increase in total integrated intensity for the C_{1s} levels is most readily understood in terms of equations 5.1 and 5.2. Before considering this however it should be noted that the angular dependent studies previously discussed reveal the inhomogeneous nature of the treated samples and by going to grazing exit angle for the photoemitted electrons we may specifically enhance the contribution to the overall spectra of surface features. In this connection it is interesting to note that for a given kinetic run if the ratio of total integrated intensity of the C_{1s} levels for the plasma treated and untreated samples are plotted as a function of take-off angle then this ratio tends to increase as take off angle approaches grazing exit. This also provides strong evidence for cross linking in the surface regions.

The total integrated intensity for the C_{1s} levels for a homogeneous sample is given as

$$I_\infty = f(\theta)F\alpha NK\lambda \qquad (5.14)$$

whereas for the surface modified system there are contributions from structural features in the surface layers and from the unmodified bulk.

$$I_{\infty}^{mod} = f(\theta)F\alpha K(N_s \lambda_s(1-e^{-d/\lambda_s \cos\theta}) + N_b \lambda_b e^{-d/\lambda_b \cos\theta}) \quad (5.15)$$

Independent studies in these laboratories have shown that for electrons of a given kinetic energy, electron mean free paths are not strongly dependent on polymer structure and we may anticipate that to a high degree of accuracy mean free paths of electrons in the cross linked surface regions are closely similar to those for the bulk (unmodified) polymer system. Indeed some evidence has already been presented in this connection since it was shown that estimates of the depth to which the fast surface reaction pertained, are eminently reasonable on both chemical and physical grounds. Since in both cases we are studying the same core level the constant factors cancel and the ratio of total integrated C_{1s} signal for the modified and unmodified polymer systems then simplifies to

$$\frac{I_{\infty}^{mod}}{I_{\infty}} = \frac{N_s(1-e^{-d/\lambda \cos\theta}) + N_b e^{-d/\lambda \cos\theta}}{N} \quad (5.16)$$

where N_s, N_b and N represent the number of carbon atoms per unit volume irradiated by the X-ray source for the surface, bulk and unmodified copolymer ($N_b = N$).

It is clear that this ratio can be > 1 provided that $N_s > N_b$. Such would be the case for a cross linked system. As a simple example where crystallographic data is available we may note that for polyethylene typical interchain distances are ~ 4.5Å.[188] This is approximately 3X the typical bond length for a carbon-carbon single bond. The net effect of cross linking is therefore to reduce interchain separation (i.e. the

surface effectively shrinks) and the number of carbon atoms per unit area in the surface thereby increases. It is also worthwhile pointing out that since cross linking inevitably involves some chain mobility it will be particularly favoured in the surface regions.

Possible mechanisms for such a process may therefore be briefly considered. The energetic species emanating from the plasma are electrons, argon ions and metastables and vacuum ultraviolet radiation. Considering firstly the electrons it is clear that since mean free paths for electrons in the energy range 0 - 10 eV are likely to be at least an order of magnitude larger than for either argon ions or metastables their role is likely to be a secondary rather than a primary one as will become apparent. Even so it is clear that the most likely primary role of the electrons, however small, should involve the production of the parent ion of a localized portion of the polymer chain. Indeed it will become apparent that this is the most likely primary process in general. It has been previously pointed out that valence ionization of the polymer is energetically feasible by direct interaction with either argon ions or metastables whilst for the short wavelength vacuum U.V. radiation the largest contribution to the attentuation coefficient is undoubtedly from photoionization and from transitions to diffuse Rydberg states which in the solid closely approximate in properties the ionized states.

A valence ionized polymer chain produced in the condensed media can undergo a number of transformations which may now be considered. The available valence ionized states correspond to removal of F_{2p} lone pairs or electrons dominantly of C-C or C-H bonding characteristics. Such ions could undergo uni-

molecular reactions such as carbon carbon or carbon hydrogen bond cleavage however in such a rigid matrix the cage effect would be expected to dominate more particularly for the former reaction and the more likely process would seem to be ion neutralization by means of the electron flux through the sample. This would lead to electronically excited systems with energies considerably higher than that required for bond cleavage and/or unimolecular elimination of a small molecule (e.g. HF or H_2). In the particular case of carbon bond cleavage in the parent ion, the relative ionization potentials and electron affinities would ensure the production of a hydrogen atom and a carbocation. The electronically excited neutral systems produced by a quenching process have sufficient localized internal energy for homolytic C-F, C-C and C-H bond cleavage. The greater mobility of hydrogen and fluorine atoms almost certainly dominate the following reaction sequences since the carbon radicals produced form part of the relatively inflexible polymer chain. Considering therefore a typical polymer repeat unit a reasonable outline of the initial stages of reaction may be elaborated as in figure 5.23. A variety of pathways are therefore available for the production of potential sites for cross linking and a consideration of the likely rates of abstraction and elimination would tend to suggest that the effective elimination of HF is an important precursor to cross linking. The production of radicals or carbocations in close proximity to any unsaturated centres provides a ready means of cross linking by either radical or electrophilic addition mechanisms. Such a scheme leads to a straightforward interpretation of the decrease in intensity of the C_{1s} levels associated with $\underline{CF}_2$ structural features and

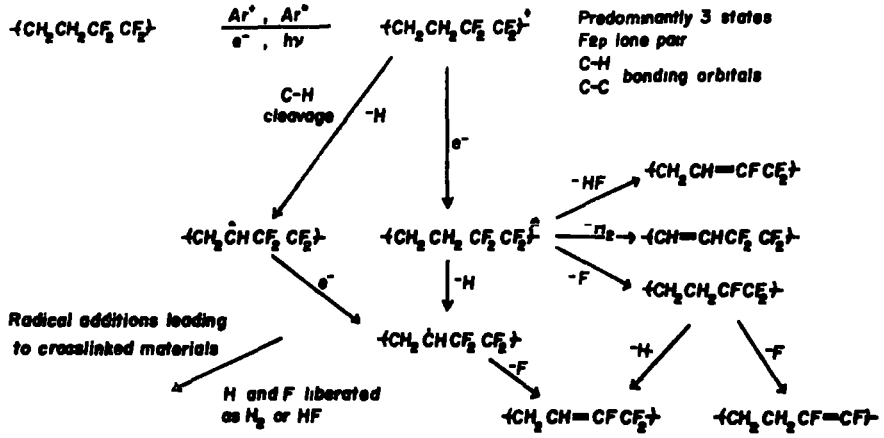

Figure 5.23. Reaction scheme for processes leading to cross-linking in an ethylene/tetrafluoroethylene co-polymer, initiated by exposure to an argon glow discharge.

the increase in intensity of those at intermediate binding energy associated with CF components.

CHAPTER SIX

Surface Modification of Polymers by Inert Gas Plasmas: Part II

1. Introduction

Chapter Five has described a detailed study of the surface modification of an ethylene/tetrafluoroethylene copolymer (52% TFE) subjected to inductively coupled radiofrequency glow discharges excited in argon. The kinetic model developed to rationalize the data was demonstrated to be an extremely good approximation over a wide range of pressures and power loadings. This chapter, as a logical extension to this work, describes investigations employing the same polymer system exposed to glow discharges excited in helium, neon, argon, krypton and xenon, and in the case of argon plasma treatment, modification as a function of polymer structure. In addition appropriate mixtures of the gases have been investigated.

It has been demonstrated that for extensively treated samples the dominant mechanism for modification involves radiative energy transfer[211] from the plasma via the ultraviolet (in this connotation taken to include the vacuum ultraviolet) component of the electromagnetic radiation. The reaction in the outermost few monolayers on the other hand is primarily due to direct energy transfer processes, involving ion neutralization[202] and Penning ionization[201] of the polymer as a result of ions and metastables interacting with the surface. Indeed the indications from Chapter Five are that the rate constants for direct energy transfer processes are typically an order of magnitude greater than those for radiative energy transfer processes.

Using an inert gas as the sustaining medium, the reaction initiated in a saturated polymer, via either energy transfer process, is thought to involve a crosslinking mechanism,[192]

in which excited states of the polymer chain undergo homolytic bond cleavage producing a wide variety of free radicals and unsaturated centres, which by radical additions produce crosslinks between adjacent polymer chains. At high power densities, ablation of small volatile chain fragments from the surface cannot be discounted.[212] However, at the relatively low power loadings employed throughout this work ablation is expected to be minimal.

The primary objective in this chapter is to compare the effects of using different inert gases for the crosslinking procedure. Information which may be gained on the average depth of penetration of the direct energy transfer processes along with the correlation of the rate constants with the fundamental properties of the plasma sustaining gas, (i.e. ionization potential, metastable energy, atomic radius) should provide qualitative information on the plasma itself. Preliminary accounts of direct electron sampling[133] from plasmas and the vacuum ultraviolet output from the plasmas as a function of power and pressure[204] are included in Section 3.

2. Experimental

2.1 Samples and Gases

Polymer samples used in this investigation were in the form of extruded films (~30 μm thick) and included the ethylene/tetrafluoroethylene copolymer, polystyrene, polyethyleneterephthalate and polytetrafluoroethylene. The only exception was polyvinylidene fluoride which was studied as a fine powder.

The inert gases used throughout this chapter were of research grade and purified by means of a sorption train as described in Chapter Five.

2.2 Kinetic Studies

The glow discharge reactor used in the kinetic studies has been previously described in Chapter Five, (reactor C). The pumping system however was modified to produce a greater pumping speed, thus reducing the partial pressure of the volatile products of the crosslinking reaction (H_2, HF). This lessens the importance of re-combination reactions of the volatiles with the polymer sample which were assumed, in the old configuration, to have been of the same order of magnitude, as far as rate constants are concerned, as the radiative energy transfer processes, effectively masking any trends that might have been observed, The new configuration, involving a 501. $min.^{-1}$ rotary pump and $\sim$3 feet of $\frac{1}{2}$" tubing, increased the flow rate for argon by a factor of $\sim$10 which is expected to reduce the 'reverse' reactions to negligible levels.

The radiofrequency equipment, ESCA equipment and experimental procedures have been previously described.

For the generation of difference spectra, spectra were recorded in the step scan mode and adequate signal to noise statistics were generated by two successive scans over 25 eV energy range with an energy increment of 0.1 eV and total count time per channel of 0.6 sec. Spectra were stored in a hard wired multi channel analyser (LABEN Spectrascope NIM8001) equipped with sufficient arithmetic facilities to allow direct addition, subtraction or integration of spectra.

2.3 Direct Electron Sampling

Direct electron sampling was achieved by employing the hemispherical double focussing electrostatic analyser (10" mean diameter)of the AEI ES 200AA spectrometer. In the usual mode

of operation of the spectrometer, the sample is conventionally mounted onto a probe tip attached to a metal probe passed into the sample chamber via an insertion lock arrangement (typical pressure in the sample chamber $\sim 5 \times 10^{-8}$ torr). On X-ray irradiation of the sample, photoemitted electrons enter a vertically mounted retarding lens system and then the analyser by means of an adjustable slit mechanism (dimensions 1.2 cms. x 0.060, 0.120, 0.200 cms.). The relatively long path length between the sample and the analyser and detector requires pressures below $\sim 10^{-5}$ torr in the analyser region to obviate any effects due to scattering involving the extraneous residual atmosphere, (typically the pressure in the analyser region is 10^{-9} torr). The possibility of irreversible damage to the electron multiplier arising from operation at relatively high pressures must also be kept in mind. The source region of the spectrometer in which the sample is irradiated is separated from the lens system by means of a teflon sleeve valve which when fully opened in normal operation provides (via restriction of pumping speed) a pressure differential between source and analyser of approximately two orders of magnitude. With this constraint it is not possible to excite a discharge in the source region of the spectrometer in the pressure range of interest in this study and directly sample the electrons. It is clear therefore that any such experiment requires a differential pumping arrangement.

The experimental arrangement is indicated schematically in figure 6.1, and involved the generation of plasmas in a $\frac{1}{2}$" pyrex tube directly pumped with a two stage 120l.min.$^{-1}$ rotary pump connected to a ballast volume maintained at $\sim 10^{-3}$ torr. The tube traversed the spectrometer sample chamber, vertically

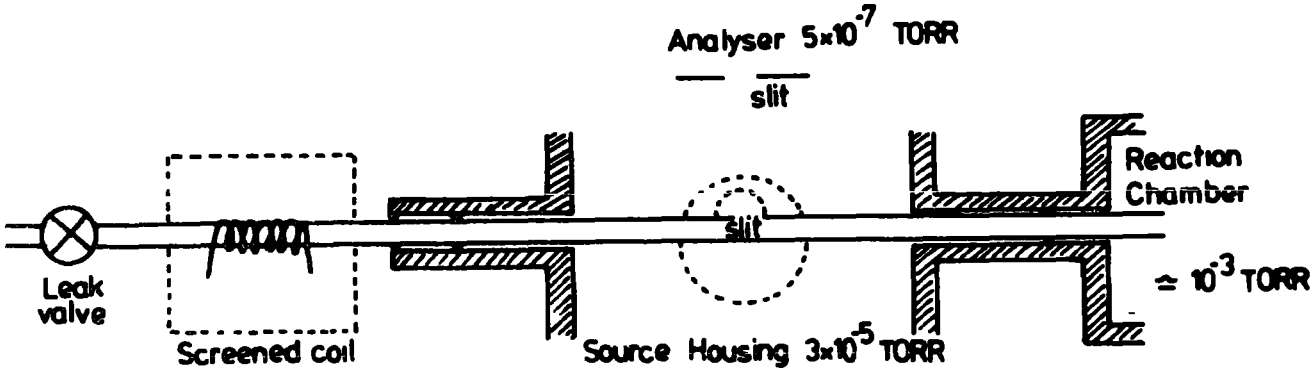

Figure 6.1. Experimental arrangement for the investigation of electron energy distributions.

below the entrance slit to the analyser via insertion locks employing viton 'O' seals. A slit 1 cm. long x 0.1 cm. wide machined along the length of the tube was aligned with the entrance slit to the analyser and a 30 turn coil of $\frac{1}{8}$" copper tubing extending to 6" was located external to the spectrometer, the centre of the coil being approximately 12" from the centre point of the slit. With the separately pumped insertion lock seals based on viton 'O' rings it was possible to rotate the tube to investigate the effect of alignment of the slits.

The differential pumping across the slit in the tube (the sample region of the spectrometer was directly pumped by a 4" diffusion pump) was such that for pressures in the range 10^{-3} - 10^{-2} torr in the discharge region the pressure in the source was maintained below 5 x 10^{-5} torr and that in the analyser below 5 x 10^{-7} torr. Inert gas was metered via the purification train into the tube and the region encompassing the coil was screened by means of a grounded wire mesh cage which

contained the electronics.

2.4 Vacuum Ultraviolet Spectra of the Plasmas

The vacuum ultraviolet spectra of the inert gas plasmas was recorded as a function of pressure and power loading, using a one-meter normal-incidence Ditchburn monochromator[213] (Rank Precision Instruments Ltd., model E 766). The grating has 600 lines per mm. and a ruled area 96 x 56 mm. It is blazed and coated for 1500Å and may be scanned mechanically from $\sim$ 200Å to the visible. The detector is a 13 stage venetian blind dynode photomultiplier (EMI type 9502 S) with a phosphor coating of sodium salicylate. This instrument gives typical linewidths (FWHM) of 1Å with entrance and exit slits of 12 μm.

In the majority of cases the plasma was excited in a 1" pyrex tube $\sim$ 45 cms. long by means of a 6 turn copper coil centred $\sim$ 8 cm. from the end of the tube adjacent to the entrance slit of the monochromator. Since the study of vacuum ultraviolet radiation largely precludes the use of window materials[196] the end of the discharge tube was open. A similar situation to that experienced for direct electron sampling in the ESCA spectrometer is apparent since the pressure in the monochromator must be $< 10^{-3}$ torr to prevent absorption of the vacuum ultraviolet radiation by the residual atmosphere. Furthermore to prevent irreversible damage to the photomultiplier the detector region is normally operated below a pressure of 10^{-4} torr. It is clear that, as for the direct electron sampling experiments, a differential pumping arrangement is necessary. The experimental configuration involved the discharge tube pumped by means of a throttled 2" diffusion pump, the monchromator

by a 6" diffusion pump and the detector region by a 2" diffusion pump, separated by the 12 μm entrance and exit slits of the monochromator. This allowed, for example, with a pressure of ~ 0.1 torr and typical flow rate of ~1.0 $cm.^3$ $min.^{-1}$ (at NTP) in the discharge tube, that the monochromator be maintained at ~10^{-3} torr and the detector at ~ 10^{-5} torr.

The leak of gas into the discharge tube was finely controlled by a servo leak valve coupled to a calibrated pirani type vacuum gauge. This arrangement is estimated to maintain the pressures quoted in the investigation accurately to ± 2%. With this arrangement the vacuum ultraviolet spectra of helium, neon, argon, krypton and xenon were recorded at power loadings of 2.5, 5, 10, 15 and 20 watts and pressures of 0.05, 0.1, 0.2 and 0.5 torr. For comparison purposes experiments were also carried out using a discharge tube in which the diameter of the discharge region (~10 cms. long, starting ~ 6 cms. from the slit) was increased to 5 cms. with a 12 turn copper coil wound centrally. This tube, although more closely approximating the configuration used in reactor C employed in the kinetic studies, was not used extensively due to problems of radiofrequency interference with the detection electronics experienced with this geometry.

3. Some Physical Aspects of Inert Gas Plasmas

Before proceeding to the elaboration of the chemical aspects of surface modification of polymers effected by plasmas excited in a variety of inert gases, it is appropriate to first consider the physical properties of the radiofrequency glow discharges in question. This section therefore summarizes the main features of the plasmas and includes preliminary accounts of the investigation of the electron energy distribution,

by means of direct electron sampling and the vacuum ultraviolet radiation emitted from the plasmas, both as functions of the pressure and power loading.

3.1 Observations on the Energy Distribution of Electrons Sampled from Radiofrequency Plasmas Excited in Inert Gases.

The series of experiments described here are different in character to those which have previously been reported in that the sampling of the plasma has been indirect but direct measurements have been made of the energy distribution. By contrast most of the previous work has involved direct sampling of the plasma, (by means of electrical probes) but an indirect estimate of the energy distribution.[199,209,214]

The results described here pertain to plasmas excited in argon, as a function of pressure and input power. The basic philosophy behind the experiments was to investigate the possibility of sampling the plasma in terms of electron energy distribution by means of an analyser located external to the tube in which the plasma was excited. There are of course distinct difficulties in such an endeavour and the results reported here are such that only a few tentative conclusions may be drawn since many more experiments would be required to evaluate the relative importance of all of the likely contributing factors.

Initial experiments indicated that a plasma excited in the tube produced an electron flux readily detected with standard counting equipment and showing a structured distribution in energy. Rotating the slit axially out of alignment with the entrance to the analyser decreased the overall count rates confirming that the electrons being sampled emanated from the slit in the tube. No attempt has been made to measure the average potential of the plasma with respect to earth and

since the pyrex tube was in any case insulated from the spectrometer there is a distinct possibility that a significant potential exists between the entrance slit to the analyser, the plasma overall and the tube in which the glow discharge was sustained. Although there was considerable emission in the visible in the region of the coil such emission was less evident for the section of tube aligned with the spectrometer slit.

The results from the first set of experiments are shown in figure 6.2, where the power ratings refer to output from the generator. In each case the matching network was adjusted

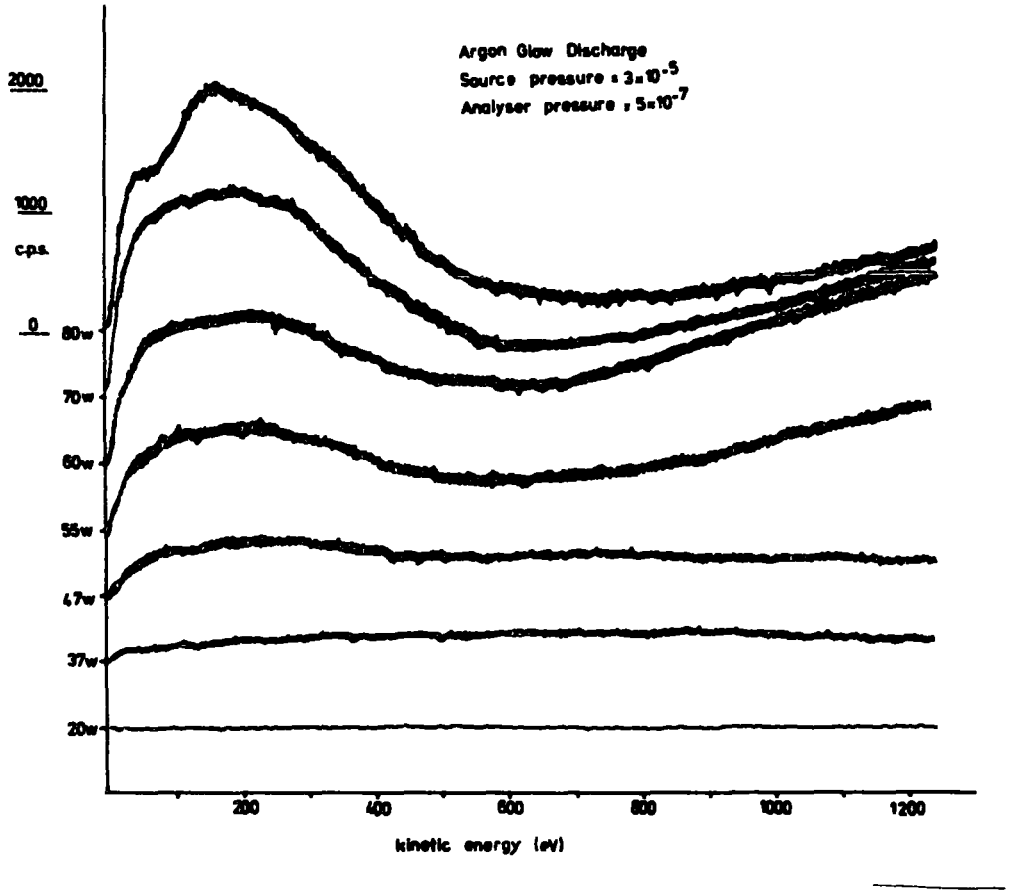

Figure 6.2. Kinetic energy distributions for electrons sampled from the plasma at various power loadings.

to minimize the standing wave ratio the latter becoming progressively larger at higher power loadings (1.5 at 20 watts - 2.3 at 80 watts). At 20 watts the count rate across the whole energy range (1250 eV) is negligible, however as the power is increased a broad energy distribution extending over $\sim$ 500 eV develops with a tail to higher kinetic energy. At 80 watts the maximum for the detected electrons centred $\sim$ 150 eV has a count rate of $\sim 2 \times 10^3$ counts/sec., and further structure develops in the low energy region with a shoulder centred $\sim$ 30 eV. The tail extending above $\sim$ 500 eV appears to be variable in nature as is clearly evidenced from the data shown in figure 6.2. Having established that an electron flux emanating from the plasma (or rather, downstream of it) can be readily detected and exhibits a structured energy distribution the effect of retuning the matching network on the low energy structure was investigated and the results are shown in figure 6.3.

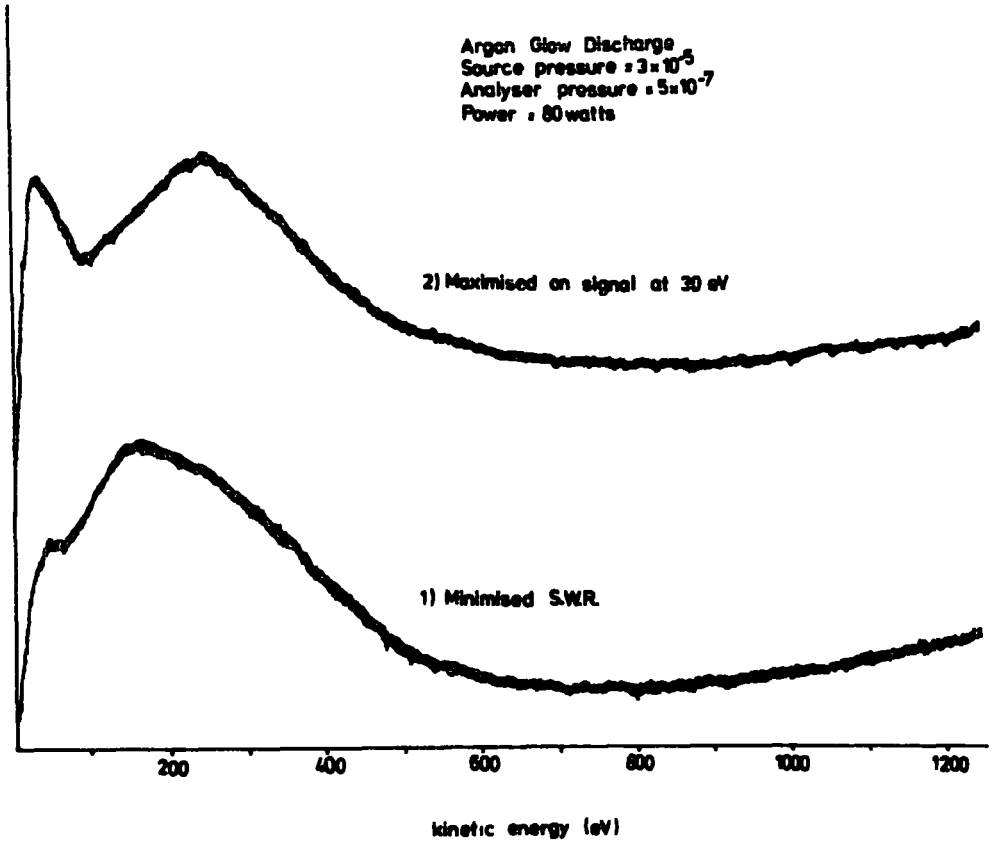

Figure 6.3. Effect of retuning the matching network.

The structure at low energy (centred ∿ 30 eV) acquires considerable intensity on retuning and separates into a distinctive peak with the semblance of a Maxwellian type distribution. The pressure dependence of this structure was investigated by adjusting the metered flow of argon into the discharge tube. The pressures in the discharge tube itself were not monitored during the experiments since the plasma interferes with both the thermocouple and pirani gauge readouts in the inlet system, however the pressures are believed to be somewhere in the range 5×10^{-3} - 5×10^{-2} torr. The pressures measured directly in the spectrometer sample chamber by means of an ion gauge were however recorded before each experiment and reflect the pressure trends in the discharge tube. It is clear from the data in figure 6.4 that the electron count increases considerably on going to lower pressures consistent with an increase in mean free path in the discharge tube.

The salient features from these experiments are therefore as follows. An electron flux emanating from the plasma may be detected and depends markedly on the power and pressure in the expected manner. The energy distribution seems to comprise three components. A low energy component with energy ∿ 30 eV at the peak maximum whose intensity can be enhanced by retuning the matching network. A broad distribution centred around ∿ 150 eV (minimised SWR) or ∿ 230 eV (maximized signal on 30 eV peak) depending on the tuning circuit, and a long tail to higher kinetic energy which tended to be less reproducible and in any case did not vary in a consistent manner either with pressure or power input to the plasma. The interpretation placed on these data must of necessity be somewhat

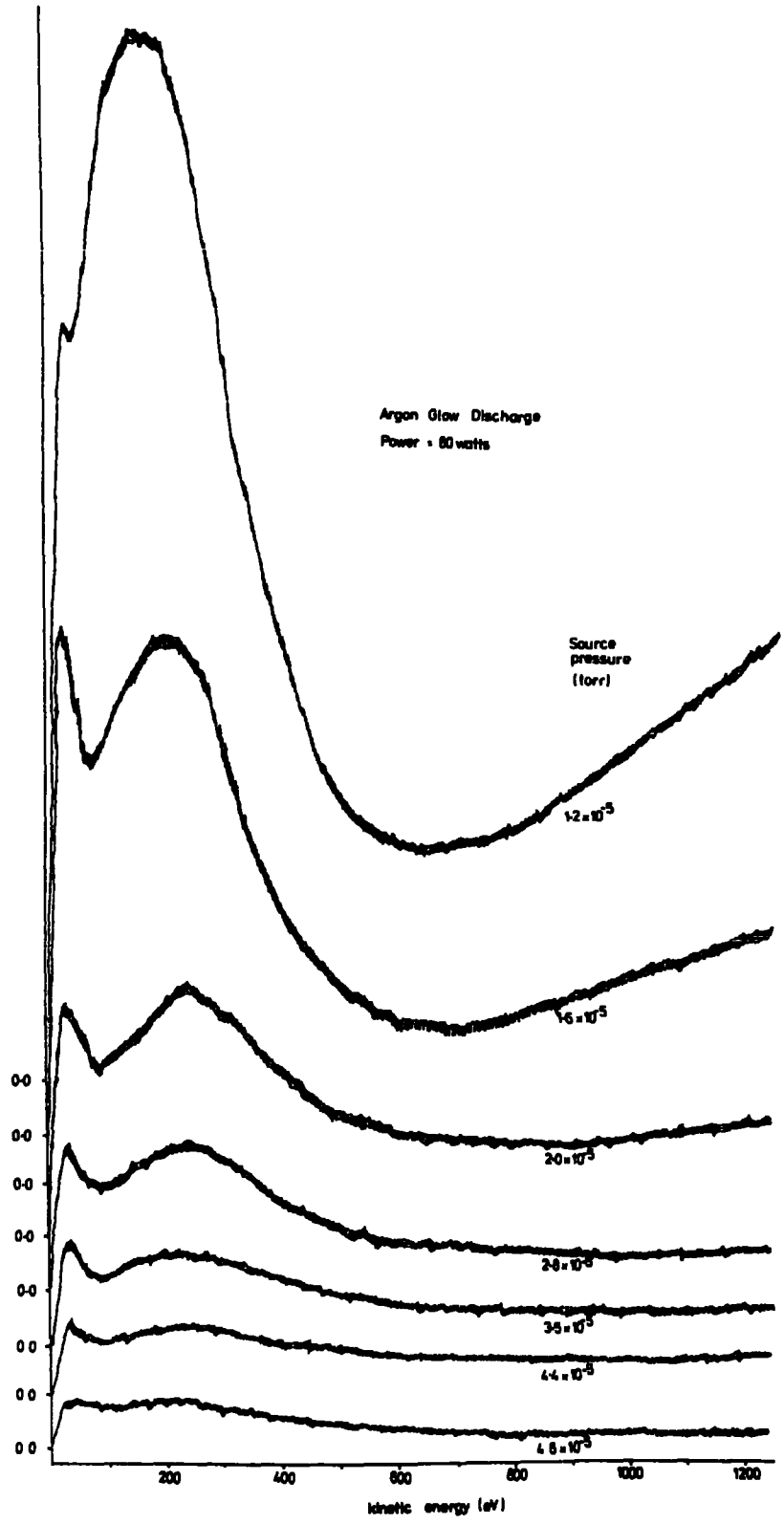

Figure 6.4. Kinetic energy distribution for electrons sampled from the plasma at various pressures.

speculative however it is tempting to assign the Maxwellian type distribution at low energy to the general distribution of electrons in the plasma. Although the trends observed in this investigation are consistent with previous work achieved by more conventional methods the measured energies of the electrons appear to be high since published data[195] suggests that in the pressure range of interest here the energy distribution function typically peaks in the region 0-10 eV. It should be pointed out however that there are problems associated with the energy reference. The kinetic energy of the electrons are measured with respect to the fermi level of the spectrometer however there is no guarantee that the average potential of the plasma approximates to earth or that the exit slit to the pyrex tube is at earth potential. Indeed the higher energy structures would suggest that space charge effects at the edges of the slit might be of some importance. Further factors which might be considered are the strong fields arising inside the spectrometer source from the plasma which could well account for the high energy components of the distributions shown in figures 6.2 to 6.4. At this stage therefore it may merely be noted that the possibility exists of combining ESCA studies with investigations of energy distributions and the preliminary results outlined here form an interesting and very useful basis for such studies.

3.2 Ions and Metastables in Inert Gas Plasmas

Whilst the kinetic energy for the ions and metastables in the plasmas is close to ambient temperature they possess a considerable amount of electronic energy which may be given up to the polymer when the ion or metastable interacts with

its surface. The relatively long lifetimes of the metastable states in particular of the inert gases allow them to undergo several elastic collisions before releasing their energy.

Typical lifetimes of the metastables in the plasma of the inert gases have been quoted in the order of a second or so for argon and in the sequence He>Ne>Ar>Kr>Xe[201] although the lifetimes will be a strong function of the plasma parameters and in particular mean free paths of the metastables in the plasma. The ionization potentials and metastable energies associated with the various inert gases are well documented in the literature and are summarized in Table 6.1.[201,215]

Table 6.1. Electronic Energies of the Ions and Metastables of Inert Gases

Atom	Ionization Potential		Metastables	
	Designation	Energy (eV)	Designation	Energy (eV)
He	$^2S_{1/2}$	24.586	2^1S	20.615
			2^3S	19.818
Ne	$^2P_{3/2}$	21.564	$^3P_0$	16.795
	$^2P_{1/2}$	21.661	$^3P_2$	16.619
Ar	$^2P_{3/2}$	15.759	$^3P_0$	11.723
	$^2P_{1/2}$	15.937	$^3P_2$	11.548
Kr	$^2P_{3/2}$	13.999	$^3P_0$	10.562
	$^2P_{1/2}$	14.665	$^3P_2$	9.915
Xe	$^2P_{3/2}$	12.130	$^3P_0$	9.447
	$^2P_{1/2}$	13.436	$^3P_2$	8.315

All of the energies shown in Table 6.1 are sufficiently large to ionize most organic systems, with the exceptions of the 9.915 eV and 8.315 eV metastable states of krypton and

xenon respectively which are too low for Penning ionization of a typical alkane.[216]

The mean free paths for inert gas ions and metastables a priori might be expected to be strongly dependent on the energy (kinetic and electronic) and size of the species in question. In a study of the inert gas ion bombardment of PbO surfaces Kim and co-workers[203] showed that the relative order of mean free paths was He>Ne>Ar>Kr. The metastables and ions in a radiofrequency plasma however would be expected to have substantially shorter mean free paths than for species produced in conventional ion guns since the kinetic energy distribution for the former corresponds roughly to ambient temperature whereas the latter are 'hot'. The depth to which direct energy transfer processes involving argon ions and metastables are important in the ethylene-tetrafluoroethylene copolymer was estimated to be ~ 8Å, based on a mean free path of ~ 10Å for electrons of ~ 960 eV kinetic energy.[100] Thus the indication from this previous work is that direct energy transfer processes involving argon ions and metastables is only of importance over the first few monolayers.

The concentration of ions in the plasma parallels that of the electrons (typically 10^{10} - 10^{12} cm.$^{-3}$) resulting in overall electrical neutrality and the concentration of metastables is of the same magnitude.

3.3 Observations on the Vacuum Ultraviolet Radiation Emitted from Radiofrequency Plasmas Excited in Inert Gases

The electromagnetic radiation associated with the inert gases is predominantly in the vacuum ultraviolet. In the pressure range pertinent to this investigation the radiation from the plasmas is in the form of the characteristic line spectra.[196]

As well as the neutral atoms a significant number are present in their first ionized state. This gives rise to two line series designated I and II. For those with atomic number > 2 the most intense lines for each series derives from transitions to the ground state from the lowest energy singly excited state, i.e. ns^2np^6 $(J=0) \leftarrow ns^2np^5(n+1)s$ $(J=0,1)$ for the neutral atom and ns^2np^5 $(J=1/2, 3/2) \leftarrow nsnp^6$ $(J=\frac{1}{2})$ for the singly ionized species, giving two component structures arising from the J splitting. For helium the situation is closely similar but having only one component in each case, i.e. $1s^2$ $(J=0) \leftarrow 1s2p$ $(J=1)$ and $1s$ $(J=\frac{1}{2}) \leftarrow 2p$ $(J=\frac{1}{2})$ for the HeI and HeII resonance lines respectively. Since these transitions are to the ground state configuration of the atom or ion the photon released is readily reabsorbed by other atoms or ions in their ground states hence the term resonance lines. A summary of the wavelength and energy of the resonance lines for the inert gases is given in Table 6.2.[215]

Table 6.2. Resonance Lines of the Inert Gases

Designation	Wavelength (A^o)	Energy (eV)	Designation	Wavelength (A^o)	Energy (eV)
HeI	584.4	21.217			
HeII	303.8	40.811			
NeI	743.7	16.671	KrI	1235.8	10.032
	735.9	16.848		1164.9	10.643
NeII	462.4	26.813	KrII	964.2	12.858
	460.7	26.910		917.4	13.514
ArI	1066.7	11.623	XeI	1469.6	8.436
	1048.2	11.823		1312.4	9.447
ArII	932.1	13.302	XeII	1244.8	9.960
	919.8	13.479		1100.4	11.266

The total attenuation cross sections for the vacuum ultraviolet radiation passing into the polymer are undoubtedly dominated by the photo-ionization component[205] resulting in the production of polymer ions.

At slightly longer wavelengths, components of the Rydberg transitions (which converge on the ionization limits) also have substantial cross sections and since for the higher members the orbitals involved are so diffuse the concept of a locally excited transition loses its meaning and effectively such excited states in their chemical behaviour will have a close similarity to the photoionized states. Such states are of considerable importance in discussing the interaction of saturated polymer systems in the particular case of KrI and several of the Xe resonance lines.

In an investigation into surface modification of polymers by exposure to inert gas plasmas, it is of considerable interest to understand how the intensities of the various spectral lines vary as a function of the pressure and power loading delivered to the plasma. Thus an extensive study has been carried out in this connection under the experimental conditions described in section 2.4. A full account of this investigation may be found elsewhere[204] and it will suffice here to summarize some of the important features of direct relevance to the present work. Apart from the resonance lines discussed above, the spectra of the inert gases exhibit lower intensity spectral series of lines extending to shorter wavelength (higher energy).[196,204] The discussion to follow however will be restricted to the trends in the intensities of the resonance lines since they are in general representative of the higher

energy lines in their respective spectral series.

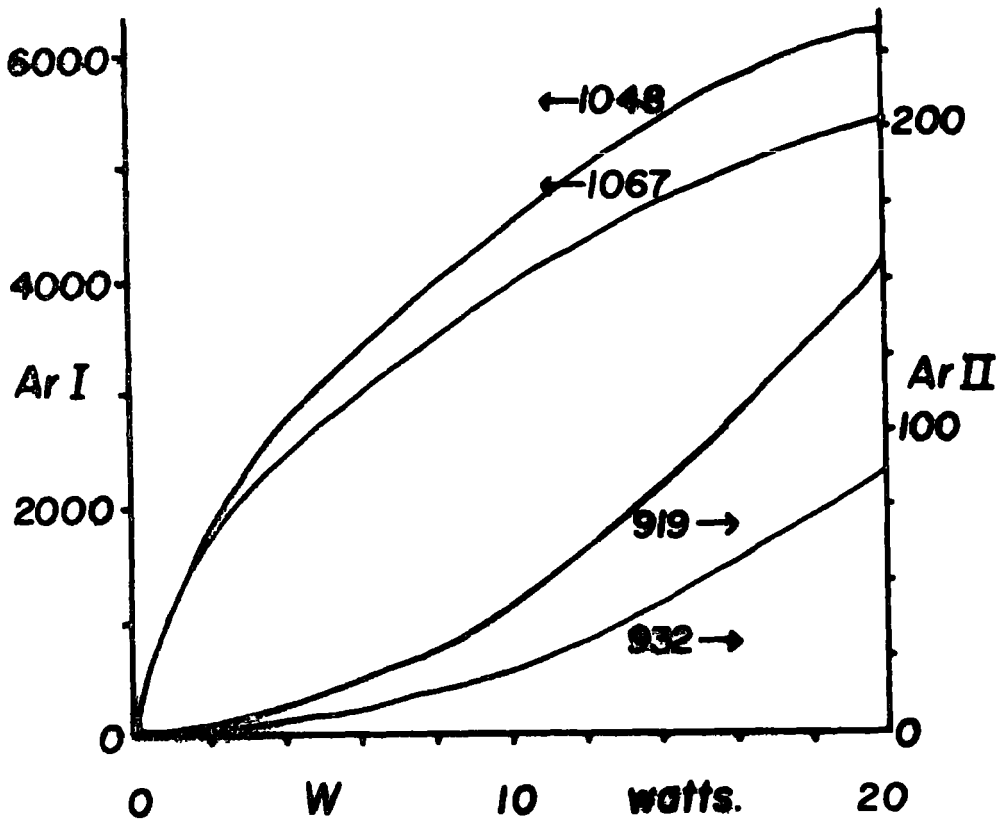

Figure 6.5. Intensity of the ArI and ArII resonance lines as a function of power loading (0.2 torr).

The intensity variations of the resonance lines as functions of the power and pressure are closely similar for all the gases in this investigation. Figure 6.5 illustrates the power dependence for the middle member of the inert gas series, argon. Not unexpectedly all the observed lines show increased intensity at higher power loadings. The ArII lines however exhibit a much greater increase than do the ArI lines. It is also a general case at the pressures of interest here that the intensity of the resonance lines of the second spectrum, associated with the ionized species is typically two orders of magnitude lower than the intensity of the resonance lines of the first

spectrum, associated with the neutral atom. Indeed, at the higher pressures the intensity of the ArII resonance lines is less than that of the higher members of the first spectrum and also the impurities (H,N,O).[204] It must be emphasized however that the cross section for photoionization of a typical polymer varies rapidly as a function of wavelength in this region,[205] hence the importance of a given line in the modification of polymers is not solely dependent on its intensity.

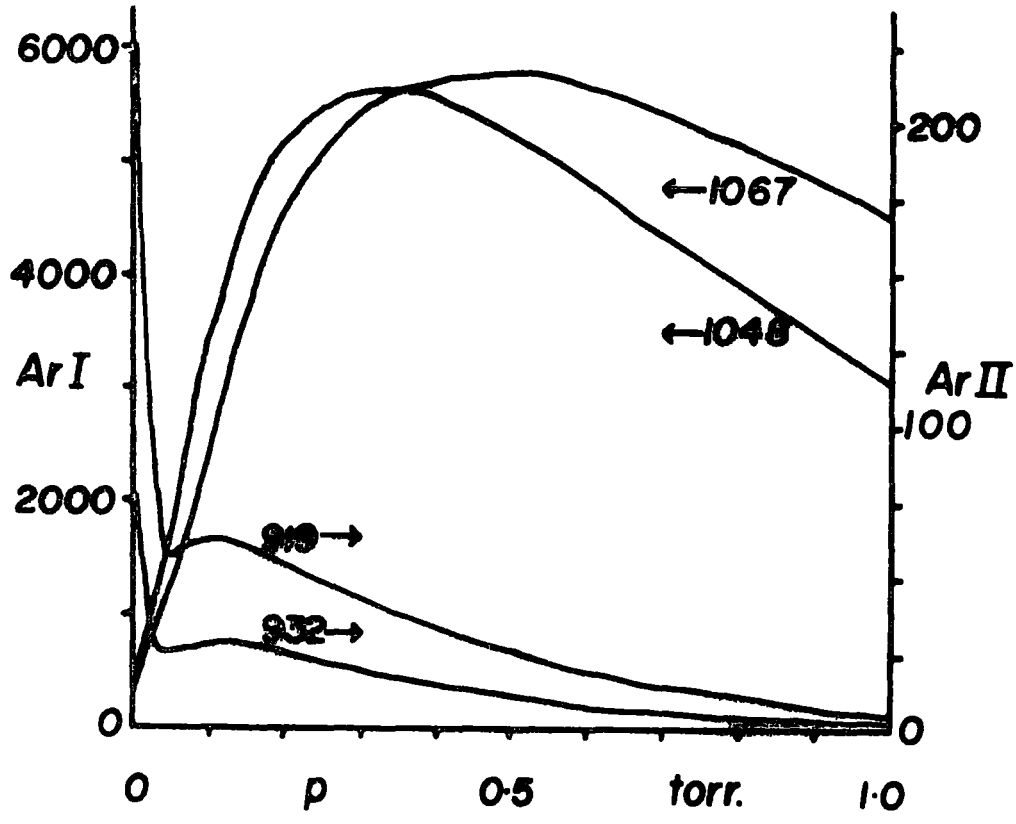

Figure 6.6. Intensity of the ArI and ArII resonance lines as a function of pressure (10 watts).

The pressure dependence of the resonance line intensities is a more complex situation as shown in figure 6.6, again using argon as the example. The sharp increase in intensity

of the ArII lines at near zero pressure suggests that the plasma breaks down to produce a totally ionized state in this region. Within the pressure limits of interest however the intensities of the lines show a maximum. The pressure at which this maximum intensity occurs is a function of the gas, the spectral line in question and the power loading. The trends in this pressure (p_{max}) can be summarized as follows. For the I resonance lines p_{max} decreases with increasing atomic number of the inert gas, whilst for the II resonance lines the opposite is true. In all cases however p_{max} increases with power.

The relative intensities of the observed lines is much more difficult to interpret since the efficiency of the monochromator grating is largely unknown over the range of wavelengths measured in this investigation. Although from ∿500Å to ∿1400Å it is not expected to vary more than an order of magnitude or so,[196] it is by no means linear in this region. The observed intensities for the resonance lines at 10 watts and 0.2 torr are summarized in Table 6.3 (for the 1" diameter discharge tube).

Table 6.3. Observed Intensities of the Resonance Lines

Inert Gas	II resonance lines* (high energy)	(low energy)	I resonance lines* (high energy)	(low energy)
He	-		20.2	
Ne	0.02	0.02	150.9	40.0
Ar	0.58	0.25	386.4	345.5
Kr	0.07	0.12	194.5	772.7
Xe	1.35	1.38	38.8	2800.0

* Intensities in arbitrary units.

Since the monochromator grating employed in this study is blazed and coated for a wavelength of 1500Å its efficiency will

show a marked increase close to this value. Hence, it is not surprising that the observed intensity of the XeI, 1469.6Å resonance line is very much greater than the other lines. Indeed the observed trend in the intensities of the low energy I resonance lines follows that which might be expected for the efficiency of the grating as a function of wavelength in the light of published data on similar systems.[196] It can be envisaged therefore that the true intensities of these lines are probably all closely similar. For the resonance lines of the ionized species however the expected trend would be an increase in intensity with atomic number since the concentration of ions in a plasma of given power loading and pressure is known to increase with atomic number.[209] This is reflected to some extent in Table 6.3.

Experiments employing the larger (5 cm diameter) discharge tube showed that p_{max} is also a function of the plasma configuration since it occurred at a higher pressure in the larger tube. Also the intensities of the lines were greatly enhanced with this tube. The effect of pulsing the discharge was also manifested in a shift in p_{max}.

This investigation, of which only a few of the general trends have been commented on here, has provided therefore a wealth of information concerning the vacuum ultraviolet emission from the inert gas plasmas. In the connection of modification of polymers by inert gas plasmas it is clear that the resonance lines of the neutral atom are likely to have greatest importance since the cross sections for ionization effected by the higher energy II resonance lines are unlikely to be two orders of magnitude larger.[217] However, it is important to know the relative intensities of all the spectral lines present

since each will have some contribution to the overall reaction. This information was obtained from this investigation and is documented elsewhere.[204]

The work outlined in this section therefore provides a sound background for the interpretation of data pertaining to the modification of polymers by the radiative energy transfer processes and has particular relevance in the context of the present investigation. Reference to the data presented in this section is made throughout the subsequent sections of this Chapter.

4. Kinetic Studies of the Glow Discharge Modification of the Ethylene/Tetrafluoroethylene Copolymer by Plasmas Excited in the Inert Gases

4.1 Plasmas Excited in Helium, Neon, Argon, Krypton and Xenon

Since the overall reaction is very similar, irrespective of the gas, power and pressure used, the ESCA spectra from any of the kinetic runs presented here show similar trends to those observed for the argon plasmas (Chapter Five, figure 5.16). The analysis of the data therefore is along identical lines to those used previously.

Figure 6.7 and figure 6.8 show logarithmic plots of the $\underline{C}F_2$ intensity (relative to its intensity at t=0) and the corresponding data for the F_{1s} levels, respectively for kinetic runs in helium, neon, argon and krypton, all at pressures of 0.2 torr and power loading of 5.0 watts. The data pertains to a fixed angle at which, in the particular spectrometer used in this study, the total integrated intensity of the C_{1s} levels is a maximum. It is clear that the analysis in terms of the two component system of equation 5.12 is straightforward. The complete set of results obtained from the kinetic runs in helium,

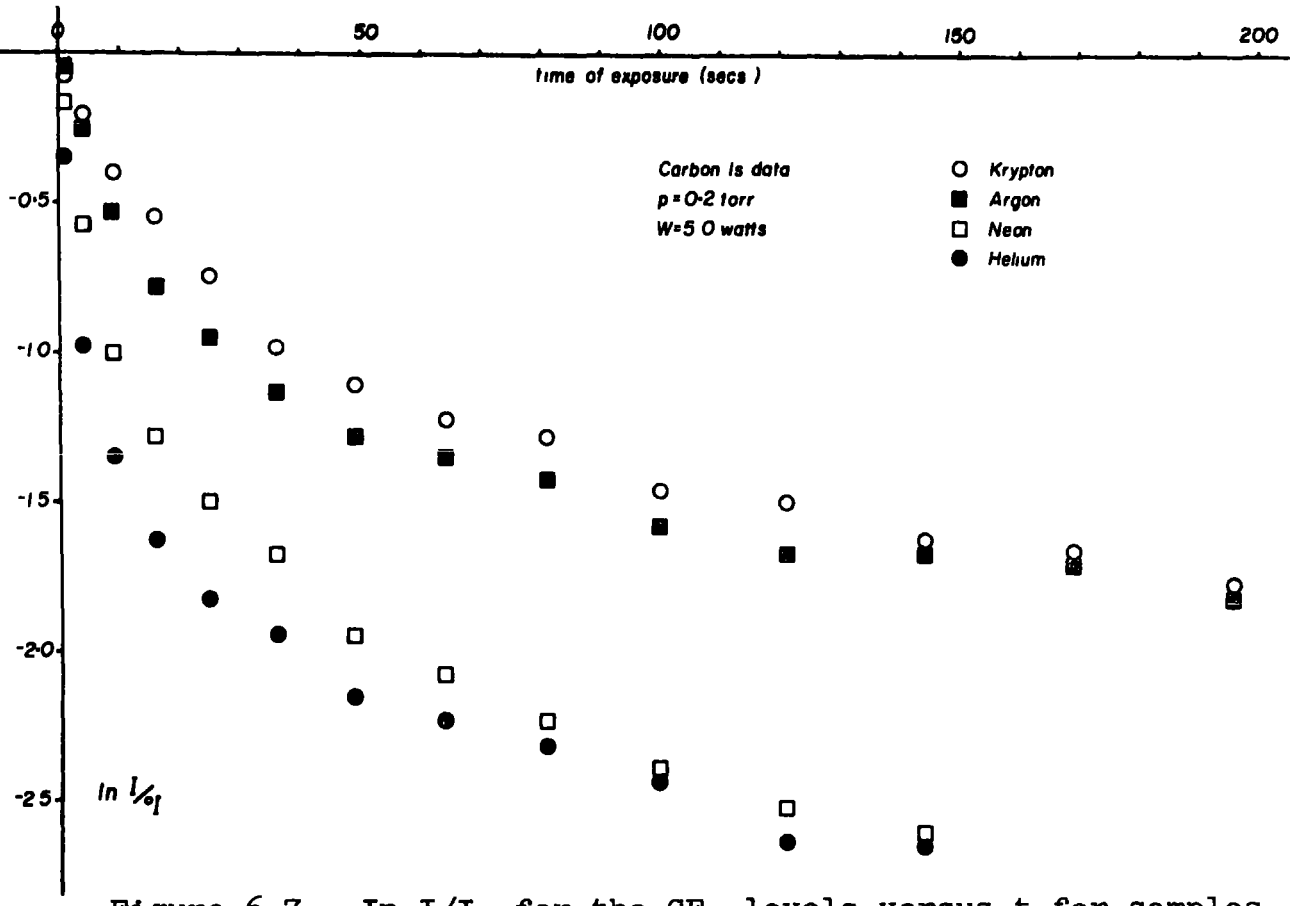

Figure 6.7. In I/I_o for the $\underline{C}F_2$ levels versus t for samples exposed to helium, neon, argon and krypton plasmas (0.2 torr, 5.0 watts).

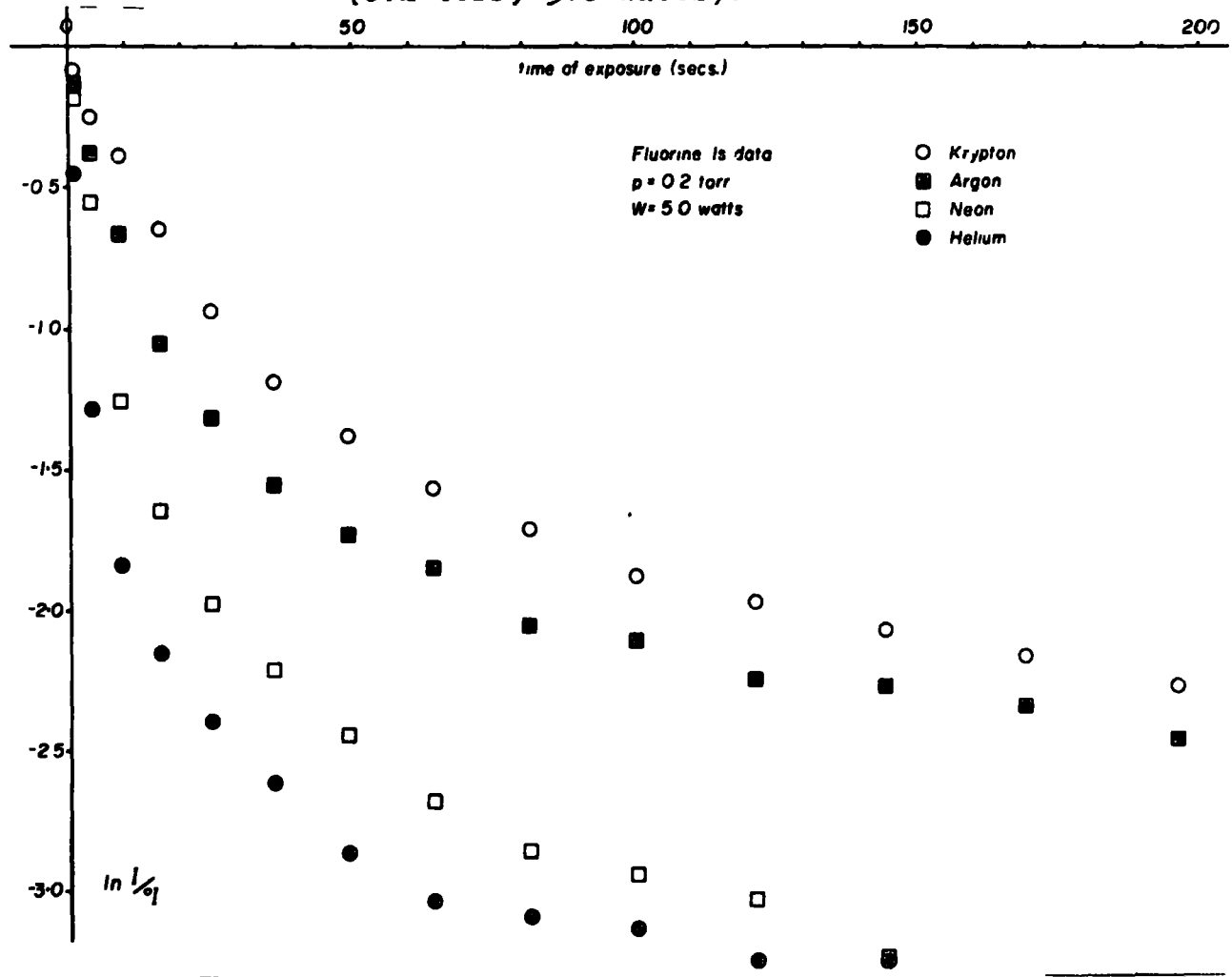

Figure 6.8. In I/I_o for the F_{1s} levels versus t for samples exposed to helium, neon, argon and krypton plasmas

neon, argon and krypton at power loadings of 0.4, 5.0 and 10.0 watts and a pressure of ∿0.2 torr are shown in Tables 6.4 and 6.5, for the CF_2 and F_{1s} levels respectively. Since for this series of experiments the thermocouple vacuum gauge used to record the pressure was not accurately calibrated the pressure of 0.2 torr is nominal. It has previously been noted in Chapter Five, however, that the rate constant for the fast surface reaction due to direct energy transfer processes is largely independent of the pressure above ∿0.2 torr for argon at the power loadings of interest here. Further evidence for this is derived from a kinetic run in helium at 5.0 watts and a pressure of ∿0.5 torr. The comparison of the results of this experiment with those for helium at 5.0 watts and 0.2 torr in Tables 6.4 and 6.5 may be summarized as follows. For the C_{1s} data K_s = 0.144(17) and 0.133(10), and K_b = 0.006(1) and 0.005(1), respectively for 0.2 and 0.5 torr, whilst for the F_{1s} data K_s = 0.136(23) and 0.145(16), and K_b = 0.005(0) and 0.010(1), respectively for 0.2 and 0.5 torr. The rate constants are the same, within the least squares error (in brackets) with the exception of the radiative energy transfer rate constant for the F_{1s} data which is increased by a factor of two by increasing the pressure. This observation is interesting in its own right since it suggests that whilst the predominantly direct energy transfer process in the surface involves the conversion of $CF_2 \rightarrow CF$, (i.e. $K_s(\underline{C}F_2) = K_s(F_{1s})$) the radiative energy transfer process in the subsurface and bulk also involves CF being further converted to carbon not directly attached to fluorine (i.e. $K_b(\underline{C}F_2) < K_b(F_{1s})$) and that this further reaction is more favourable at higher pressures. A similar observation can be made by again grouping the K_b values for the $\underline{C}F_2$ and F_{1s} data pertaining to the argon study in Chapter Five.

Table 6.4. Composite rate constants, pre-exponential terms and depth information derived from the CF_2 data.

Inert Gas	Pressure (Flow rate)*	Power (watts)	$(1-e^{-d}/\lambda\cos\theta)$	K_s † ($sec.^{-1}$)	$e^{-d}/\lambda\cos\theta$	K_b † ($sec.^{-1}$)	d** (A^o)	Σr^2 ††
Helium	0.2 torr	0.4	0.62	0.093(10)	0.23	0.006(1)	12	0.11
	(128 $cm^3 sec.^{-1}$)	5.0	0.54	0.144(17)	0.17	0.006(1)	15	0.14
		10.0	0.55	0.203(31)	0.21	0.005(2)	13	0.16
Neon	0.2 torr	0.4	0.64	0.090(3)	0.31	0.008(1)	10	0.02
	(85 $cm.^3 sec.^{-1}$)	5.0	0.62	0.117(12)	0.23	0.009(1)	12	0.09
		10.0	0.64	0.153(18)	0.24	0.007(1)	12	0.07
Argon	0.2 torr	0.4	0.54	0.042(2)	0.44	0.004(0)	7	0.02
	(81 $cm.^3 sec.^{-1}$)	5.0	0.62	0.084(3)	0.34	0.005(1)	9	0.02
		10.0	0.58	0.095(6)	0.26	0.004(1)	11	0.06
Krypton	0.2 torr	0.4	0.30	0.034(2)	0.67	0.004(0)	3	0.01
	(67 $cm.^3 sec.^{-1}$)	5.0	0.58	0.078(5)	0.42	0.005(0)	7	0.01
		10.0	0.60	0.084(4)	0.44	0.006(1)	7	0.04

† Figures in brackets refer to errors calculated in the least squares analysis.

†† Sum of the squares of the residuals of the experimental data and the recalculated data.

* Flow rates refer to the pressure at which the experiment was carried out (i.e. 0.2 torr).

** d is calculated from $e^{-d}/\lambda\cos\theta$ where $\lambda_{C_{1s}}$ is taken as 10Å and θ is the angle at which the spectra were run (i.e. 34°).

Table 6.5. Composite rate constants, pre-exponential terms and depth information derived from the F_{1s} data.

Inert Gas	Pressure (Flow rate)*	Power (watts)	$(1-e^{-d}/\lambda\cos\theta)$	K_s† ($sec.^{-1}$)	$e^{-d}/\lambda\cos\theta$	K_b† ($sec.^{-1}$)	d** (A^o)	Σr^2††
Helium	0.2 torr	0.4	0.63	0.099(10)	0.15	0.012(0)	11	0.15
	(128 $cm.^3sec.^{-1}$)	5.0	0.52	0.136(23)	0.07	0.005(1)	15	0.38
		10.0	0.59	0.197(35)	0.11	0.005(1)	13	0.27
Neon	0.2 torr	0.4	0.68	0.090(3)	0.23	0.013(1)	9	0.02
	(85 $cm.^3sec.^{-1}$)	5.0	0.71	0.131(10)	0.13	0.009(1)	12	0.09
		10.0	0.72	0.175(18)	0.14	0.009(2)	11	0.09
Argon	0.2 torr	0.4	0.55	0.047(2)	0.37	0.006(0)	6	0.02
	(81 $cm.^3sec.^{-1}$)	5.0	0.70	0.089(3)	0.22	0.006(1)	9	0.03
		10.0	0.63	0.100(8)	0.16	0.004(1)	11	0.12
Krypton	0.2 torr	0.4	0.33	0.040(1)	0.61	0.006(1)	3	0.02
	(67 $cm.^3sec.^{-1}$)	5.0	0.65	0.072(2)	0.34	0.007(1)	6	0.02
		10.0	0.65	0.085(4)	0.29	0.008(1)	7	0.02

† Figures in brackets refer to errors calculated in the least squares analysis.

†† Sum of the squares of the residuals of the experimental data and the recalculated data.

* Flow rates refer to the pressure at which the experiment was carried out (i.e. 0.2 torr).

** d is calculated from $e^{-d}/\lambda\cos\theta$ where $\lambda_{F_{1s}}$ is taken as 7Å and θ is the angle at which the spectra were run (i.e. 34^o).

Returning to the data presented in Tables 6.4 and 6.5 it is important to consider firstly how well the kinetic model fits the experimental data. The sums of the terms pertaining to the depth information should be unity for a perfect fit of equation 5.12 to the experimental data. However, as K_s becomes large this requirement is not so closely obtained. This effect is also reflected in the sums of the squares of the residuals of the experimental data and data recalculated from the pre-exponents and exponents obtained from the analysis. This merely reflects the difficulties of analysing the data along the lines presented here if the difference in surface and subsurface and bulk reactions become widely disparate. This is clearly the case for helium where the crude analysis presented here indicates differences in composite rate constants K_s and K_b of greater than two orders of magnitude. In such circumstances an extrapolation is not entirely adequate. The differences however between the rate constants for the surface reactions, for different gases and power loadings are larger than the errors involved which is evident in the fact that clear trends are readily observed. Considering the approximations involved in the development of the kinetic model including the use of composite terms for rate constants, concentrations of ions and metastables and intensities and attenuation factors for the whole of the electromagnetic spectrum, the fit with the experimental data over the extensive range of plasma conditions in this investigation is surprisingly good.

The trends in the rate constants for the surface reaction as a function of power are illustrated by figure 6.9 whilst figure 6.10 correlates K_s with the ionization potential of the sustaining gas. The ionization potential has been chosen here

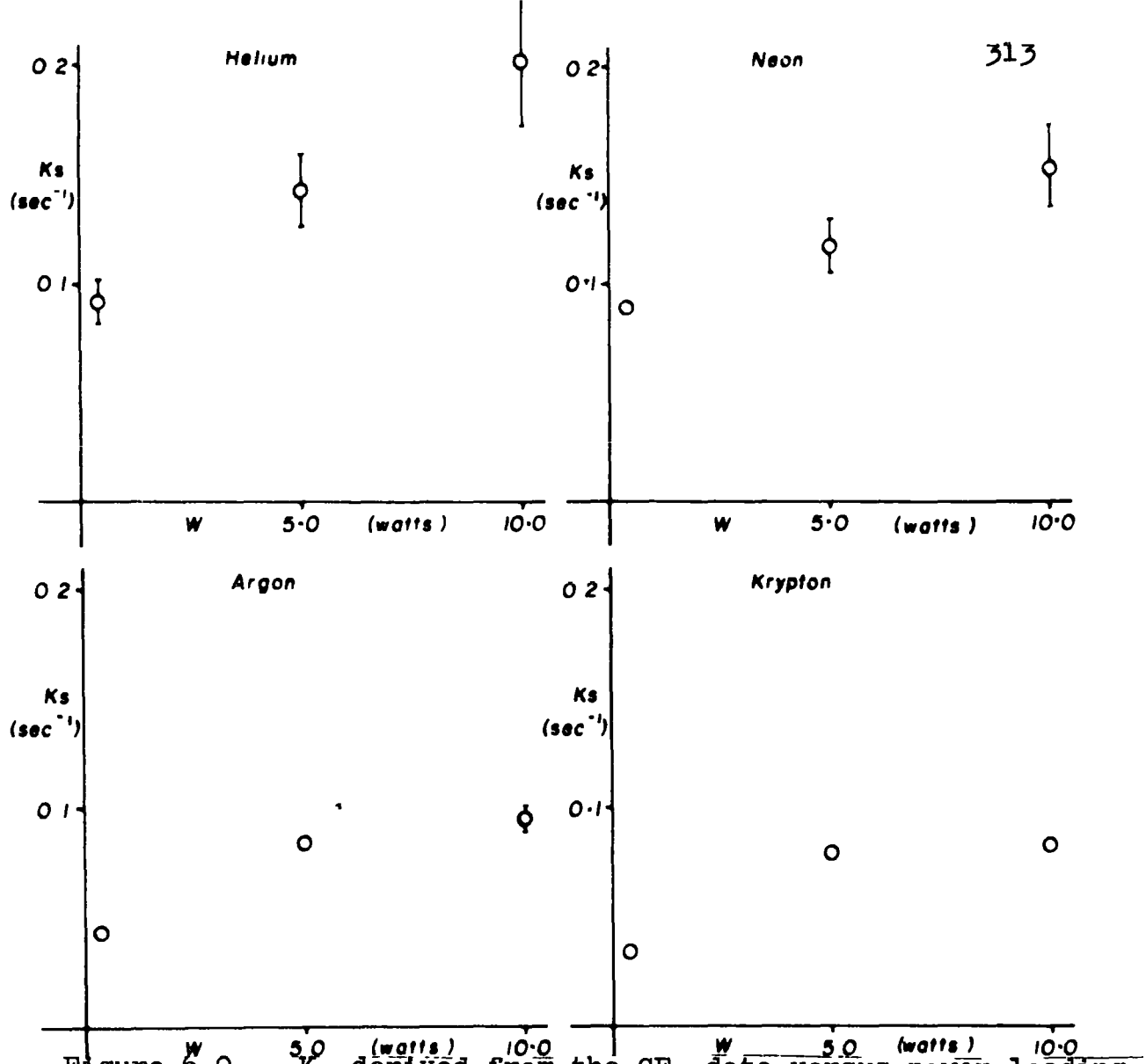

Figure 6.9. K_s derived from the CF_2 data versus power loading.

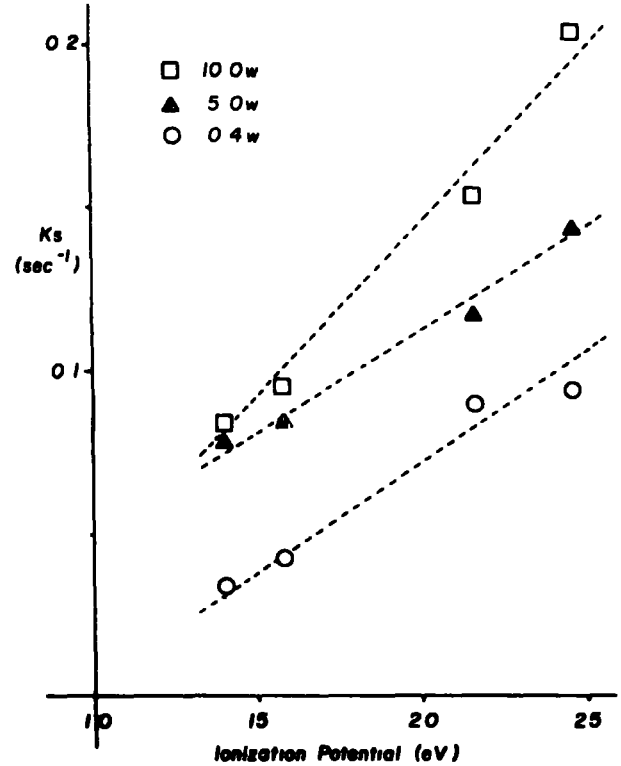

Figure 6.10. K_s derived from the CF_2 data versus ionization potential of the sustaining gas (0.2 torr, 0.4, 0.5 and 10.0 watts).

merely for convenience as similar correlations clearly exist for other physical properties of the gases (e.g. metastable energy, atomic radius, etc.). It should be noted that the pseudo rate constants detailed in Tables 6.4 and 6.5 involve a convolution of true rate constants and amongst other things for the surface reactions, the concentrations of ions and metastables. For a given power loading however the concentration of ions and metastables will be in the order Kr > Ar > Ne > He[209] which implies that the differences in apparent rates for the surface reactions of a given polymer system with the inert gas plasmas will represent lower limits to the span of reactivities. Viz. since for a given power loading the concentration of ions and metastables should be lower in helium than in krypton, the relative rates at a power loading of 10 watts of 25:1 may well represent a lower limit to the difference in reactivity.

K_s is clearly a function of both the power and the fundamental properties of the inert gases. At higher power loadings the rate constant tends to increase less with power which is entirely consistent with previous work and not unexpected in the light of work published by other workers concerning the concentration of ions and metastables as a function of power, in similar systems.[209,210] Figure 6.10 clearly demonstrates an apparent linear correlation between K_s and the ionization potentials at each of the three power loadings employed in this investigation spanning a range of one and a half orders of magnitude. It is interesting to note in this connection that the data displayed in figures 6.7 and 6.8 clearly fall into two bands arising dominantly from the differences in K_s, and the ionization potentials similarly fall into two bands. This is

strong confirmatory evidence for the assignment of the faster of the two rate processes as that arising from direct energy transfer. The slope of the plots in figure 6.10 increases with increasing power with the slope at 0.4 w being ~ 0.0035 and that at 10.0 w being ~ 0.0055, where K_s is in units of reciprocal seconds and the ionization potentials in electron volts.

The data pertaining to the pseudo rate constants for the radiative energy transfer reaction in the subsurface and the bulk polymer, K_b show an order of magnitude similarity for all kinetic runs. Grouping the data is expected to improve its statistical meaningfulness and taking the average value (over the three power loadings) for each gas it becomes clear that the magnitudes of K_b are in the order Ne>He>Kr>Ar. These values are plotted against the ionization potential in figure 6.11, for the $\underline{CF}_2$ and F_{1s} levels.

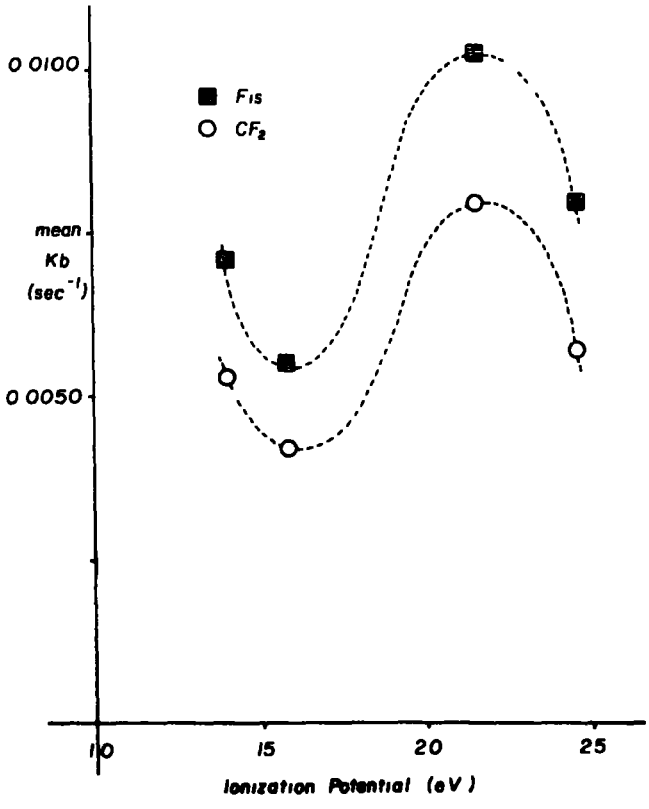

Figure 6.11. The mean value of K_b versus ionization potential of the sustaining gas.

Although no conclusive explanation can be offered for these results it will be seen that it is eminently reasonable to obtain this type of distribution. Section 3.3 has demonstrated that although the absolute intensities of the various spectral lines in the vacuum ultraviolet emitted from these plasmas are not directly measurable, the intensity of any given line shows clear trends. Thus at any given power, pressure, reactor geometry and pumping configuration the intensity of a spectral line depends on the position of p_{max}, (as designated in figure 6.6). Thus for this series of experiments whether 0.2 torr is greater than or less than p_{max} for a given gas the intensity of a spectral line will be somewhat less than its maximum possible value, for the given power loading. Hence even though p_{max} versus ionization potential (of the gas) may-be an increasing or decreasing function (see section 3.3) the intensity of the relevant spectral lines versus ionization potential will show a maximum. (This may well occur at neon). It must also be noted that the efficiency of photoionization of the polymer is a strong function of the wavelength of the incident radiation. The involvement of overlap terms would therefore be expected to produce a 'non-continuous' correlation as in figure 6.11. This aspect is discussed in greater detail in section 5.3.

It is worthwhile at this point to also reconsider the data for the radiative energy transfer rate constant, as a function of pressure for argon (figure 5.19) presented in the previous Chapter. K_b decreased with increasing pressure which suggests that with the given reactor and pumping system, p_{max} for the radiation causing the modification (or more likely the composite p_{max} for several spectral lines) occurred at a pressure lower than those investigated, i.e. <0.1 torr, whilst the

plot of K_b versus W/p (figure 5.20) showing a maximum value is consistent with a convolution of the line intensities decreasing with pressure and increasing with power.

In figure 6.11 the magnitude of the mean K_b derived from the F_{1s} data is always in excess of that derived from the $\underline{C}F_2$ component of the C_{1s} data. A similar comparison of K_s values shows that they are virtually the same when derived from either $\underline{C}F_2$ or F_{1s} data. (Tables 6.4 and 6.5).

The C_{1s} data only monitors the disappearance of $\underline{C}F_2$ type structural features since the signal due to $\underline{C}F$ environments is not included in the analysis. On the other hand, however, the F_{1s} data not only monitors the disappearance of $C\underline{F}_2$ but also $C\underline{F}$ structural features, arising from the fact that the fluorine 1s signals for these distinct environments are unresolved in the ESCA spectra. It is apparent then from the relative values of K_s and K_b obtained from the two sources of data that the direct energy transfer process only involves CF_2 being converted to CF, whereas the radiative energy process proceeds further to convert CF to C (carbon not attached to fluorine). Both radiative and direct energy transfer processes will also include $CH_2 \rightarrow CH \rightarrow C$ but the relatively small changes in C_{1s} binding energies for this process and also production of $\underline{C}$, from the conversion of CF_2, which will of course fall at a similar binding energy, makes it difficult to study this aspect of the reaction.

The dependence of d, the depth to which direct energy transfer processes are important, on the inert gas employed for the crosslinking process is quite striking (Tables 6.4 and 6.5) and can be correlated well with the ionization potential (metastable energy, atomic radius, etc.) of the gas

(figure 6.12). Figure 6.12 shows such a correlation for the mean (over the three power loadings) values of d. Tables 6.4 and 6.5 also show that d has a dependence on the power loading with a marked tendency for a smaller value of d to be correlated with a lower power loading. This provides circumstantial but independent evidence for the assignment of the surface reaction as that due to direct energy transfer from ions and metastables since the Boltzmann temperature for these reactive species would be expected to increase at higher power loadings. The depth of penetration of the active species in the polymer under the conditions employed here ranges from roughly one monolayer for krypton to three monolayers for helium.

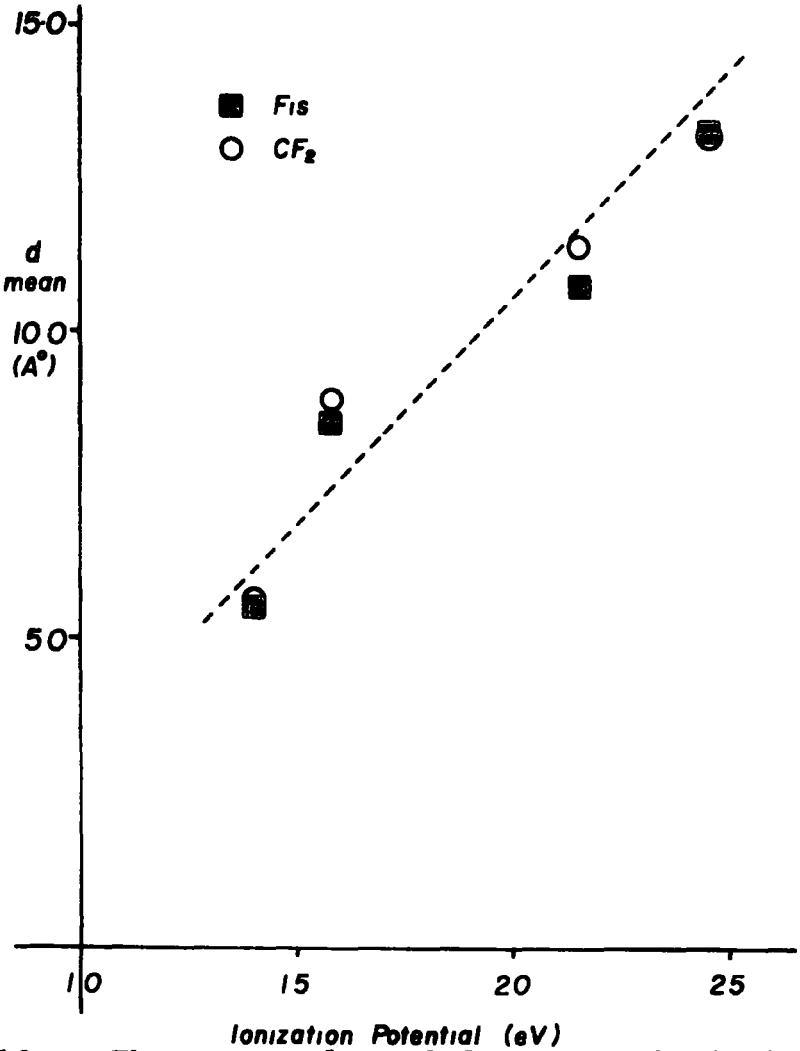

Figure 6.12. The mean value of d, versus ionization potential of the sustaining gas.

The extension of this investigation to include xenon produced experimental difficulties, in that a true pressure of ∿ 0.2 torr produces a relatively small deflection on the thermocouple vacuum gauge control and hence this pressure was difficult to maintain. However it is of interest to consider the results from a kinetic run in xenon at a somewhat higher pressure (∿1.0 torr) and 10.0 watts. The relevant data is presented in Table 6.6.

Table 6.6. C_{1s} and F_{1s} Data for Xenon (10 watts, 1.0 torr)

Data	$(1-e^{-d/\lambda\cos\theta})$	K_s (sec^{-1})	$e^{-d/\lambda\cos\theta}$	K_b (sec^{-1})	$\frac{d}{\sigma}$ (Å)
C_{1s}	0.48	0.042(2)	0.41	0.003(0)	7
F_{1s}	0.56	0.040(1)	0.37	0.004(0)	6

These data fall nicely into line with that already discussed for the other inert gases which again suggest that the rate constants have only a small dependence on pressure.

It is readily apparent from the preceding discussion that for the saturated polymer system, the lighter inert gases have superior crosslinking properties for the initial stages at relatively low power/pressure ratios (<50), in terms of both rate and depth of penetration, the reaction being dominated by direct energy transfer processes. For crosslinking to a depth greater than ∿20Å however this is not the case since the reaction is exclusively due to radiative energy transfer processes. The data presented here clearly shows that for long term treatments neon is the most efficient gas for the crosslinking of the ethylene/tetrafluoroethylene copolymer. It is interesting to draw a comparison here with the work of Schonhorn

and Hansen[192] on the crosslinking of polyethylene with helium and neon plasmas. Their data is consistent with the conclusions drawn here in that they observed, for samples exposed for extended periods of time, a greater depth of crosslinking for neon treated samples compared to samples treated in helium under the same conditions, for the same period of time.

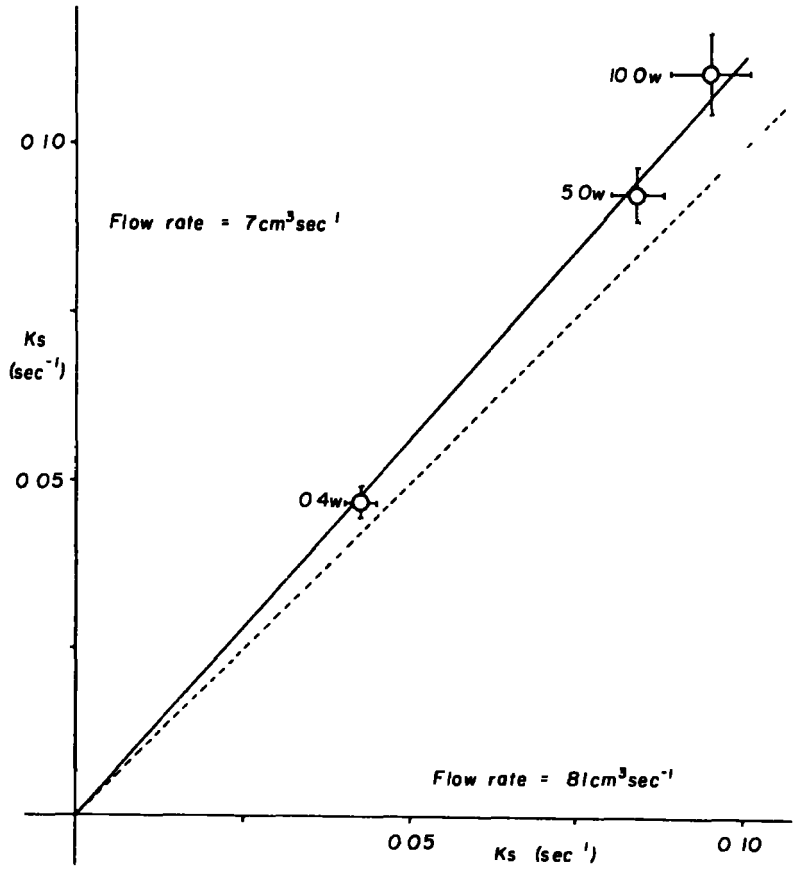

Figure 6.13. K_s at a flow rate of argon of $\sim$ 7 cm.^{3}sec.$^{-1}$ versus K_s at a flow rate of $\sim$ 80 cm.^{3}sec.$^{-1}$ (0.2 torr, 0.4, 5.0 and 10.0 watts)

By comparison of the data for argon plasmas obtained in this work with that inferred from the data in the previous Chapter, the effect of the flow rate on the surface reaction may be investigated. Figure 6.13 shows a plot of K_s values

obtained from C_{1s} data at 0.2 torr pressure and power loadings of 0.4, 5.0 and 10.0 watts. The vertical axis refers to experiments run at a flow rate of $\sim$ 7 $cm.^3$ $sec.^{-1}$ whilst the horizontal axis refers to a flow rate of $\sim$ 80 $cm.^3$ $sec.^{-1}$.

The broken line represents a slope of unity. It is evident that with the experimental configuration used in these investigations, the rate constant for the surface reaction is relatively insensitive to variation of flow rate at a constant pressure. In reality the rate constant is slightly greater for experiments at lower flow rates. This effect although not necessarily predictable may be explained as a convolution of two major effects. Firstly, an increase in flow rate will result in more efficient removal of volatile products (i.e. H_2, HF) causing a decrease in their partial pressure in the immediate vicinity of the sample surface and hence tend to increase the rates of reaction. Secondly, an increase in flow rate will decrease the partial pressure of ions and metastables in the plasma and hence tend to decrease the rates of reactions. For the example presented in figure 6.13 the second effect is evidently slightly greater than the first over an order of magnitude increase in flow rate.

4.2 Plasmas Excited in Gas Mixtures

It is also of interest, in the context of this discussion to consider the effects of employing mixtures of the inert gases for the plasma modification process. In this section the results derived from kinetic studies using mixtures of helium and krypton are presented. It is known that for most instances of discharges excited in mixtures of gases of different ionization potential the line spectra emitted is characteristic of the gas of lower ionization potential.[196] This may be con-

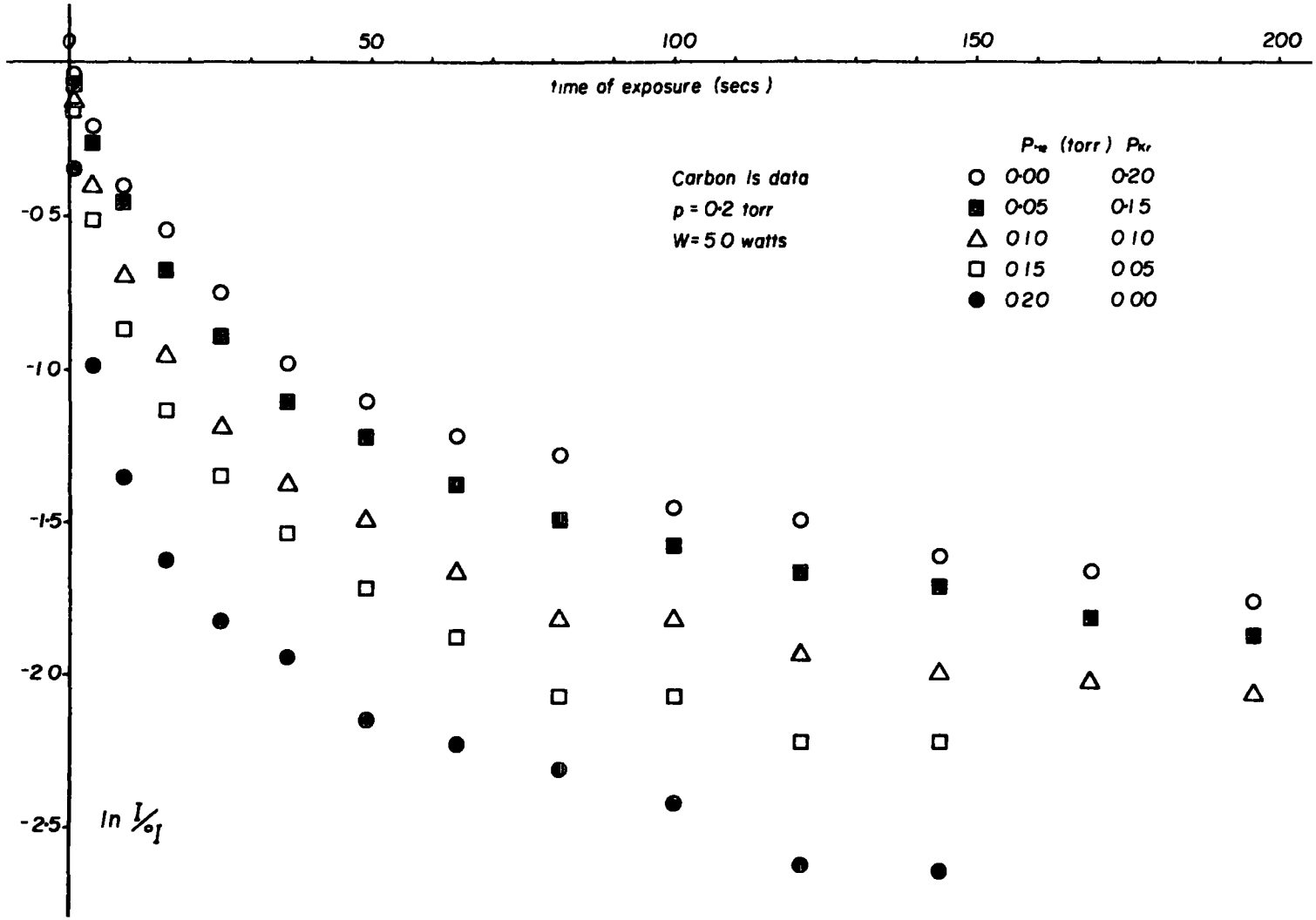

Figure 6.14. In I/I_o for the $\underline{C}F_2$ levels, versus t for samples exposed to plasmas excited in helium/krypton mixtures.

firmed superficially by observation of the colour (i.e. visible component) of the discharges. Furthermore ion neutralization and Penning ionization processes occur in the gas phase as in the reactions

$$He^+ + Kr \rightarrow He + Kr^+$$

$$He^* + Kr \rightarrow He + Kr^*$$

These are processes by means of which energy may be transferred from the helium component of the plasma to the krypton component. This complex nature of the plasma along with the lack of information on the fractional power input to each component does not allow for a quantification of the relative importance of each component.

Figure 6.14 shows plots of $\ln I^t/I_o^{TOT}$ for the $\underline{C}F_2$ component of the C_{1s} spectra for kinetic runs using pure krypton, pure helium and various mixtures. In all cases the power loading was 5.0 w and the total pressure was 0.2 torr. The three mixtures were devised to have nominal partial pressures of helium of 0.05, 0.10 and 0.15 torr. The analysis in terms of the kinetic model is shown in Table 6.7 for both the $\underline{C}F_2$ component of the C_{1s} levels and the F_{1s} levels. The fit with the experimental data is quite remarkable, considering that rate processes for both krypton and helium species are combined in the composite rate constants, and the trends are clear. Figures 6.15 and 6.16 show plots of K_s and d versus the partial pressure of helium respectively. The data has a closely linear correlation with the partial pressure of helium although there is a small tendency for the values of the mixtures to fall below the line joining the data pertaining to the pure krypton and helium discharges.

Table 6.7. Composite rate constants, pre-exponential terms and depth information derived from the CF_2 and F_{1s} data for samples treated in helium/krypton mixtures.

Data	Partial pressures † P_{He}(torr)	P_{Kr}	Flow rate* ($cm.^3 sec.^{-1}$)	$(1-e^{-d/\lambda\cos\theta})$	K_s †† ($sec.^{-1}$)	$e^{-d/\lambda\cos\theta}$	K_b †† ($sec.^{-1}$)	d** (Å)	Σr^2 †††
C_{1s}	0.20	0.00	128	0.54	0.144(17)	0.17	0.006(1)	15	0.14
	0.15	0.05	111	0.62	0.104(9)	0.24	0.006(1)	12	0.08
	0.10	0.10	102	0.64	0.100(5)	0.28	0.006(1)	11	0.04
	0.05	0.15	81	0.59	0.080(3)	0.38	0.006(1)	8	0.02
	0.00	0.20	67	0.58	0.078(5)	0.42	0.005(0)	7	0.01
F_{1s}	0.20	0.00	128	0.52	0.136(23)	0.07	0.005(1)	15	0.38
	0.15	0.05	111	0.68	0.117(10)	0.15	0.006(1)	11	0.11
	0.10	0.10	102	0.70	0.110(5)	0.21	0.008(1)	9	0.04
	0.05	0.15	81	0.66	0.093(5)	0.32	0.008(1)	7	0.03
	0.00	0.20	67	0.65	0.072(2)	0.34	0.007(1)	6	0.02

† Partial pressures are nominal.

†† Figures in brackets refer to errors calculated in the least squares analysis.

††† Sum of the squares of the residuals of the experimental data and the recalculated data.

* Flow rates refer to the total pressure at which the experiment was carried out (i.e. 0.2 torr).

** d is calculated from $e^{-d/\lambda\cos\theta}$ where $\lambda_{C_{1s}}$ and $\lambda_{F_{1s}}$ are taken as 10Å and 7Å respectively and θ is the angle at which the spectra were run (i.e. 34°).

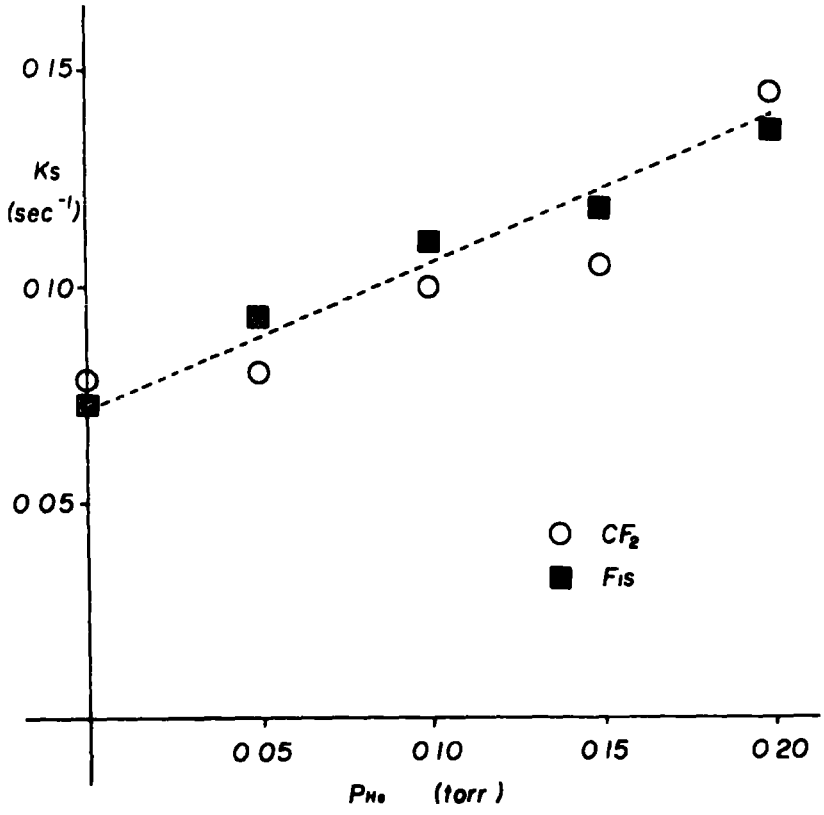

Figure 6.15. K_s verus the nominal partial pressure of helium.

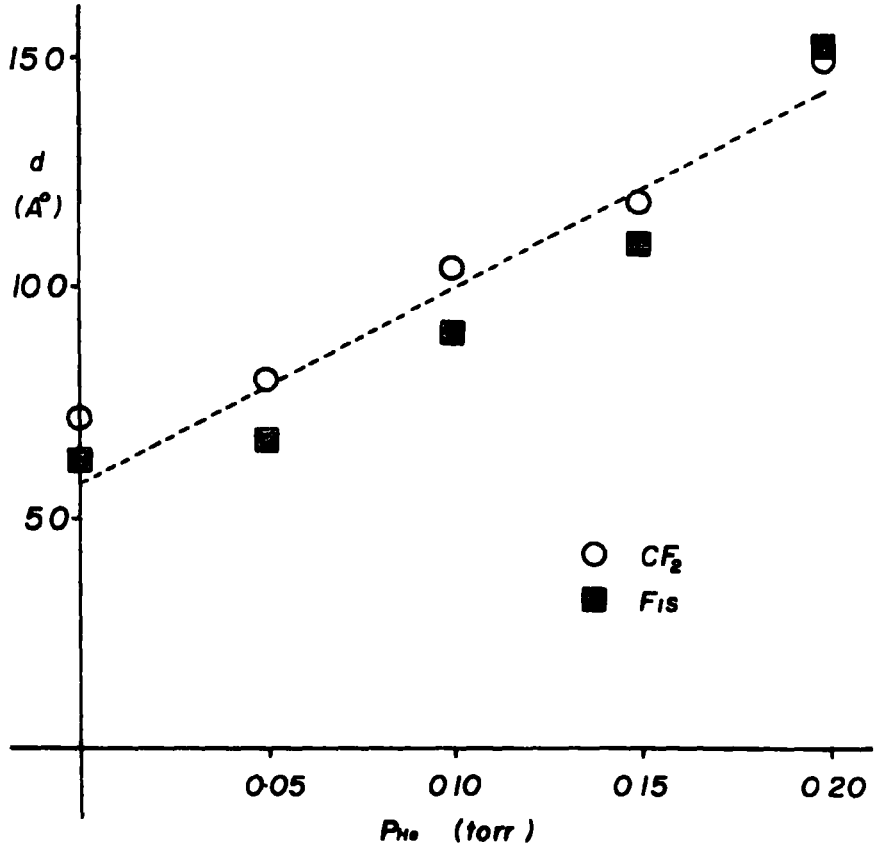

Figure 6.16. d versus the nominal partial pressure of helium.

4.3 Modification of Other Polymers by Inert Gas Plasmas

The treatment of non-fluorine containing polymers may not be followed in such detail as that for the ethylene/tetrafluoroethylene copolymer, however it is appropriate to include several observations here. The exposure of a polystyrene film to an argon glow discharge results in extensive surface oxidation even after careful purification of the gas. The possible origins of the oxygen containing species has been previously discussed in Chapter Five. With polystyrene the effect of the oxidation side reactions are much more severe than for the ethylene/tetrafluoroethylene copolymer due to the greater susceptibility of the unsaturated centres to attack by active oxygen species. (This point will be elaborated in the following Chapter). However the problem can be alleviated to some extent by covering the sample with a quartz slide, thus screening the polystyrene film from the reactive species in the plasma and filtering out the vacuum ultraviolet radiation of wavelength less than $\sim$1600Å. In this experimental arrangement the polystyrene is crosslinked extremely slowly as evidenced by a small decrease in the shake up intensity after an extended treatment time at high power.

The exposure of a polyethyleneterephthalate film to an argon plasma results in a decrease in the shake up intensity and also a decrease in the oxygen intensity, such that the signals in the O_{1s} and C_{1s} regions due to carbon doubly bonded to oxygen show a greater decrease than do the signals due to carbon singly bonded to oxygen. These observations may also be explained in terms of a crosslinking mechanism. This polymer shows a very similar reaction when covered by a quartz slide.

For polytetrafluoroethylene the opportunity presents itself

to follow the reaction as a function of time in an analogous fashion to that previously described for the ethylene/tetrafluoroethylene copolymer, and Table 6.8 contains the results obtained by monitoring the C_{1s} and F_{1s} levels for such a kinetic run at 0.2 torr and 5.0 watts in argon along with the corresponding data for the copolymer extracted from Tables 6.4 and 6.5.

Table 6.8. Data Derived from Plasma Treatment of Polytetrafluoroethylene.

Data		$(1-e^{-d/\lambda\cos\theta})$	K_s (sec.$^{-1}$)	$e^{-d/\lambda\cos\theta}$	K_b (sec.$^{-1}$)	$\frac{d}{\sigma}$ (Å)
P.T.F.E.	C_{1s}	0.70	0.058(2)	0.23	0.008(1)	12
	F_{1s}	0.70	0.061(3)	0.18	0.008(0)	10
Copolymer	C_{1s}	0.62	0.084(3)	0.34	0.005(1)	9
	F_{1s}	0.70	0.089(3)	0.22	0.006(1)	9

In the absence of a great deal more data the conclusion drawn from these data can only be tentative. However it appears from Table 6.8 that in comparing polytetrafluoroethylene with the ethylene/tetrafluoroethylene copolymer, the surface rate constant involving predominantly direct energy transfer is smaller and the radiative energy transfer process rate constant is larger, for PTFE. These observations are readily understood since the cross section for photoionization of the copolymer by argon radiation is dominated by that associated with the F_{2p} lone pairs (see section 5.3). The direct energy transfer reaction on the other hand is expected to be slower since the elimination of fluorine atoms is not likely to be as efficient as that of hydrogen atoms.

Experiments comparing polyvinylidenefluoride powder and the copolymer appear in the next section.

4.4 Angular Dependence Studies

The great potential of studying the angular dependence of absolute and relative peak intensities has been previously pointed out in Chapter Five. It is of considerable interest therefore to investigate the effects of the electron take off angle, in connection with the kinetic studies. Thus, figure 6.17 shows a logarithmic plot of I^t/I_o^{TOT} versus exposure time for a kinetic run performed on the ethylene/tetrafluoroethylene copolymer in argon (0.2 torr, 5.0 watts) for C_{1s} data recorded at electron take off angles of 34^o, 50^o and 70^o.

It is gratifying to note from the outset that as t becomes large the three curves tend to linearity and are closely parallel. This is consistent with the kinetic model since the slopes of the lines at large t are determined solely by the pseudo rate constant for the radiative energy transfer processes in the subsurface and bulk of the polymer, and hence are independent of the electron take off angle employed when analysing the samples.

The data is more readily appreciated after analysis in terms of the kinetic model and the data is listed in Table 6.8.

Table 6.8. Kinetic Data for the Ethylene/Tetrafluoroethylene Copolymer at Various Electron Take Off Angles

Data	θ^o	$(1-e^{-d/\lambda\cos\theta})$	K_s (sec^{-1})	$e^{-d/\lambda\cos\theta}$	K_b (sec^{-1})	$\frac{d}{\lambda}$ (Å)
C_{1s}	34	0.63	0.094(4)	0.24	0.006(1)	12
	50	0.62	0.105(5)	0.23	0.008(0)	10
	70	0.63	0.117(7)	0.14	0.006(2)	7
F_{1s}	34	0.69	0.090(4)	0.21	0.010(1)	9
	50	0.70	0.098(6)	0.17	0.011(1)	8
	70	0.69	0.101(9)	0.10	0.011(3)	6

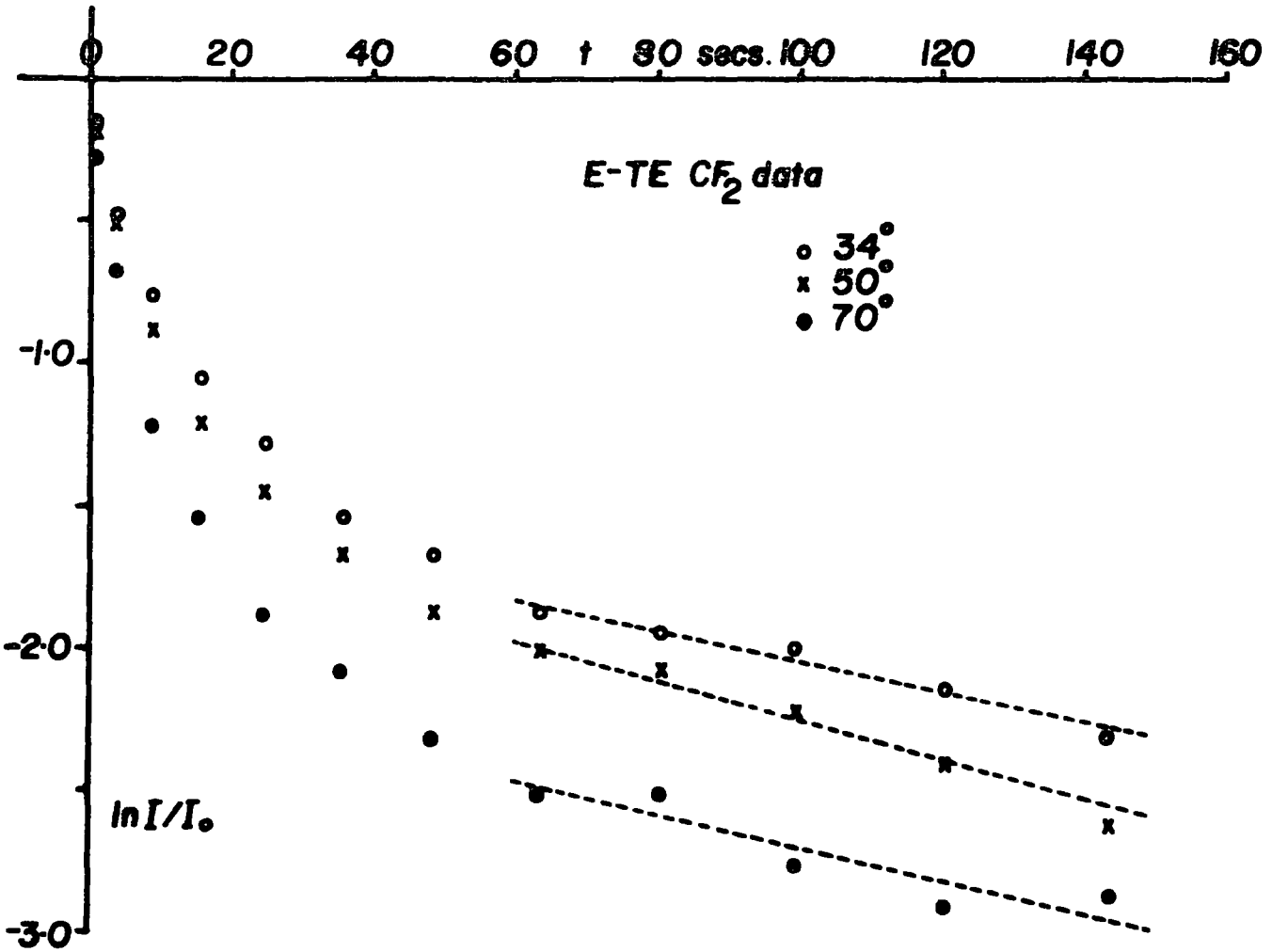

Figure 6.17. In I/I_o for the $\underline{C}F_2$ levels at electron take off angles of 34°, 50° and 70° versus t, for a sample of the copolymer treated in an argon plasma (0.2 torr, 5.0 watts).

It is clearly evident from Table 6.8 that the rate constants for both the surface and bulk reactions are essentially independent of θ, as might have been anticipated. The depth to which direct energy transfer processes are important however appears to be dependent on the angle. This is probably more apparent than real if the errors in the method are considered. As the angle is increased the kinetic model fits less well to the available data (as evidenced by the sum of the terms pertaining to the depth information) since the peak intensities in the ESCA spectra at near grazing electron take off are low and therefore have lower statistical accuracy, and at grazing angle the effects of the surface reaction are essentially isolated with very small changes in the spectrum occurring as a result of the bulk processes. Furthermore small errors in the measurement of large values of the angle result in greater errors in the analysis since $1/\cos\theta$ is involved. On the other hand however the dependence of d on θ could also be explained if the reaction does not proceed uniformly into the sample over the whole surface area. If this is the case then angular studies become extremely important for monitoring this phenomenon since interpretation in terms of the kinetic model alone gives only an average value of d.

It is of interest also to compare the results in Table 6.8 with similar data derived for a powdered sample which should exhibit very little or no angular dependence. Figure 6.18 shows $\ln I^t/I_o^{TOT}$ for a similar experiment performed on a polyvinylidenefluoride powder. Comparison with figure 6.17 clearly shows that for the powdered sample the dependence of the signal intensities on θ is very slight.

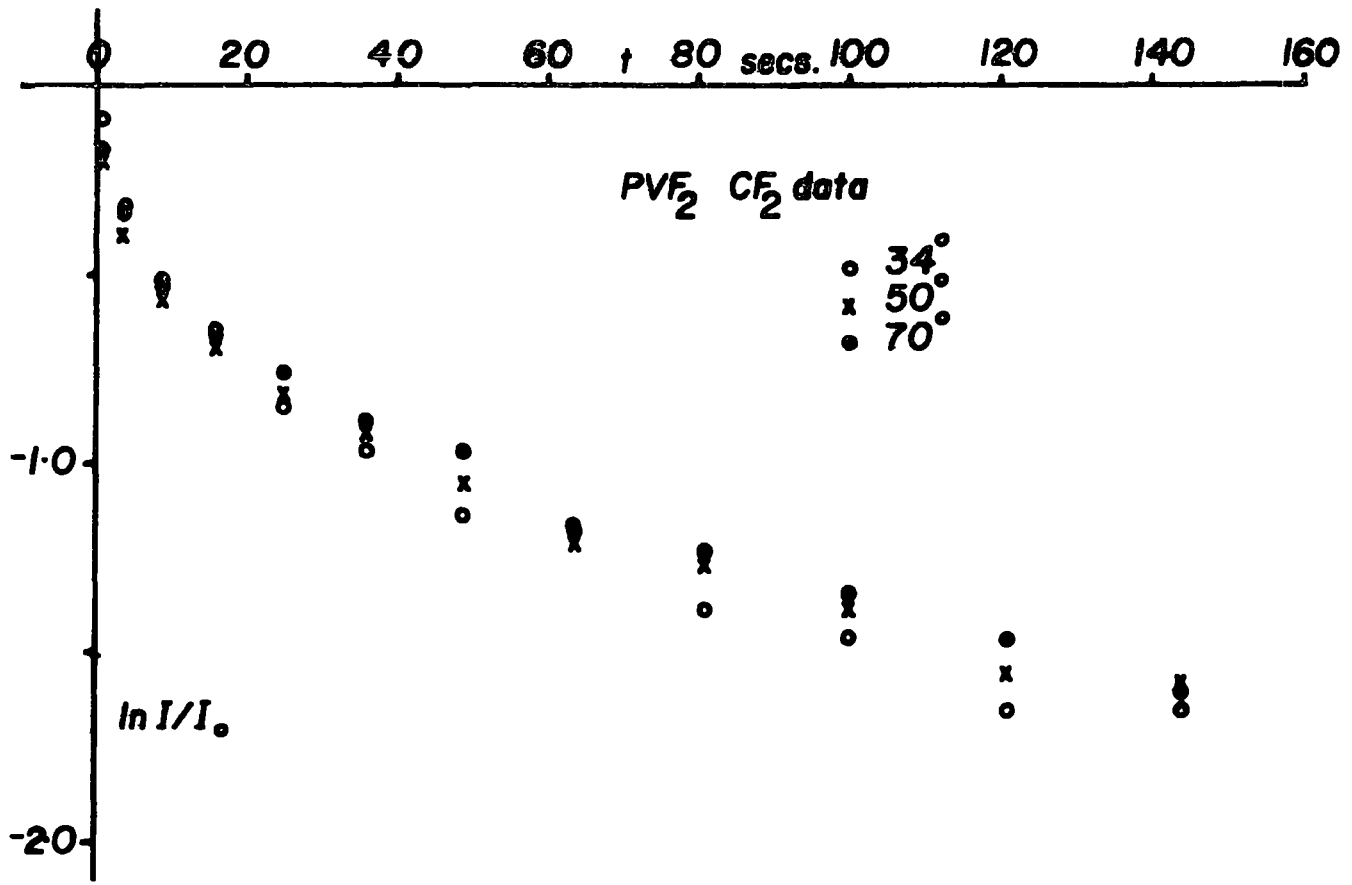

Figure 6.18. In I/I_o for the $\underline{C}F_2$ levels at electron take off angles of 34°, 50° and 70°, versus t, for polyvinylideneflyoride powder treated in an argon plasma (0.2 torr, 5.0 watts).

4.5 Charging Phenomena

The crosslinking of the ethylene/tetrafluoroethylene copolymer by exposure to inert gas plasmas results in the production of a surface which has a greatly reduced fluorine content. Since the charging characteristics of the copolymer and of a solely hydrocarbon based polymer such as polyethylene are so different (see Chapter Four) it might be anticipated that changes in equilibrium charge would provide a sensitive monitor for changes in surface composition. This is indeed the case as illustrated in figure 6.19. In all cases the equil-

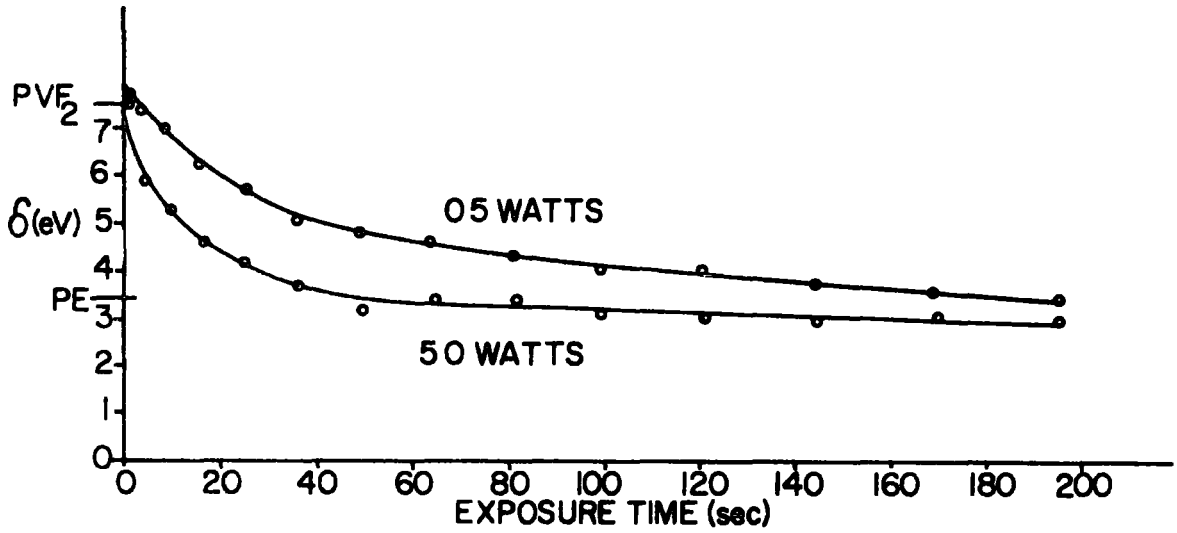

Figure 6.19. Sample charging of the ethylene/tetrafluoroethylene copolymer as a function of time of exposure to plasmas excited in argon (0.5 torr, 0.5 and 5.0 watts).

ibrium charge for extended reaction time approaches that of polyethylene and indeed with a knowledge of electron mean free paths as a function of kinetic energy it is possible to estimate the thickness of the surface layer at which this situation

obtains.[99,100] In each case the estimate suggests a depth of ~3 monolayers which is entirely reasonable in the light of the data previously presented in Chapter Four. It has been seen that for the data present in figure 6.19 the rate of reaction at 5.0 watts is greater than that at 0.5 watts and the charging data alone illustrate this most convincingly. Thus the rate of decrease of sample charging, which reflects the decreased fluorine content of the surface region, also falls in the same order. It is clear, therefore, that sample charging phenomena can add an extra dimension to such investigations and is eminently worthwhile studying in its own right.

5. Elucidation of Some Mechanistic Aspects of the Initial Stages of Crosslinking

It can be seen from the discussion that the crosslinking of saturated polymers by means of a radiofrequency glow discharge can be, contrary to popular belief, an extremely mild treatment technique. With correct optimization of the plasma parameters it is possible to crosslink as little as a fraction of a monolayer of the outermost surface of the sample, whilst bulk properties remain unchanged. In order to elucidate structural changes occurring in the initial few seconds of reaction it is necessary to accompany the ESCA experiment by theoretical and data handling techniques[136] as will become apparent in the ensuing discussion.

5.1 Theoretical Interpretation of the ESCA Spectra of the Crosslinked Copolymer

The theoretical treatment of results so far has been in terms of the reaction kinetics of the system. However, ESCA provides, through the consistency of the line shapes of the component signals, a means of theoretically simulating the overall spectral envelopes from their individual signals.

It has been shown[1] that the binding energy of an electron in a particular core orbital as seen by ESCA can be closely approximated using the Madelung Charge Potential Model as expressed in Chapter One, equation 1.13. In the following theoretical interpretations values for k and E^{o} of 25.2 and 284.6 eV respectively have been chosen.[114]

The charge potential model has been applied extensively to small molecules and agreement with experimental data has proved to be good.[1] Recently the model has been applied to larger systems (i.e. polymers) and it has been shown that the spectrum of a polymer may be adequately derived from charge distributions obtained for two or three units.[114,125] This is a direct consequence of the $^{1}/_{r}$ dependence of the potential term. For the example of this work (crosslinked ethylene/tetrafluoroethylene copolymer) the situation is very complex and it is therefore not expected to be able to achieve a definitive description since the mechanism of the crosslinking reaction is not well understood and the number of models required to describe an extensively crosslinked system is prohibitive. The analysis is therefore confined to the very initial stages of the process. Calculations of the charge distributions of the models described below were accomplished within the all-valence electron CNDO/2 SCF MO formalism† as previously outlined.[1]

The structure of the ethylene-tetrafluoroethylene copolymer (52% TFE) has been previously determined[121] (see Chapter Two)

---

† The CNDO/2 program used in this investigation could handle a maximum of 120 basis functions (atomic orbitals) which imposed restrictions on the size of the model systems for which the charge distributions could be computed.

along with the binding energies of the C_{1s} levels of the individual carbon atoms. The six starting models used in this investigation[121] are derived from this work and are listed in Table 6.9.

Table 6.9. Starting Models

Model	% Abundance[121]
291.0 291.2 291.2 CH_3-CH_2-CF_2-CF_2-CF_2-CF_2-CH_3	6.7
286.3 291.0 291.0 CHF_2-CH_2-CH_2-CF_2-CF_2-CH_2-CH_3	36.2
286.3 291.0 291.2 CHF_2-CH_2-CH_2-CF_2-CF_2-CF_2-CHF_2	6.7
286.3 290.5 291.0 CH_3-CH_2-CH_2-CF_2-CF_2-CH_2-CH_3	1.3
286.3 286.3 291.0 CHF_2-CF_2-CH_2-CH_2-CF_2-CF_2-CHF_2	44.8
286.1 286.1 286.3 CHF_2-CH_2-CH_2-CH_2-CH_2-CF_2-CHF_2	1.3

The binding energies of the central three carbon atoms are given in eV. CNDO/2 and charge potential calculations were carried out for all the possible crosslinks between the central atoms of the six starting models to give thirty-six crosslinked model systems. Each crosslinked model contained two of the starting models with one crosslink between their central atoms, i.e.

C-C-C-C-C-C-C
|
C-C-C-C-C-C-C

These models give the modified binding energies of the central six carbon atoms with an estimated accuracy of $\pm$ 0.1 eV.

It is clear that the addition of one or more polymer starting models onto a crosslinked model would increase the number of models required to a very large number, and the number of atoms per model would exceed the maximum which could be handled by the CNDO/2 program available. The best that can be obtained from such models therefore is a description of the initial stages of the crosslinking reaction where the crosslinks are remote from one another (i.e.< 1 crosslinked atom per 4 chain carbon atoms, or <12.5% crosslinked).

Without a detailed knowledge of the reaction mechanism the starting assumption is that all crosslinks are equally probable. The relative abundance of each of the thirty-six crosslinked models is then merely the product of the relative abundance of the two starting models, in the initial copolymer, of which it consists. Having calculated the core level spectra appropriate to a given degree of crosslinking and knowing the lineshape and linewidths for individual components it is a straightforward matter to produce a difference spectrum which may then be appropriately scaled to produce composite spectra appropriate for direct comparison with experimental data (figure 6.20). It should be noted that as a first approximation in generating the difference spectra it has been assumed that the atom density of the crosslinked and uncrosslinked material are the same. Only a small error is involved in considering only the three central carbon atoms in each case, and gaussian lineshapes were used throughout.

Figure 6.20 shows a complete C_{1s} spectrum of the ethylene/tetrafluoroethylene copolymer simulated from the six starting models,[121] along with a spectrum obtained by the method des-

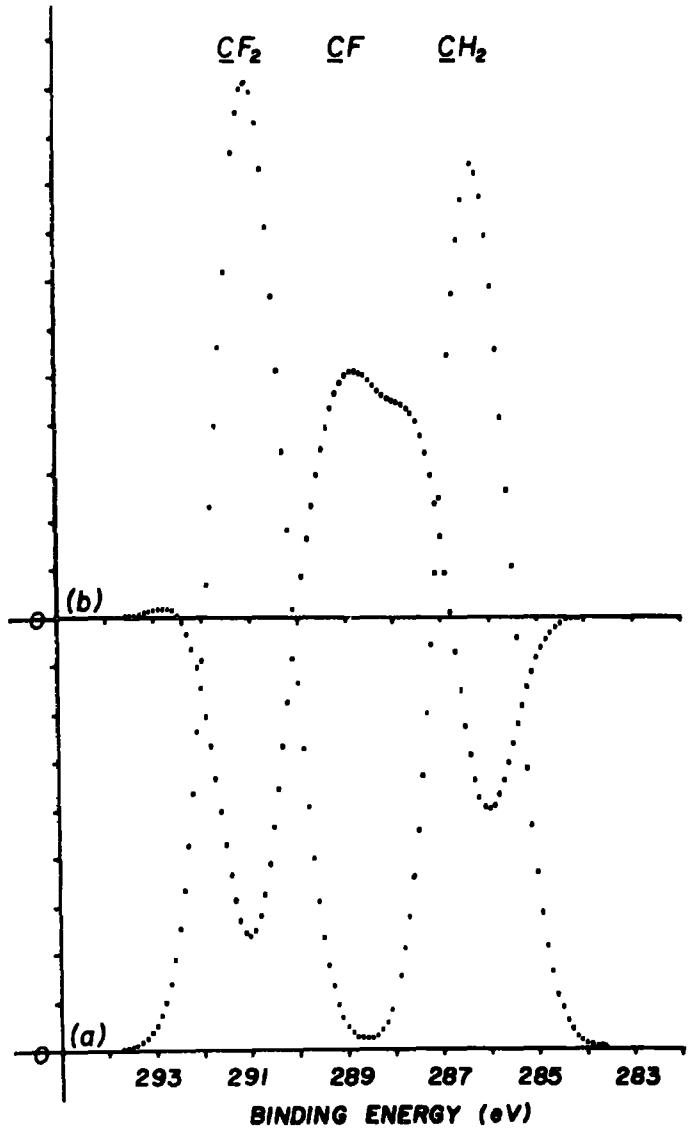

Figure 6.20. (a) Complete C_{1s} spectrum of the starting material, theoretically simulated from the starting models.
(b) Spectrum simulated from the crosslinked models. (Note that the origin is shifted). The intensity is in arbitrary units.

cribed above invoking the use of binding energies of the three central carbon atoms in the models. It is evident from figure 6.20 that the crosslinking reaction manifests itself in the initial stages as a decrease in signal intensity due to $\underline{C}F_2$

and $\underline{C}H_2$ environments with a concomitant increase in signals of intermediate binding energy due to $\underline{C}F$ and $\underline{C}H$ type structural features. The two major components of this signal are clearly observable and are due to $\underline{C}H$ and $\underline{C}F$ with the latter at a higher binding energy.

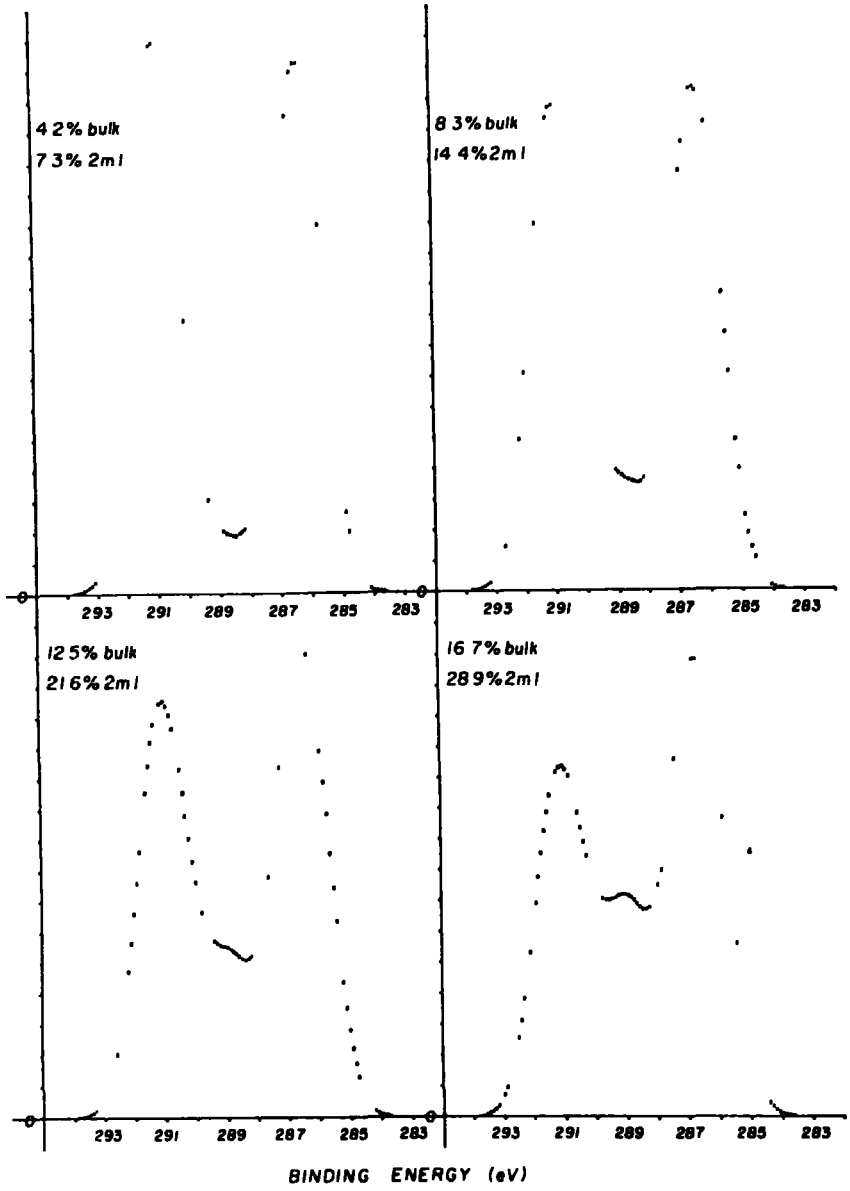

Figure 6.21. Theoretically simulated spectra for samples of varying degrees of crosslinking. The intensity is in arbitrary units.

Figure 6.21 shows the weighted additions of figure 6.20 (a) and (b) producing C_{1s} spectra of systems having varying

degrees of crosslinking. Each spectrum may be correlated to bulk polymer crosslinked to a degree of x% or a system in which the surface only is crosslinked, to a depth d, to a degree of $(x/(1-e^{-d/\lambda C_{1s}\cos\theta}))\%$.

Figure 6.21 gives for each simulation the degree of crosslinking for bulk polymer and a polymer in which only the outermost two monolayers (2m.l.) are crosslinked. If the simulated spectra in figure 6.21 are compared to experimental data very close similarities are seen in the initial stages of the reaction. The first spectrum in figure 6.21 shows the simulation of the copolymer crosslinked to a degree of 7.3% in the outermost two monolayers (i.e. ∿1 crosslinked atom per 7 chain carbon atoms). This model falls within the approximations of the theoretical model and the agreement with experiment is very good. (cf. Chapter Five, figure 5.16). However as the degree of crosslinking increases the theoretical model tends to overestimate signals due to CF structural features at the expense of signals at lower binding energy arising from features involving carbon not directly attached to fluorine. This is inherent in the exclusion of $\underline{C}F \rightarrow \underline{C}$ type reactions in the theoretical model, but is also informative since it presents independent evidence of the importance of $\underline{C}F \rightarrow \underline{C}$ type conversions in extensively treated samples.

Figure 6.21 also demonstrates that the overall shape of the spectral envelope is changed relatively little by a large increase in the degree of crosslinking in the surface regions. The decrease in the intensity of the CF_2 component of the C_{1s} spectrum exhibited by the most extensively crosslinked polymer spectrum in figure 6.21 is readily effected experimentally by just a few seconds exposure to an inert gas plasma, whilst

extended exposure times result in more dramatic changes in the shape of the spectrum. This, along with the very low fluorine levels observed for these samples is clearly indicative of the extensive nature of the crosslinking in the outermost monolayer or so, that may be achieved.

Closer scrutiny of the simulated spectra reveals further information concerning the processes involved in the crosslinking mechanism, encoded in the shape of the well between the two major peaks of the spectrum. In the simulated spectra the centroid of the intermediate binding energy components is to slightly higher binding energy than observed experimentally (see Chapter Five, figure 5.16). This may be rectified by either including a small signal at $\sim$ 288.0 eV due to carbonyl carbon[125] or by increasing the contributions due to crosslinks involving CH features. The latter would reflect a greater reactivity of the CH_2 sites to crosslinking, since the initial assumption was that all crosslinks were equally probable.

5.2 Difference Spectra

For the early stages in the surface modification fine details of structural changes which would normally be inferred from a detailed consideration of the overall line profiles for individual core levels become somewhat difficult to study directly since the spectra arise as a convolution of that appropriate to a modified surface and essentially unmodified subsurface and bulk.

Whilst the use of difference spectroscopy has been widespread in certain areas (e.g. I.R.) the application in photoelectron spectroscopy has only been exploited in more recent times with particular reference to detecting changes in valence

band structures consequent upon the physisorption or chemisorption of small molecules on metal surfaces.[218-220] Potentially, however, the technique should be of considerable utility in studying surface changes in general more particularly if difference spectra are calculated for both core and valence levels which span different ranges of mean free paths for the photoemitted electrons.

The changes in core level spectra for the copolymer system arising from interaction with plasmas excited in inert gases, have been described in Chapter Five. The salient features are that the F_{1s} levels decrease in intensity, as does the higher binding energy component of the C_{1s} spectra arising from $\underline{C}F_2$ structural features. In the C_{1s} spectra a region of intermediate binding energy appears which is attributable to $\underline{C}F$ and $\underline{C}H$ structural features, however, for early stages of reaction these changes in the C_{1s} levels may only be extracted by detailed line shape analysis.

Figure 6.22 shows the F_{1s} and C_{1s} levels for the initial copolymer system and that reacted for 4 secs.together with the corresponding difference spectra. The latter are dramatically revealing and give an immediate pictorial description of the substantial structural changes accompanying interaction of the polymer with the plasma excited in argon. In particular the C_{1s} difference spectrum clearly accentuates the region of intermediate binding energy and the asymmetric nature of the peak provides strong confirmatory evidence for the previous conclusions based on more extensively reacted samples for the variety of $\underline{C}F$ and $\underline{C}H$ sites that are produced in the crosslinking process, viz.

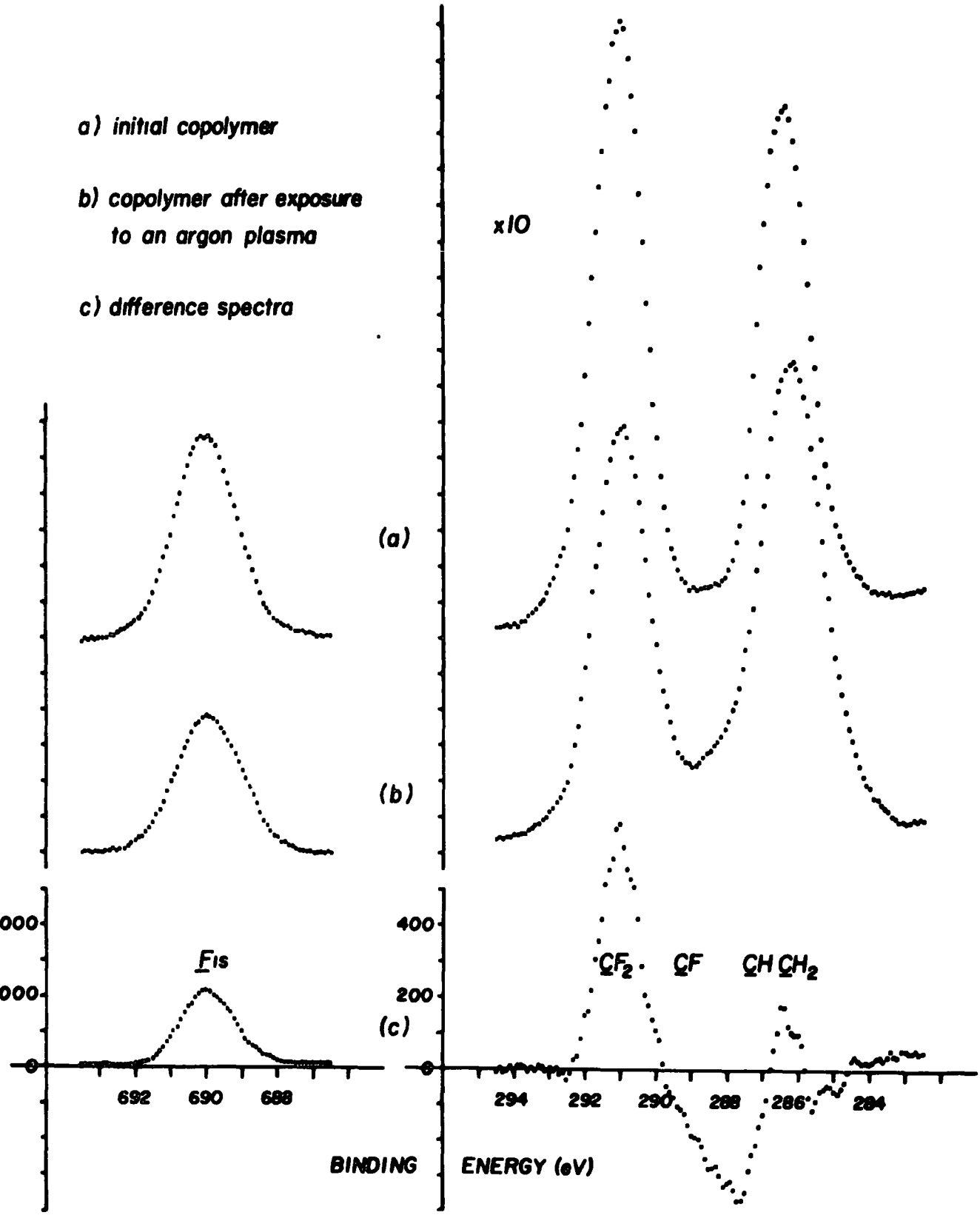

Figure 6.22. F_{1s} and C_{1s} core level spectra for the initial copolymer and a sample treated for 4 secs. in an argon plasma (0.2 torr, 5.0 watts) along with the difference spectra. (The vertical scales are in counts per channel of the MCA, i.e. counts per 0.6 sec. per 0.1 eV increment).

$-CF_2-\underline{C}F-CH_2-$ $-CF_2-\underline{C}F-CH_2-$ $-CF_2-\underline{C}H-CH_2-$

$-CF_2-\underline{C}H-CH_2-$ $-CH_2-\underline{C}F-CF_2-$ $-CF_2-\underline{C}H-CH_2-$ etc.

It is interesting to note the profound differences in relative intensities of the difference spectra with respect to the corresponding data for the original polymer system. If the depth to which the modification extends is short compared with the electron mean free path then the difference will be quite small and the attenuation factor correspondingly large. Thus despite the fact that the difference valence band spectrum is remarkably similar (figure 6.23) to that of the original polymer if the essentially core like F_{2s} levels are considered it is clear that the attenuation in going from original to difference is large ($\sim$5X) indicating that the depth to which the surface modification pertains is small compared with the mean free path of electrons of kinetic energy $\sim$ 1220 eV. By contrast the difference F_{1s} spectra are only a factor of three different in intensity than the original indicating that the depth of modification is comparable to the electron mean free path at $\sim$ 560 eV kinetic energy. The important conclusion to be drawn from this is that even when the modification in structure produces small changes in the overall band profile (e.g. as is the case with the valence band) the difference spectra are sufficiently sensitive to detect this more particular if the difference is compared in intensity with the original spectra.

In considering the C_{1s} difference spectra it is immediately evident that $\underline{C}F_2$ structural features in the original copolymer are transformed largely into $\underline{C}F$ environments and $\underline{C}H_2$ structural features converted into both $\underline{C}H$ sites with an increased number

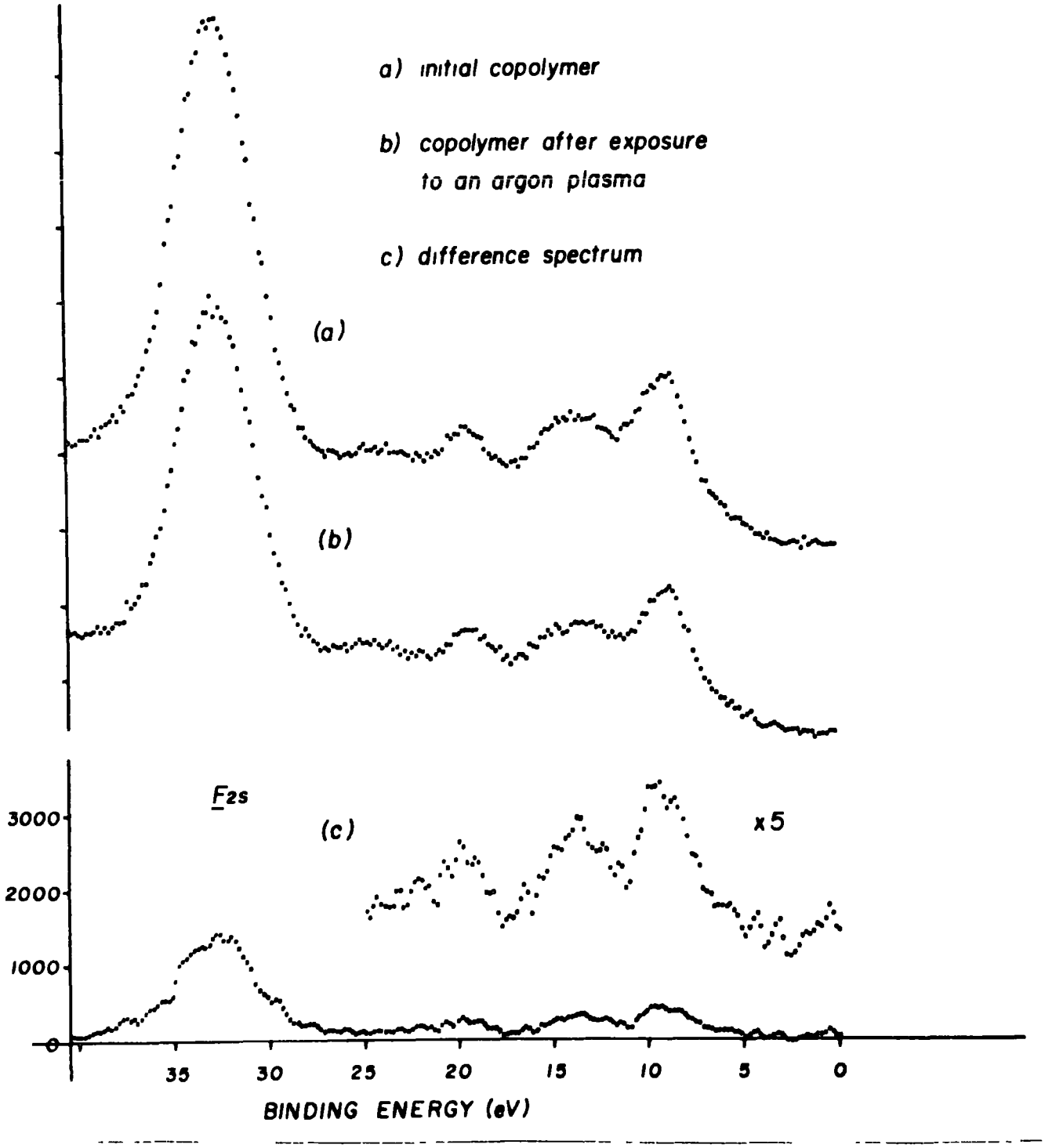

Figure 6.23. Valence band spectra for the initial copolymer and a sample treated for 4 secs. in an argon plasma (0.2 torr, 5.0 watts) along with the difference spectrum. (Vertical scales are in counts per 10.8 secs. per 0.2 eV increment).

of adjacent carbon fluoride bonds (β shift parameter ∿ 0.7 eV) which shift the centroid of the lower binding energy region to ∿ 287.6 eV and in addition produce lower binding energy $\underline{C}H_2$ sites in which the number of β carbon fluorine bonds is decreased compared with the original largely alternating structure. This confirms the previous conclusions concerning the crosslinking in such systems based on an analysis of relative intensities and of line shapes.

Comparison of figure 6.22 with the theoretically simulated difference spectrum in figure 6.20(b) (inverted) reveals a striking similarity. It is clear however that the component due to $\underline{C}H$ structural features is larger in the experimentally derived spectrum. This is strong confirmatory evidence that all crosslinks are not equally probable and that the $\underline{C}H_2$ sites do indeed exhibit a greater reactivity.

Although the production of difference spectra is time consuming and needs considerable attention to detail, in appropriate cases as this work has demonstrated it is a worthwhile exercise since details of change in structure and bonding are immediately revealed even for systems in which the extent of reaction is extremely small. In the samples discussed here for example it would be estimated that the modified sample is crosslinked to an extent of < 20% in the first two monolayers. Clearly difference spectra of adequate signal to noise ratio could be generated at a much earlier stage when inspection of the raw data for the core levels themselves might reveal little detail of the modification.

5.3 Valence Band Spectra

It has been previously noted that the interaction of an atom or molecule with a soft X-ray photon source leads to photoemission of both core and valence electrons, the cross section for the former being substantially larger than for the latter. The study of spectra arising from the core levels is straightforward and provides, by indirect monitoring of the valence electrons, information concerning the structure and bonding of the system. In principle the study of valence band spectra should provide this information directly. In practice however the valence bands for solid materials are generally broad and of a low resolution, and their study has been confined to simple systems and in particular as a fingerprint technique.[125] (see Chapter Two).

Since the proposed mechanism for modification of the ethylene/tetrafluoroethylene copolymer system by radiative energy transfer, dominantly involves photoionization (and transitions to diffuse Rydberg states) it is pertinent to compare the overall match between the dominant characteristic line spectra excited in the inert gas plasmas and the valence band of the copolymer shown in figure 6.24. At first sight there seems to be a problem in comparing these data since the valence band spectrum is referenced to the fermi level of the solid. However since reactions may occur subsequent to the photoionization of the polymer leaving the electron in the solid a direct comparison is possible.

Several studies have been reported of differential cross sections for photoionization of valence 2s and 2p subshells as a function of photon energy in the region of interest to

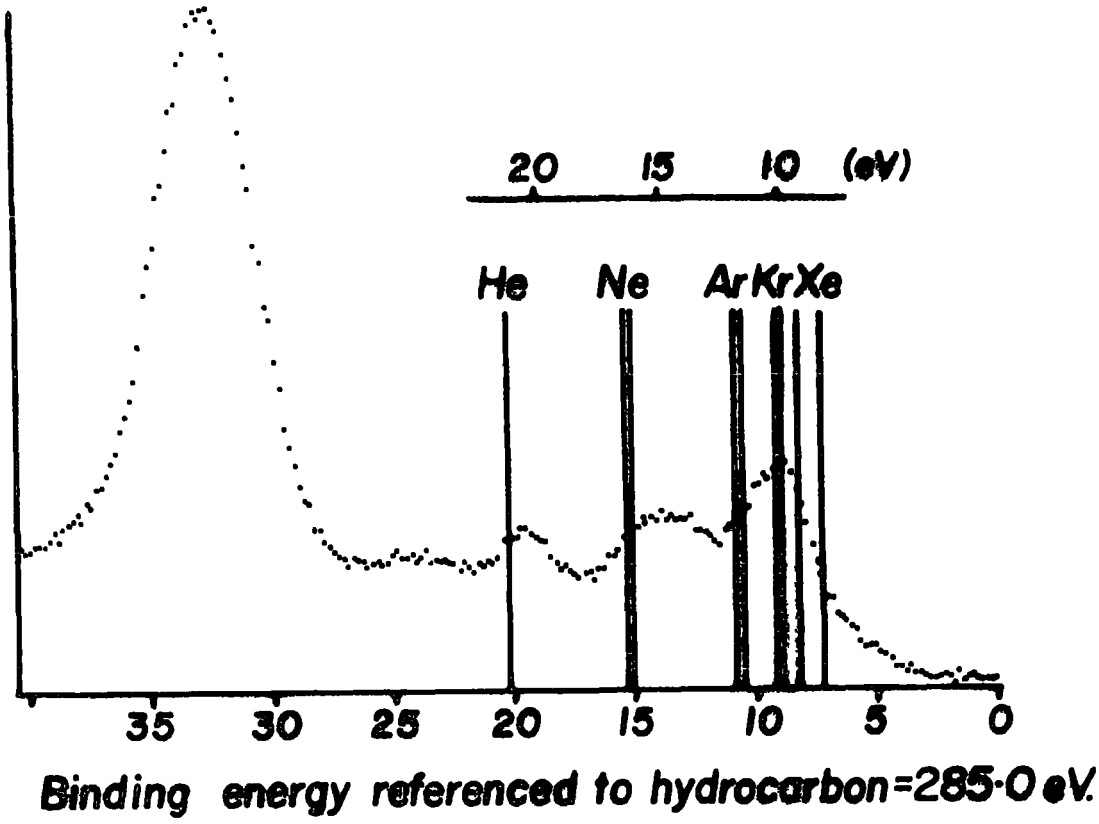

Figure 6.24. Valence band spectrum of the copolymer with the inert gas resonance lines superimposed.

this work[217,221] (viz. HeI, 20.2 eV - XeI, 8.4 eV). The main features which emerge from these investigations are as follows:

(1) The cross sections increase dramatically at the threshold and vary over a relatively small range over the energy window of interest.

(2) The differential cross sections for photoemission from a valence 2p orbital decreases relatively slowly as a function of the photon energy.

(3) Since the most intense outputs in the vacuum U.V. for the inert gas plasmas studied under the conditions appropriate to this work are for the resonance lines (HeI-XeI) there is expected to be little contribution to the overall radiative

component from photoemission involving molecular orbitals with significant 2s character.

The ordering of the rates for the radiative energy transfer processes for the modification by the inert gas plasmas as seen in figure 6.11 and Table 6.6 can be summarized as Ne >He >Kr >Ar >Xe, and this can be appreciated in terms of the crude model illustrated by figure 6.24. The lowest energy resonance lines arising from xenon (XeI) do not possess sufficient energy to cause ionization of the F_{2p} levels and the reaction must proceed via ionization of C-H bonding orbitals and excitations to Rydberg states. The energy of the KrI resonance lines however coincide with the ionization threshold for the F_{2p} lone pairs and hence the ionization is expected to be more efficient, whilst the cross section for the ArI lines of higher energy will be somewhat lower. The NeI resonance lines have sufficient energy to ionize the C-F bonding orbitals, F_{2p} lone pairs or C-H bonding orbitals and the rate of modification would be expected to be fast. For the HeI resonance lines sufficient energy is available to ionize all but the F_{2s} levels. The cross section for orbitals of s character for the example of methane falls off more rapidly than for those of p character with increasing photon energy.[217] The same might be expected to be true for the case of the C_{2s} levels in the copolymer. The rate for helium, on this basis and also considering the disparity of its energy with that of the remaining levels might be expected to have a rate similar to that of neon.

It is clear that this crude simplistic analysis has provided a qualitative description of the observed trends in the pseudo rate constants for the radiative energy transfer processes occurring in the bulk of the polymer. It must be

emphasized however, that no consideration has been made of the relative intensities of the respective spectral lines which may modify the situation slightly, although it has been noted in section 3.3 that their intensities are probably closely similar.

6. Conclusions

The conclusions drawn in this and the previous Chapter although largely pertaining to a specific system, give strong guidelines for the study of most other saturated polymeric systems exposed to an inert gas plasma and indeed the broad outlines may be extrapolated to unsaturated systems although the U.V./visible radiation will be anticipated to play a relatively more important role. It has been undertaken to apply as many facets of the ESCA experiment as possible in this investigation in order to demonstrate the great potential of ESCA as a spectroscopic tool in the area of surface modification of polymers, and this fact should be readily apparent from the foregone discussions.

CHAPTER SEVEN

Surface Modification of Polymers by Oxygen Plasmas

1. Introduction

An area of considerable technological and academic importance is the surface oxidation of polymers, in terms of both improvement of surface properties by increasing their surface free energy or wettability, and in the understanding of oxidative degradation in general. The essence of degradation is a change in structure and bonding which may permeate through the surface, subsurface and bulk but usually gives rise to inhomogeneities in these regions. This being the case, and since degradation is invariably initiated at the surface, then a prime requisite for a definitive study of polymer degradation in general is the complete elaboration of surface structure for the initial and modified systems.[52,130,132] Prior to the advent of ESCA the important question as to whether surface composition of a polymer is the same as that of the bulk and if not, in what way it differs could only be inferred indirectly in favourable cases whilst the specific differentiation of these regions in inhomogeneous samples could not be encompassed.[148]

Within the past few years several observations have appeared in the literature on the use of ESCA to study the surface oxidation of polymers, effected by a variety of agents and the difficulties of such an undertaking due to the unresolved nature of the spectra have been readily apparent.[125,132,222-225] With a suitable background knowledge however, it is possible to unravel the complexities to some extent and it is to this problem that this chapter is particularly addressed.[137] An investigation is therefore described of the oxidation of polyethylene, polypropylene and polystyrene effected by radiofrequency glow discharges excited in oxygen and helium/oxygen mixtures.

The choice of purely hydrocarbon polymers enables distinct monitoring of all of the likely carbon-oxygen features which are likely to be produced, in the absence of complications due to the production of reactive species consequent upon ablation of oxygen containing fragments from the polymer surface.[148] A direct comparison with related polymer systems of known structure is then readily accomplished. The choice of the method used to oxidize the samples is also of considerable importance. For example a thermal oxidation process by simply heating in air, is not easily controlled and generally causes oxidation extending into the bulk of the sample.[123-125,224,225] Solution techniques (e.g. chromic acid etching[223]) suffer from similar difficulties and in addition the loss of low molecular weight fragments cannot be discounted. Problems may also occur via solvent incorporation with the product. It will be seen from this investigation that as a starting point the employment of inductively coupled radiofrequency glow discharges provides the flexibility, on/off power control and clean reaction conditions necessary to demonstrate the phenomena with the desired degree of clarity. Previous chapters of this thesis have already attested to the fact that such plasmas under conditions of low input power levels provide a means for extremely mild modification of polymer surfaces to a depth corresponding to only a few monolayers. Indeed stable plasmas may be sustained at average power loadings as low as 0.1 watt by means of pulsing the radiofrequency power input on the microsecond time scale.

The oxygen plasma is highly complex, containing a variety of both positive and negative ions, atoms, ozone and metastables

of both atomic and molecular oxygen[195] as well as electrons and a broad electromagnetic spectrum.[196] However the interaction of the plasma with a hydrocarbon polymer at least as far as the surface regions are concerned is almost certainly dominated by the oxygen atoms, which have the greatest reactivity towards the polymer, resulting in a wide range of free radicals which may then react with molecular oxygen, etc. to produce a variety of oxygen containing species at the polymer surface.[148] This situation will clearly allow the elaboration of all of the likely areas of utility of ESCA in this field.

2. Experimental

The samples of polyethylene, polypropylene and polystyrene used in this investigation were in the form of freestanding extruded films, and contained no additives. The ESCA instrumentation has been amply described in earlier chapters of this thesis and the glow discharge reactor and pumping arrangement was the same as that employed in Chapter Six. The method of successively exposing the samples to the plasma and passing them into the ESCA spectrometer for analysis was also along similar lines to those previously outlined. For comparison purposes samples of polyethylene treated in a corona discharge in air,[132] and samples prepared by pressing non-degassed polyethylene powder between aluminium foil sheets at $\sim 200^{\circ}C$ under a nitrogen atmosphere, have also been studied.[225] The oxygen and helium used in this study were of research grade and used without further purification.

3. Absolute and Relative Binding Energies of Carbon-Oxygen Structural Features

The possibility of using ESCA to study non fluorine

containing polymers has only been exploited within the past year or so with the completion of an extensive report on a series of more than one hundred standard polymer samples.[125-127] In particular the data pertaining to a series of polyalkylacrylates,[125] polyalkylmethacrylates[126] and a variety of other oxygen containing polymers[127] along with related small molecules might be expected to provide much of the background information necessary for the unravelling of the complexities of the surface oxidation of polymers in terms of absolute and relative binding energies of oxygen containing structural features. Table 7.1 summarizes the data of relevance to the present work.

Table 7.1. Binding Energies of Oxygen Containing Structural Features

Feature	Material	Binding Energy* C_{1s} (eV)	Binding Energy* O_{1s} (eV)	Reference
C-OH	ethanol, methanol	286.6	533.6	125
>C=O	acetone	287.9	533.6	125
C-O-C	diethylether	286.5	533.6	125
-C=O O-C	acetates	289.2 286.6	533.4 534.4	125
-C=O O-H	polyacrylic acid	289.1	533.0 534.3	125
-C=O O-C	polyalkylacrylates	288.9 286.6	532.8 534.3	125
-C=O O-C	polyalkylmethacrylates	288.8 286.7	533.0 534.4	126
-C-O-C-O-	polymethyleneoxide	287.8	533.6	127
>C=O	polyacetyl-p-xylylene	287.6	533.6	127
-O C=O -O	polycarbonates	290.4	534.9 533.0 534.9	127

* All binding energies are quoted with an accuracy of $\sim \pm$ 0.1 eV.

Several important features, which are crucial to the analysis of the spectra to be presented in this chapter, are immediately obvious and are as follows. Although a wide variety of environments are depicted in Table 7.1 the carbon 1s and oxygen 1s binding energies tend to occur in groups. Thus for carbon singly bonded to one oxygen atom the binding energy is ∿286.6 eV. Carbon singly bonded to two oxygen atoms and carbon doubly bonded to one oxygen atom may be grouped together at a binding energy of ∿ 287.9 eV, whilst carboxylate and carbonate carbons occur at ∿ 289.0 and 290.4 eV respectively. A similar situation is also apparent for the oxygen signals. Hence for simple carbonyl compounds, alcohols and ethers the binding energies for the O_{1s} levels are essentially the same, ∿533.6 eV. By comparison, for esters and acids the singly and doubly bonded oxygens have binding energies of ∿ 534.3 and 532.9 eV. For carbonates the splitting between the oxygen environments is somewhat larger, the singly and doubly bonded oxygens having binding energies of ∿ 535.0 and 533.0 eV respectively, the latter being similar to that for the corresponding ester oxygen.

Experimentally determined binding energies for other features which might be expected to be present in the oxidized polymer systems, i.e. peroxides and peroxyacids, are not available at the present time from the literature. However, non-empirical calculations on an extensive series of model systems have provided valuable information in this respect. Computations with STO 4.31G basis sets in the ΔSCF formalism provide an excellent description of both relative binding and relaxation energies at reasonable computational expense. In absolute

terms binding energies tend to be overestimated by ~ 1% largely due to the underestimation of relaxation energies. The adequacy of the basis set in discussing relative values however is demonstrated by considering a simple example such as methyl acetate. The computed C_{1s} shifts are (relative to the carbon atom not directly attached to oxygen) -O$\underline{C}H_3$, 1.3 eV; O-$\underline{C}$=O, 3.9 eV compared with the experimentally determined values of 1.6 eV and 4.0 eV respectively.[125] For the O_{1s} levels the calculated shift of 1.4 eV may be compared to that determined for a series of esters of 1.4 eV,[125] with the doubly bonded oxygen at lower binding energy. A detailed account of these calculations can be found elsewhere,[226] and it will suffice here to briefly summarize the results. Figure 7.1 shows the calculated C_{1s} and O_{1s} binding energies of several model compounds. It can be readily shown that the replacement of a methyl group by hydrogen causes a shift to higher binding energy of the remaining atoms by approximately half an eV.[226] It might be envisaged therefore that several of the binding energies displayed in figure 7.1 may well be modified slightly when the structural feature is incorporated into a polymer system. The binding energy scale in figure 7.1 shows both the calculated values and values approximately corrected for the 1% overestimation noted above and for the work function of the polymer since the reference levels for the calculated and experimental binding energies are different (i.e. the vacuum versus the fermi level). The total correction is approximately 9 eV.

Considering the first five models in figure 7.1, which contain features for which the experimental data has already been discussed, with the sole exception of the oxygen assoc-

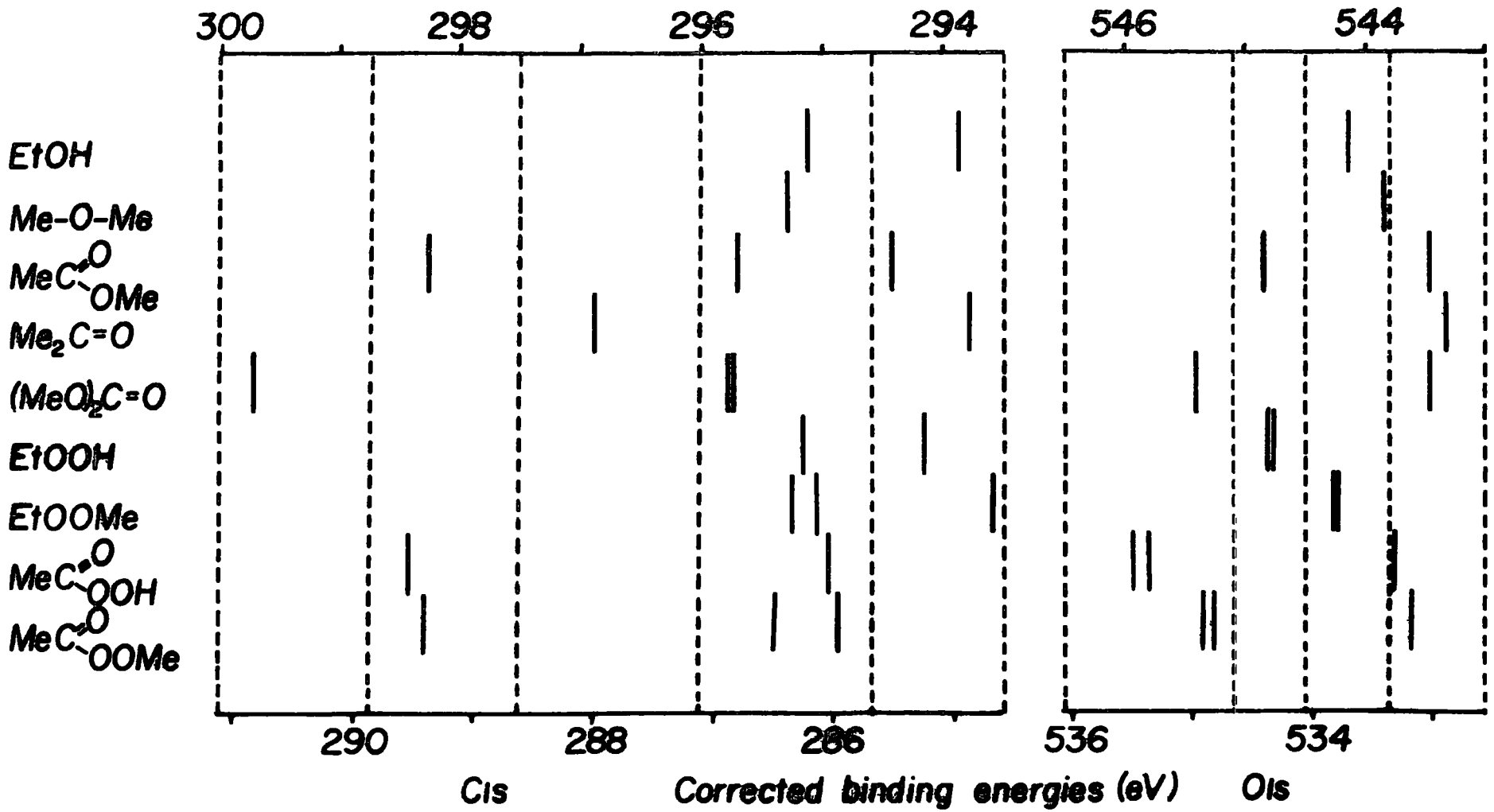

Figure 7.1. Theoretical C_{1s} and O_{1s} core level binding energies of model compounds.

ıated with acetone both the C_{1s} and O_{1s} binding energies fall into groups entirely consistent with the discussion of the data presented in Table 7.1. It is clear, therefore, that the calculations of bindıng energies for small molecules provide a sound basis for the discussion of similar oxygen environments in oxygen containing polymer systems.[226] The probable binding energy ranges for the peroxide and peroxyacid type structural features may therefore be predicted with a fair degrec of confidence. The data pertaining to these systems in figure 7.1 clearly suggest that the binding energies of the carbon atoms singly bonded to oxygen are encompassed by the grouping centred at ∿ 286.6 eV whılst that for the carbon atom attached to two oxygen atoms in the peroxyacids and peroxyesters has a binding energy close to that appropriate to a simple carboxylate carbon. The comparison of RO.OR′ with R(CO)O.OR′ in the O_{1s} region has a close correspondence with a sımılar exercise involving ROR′ and R(CO)OR′ in that the O_{1s} binding energy of the former lies between the two components of the doublet structure observed for the latter. However a clear difference is that the binding energy for the singly bonded oxygen atoms in the peroxyacid systems is somewhat higher than the correspondıng figure for sımple acid systems. In terms of the grouping the doubly bonded oxygen atoms may be included in the group centred at ∿533.0 eV whilst the singly bonded oxygen atoms in the peroxyacid systems have a binding energy similar to the high binding energy component observed for a carbonate (∿535.0 eV). For the peroxides the two examples (R=H,Me) give oxygen binding energies in different groups.

All of the available data therefore suggests that the primary substituent effect of oxygen may be summarized ın terms of

a simple additive model. The shift in binding energy of a given carbon 1s core level subsequent upon replacing hydrogen or carbon atoms by oxygen is ∿1.5 ± 0.2 eV per carbon-oxygen bond. The binding energies in the C_{1s} spectrum therefore fall into four groups increasing in binding energy thus:

$$\underline{C}\text{-}O < \underline{C}\text{=}O \sim O\text{-}\underline{C}\text{-}O < O\text{=}\underline{C}\text{-}O < O\text{=}\underline{C}\begin{matrix}\nearrow O \\ \searrow O\end{matrix}$$

$$\sim 286.6 \quad \sim 287.9 \quad \sim 289.0 \quad \sim 290.4 \qquad (eV)$$

the secondary substituent effect of oxygen being small. The situation in the oxygen spectrum is not so straightforward as might have been expected, since the relaxation energies associated with O_{1s} core ionization are not in general a simple function of structure.[42]

It would seem reasonable based on this method of collecting the varied types of oxygen environment into four main groups in the carbon region that the analysis of the spectra may well be accomplished by a greatly simplified curve fitting procedure employing only four components in the C_{1s} spectrum (in addition to a signal at ∿285.0 eV due to carbon atoms not attached to oxygen) at binding energies appropriate to the centroids of the groups and with FWHM slightly larger than that obtained for a typical homopolymer (∿1.4 eV), to encompass several structural environments. That this is indeed the case may be demonstrated by the data in figures 7.2 and 7.3, which show the C_{1s} spectra for the initial polyethylene and polystyrene and for samples exposed to an oxygen plasma (0.2 torr, 0.4 watts) for one second and five seconds. At first sight the unresolved spectra (figure 7.3) would appear too complex to attempt any curve fitting procedure. However by setting curves at binding energies of ∿ 286.6, 287.9, 289.0 and 290.4 eV and treating the

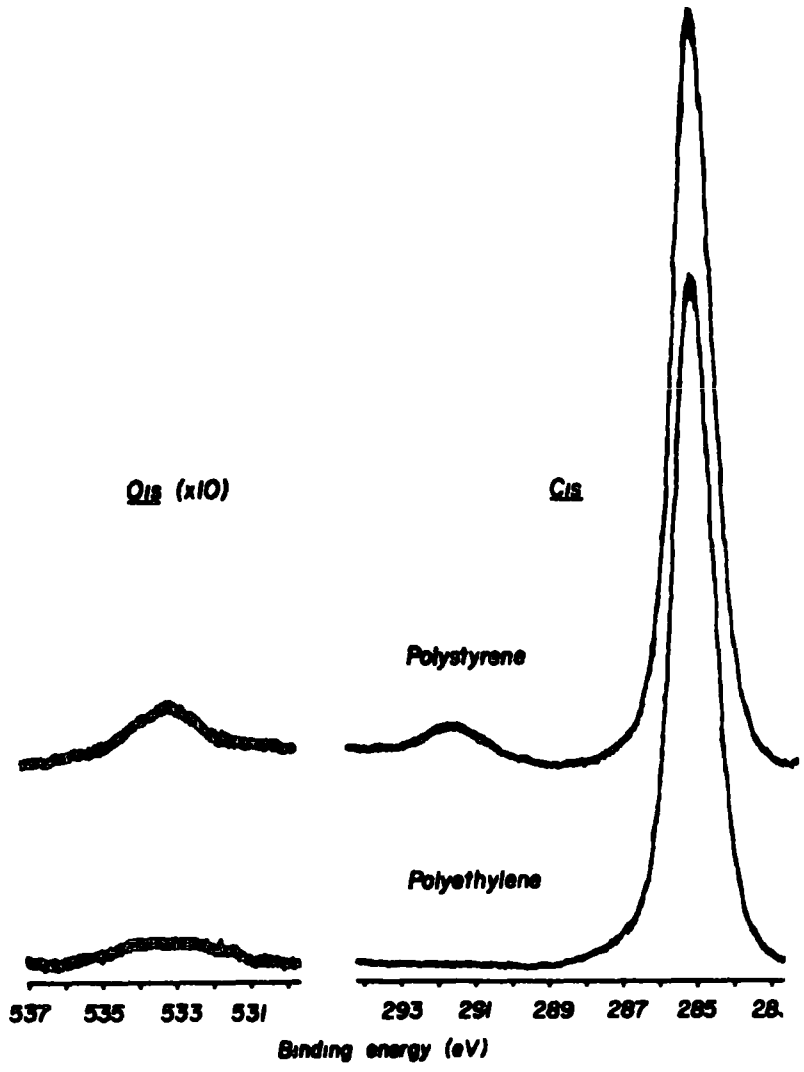

Figure 7.2. Polyethylene and Polystyrene.

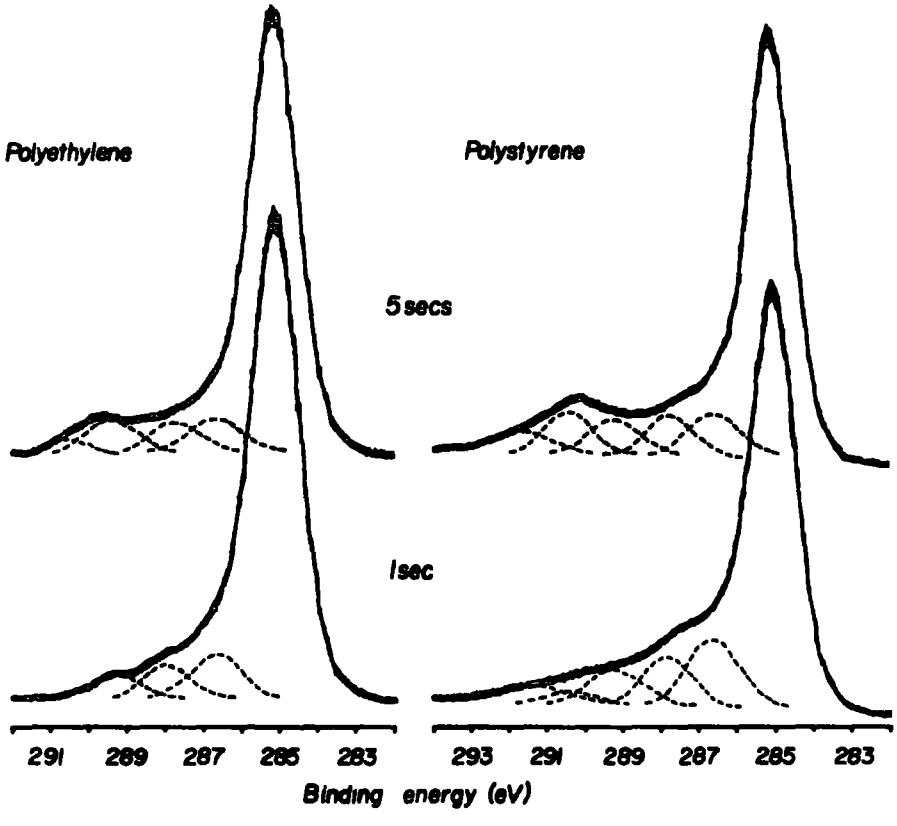

Figure 7.3. C_{1s} spectra for samples exposed to an oxygen plasma (0.2 torr, 0.4 watt) for 1 sec. and 5 secs.

height as a variable a unique deconvolution can be achieved with a FWHM of 1.7 eV. This is entirely reasonable and a similar procedure is used for all the examples given in this chapter, giving good fits to the experimental envelope in all cases. It must be noted here that for polystyrene a peak corresponding to shake up satellites is also necessary at a position ~6.6 e V from the signal at 285.0 eV. A similar analysis of the oxygen spectra of these samples is more ambiguous since the shift in binding energies between the O_{1s} groupings is less, and the groups themselves are much less well defined.

The semi-quantitative analysis of the C_{1s} envelopes, although encompassing several environments in each curve, greatly extends the scope of study of surface oxidation processes in polymers as will become apparent in the ensuing discussions. It must be stressed however that the conclusions drawn, based on this source of evidence alone is within the obvious limitations of the method.

4. Modifications Effected by Oxygen Containing Plasmas

4.1 Pure Oxygen Plasmas

The core level spectra of the polyethylene and polystyrene used in this investigation are shown in figure 7.2. Both samples show a very low level of oxidation, the O_{1s} spectra being magnified by a factor of 10. The polypropylene sample employed shows a closely similar spectrum to that of polyethylene. The C_{1s} spectrum of polystyrene shows the distinctive satellite structure associated with low energy shake up transitions accompanying core ionization (cf. Chapter Three). The monitoring of the relative intensity of the shake up satellite

with respect to the direct photoionization peak clearly shows the integrity of the surface of the sample (i.e. no hydrocarbon contamination of the samples was evident). The data in figure 7.3 refer to an experiment in which the samples of polyethylene and polystyrene were exposed to the plasma (0.2 torr, 0.4 watts) simultaneously mounted on opposite sides of the probe tip (cf. Chapter Five) allowing a direct comparison of the reactions occurring in the saturated versus unsaturated systems.

In both cases the reaction is rapid and essentially complete (as far as the change in surface composition is concerned) after 5 secs. These data clearly demonstrate the potential ability of ESCA coupled with glow discharge techniques, to monitor the reaction at a much earlier stage since in comparing the spectra for samples treated for 1 sec. and 5 secs. distinct differences are apparent in the spectrum pertaining to the oxygen containing structural features. Furthermore a semi-quantitative description of these differences is possible within the curve fitting procedure advocated in the previous section.

The greater susceptibility of the unsaturated system is clearly evident from this preliminary experiment, in that the total fraction of the C_{1s} envelope associated with oxygen environments is greater for the polystyrene sample, and for the samples treated for 5 secs. the intensity ratio of the O_{1s} to C_{1s} signals is 0.36 and 0.50 for polyethylene and polystyrene respectively. The unsaturated system also prefers the formation of carbonate structures as evidenced by the signal at $\sim$290.4 eV, which is also consistent with the greater uptake of oxygen for this sample.

Having established that the oxidation reactions at the

surface of polymer samples exposed to oxygen plasmas can be readily detected by means of ESCA it is of interest, as a logical extension, to monitor the oxidation as a function of time of exposure to the plasma. Such an exercise coupled with studies of the angular dependence of the absolute and relative peak intensities (with respect to the electron take off angle in the ESCA spectrometer) might be expected to add a further dimension to the investigation. Thus for example figure 7.4 shows the C_{1s} and O_{1s} core level spectra of a polyethylene sample as a function of time of exposure to an oxygen plasma at a power loading of 0.1 watt (pressure = 0.2 torr). The data in figure 7.4 pertains to an electron take off angle of 70^{o}. It is clear even from a cursory examination of these data that in the very initial stages of reaction a greater proportion of singly bonded oxygen is produced, both from the C_{1s} spectrum and in a distinct shift in the centroid of the O_{1s} spectral envelope to higher binding energy as the reaction proceeds. The same is also true for polypropylene and polystyrene.

Before examining these data in greater detail it is interesting to consider the outcome of the angular study on the absolute and relative peak intensities, in order to estimate the depth to which the oxidation processes occur under the conditions used in this investigation. Figure 7.5 shows the C_{1s} and O_{1s} spectra of polyethylene and polystyrene samples treated for 16 secs., recorded at electron take off angles of 34^{o} and 70^{o} respectively. The enhancement of relative intensities of the signals associated with the carbon-oxygen features at near grazing electron take off angle (70^{o}) demonstrates the surface nature of the modification. The absolute intensity of these

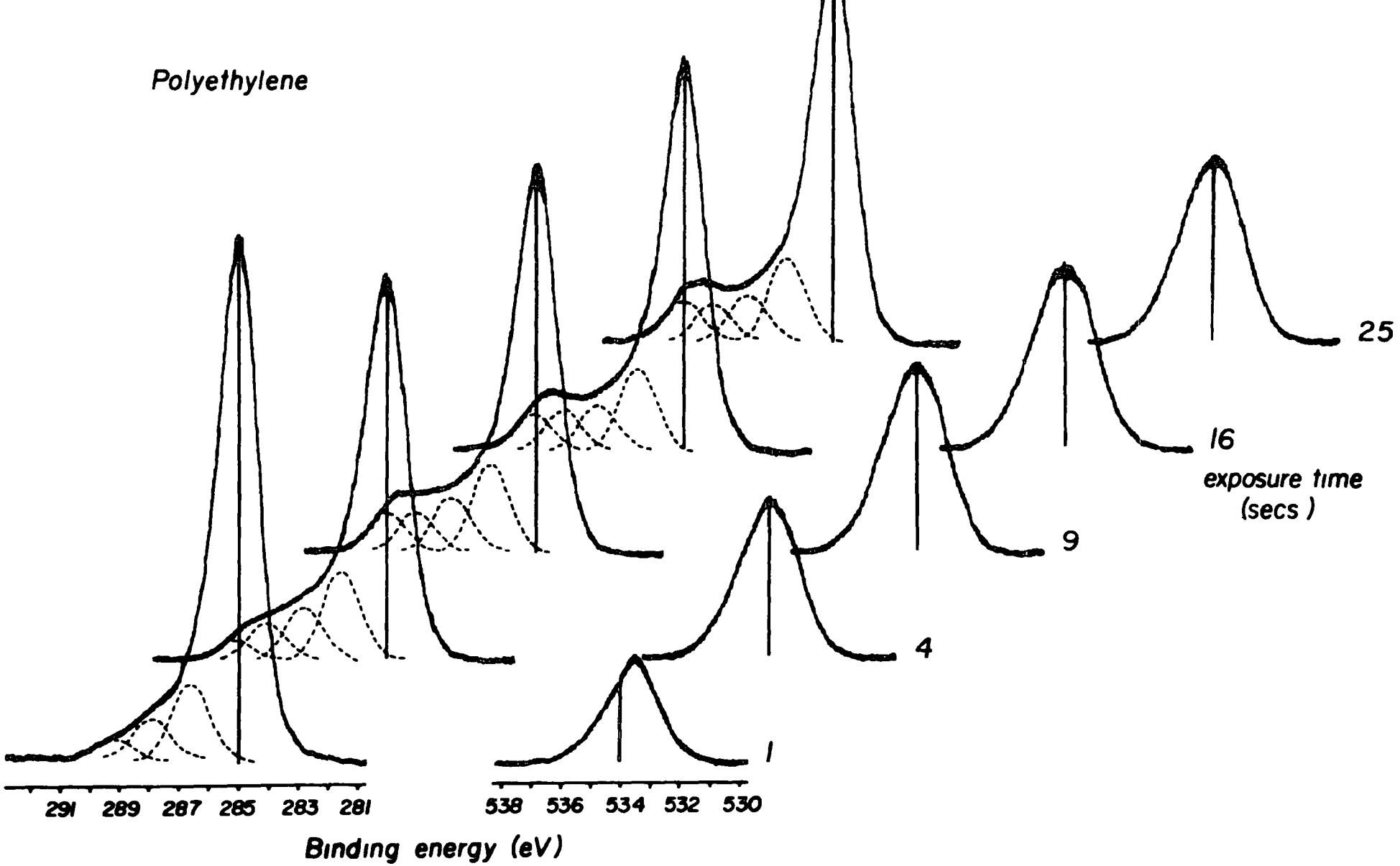

Figure 7.4. C_{1s} and O_{1s} spectra of polyethylene versus time of exposure to an oxygen plasma (0.2 torr, 0.1 watt).

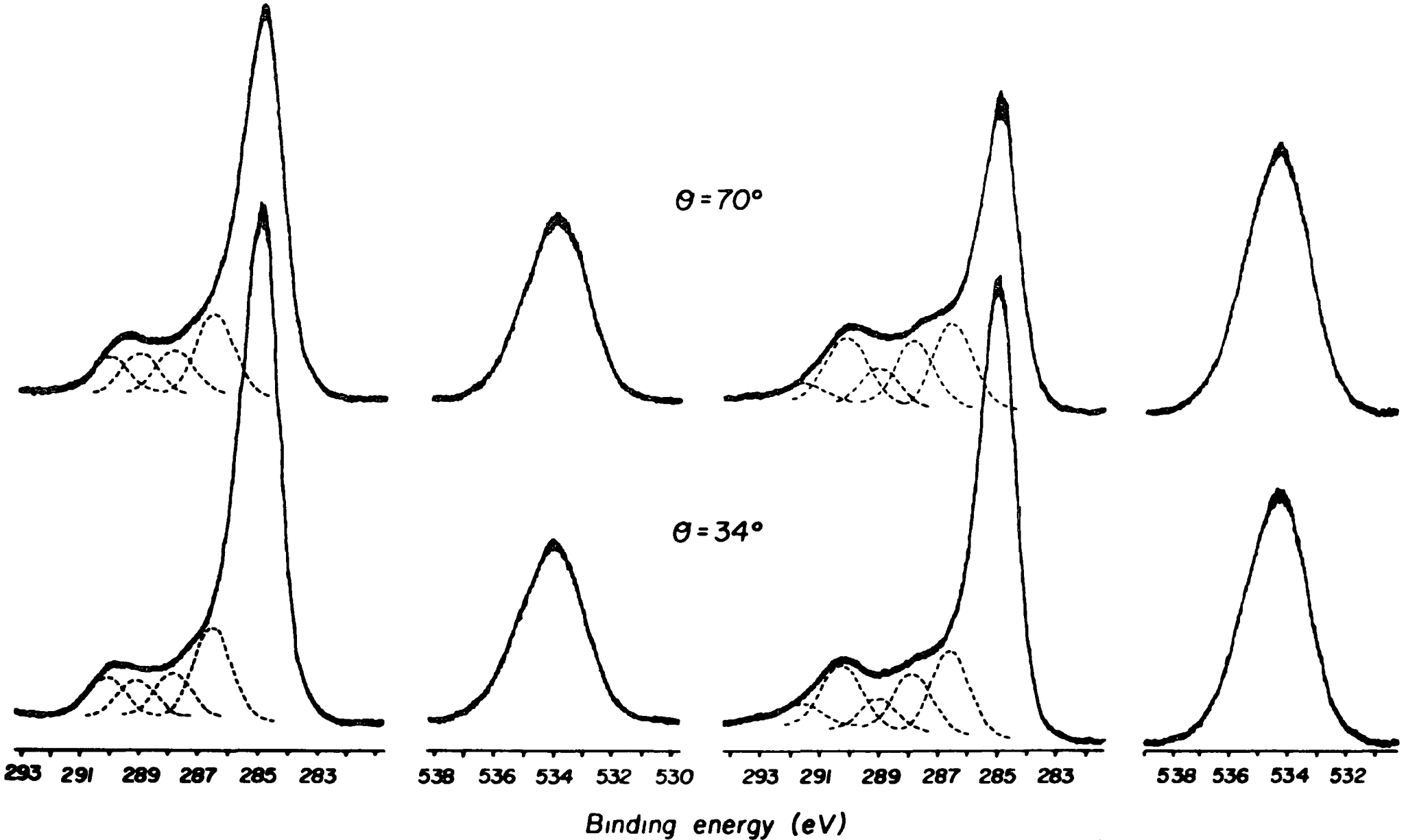

Figure 7.5. C_{1s} and O_{1s} spectra (recorded at electron take off angles of 34° and 70°) of polyethylene and polystyrene exposed for 16 secs. (0.2 torr, 0.1 watt).

signals also increases suggesting that the carbon-oxygen features are contained in a layer of thickness appropriate to that of a monolayer or so. To substantiate this statement it is necessary to draw a comparison between the data in figure 7.5 and corresponding data for polyethylene samples which have been oxidized by (1) corona discharge in air[132] and (2) pressing polyethylene powder between aluminium foil sheets (at $\sim 200^{\circ}C$) under a nitrogen atmosphere but without prior degassing of the sample.[123,225] Firstly figure 7.6 shows the O_{1s}, N_{1s} and C_{1s} spectra of the corona discharge treated sample at angles of 34° (a) and 70° (b). The relative intensity of the oxygen and carbon signals is the same at both angles which is clearly consistent with the sample being homogeneous on the ESCA sampling depth scale. Viz. the modification extends more than 50 Å into the sample which is eminently reasonable in terms of the relatively high kinetic energy of the reactive species involved in the process. A different situation is obtained for the sample thermally oxidized at its surface (figure 7.7). In this case the O_{1s} signal intensity relative to that of the C_{1s} intensity increases in going to near grazing electron take off angle. The depth to which the modificiation has occurred in this sample has been estimated to be of the order of three monolayers or so.[123,124,225] However for this sample the absolute intensity of the O_{1s} signal decreases in going from a take off angle of 34° to 70°. Thus in terms of the general form of equation 5.2 in Chapter Five the O_{1s} signal intensity will be a maximum at an angle between 34° and 70°, and closer to 34°. (For a completely homogeneous sample the signal intensities maximise at 34° for the particular spectrometer geometry employed here). Now returning to figure 7.5 it is clear that

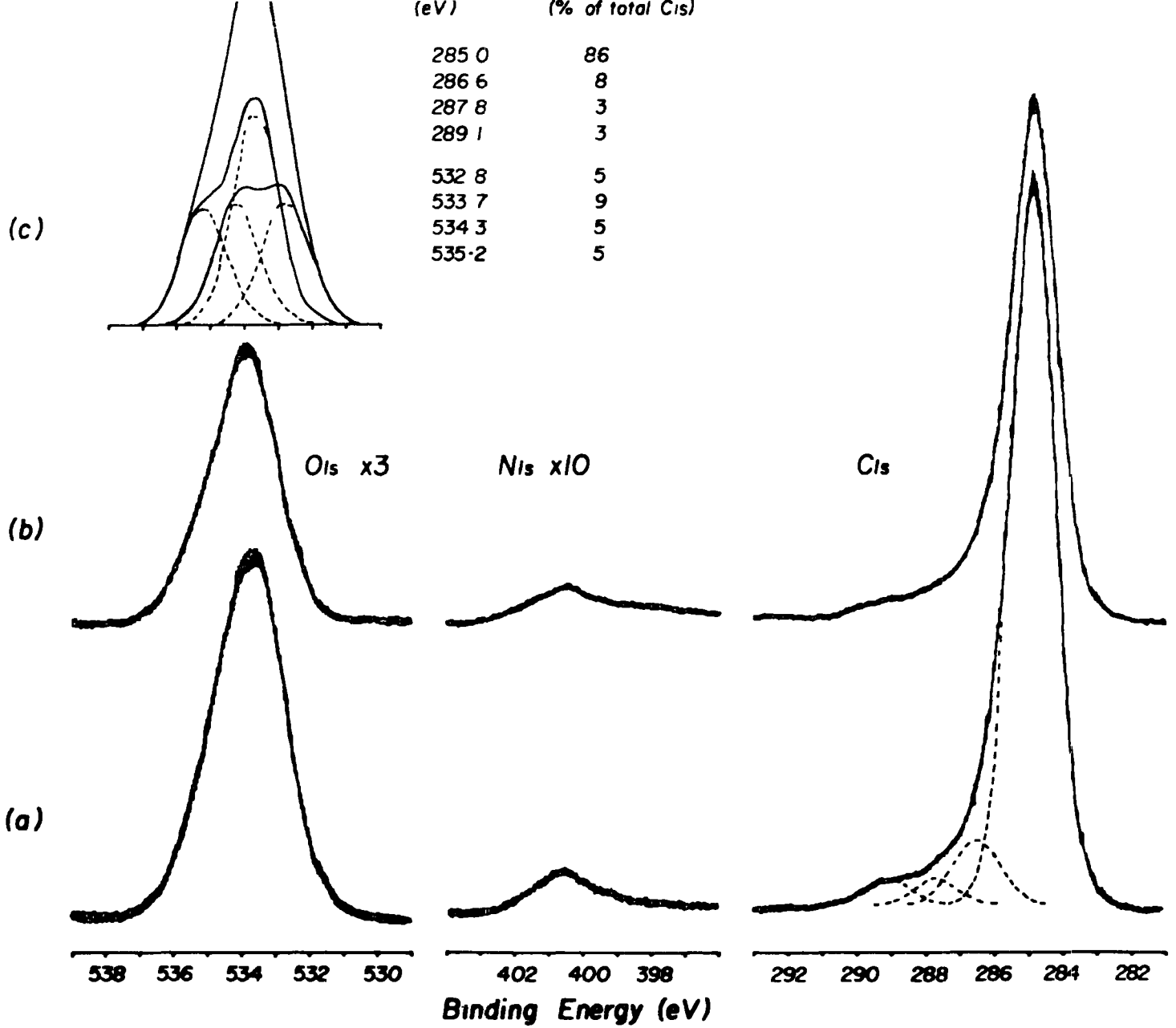

Figure 7.6. O_{1s}, N_{1s} and C_{1s} spectra of a polyethylene sample treated in a corona discharge in air, at electron take off angles of 34° (a) and 70° (b). (c) represents a deconvolution of the O_{1s} spectrum.

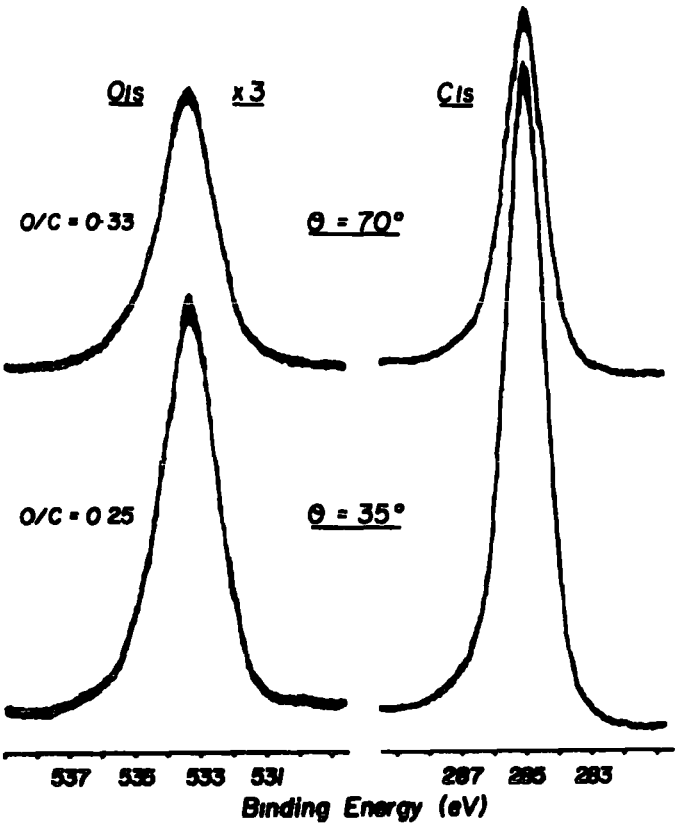

Figure 7.7. O_{1s} and C_{1s} spectra for polyethylene pressed under a nitrogen atmosphere, at electron take off angles of 34^{o} and 70^{o}.

in addition to the signals due to surface features increasing in intensity relative to the total C_{1s} intensity they also increase in absolute terms. Thus in terms of equation 5.2 the signals due to surface features maximise between 34^{o} and 70^{o}, at an angle closer to 70^{o}. This situation can only obtain for a sample modified in the outermost monolayer or so. Indeed it may even be envisaged on the basis of this argument that for polystyrene many of the oxygen atoms may be oriented away from the sample surface. Table 7.2 shows the relevant data for samples of polyethylene (PE), polypropylene (PP) and polystyrene (PS) treated for 4 secs. and 16 secs. respectively in the oxygen plasma (0.2 torr, 0.1 watt).

Table 7.2. Absolute Intensities for C_{1s} and O_{1s} Core Levels Associated with Carbon-Oxygen Environments.

	Carbon*		Oxygen		O_{1s}/C_{1s}*	
	34°	70°	34°	70°	34°	70°
4 secs. PE	22.2	25.1	31.8	35.5	1.43	1.41
PP	27.2	29.3	42.1	43.4	1.55	1.48
PS	30.5	36.0	48.0	55.2	1.57	1.53
16 secs. PE	23.7	23.9	36.3	36.8	1.53	1.54
PP	26.0	26.4	48.9	49.4	1.88	1.87
PS	30.9	34.9	55.5	60.1	1.80	1.72

* Refers to the carbon atoms associated with oxygen only (i.e. the total intensity less the signal at 285.0 eV and shake up at 291.6 eV).

All intensities are in arbitrary units.

Table 7.2. also shows the relative intensity of the total O_{1s} signal to that for the carbon atoms directly attached to oxygen. With a knowledge of the electron mean free paths for C_{1s} and O_{1s} core levels it can be estimated that for an overall stoichiometry of 1:1 the O_{1s}:C_{1s} integrated area ratio is 1.87 and 1.79, if the modification is confined to the outermost monolayer, for electron take off angles of 34° and 70° respectively. (Taking the electron mean free paths for C_{1s} and O_{1s} core levels as 10 Å and 8.5 Å respectively,[100] the depth appropriate to one monolayer as 5 Å [188] and the relative sensitivity of O_{1s} to C_{1s} as 1.67[125]). On comparing these estimated values with those in Table 7.2 it is evident that the overall oxygen:carbon stoichiometry for the oxygen containing features is always less than or equal to one. This type of analysis is possible due to the short range nature of substituent effects and clearly the total

number of oxygen atoms ratioed to the total number of carbon atoms is a lower figure. Since for structural features such as acids, peroxyacids and hydro-peroxides the O:C stoichiometry is greater than one on this basis the modified polymer surface must contain a significant quantity of ether linkages to compensate, since they have an O:C stoichiometry of one half, in the sense of this discussion. This is supported to some extent by the C_{1s} spectrum in which the signal due to carbon singly bonded to oxygen typically accounts for 10-15% of the total carbon signal, for the treated samples (Table 7.3).

The data in Table 7.2 clearly demonstrate the relative order of reactivity of the three polymers towards the oxygen glow discharge as; polystyrene > polypropylene > polyethylene, which is entirely reasonable in terms of the relative reactivities of unsaturated versus saturated systems and of tertiary versus primary and secondary C-H bonds.

So far in the discussion no attempt has been made to resolve the O_{1s} spectra, for reasons previously noted in section 3, namely that the centroids of the binding energy groupings are separated by typically less than 1 eV, and that the groups are less well defined than those for the C_{1s} core levels. However figure 7.6 has already shown one example of the curve fitting method for an O_{1s} spectrum based on four peaks and in general good fits can be obtained in the same fashion to all of the O_{1s} spectra of samples exposed to oxygen plasmas in this work, although the fit is not always unique. Indeed, in the example (figure 7.6) the relative intensities of the oxygen signals shown cannot be directly correlated with those of the related carbon signals, however judicious optimization of the height and FWHM of the component curves may well improve matters in

this direction. The most important information derived from the curve fitting with respect to the O_{1s} spectrum is that associated with the high binding energy component at 535.2 eV. It has been seen in section 3 that this grouping contains the singly bonded oxygen atoms of carbonates peroxyacids and peroxyesters. For the corona discharge treated sample (figure 7.6) the C_{1s} spectrum shows no evidence for carbonate features, providing strong evidence for the presence of peroxyacids and peroxyesters in the sample since their C_{1s} binding energy coincides with that associated with simple acids and esters (289.0 eV). For the oxygen glow discharge treated samples however (figure 7.5) carbonate features are readily observed in the C_{1s} spectra (290.4 eV) and the high binding energy oxygen component is more prominent as evidenced by the centroid of the O_{1s} spectrum being at higher binding energy. It is likely that both carbonate and peroxyacid type features are present at the surface of these samples.

For the particular case of polystyrene the low energy shake up satellite structure provides an extra level of information and allows direct monitoring of the degree of unsaturation in the surface regions of the sample. To date shake up satellites have not been observed associated with $\geq C=O$ type pi systems in polymers largely due to their low intensity and the kinetic energy of the emitted electrons which falls in a region where they are likely to be masked by the tail arising from inelastic scattering events. The discussion here therefore is confined to the shake up satellites associated with the benzenoid ring systems and carbon-carbon double bonds. Figure 7.8 shows plots of the shake up intensity expressed as a percentage of the total C_{1s} intensity and of the signal due to

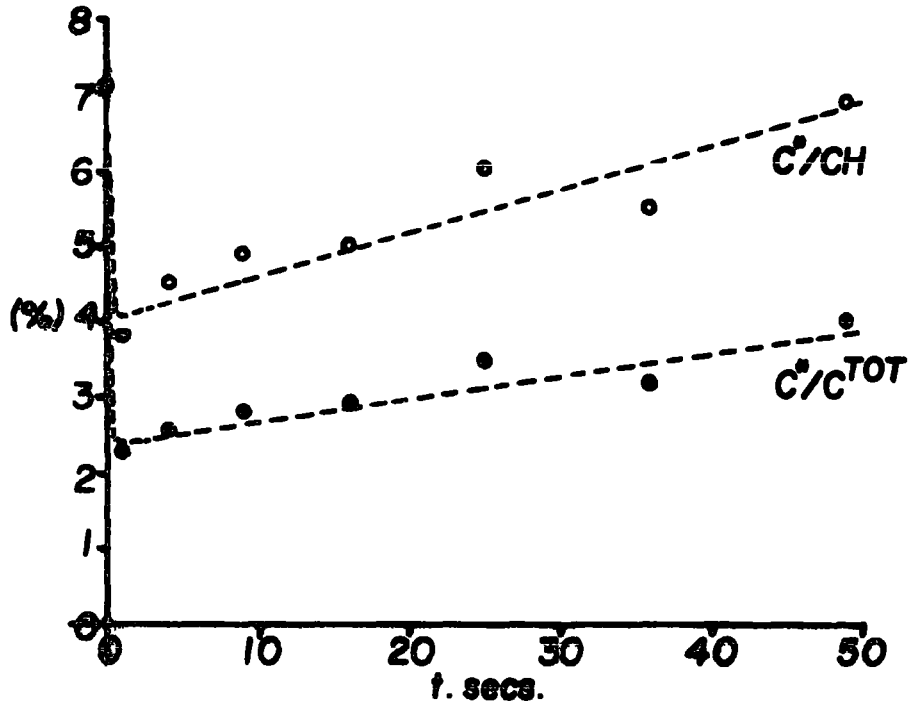

Figure 7.8. Shake up intensity relative to C_{1s}^{TOT} and CH (carbon not attached to oxygen) versus time of exposure to the plasma.

carbon atoms not directly attached to oxygen. In the initial second of reaction the shake up signal decreases drastically due to a loss of unsaturation in the surface regions of the sample and to a lesser extent, substituent effects consequent upon replacing ring hydrogen by an oxygen containing functionality. The relatively constant value of the intensity relative to the total C_{1s} signal suggests that the loss of unsaturation occurs to a definite depth into the sample very quickly although it is likely that unsaturation of the subsurface and bulk regions will be lost at a much slower rate by a radiative energy transfer mechanism throughout the reaction. Thus the

apparent slight increase in the shake up intensity with respect to the total must be due to 'swelling' of the surface regions consequent upon the insertion of oxygen atoms. This would reduce the number density of carbon atoms in the surface and decrease the total C_{1s} intensity. Since the signal due to carbon atoms not attached to oxygen at 285.0 eV becomes reduced in intensity as the reaction proceeds the shake up intensity relative to this, not surprisingly, increases after the first second of reaction. However the interesting point to note is that this curve is tending to a value similar to that for the starting material[129] which clearly indicates that after 50 secs. very nearly all of the carbon atoms in the outermost surface of the sample are attached to at least one oxygen atom and thus make no contribution to the signal at 285.0 eV. The spectrum in this situation would be expected to be consistent with that of polystyrene overlayed with a highly oxygenated surface.

The development of the various carbon-oxygen features can be straightforwardly monitored as a function of time as illustrated in figure 7.9 for polyethylene and polystyrene. The data were accumulated at an electron take off angle of 34^{o} and resolved into four components as described in section 3. There is a clear tendency for the signals associated with $\underline{C}$-O and $\underline{C}$=O/O-$\underline{C}$-O to reach a maximum value soon after the start of the reaction and then decrease to a constant level, whilst the signals associated with O=$\underline{C}$-O and $\underline{C}O_3$ steadily rise to a constant level. Under the conditions employed in this investigation all of the components of the C_{1s} spectrum reach a constant intensity after approximately 16 secs. Whether this is due to the reaction reaching a limit and stopping or that the surface is continually renewed by the evolution of small volatile mole-

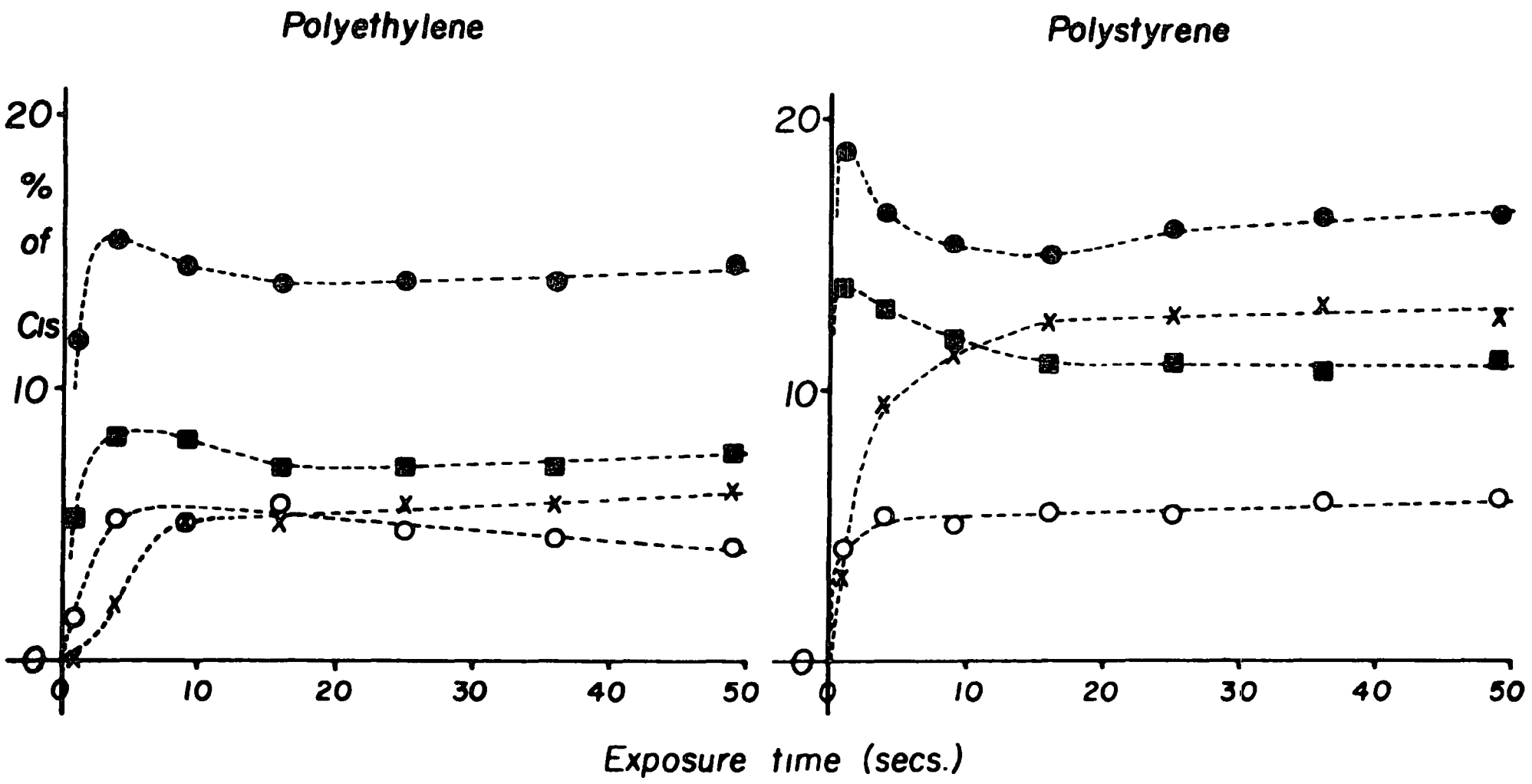

Figure 7.9. Intensity of the various components of the C_{1s} spectrum of polyethylene and polystyrene relative to C_{1s}^{TOT}, versus time of exposure to the oxygen plasma (0.2 torr, 0.1 watt).

cules (e.g. CO, CO_2, H_2O, etc.) cannot be determined from the ESCA data. For similar investigations employing higher power loadings the latter case has been demonstrated both by sample weight loss[227] and the detection of the volatile products.[228] However at the extremely low power loading employed in this investigation this is not necessarily the case although considering the high extent of oxidation observed at the surface it cannot be discounted. The constant values of the C_{1s} component peak intensities averaged for spectra recorded after 16, 25, 36 and 49 seconds exposure to the plasma are collected in Table 7.3 for polyethylene, polypropylene and polystyrene. The error limits have been estimated at 10%, although the total area of the four components is accurate to 5% as is the O_{1s} intensity. It is interesting to note that in each case the total intensity of the signals due to carbon attached to oxygen have a close correspondence to the fraction of the total C_{1s} signal appropriate to one monolayer.

Table 7.3. Final Composition of the Plasma Oxidized Polymers in Pure Oxygen.

	Total O_{1s}*	C_1 (286.6eV)*	C_2 (287.9eV)*	C_3 (289.0eV)*	C_4 (290.4eV)*	Total C_{1s}*
PE	42.1±2.1	12.8±1.3	5.2±0.5	3.7±0.4	5.0±0.5	26.7±1.3
PP	58.7±2.9	14.3±1.4	6.4±0.6	3.8±0.4	5.7±0.6	30.2±1.5
PS	60.4±3.0	12.7±1.3	8.2±0.8	3.2±0.3	9.5±1.0	33.6±1.7

* Expressed as a percentage of the total C_{1s} intensity.

The marked trends displayed by the data in Table 7.3 demonstrate the overall consistency of the analysis. For the three samples C_1 (C-O) and C_3 (O=C-O) have a closely similar intensity although their rate of production is fastest in polystyrene (figure 7.9). The greater incorporation of oxygen in

polystyrene is clearly in the form of ketone/methylene-diether, (C_2), and carbonate, (C_4), environments. Clearly this degree of information is only available from ESCA investigations.

4.2 Helium/Oxygen Plasmas

The addition of helium to the system might be expected to produce profound changes in the processes occurring at the surface of the samples. Apart from the obvious effects of a diluent, helium has been demonstrated to be the most efficient of the inert gases for the crosslinking of the outermost few monolayers of a polymer (cf. Chapter Six) due to its size and the large amount of energy it is able to transfer to the polymer surface via ion neutralization and Penning ionization processes. To investigate this experiments have been carried out in plasmas excited in helium/oxygen mixtures approximately 95/5 and 75/25% by volume at a pressure of 0.2 torr and power loading of 0.1 watt to facilitate direct comparison with the corresponding data for the pure oxygen plasmas. Thus figure 7.10 shows plots of the intensities of the various carbon-oxygen components of the C_{1s} spectrum as a function of time of exposure to the plasma and Table 7.4 summarizes the constant values of the intensities averaged for spectra recorded after 16, 25, 36 and 49 seconds exposure. The most striking feature in figure 7.10 and Table 7.4 is that the three samples all react very similarly in terms of both the rate of production of the carbon-oxygen features and their final composition. Section 4.1 has clearly demonstrated that the overall composition of the product of oxidation by a pure oxygen plasma at low power is a sensitive function of the molecular structure of the starting material. It would seem highly likely then that the oxidation in the helium/oxygen mixture is preceded by an extremely rapid crosslinking of the

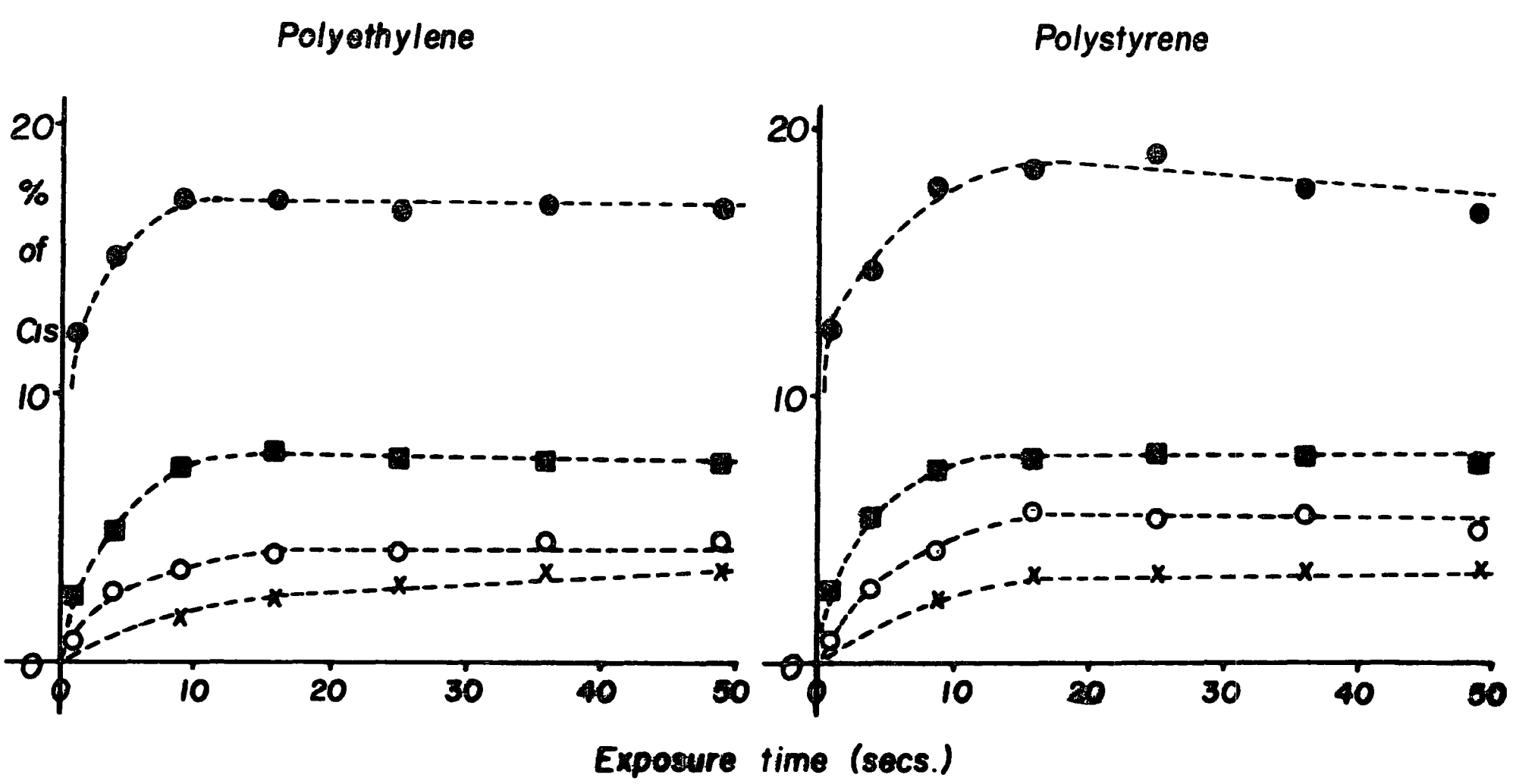

Figure 7.10. Intensity of the various components of the C_{1s} spectrum of polyethylene and polystyrene relative to C_{1s}^{TOT}, versus time of exposure to the helium/oxygen mixture plasma (0.2 torr, 0.1 watt).

surface regions of the polymers, thus producing closely similar molecular structures in these regions for the three polymer systems and hence the same product for the three samples on subsequent oxidation.

Table 7.4. Final Composition of the Plasma Oxidized Polymers in Helium/Oxygen Mixtures (95:5 by volume)

	Total O_{1s}*	C_1 (286.6eV)*	C_2 (287.9eV)*	C_3 (289.0eV)*	C_4 (290.4eV)*	Total C_{1s}*
PE	46.9±2.3	16.9±1.7	7.7±0.8	4.3±0.4	3.1±0.3	32.0±1.6
PP	48.0±2.4	17.0±1.7	7.8±0.8	4.7±0.5	3.1±0.3	32.6±1.6
PS	44.6±2.2	18.0±1.8	7.7±0.8	5.4±0.5	3.4±0.3	34.5±1.7

* Expressed as a percentage of the total C_{1s} intensity.

It is also clearly apparent from figure 7.10 and Table 7.4 that for the samples oxidized in helium/oxygen mixtures there is a greater proportion of C-O and O-C-O/C=O structural features at the expense of O=C-C and CO_3 compared to the corresponding data for samples oxidized with pure oxygen. The angular dependence of the absolute and relative oxygen intensity for these samples however follow a closely similar pattern to those of the sample oxidized in pure oxygen indicating that the oxidation is largely confined to the outermost monolayer.

Comparison of the data in figure 7.10 and Table 7.4 with those in figure 7.9 and Table 7.3 allow several features of the possible processes involved in these reactions to be elaborated, as will become clear from the following section.

5. Mechanistic Aspects of the Plasma Oxidation of Hydrocarbon Polymers

In this section is discussed the most likely processes involved in the oxidation of the three polymers studied in this

work by exposure to oxygen containing plasmas, consistent with the observed experimental data. In comparing figures 7.9 and 7.10 a clear distinction is seen in the shape of the curves corresponding to C-O and O-C-O/C=O environments. For samples oxidized in pure oxygen the intensity of the C_{1s} core level signals due to these features shows a maximum in the early stages of the reaction. This phenomenon is not observed for samples exposed to the helium/oxygen mixture (95% He). The most likely explanation for the fact that all three polymers give the same product when oxidized by the mixture has been suggested to be that the polymers are highly crosslinked in the initial stages of the reaction by the highly energetic (in the sense of electronic rather than kinetic energy) helium ions and metastables, thus:

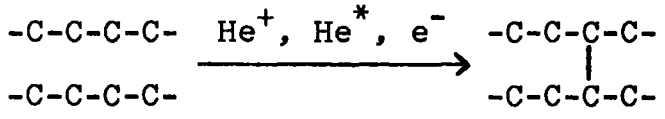

(i)

for which mechanisms have been proposed in Chapter Five. It would not be unreasonable, therefore, to suggest that similar crosslinking may occur in the pure oxygen plasma, effected by active species therein, expressed schematically thus:

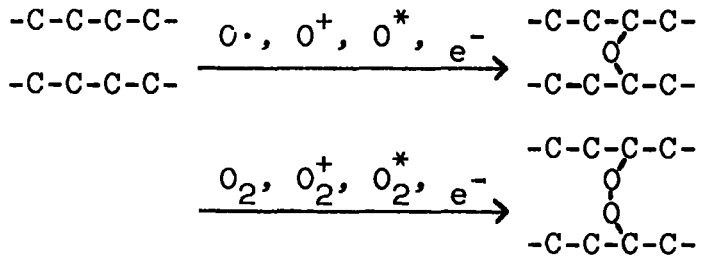

(ii)

These types of reaction however would be expected to be far more selective than those associated with helium ions and metastables which have a greater amount of electronic energy available to the polymer. Hence the polymers retain some of their identity. The observation of maximum values for the components

of the C_{1s} spectrum due to C-O and O-C-O in the initial stages of the reaction is readily rationalized on this basis. Subsequent addition of further oxygen atoms to the then highly crosslinked surface layer produces several types of oxygen environment. Clearly the opportunity to form tri-substituted carbon atoms is far greater for the second case (reaction (ii)). This is reflected in the greater quantity of CO_3 type features found for samples treated in pure oxygen.

Table 7.5 summarizes the data for polyethylene and polystyrene samples treated in plasmas of a total pressure of 0.2 torr and power loading of 5 watts in mixtures of helium and oxygen; 0/100, 75/25 and 95/5% by volume, respectively. The data refers to the constant values of the intensities, attained at the dynamic equilibrium, averaged for spectra recorded after 16, 25, 36 and 49 seconds exposure. The errors are estimated to be within the limits of ± 10% for the C_{1s} components and

Table 7.5. Final Compositions as a Function of Gas Mixture

Polyethylene:

He/O_2	O_{1s}	C_1(286.6eV)	C_2(287.9eV)	C_3(289.0eV)	C_4(290.4eV)
95/5	46.9	16.9	7.7	4.3	3.1
75/25	48.9	14.1	6.9	5.1	3.9
0/100	42.1	12.8	5.2	3.7	5.0

Polystyrene:

He/O_2	O_{1s}	C_1(286.6eV)	C_2(287.9eV)	C_3(289.0eV)	C_4(290.4eV)	Shake up
95/5	44.6	18.0	7.7	5.4	3.4	3.6
75/25	57.1	13.4	7.1	3.6	6.8	3.8
0/100	60.4	12.7	8.2	3.2	9.5	3.4

± 5% for the total O_{1s} intensity.

It is interesting to speculate, on the basis of the available data,[195,229,230] about the behaviour of the plasmas excited in inert gas/oxygen mixtures. The likely contributions of reactions from inert gas ions and metastables versus oxygen containing species with the polymer presents a highly complex problem. However an approximate solution can be obtained by considering the published cross section data for ionization by electron impact as models. It would appear reasonable that the typical cross sections for these processes (based on electron energies in the region of 25 eV) are an order of magnitude larger for oxygen than for helium.[229] On this basis a crude estimate of the likely relative concentrations of reactive species derived from either helium or oxygen in the plasmas excited in mixtures is possible. Thus for the 95% and 75% helium mixtures the relative concentrations of reactive species of helium: oxygen are of the order of 2:1 and 1:3 respectively.

By comparison of the data in figures 7.9 and 7.10 with data pertaining to the rate of crosslinking of a typical polymer effected by a direct energy transfer process in plasmas excited in helium, (derived in Chapter Six), it is readily apparent that the overall rates of crosslinking for pure helium and pure oxygen are comparable and that the rate for the mixtures is also of the same order. It would seen likely therefore that the crosslinking reaction in the initial stages of oxidation by exposure to plasma excited in helium/oxygen mixtures will involve contributions from both inert gas species and oxygen species in the plasma.

Returning to the experiment data, the evidence in favour of these speculations is as follows. For polystyrene the oxygen addition reactions seem likely to be secondary processes

preceded by the crosslinking process effected by both helium and oxygen species at similar rates. The probable mechanism for these crosslinking reactions has been previously discussed in Chapter Five and the initial stages, after energy transfer and possibly neutralization of the polymer ions, result in the production of unsaturated sites, and these will almost certainly be in the backbone. The unsaturation in the starting material for polystyrene will ensure that this type of reaction is rapid. Therefore on the time scale on which the dynamic equilibrium at the surface is established the surface is crosslinked and the number of tertiary C-H bonds is reduced. Hence the rate of production of oxygen containing structural features is less for the helium/oxygen mixtures, as evidenced by the total O_{1s} intensity (Table 7.5). The lower partial pressure of oxygen is also expected to produce such a trend, although the lack of a direct correlation is evident from Table 7.5 for polystyrene since for the 75/25% helium/oxygen mixture the composition of the product is close to that obtained from pure oxygen, as might have been expected since the ratio of helium:oxygen reactive species in the plasma is estimated to be 1:3.

The close similarity of the shake up intensity for the three experiments involving polystyrene also provides some evidence that the crosslinking processes predominantly involve the backbone of the polymer and the loss of the original unsaturation due to the phenyl rings is a consequence of the oxidation reaction rather than the initial crosslinking processes. This is further supported from experimental data in the earlier stages of reaction, where the shake up intensity decreases at a faster rate for the pure oxygen system. Thus for a 4 second exposure to the pure oxygen plasma and the 95/5% helium/oxygen mixture the shake up intensities are 2.6 and 3.6% respectively.

An interesting situation occurs for polyethylene on the other hand (Table 7.5). The crosslinking process is slower due to the lower rate of production of unsaturated sites in the initial stages, however subsequent oxidation of the tertiary C-H bonds so produced is more favourable than the oxidation of the CH_2 sites of the initial system. The data pertaining to the amount of oxygen incorporated into the polymer therefore indicates a small but significant enhancement of oxidation at higher helium partial pressures for this system suggesting that helium is somewhat more efficient than oxygen in crosslinking the saturated structure. This is entirely reasonable since for saturated systems the rate of crosslinking via a direct energy transfer mechanism was found to be directly related to, amongst other things, the amount of energy available (see Chapter Six).

6. Conclusions

In the early work on the investigation of structure and bonding in fluoropolymers[114] the concept of primary and secondary effects of substituting hydrogen by fluorine was well established. The primary shift being $\sim 2.9 \pm 0.3$ eV and the secondary shift being $\sim 0.7 \pm 0.2$ eV.[114] The shift on substituting more than one fluorine atom is roughly additive. The present work has extended this concept to oxygen containing systems and it is found that a closely similar situation exists. The primary shift for oxygen being $\sim 1.5 \pm 0.2$ eV per oxygen bond and by comparison with the fluorine data the secondary shift may be estimated to be of the order of ~ 0.3 eV. The lower value of the primary shift compared to that for fluorine manifests itself in less well resolved C_{1s} spectra for these systems, however the lower value of the secondary shift is advantageous since it allows a closer grouping of various oxygen environments.

(e.g. C-OH and C-OOH have closely similar binding energies whilst C-C-OH and HO-C-C-OH have virtually the same binding energy). It has also been demonstrated that the effect is again roughly additive. Consequently the resolution of complex spectra of even highly oxidized samples is possible within an acceptable degree of accuracy.

It should be clear from this Chapter that the application of this concept to the academically and industrially important field of polymer oxidation can provide much information which is beyond the scope of more conventional spectroscopic techniques. Indeed, fine details of the mechanistic aspects of the oxidation of the outermost monolayer of hydrocarbon polymers effected by oxygen containing radiofrequency glow discharges have been straightforwardly obtained, showing that the reactions are initiated by a fast crosslinking process. The relative concentrations of the various types of carbon-oxygen environments have also been estimated by this method, leaving little doubt that ESCA studies are mandatory for the investigation of the surface modification of polymers.

REFERENCES

1. D.T. Clark, 'Chemical Aspects of ESCA', in 'Electron Emission Spectroscopy', Ed. W. Dekeyser and D. Reidel. D. Reidel Publishing Company, Dordrecht, Holland, 373 (1973)
2. H. Robinson and W.F. Rawlinson, Phil.Mag., 28 277 (1914)
3. H. Robinson, Proc.Roy.Soc. A104 455 (1923)
4. H. Robinson, Phil.Mag., 50 241 (1925)
5. M. de Broglie, Compt.Rend., 172 274 (1921)
6. J.A. van Akker and E.C. Watson, Phys.Rev., 37 1631 (1931)
7. M. Ference, Jr., Phys.Rev., 51 720 (1937)
8. A. Bazin, Zhurnal Eksperimental noi i Theoreticheskoi Fiziki, 14 23 (1944)
9. R.G. Steinhardt, Jr., F.A.D. Granados and G.I. Post Anal.Chem., 27 1046 (1955)
10. B.L. Henke, Tech.Report No. 6, Contract No. AF49(638) Air Force Office of Scientific Research (1962)
11. K. Siegbahn and K. Edvarson, Nucl.Phys. 1 137 (1956)
12. C. Nordling, E. Sokolowski and K. Siegbahn, Phys.Rev., 105, 1676 (1957)
13. A.E. Lindh, in 'Handbuch der Experimentalphysik', 24 2 Ed. W. Wien and F. Haines, Leipzig (1930)
14. H.W.B. Skinner and J.E. Johnston, Proc.Roy.Soc., A161 420 (1937)
15. C. Nordling, E. Sokolowski and K. Siegbahn, Arkiv,Fys. 13 483 (1958)

16. S. Hagstrom, C. Nordling and K. Siegbahn, Phys.Lett. 9 235 (1964)

17. C. Nordling, S. Hagstrom and K. Siegbahn, Z. Physik, 178 433 (1964)

18. K. Siegbahn, C. Nordling, A. Fahlman, R. Nordberg, K. Hamrin, J Hedman, G. Johansson, T. Berkmark, S.E. Karlsson, I. Lidgren and B. Lindberg, 'ESCA, Atomic, Molecular and Solid State Structure Studied by Means of Electron Spectroscopy', Almquist and Wiksells, Uppsala (1967)

19. K. Siegbahn, C. Nordling, G. Johansson, J. Hedman, P.F. Heden, K. Hamrin, U. Gelius, T. Berkmark, L.D. Werme, R. Manne and Y. Baer. 'ESCA Applied to Free Molecules', North-Holland Publ.Co., Amsterdam (1969)

20. C.D. Wagner, Farad.Disc.Chem.Soc., 60 306 (1975)

21. D.T. Clark, 'Structure and Bonding in Polymers as Revealed by ESCA' in 'Electronic Structure of Polymers and Molecular Crystals', Ed. J. Ladik and J.M. Andre, Plenum Press, New York (1975)

22. J.F.McGilp and I.G. Main, J.Elect.Spec. 6 397 (1975)

23. P. Ascarelli and G. Missoni, J.Elect.Spec. 5 417 (1974)

24. G. Johansson, J. Hedman, A. Berndtsson, M. Klasson and R. Nilsson, J.Elect.Spec. 2 295 (1973)

25. P. Auger, J.Phys.Radium 6 205 (1925)

26. P. Auger, Compt.Rend. 65 180 (1925)

27. J.J. Lander, Phys.Rev. 91 1382 (1953)

28. Cf. T.A. Carlsson, 'Photoelectron and Auger Spectroscopy', Plenum Press, New York (1975)

29. D. Coster and R. de L. Kronig, Physica 2 13 (1935)

30. E.H.S. Burhop, 'The Auger Effect and Other Radiationless Transitions', Cambridge University Press (1952)

31. C.C. Chang, Surface Sci., 25 53 (1971)

32. J.P. Coad, M. Gettings and J.G. Riviere, Farad.Disc. Chem.Soc., 60 269 (1975)

33. A.E. Sandström in 'Handbook of Physics', Vol.XXX, 'X-rays', 164 Ed. S.F. Flugge Springer-Verlag, Berlin (1957)

34. C.D. Wagner, Disc.Farad.Soc. 60 291 (1975)

35. A. Rosen and I. Lindgren, Phys.Rev., 176 114 (1968)

36. P.S. Bagus, Phys.Rev., 139A 619 (1965)

37. D.A. Shirley in, 'Advances in Chemical Physics', 23 85 Ed. I. Prigogine and S.A. Rice, Wiley, New York (1973)

38. U. Gelius and K. Siegbahn, Farad.Disc.Chem.Soc. 54 257 (1972)

39. L.C. Snyder, J.Chem.Phys., 55 95 (1971)

40. D.B. Adams and D.T. Clark, Theoret.Chim.Acta., 31 171 (1973)

41. M.F. Guest, I.H. Hillier, V.R. Saunders and M.H. Wood, Proc.Roy.Soc. A333 201 (1973)

42. D.T. Clark, I. Scanlan and J. Müller, Theoret.Chim.Acta. (Berl) 35 341 (1974)

43. T.A. Koopmans, Physika, 1 104 (1933)

44. E. Clementi and H. Popkie. J.Amer.Chem.Soc. 94 4057 (1972)

45. W. Meyer, J.Chem.Phys. 58 1017 (1973)

46. B. Levy, P.H. Millie, J. Ridard and J. Vinh, J.Elect.Spec. 4 13 (1974)

47. L.C. Snyder and H. Basch, J.Amer.Chem.Soc., 91 2189 (1969)

48. H. Hartman and E. Clementi, Phys.Rev., A133 1295 (1964)

49. C.W. Scherr, J.N. Siverman and F.A. Matsen, Phys.Rev., 127 830 (1962)

50. C.S. Fadley, S.B.M. Hagstrom, M.P. Klein and D.A. Shirley, J.Chem.Phys., 48 3779 (1968)

51. D.T. Clark and I.W. Scanlan, J.Chem.Soc. Farad.Trans.II 70 1222 (1974)

52. D.T. Clark, 'ESCA Applied to Polymers' in 'Advances in Polymer Science', Springer-Verlag, Berlin, in press (1977)

53. D.T. Clark in 'Progress in Theoretical Organic Chemistry' Vol.2. Ed. I.G. Csizmadia, Elsevier, Holland in press (1976)

54. D.T. Clark and D.B. Adams, J.Elect.Spec., 7 401 (1975)

55. D.T. Clark, A. Dilks, J. Peeling and H.R. Thomas, Farad. Disc.Chem.Soc. 60 183 (1975)

56. D.T. Clark, D.B. Adams, A. Dilks, J. Peeling and H.R. Thomas, J.Elect.Spec. 8 51 (1976)

57. R. Manne and T. Åberg, Chem.Phys.Lett, 7 282 (1970)

58. J.N. Murrell and B.J. Ralston, J.Chem.Soc.Farad.Trans.II 68 1393 (1972)

59. M.E. Schwartz, Chem.Phys.Lett, 6 631 (1970)

60. D.A. Shirley, Chem.Phys.Lett, 15 325 (1972)

61. W.L. Jolly and D.N. Hendrickson, J.Amer.Chem.Soc., 92 1863 (1970)

62. J.M. Hollander and W.L. Jolly, Acc.Chem.Res. 3 193 (1970)

63. D.T. Clark and D.B. Adams, J.Chem.Soc.Farad.Trans.II 68 1819 (1972)

64. D.B. Adams and D.T. Clark, J.Elect.Spec. 2 201 (1973)

65. W.J. Hehre, R.F. Stewart and J.A. Pople, J.Chem.Phys. 51 2657 (1969)

66. R. Ditchfield, W.J. Hehre and J.A. Pople, J.Chem.Phys. 54 724 (1971)

67. J.A. Pople and D.L. Beveridge, 'Approximate Molecular Orbital Theory', McGraw-Hill, New York (1970)

68. R.E. Watson and A.J. Freeman in 'Hyperfine Interactions' Ed. A.J. Freeman and R.B. Frankel, Academic Press, New York, 1967

69. C.S. Fadley, D.A. Shirley, A.J. Freeman, P.S. Bagus and J.V. Mallow, Phys.Rev.Lett., 23 1397 (1969)

70. J.H. van Vleck, Phys.Rev.Lett., 45 405 (1934)

71. C.S. Fadley in 'Electron Spectroscopy', Ed. D.A. Shirley, 781, North Holland (1972)

72. D.W. Davis and D.A. Shirley, J.Chem.Phys. 56 669 (1972)

73. J.C. Carver, C.A. Thomas, L.C. Cain and G.K. Schweitzer in 'Electron Spectroscopy' Ed. D.A. Shirley, 803, North Holland (1972)

74. Cf. P.W. Atkins, 'Molecular Quantum Mechanics', Oxford University Press, London (1970)

75. Cf. F.A. Cotton and G. Wilkinson, 'Advanced Inorganic Chemistry', John Wiley, New York (1972)

76. T. Novakov and J.M. Hollander, Bull.Amer.Phys.Soc., 14 524 (1969)

77. T. Novakov and J.M. Hollander, Phys.Rev.Lett. 21 1133 (1968)

78. G.K. Wertheim, 'Mossbauer Effect: Principles and Applications', Academic Press, New York (1964)

79. T. Novakov, Ref.26 of C.S. Fadley in 'Electron Spectroscopy' Ed. D.A. Shirley, North Holland (1972)

80. G.M. Bancroft, I.Adams, H. Lampe and T.K. Sham, Chem. Phys.Lett., 32 173 (1975)

81. R.P. Gupta and S.K. Sen, Phys.Rev.Lett., 28 1311 (1972)

82. D.W. Turner, C. Baker, A.D. Baker and C.R. Brundle, 'Molecular Photoelectron Spectroscopy', John Wiley, New York (1970)

83. D.S. Urch and M. Webber, J.Elect.Spec., 5 791 (1974)

84. D. Betteridge, J.C. Carver and D.M. Hercules, J.Elect.Spec. 2 327 (1973)

85. C.R. Ginnard and W.M. Riggs, Anal.Chem. 46(9), 1306 (1974)

86. Cf. R.S. Swingle II and W.M. Riggs, CRC Crit.Rev.Anal.Chem. 5 267 (1975) CRC Press, Cleveland.

87. D.A. Huchital and R.T. McKeon, Appl.Phys.Lett. 20 158 (1972)

88. D.T. Clark, A.Dilks, H.R. Thomas and (in part) D. Shuttleworth in preparation (1977)

89. T.A. Carlson and G.E. McGuire, J.Elect.Spec. 1 161 (1972)

90. C.S. Fadley, R.J.Baird, W. Siekhaus, T. Novakov and S.Å.L. Bergström, J.Elect.Spec. 4 93 (1974)

91. B.L. Henke, J.Phys.(Paris) C4, 115 (1971)

92. B.L. Henke, Adv.X-ray Analysis, 13 1 (1969)

93. J.H. Scofield, Lawrence Livermore Laboratory Report UCRL-51326, Jan (1973)

94. J.H. Scofield, J.Elect.Spec., 8 129 (1976)

95. J. Cooper and R.N. Zare, J.Chem.Phys. 48 942 (1968)

96. F.O. Ellison, J.Chem.Phys. 61 507 (1974)

97. J.J. Huang, J.W. Rabalais and F.O. Ellison, J.Elect.Spec. 6 85 (1975)

98. D.R. Penn, J.Elect.Spec. 9 29 (1976)

99. D.T. Clark and H.R. Thomas, J.Polym.Sci.Polym.Phys.Edn. in press (1977)

100. D.T. Clark and D. Shuttleworth, J.Polym.Sci., Polym.Chem. Edn. in press (1977)

101. Cf. N. Beatham and A.F. Orchard, J.Elect.Spec. 9 129 (1976)

102. A.T. Giese and C.S. French, Appl.Spectr. 9 78 (1955)

103. J.M. Vanderbuilt and C. Henrich, Appl.Spectr. 7 171 (1953)

104. E. Gunders and B. Kaplam, J.Opt.Soc.Amer. 55 1094 (1965)

105. A.E. Martin, Nature (London) 180 231 (1957)

106. H.F. Smith, P-E UV/FL Prod.Dept.Tech. Memo. No.34 (1970)

107. G.L. Green and T.C. O'Haver, Anal.Chem. 46 2191 (1974)

108. R.M. Eisenberg, 'Fundamentals of Modern Physics' Ch.14, John Wiley and Sons, New York (1961)

109. U. Gelius, E. Basilier, S. Svensson, T. Bergmark and K. Siegbahn J.Elect.Spec., 2 405 (1974)

110. I.W. Drummond, G.A. Errock and J.M. Watson, GEC.J.Sci. Tech. 41 94 (1974)

111. D.T. Clark, H.R. Thomas, A. Dilks and D. Shuttleworth, J.Elect.Spec., 10 455 (1977)

112. E.M. Purcell, Phys.Rev. 54 818 (1938)

113. J.C. Helmer and N.H. Weichert, Appl.Phys.Lett. 13 268 (1968)

114. D.T. Clark and W.J. Feast J. Macromol.Sci., Reviews in Macromol.Chem. C12 191 (1975)

115. D.T. Clark in 'Structural Studies of Macromolecules by Spectroscopic Methods' Chapter 9, Ed.K. Ivin, J. Wiley and Sons, London (1976)

116. D.T. Clark in 'Advances in Polymer Friction and Wear', Vol.5A Ed. L.H. Lee, Plenum Press, New York (1975)

117. D.T. Clark 'Some Chemical Applications of ESCA' in 'Molecular Spectroscopy' Ed. A.R. West, Heydon and Sons, London (1976)

118. D.T. Clark in 'Advances in Characterization of Polymer and Metal Surfaces' Ed. L.H. Lee, Academic Press, New York (1976)

119. D.T. Clark, D. Kilcast, W.J. Feast and W.K.R. Musgrave, J.Polym.Sci., Polym.Chem.Edn., 11 389 (1973)

120. D.T. Clark, D. Kilcast, W.J. Feast and W.K.R. Musgrave, J.Polym.Sci., A1, 10 1637 (1972)

121. D.T. Clark, W.J. Feast, I. Ritchie, W.K.R. Musgrave, M.Modena and M. Ragazzini, J.Polym.Sci., Polym.Chem.Edn., 12 1049 (1974)

122. D.T. Clark, J. Peeling and J.M. O'Malley, J.Polym.Sci., Polym.Chem.Edn., 14 543 (1976)

123. D.T. Clark, W.J. Feast, W.K.R. Musgrave and I. Ritchie, J. Polym.Sci., Polym.Chem.Edn., 13 857 (1975)

124. D.T. Clark, W.J. Feast, W.K.R. Musgrave and I. Ritchie in 'Advances in Polymer Friction and Wear', Vol.5A, Ed. L.H. Lee, Plenum Press, New York, (1975)

125. D.T. Clark and H.R. Thomas, J.Polym.Sci., Polym.Chem.Edn, 14 1671 (1976)

126. D.T. Clark and H.R. Thomas, J.Polym.Sci.,Polym.Chem.Edn., 14 1701 (1976)

127. D.T. Clark and H.R. Thomas, J.Polym.Sci.,Polym.Chem.Edn., in press (1977)

128. D.T. Clark and A. Dilks, J.Polym.Sci.,Polym.Chem.Edn., 14 533 (1976)

129. D.T. Clark and A. Dilks, J.Polym.Sci., Polym.Chem.Edn., 15 15 (1977)

130. D.T. Clark, A. Dilks and D. Shuttleworth, proceedings of 'Durham Polymer Surfaces Symposium', Ed.D.T. Clark and W.J. Feast, J. Wiley and Sons, London, in press (1977) and references therein.

131. D.T. Clark and D. Shuttleworth, to be submitted (1977)

132. D.T. Clark, A. Dilks and H.R. Thomas, 'The Application of ESCA to Polymer Degradation' in 'Degradation of Polymers' Ed. N. Grassie, in press (1977), and references therein.

133. D.T. Clark and A. Dilks, A.C.S. Centennial Meeting, New York, April 1976, 'International Symposium on Advances in Characterization of Metal and Polymer Surfaces', Ed. L.H. Lee, Vol.2, page 101, Academic Press, New York (1976)

134. D.T. Clark and A. Dilks, J.Polym.Sci.,Polym.Chem.Edn., in press (1977)

135. D.T. Clark and A. Dilks, J.Polym.Sci.,Polym.Chem.Edn., in press (1977)

136. D.T. Clark and A. Dilks, J.Elect.Spec. 11 225 (1977)

137. D.T. Clark and A. Dilks, J.Polym.Sci.,Polym.Chem.Edn., in preparation (1977)

138. D.T. Clark, A. Dilks and H.R. Thomas, J.Polym.Sci.,Polym. Chem.Edn. in press (1977)

139. J.M. André, J. Delhalle, S. Delhalle, R. Caudano, J.J. Pireaux and J.J. Verbist, Chem.Phys.Lett. 23 206 (1973)

140. J. Delhalle, J.M. André, S. Delhalle, J.J. Pireaux, R. Caudano and J.J. Verbist, J.Chem.Phys. 60 595 (1974)

141. J.J. Pireaux, J. Riga, R. Caudano, J.J. Verbist, J.M. André, J. Delhalle and S. Delhalle, J.Elect.Spec. 5 531 (1974)

142. M. Millard, 'Synthesis of Organic Films in Plasmas' in 'Techniques and Applications of Plasma Chemistry', Ed. J.R. Hollahan and A.T. Bell, J. Wiley and Sons, New York (1974) and references therein.

143. J. Macromolecular.Sci.,Chem. Volume A10(3) (1976)

144. B.D. Washo, J.Macromol.Sci.,Chem. A10(3) 559 (1976)

145. D.W. Rice and D.F. O'Kane, J.Electrochem.Soc. 123 1308 (1976)

146. R.H. Hansen and H. Schonhorn, Polymer Letters, 4 203 (1966)

147. J. Gray 'Surface Treatment for Plastics, Films and Containers' in 'Plastics: Surface and Finish', Ed. S.H. Pinner and W.G. Simpson, Butterworths, London (1971)

148. M. Hudis, 'Plasma Treatment of Solid Materials' in 'Techniques and Applications of Plasma Chemistry' Ed. J.R. Hollahan and A.T. Bell, J. Wiley and Sons, New York (1974)

149. M. M. Millard and A.E. Pavlath, J.Macromol.Sci.,Chem. A10(3) 579 (1976)

150. A. Pavlath and K.S. Lee, J.Macromol.Sci.,Chem. A10(3) 619 (1976)

151. D.M. Soignet, R.J. Berni and R.R. Benerito, J.Appl.Polym. Sci., 20 2483 (1976)

152. M.M. Millard, Anal.Chem. 44 828 (1972)

153. M.M. Millard, K.S. Lee and A.E. Pavlath, Textile.Res.J., 42 307 (1972)

154. M.M. Millard and A.E. Pavlath, Textile.Res.J. 42 460 (1972)

155. D.T. Clark, A. Paton and W. Salanek, J.Appl.Phys. 47 144 (1976)

156. R.D. Chambers, D.T. Clark, D. Kilcast and S. Partington, J.Polym.Sci.,Polym.Chem.Edn. 12 1647 (1974)

157. Cf. T.A. Carlson, J.C. Carver, L.J. Saethre, F.G. Santibanez and G.A. Vernon, J.Elect.Spec., 5 247 (1974)

158. D.H. Richards, N.F. Scilly and F.J. Williams, Polymer, 10 603 (1969)

159. U. Gelius, C.J. Allan, D.A. Allison, H. Siegbahn and K. Siegbahn, J.Chem.Phys.Lett. 11 224 (1971)

160. J.N. Murrell, 'The Theory of the Electronic Spectra of Organic Milecules', Methuen and Co. Ltd., London (1963)

161. M.M. Jaffe and M. Orchin, 'Theory and Applications of Ultraviolet Spectroscopy', John Wiley and Sons, New York, (1962)

162. J. Petruska, J.Chem.Phys. 34 1120 (1961)

163. D.T. Clark, Theor.Chim.Acta.10 111 (1968)

164. J.M. Sichel and M.A. Whitehead, Theor.Chim.Acta, 7 32 (1967)

165. M. Wolfsberg and L. Helmholtz, J.Chem.Phys. 20 837 (1952)

166. D.T. Clark, Tetrahedron, 24 2663 (1968)

167. E. Clementi and D.L. Raimonde, J.Chem.Phys. 38 2686 (1963)

168. N. Mataga and K. Nishimoto, Z.Phys.Chem. Frankfurt 13 140 (1957)

169. L.E. Sutton, 'Tables of Interatomic Distances', Chemical Society, London, Special Publication, No. 18 (1965)

170. D.T. Clark, D. Kilcast and W.K.R. Musgrave, Chem.Comm., 516 (1971)

171. D.T. Clark, R.D. Chambers, D. Kilcast and W.K.R. Musgrave, J.Chem.Soc., Faraday Trans. II, 68 309 (1972)

172. D.T. Clark and D. Kilcast, J.Chem.Soc.(A), 3286 (1971)

173. Cf. D.M.J. Lilley, Ph.D. Thesis, University of Durham, England (1973)

174. J.R. Platt, J.Chem.Phys. 19 1418 (1951)

175. T. Ohta, T. Fujikawa and H. Kuroda, Bull.Chem.Soc. Japan 48 2017 (1975)

176. G. Loux and G. Weill, J.Chim.Physique, 6 484 (1964)

177. D.T. Clark and J. Müller, Theor.Chim.Acta, 41 193 (1976)

178. I.H. Hillier and J. Kendrick, J.Chem.Soc., Faraday Trans.II, 71 1369 (1975)

179. H. Basch, Chem.Phys.Lett., 5 337 (1970)

180. D.T. Clark and D.B. Adams, Theor.Chim.Acta, 39 321 (1975)

181. D.J. Hnatowich, J. Hudis, M.L. Perlman and R.C. Ragaini, J.App.Phys. 42 4883 (1971)

182. C.K. Jørgensen and H. Berthon, Chem.Phys.Lett. 31 416 (1975)

183. J.R. McCreary and R.J. Thorn, J.Elect.Spec. 8 425 (1976)

184. M.F. Ebel and H. Ebel, J.Elect.Spec., 3 169 (1974)

185. T. Dickinson, A.F. Povey and P.M.A. Sherwood, J.Elect.Spec. 2 441 (1973)

186. T.E. Madey, C.D. Wagner and A. Joshi, J.Elect.Spec. 10 359 (1977)

187. International Tables for X-ray Crystallography, Vol.III, Ed. C.H. Macgilla, G.D. Rich and K. Lonsdale, The Kynoch press, Birmingham (1962)

188. B. Wunderlich, 'Macromolecular Physics' Vol.I, Academic Press, New York (1973)

189. G.A. Byrne and K.C. Brown, J.Soc.Dyers and Colourists, 88 113 (1972)

190. J.R. Hall, C.A.L. Westerdahl, A.T. Devine and M.J. Bodnar, J.Appl.Polym.Sci., 13 2085 (1969)

191. M. Hudis, J.Appl.Polym.Sci., 16 2397 (1972)

192. H. Schonhorn and R.H. Hansen, J.Appl.Polym.Sci., 11 1461 (1967)

193 H. Yasuda, J. Macromol.Sci.-Chem. A10 383 (1976)

194. H. Schonhorn, proceedings of 'Durham Polymer Surfaces Symposium', Ed. D.T. Clark and W.J. Feast, J. Wiley & Sons, London in press (1977)

195. Cf. A.T. Bell, 'Fundamentals of Plasma Chemistry' in 'Techniques and Applications of Plasma Chemistry', Ed. J.R.Hollahan and A.T. Bell, J. Wiley and Sons, New York (1974)

196. J.A.R. Samson, 'Techniques of Vacuum Ultra Violet Spectroscopy' J. Wiley and Sons, New York (1967)

197. G. Francis, 'Ionization Phenomena in Gases', Butterworth Publications Ltd., London (1960)

198. E.O. Johnson and L. Malter, Phys.Rev., 80 58 (1950)

199. J.D. Swift and M.J.R. Schwar, 'Electrical Probes for Plasma Diagnostics', Iliffe Books Ltd., London (1970) and references therein.

200. J.J.Quinn, Phys.Rev. 126 1453 (1962)

201. E.E. Muschlitz., Jr.Science, 159 599 (1968)

202. H.D. Hagstrum in 'Techniques of Metals Research', Ed. R.F. Bunshak, J. Wiley and Sons, New York (1972)

203. K.S. Kim, W.E. Baitinger and N. Winograd, Surface Science 55 285 (1976)

204. D.T. Clark, A. Dilks and G.H.C. Freeman, in preparation.

205. R.H. Partridge, J.Chem.Phys. 45 1685 (1966)

206. H. Yasuda, H. Marsh, S. Brandt and C.N. Reilley, J.Polym.Sci., Polym.Chem.Edn., 15 991 (1977)

207. B. Ranby and J.F. Rabek, 'Photodegradation, Photo-oxidation and Photostabilization of Polymers', J. Wiley and Sons, New York (1975)

208. 'Handbook of Spectroscopy' Ed. J.W. Robinson, Vol.1, CRC Press, Cleveland (1974)

209. K.W. Busch and T.J. Vickers, Spectrochimica Acta, 29B 85 (1973)

210. P. Brassem and F.J.M.J. Maessen, Spectrochimica Acta, 29B 203 (1974)

211. M. Hudis and L.E. Prescott, J.Polym.Sci.,Polym.Lett.Edn., 10 179 (1972)

212. E. Mathias and G.H. Miller, J.Phys.Chem. 71 2671 (1967)

213. R.W. Ditchburn, Proc.Roy.Soc. (London) A229, 44 (1955)

214. Cf. J.E. Osher in 'Plasma Diagnostic Techniques' Ed. R.H.Huddlestone and S.L. Leonard, Academic Press, New York (1965)

215. Cf. C.E. Moore, 'Atomic Energy Levels', U.S.A. National Bureau of Standards, Washington, Vols.I to III (1958)

216. D.W. Turner in 'Determination of Organic Structure by Physical Methods', Vol.2 Ed. Nachod and Phillips, New York (1962)

217. J.W. Rabalais and T.P. Debies, J.Elect.Spec. 5 847 (1974)

218. Several discussions appear in Disc.Faraday Soc. 60 (1975)

219. I.P. Batra and C.R. Brundle, Surface Science, 57 12 (1976)

220. C.F. Brucker and T.N. Rhodin, Surface Science, 57 523 (1976)

221. J.Electron Spectroscopy 5 (1974) and references therein.

222. G.C.S. Collins, A.C. Lowe and D. Nicholas, Europ.Polym.J., 9 1173 (1973)

223. D. Briggs, D.M. Brewis and M.B. Konieczko, J.Materials Sci. 11 1270 (1976)

224. D. Briggs, D.M. Brewis and M.B. Konieczko, J.Materials Sci. 12 429 (1977)

225. D.T. Clark, A.Dilks and D. Shuttleworth, J.Materials Sci., in press (1977)

226. D.T. Clark, B.J. Cromarty and A. Dilks, in preparation (1977)

227. R.H. Hansen, J.V. Pascale, T. de Benedictis and P.M. Rentzepis, J.Polym.Sci. A3 2205 (1965)

228. C. Mayoux, A. Antoniou, Bui Ai and R. Lacoste, Europ.Polym.J. 9 1069 (1973)

229. H.S.W. Massey and E.H.S. Burhop, 'Electronic and Ionic Impact Phenomena' Clarendon Press, Oxford (1952)

230. R.I. Reed, 'Ion Production by Electron Impact', Academic Press, New York (1962)